SIMONE DELL'ACQUA
Licenciado em Química

CHARACTERIZATION OF THE ACTIVITY OF NITROUS OXIDE REDUCTASE: BIOCHEMICAL, SPECTROSCOPIC AND MIMETIC APPROACHES

Dissertação apresentada para a obtenção do Grau de Doutor em Química Sustentável pela Universidade Nova de Lisboa, Faculdade de Ciências e Tecnologia

Orientador: Doutor José João Galhardas de Moura, Professor Catedrático Aposentado da Faculdade de Ciências e Tecnologia da Universidade Nova de Lisboa
Co-orientador: Doutor Luigi Casella, Professor Catedrático da Facoltà di Scienze MM.FF.NN. da Università degli Studi di Pavia

Júri
Presidente: Doutora Isabel Maria Andrade Martins Galhardas de Moura
Arguentes: Doutora Maria Conceição Santos Silva Rangel Gonçalves
Doutor Cláudio Manuel Simões Loureiro Nunes Soares
Vogais: Doutora Sofia Rocha Pauleta
Doutor Luigi Casella
Doutor José João Galhardas de Moura

Lisboa
2011

Characterization of the activity of Nitrous Oxide Reductase: Biochemical, Spectroscopic and Mimetic Approaches

Janeiro 2011

Nº Arquivo

A Francesca e Alessandro,

la mia piccola grande famiglia.

Acknowledgments

Sono davvero molte le persone che vorrei ringraziare in questo momento, perché grande è il mio riconoscimento verso tutti coloro che hanno contribuito alla realizzazione di questa tesi.

Queste poche righe esprimono solo una piccola parte della gratitudine che provo per tutti voi.

Ao Professor José Moura, agradeço o entusiasmo e a solidariedade manifestada, e a sua grande paixão pela ciência e pela vida.

À Professora Isabel Moura, agradeço todo o apoio e todas as discussões sobre a química e também sobre o futebol.

Obrigado, José e Isabel, por terem-me acolhido desde o início no vosso grupo, como um filho numa grande família.

Ringrazio il Professor Luigi Casella per avermi guidato sempre, da giovane studente fino ad oggi, senza farmi mai mancare grande supporto e disponibilità.

Um agradecimento especial à Sofia, pela sua ajuda e pela sua contribuição para esta tese, trabalhando sempre incansavelmente.

Al mitico Prof. Enrico Monzani, un grandissimo grazie, per tutto quello che mi ha insegnato e per la grande generosità e umiltà con la quale trasmette amicizia e scienza allo stesso tempo.

Agradeço à Ana Teresa e à Célia por toda a ajuda "burocrática".

To Professor Edward Solomon, I want to express my gratitude for receiving me in his lab and to Esther for the friendship and welcome shown to me.

Aos colegas do Bioin e Bioprot, quero agradecer a vossa boa disposição e ajuda, fizeram-me sentir um português (embora ainda não tenha aprendido a língua!).

A Pablo, Gabi y Avril, gracias, son nuestra familia en Portugal.

A tutti i colleghi del LabCas un infinito grazie, ad ogni ritorno mi avete sempre fatto sentire a casa.

Ringrazio il mio Fiestino e il volo Easyjet MXP-LIS per tutti i viaggi sull'asse Italia-Portogallo.

Ringrazio tutta la mia family, i "Pais Simo", le mie sorelle & le loro famiglie in espansione, mia nonna e i "Pais Fra" per tutto l'affetto che mi dimostrano e il continuo sostegno.

Finally, I thank for the financial support Fundação para a Ciência e a Tecnologia (SFRH/BD/30414/2006).

Abstract

The multicopper enzyme nitrous oxide reductase (N_2OR) catalyses the final step of denitrification, the two-electron reduction of N_2O to N_2. This enzyme is a functional homodimer containing two different multicopper sites: CuA and CuZ. CuA is a binuclear copper site that transfers electrons to the tetranuclear copper-sulfide cluster CuZ, the catalytic site.

In this thesis, *Pseudomonas nautica* cytochrome c_{552} was identified as the physiological electron donor of N_2OR. The kinetic data present differences when comparing physiological and artificial electron donors (cytochrome versus methylviologen). For cytochrome c_{552}, both the kinetic characterization and a docking study indicate the presence of a hydrophobic patch near the CuA, which is the electron entry site. The electron transfer complexes analysis has been extended to N_2OR from other bacterial sources, *Paracoccus denitrificans* and *Achromobacter cycloclastes*, that are characterized by an interaction with the electron donor (cytochrome *c* or pseudoazurin) mainly driven by electrostatic forces. A set of well conserved residues on the N_2OR surface are proposed to be involved in the electron pathway from the redox partner to nitrous oxide reductase. A structural model is then described for the *Wolinella succinogenes* N_2OR that, unlike the other N_2OR structures known, presents a C-terminal extension containing a *c*-type heme binding motif.

The reaction of the activated form of N_2OR with stoichiometric amounts of substrate enabled the identification of a new active CuZ° form in the turnover cycle of the enzyme, which is characterized by an absorption band at 680 nm and is different from the resting and inactive CuZ form, previously observed. Both the reaction of stoichiometric amounts of substrate and the electrochemical studies mediated by the physiological electron donor cytochrome c_{552} show that the active CuZ° species, generated in the absence of reductants, can rearrange to the resting non-active CuZ state. In this light, new aspects of the catalytic and activation/inactivation mechanisms of the enzyme are discussed.

Moreover, it is known that by changing the purification conditions it is possible to obtain CuZ in different redox states. Here we have purified N_2OR from *P. nautica* in the "purple" form, in which the CuZ is in the oxidized $2Cu^{2+}$-$2Cu^{+}$ redox state, a redox active species. This form is redox active but it is not catalytically competent, since its specific activity is lower then the active fully reduced state and comparable to the inactive resting state.

Finally, a biomimetic approach to the catalytic centre CuZ is presented. Reaction of mononuclear and binuclear Cu^{I} complexes supported by different N-donor ligands with S_8 was studied in order to mimic the μ4-sulfido-tetranuclear copper cluster present in N_2OR.

Resumo

A enzima redutase do óxido nitroso (N_2OR) catalisa a etapa final do processo de desnitrificação, a redução de dois electrões de N_2O para N_2. Esta enzima é um homodímero funcional contendo dois centros diferentes multi-cobre: CuA e CuZ. CuA é um local binuclear de cobre que transfere electrões para o centro tetranuclear de cobre CuZ, o centro catalítico.

Nesta tese, o citocromo c_{552} de *Pseudomonas nautica* foi identificado como doador de electrões fisiológico. Os dados cinéticos apresentam diferenças se comparados com os doadores de electrões, quer o fisiológico quer o artificial (citocromo *versus* methylviologen). Para o citocromo c_{552}, tanto a caracterização cinética como um estudo de *docking* indicam a presença de uma área hidrofóbica próximo do centro CuA, que é a local de acesso para os electrões. A análise dos complexos de transferência eletrónica tem sido extendida para a N_2OR de outras bactérias, *Paracoccus denitrificans* e *Achromobacter cycloclastes*, que se caracterizam por uma interação com o doador de electrões (citocromo *c* ou pseudoazurina), principalmente guiado por forças electrostáticas. Um conjunto de resíduos bem conservados na superfície da N_2OR é proposto estar envolvido na via de transferência eletrónica. É aqui descrito um modelo estrutural para a N_2OR de *Wolinella succinogenes* que, ao contrário das outras estruturas conhecidas, apresenta uma extensão C-terminal que contém um motivo de citocromo *c*.

A reacção da forma activada de N_2OR com uma quantidade estequiométrica do substrato permitiu a identificação de uma nova forma activa, designada CuZ°, que é caracterizada por uma banda de absorção em 680 nm e é diferente da forma do CuZ não activa anteriormente observada. Tanto a reação com quantidade estequiométrica de substrato como os estudos electroquímicos mediados pelo citocromo c_{552}, doador fisiológico de electrões, mostram que a espécie activa CuZ°, gerada na ausência de redutores, pode reorganizar-se no estado de CuZ não activo. Nesta perspectiva, são discutidos novos aspectos da activação catalítica e do mecanismo de inactivação da enzima.

Além disso, alterando as condições de purificação, é possível obter o centro CuZ em diferentes estados de oxidação. Aqui foram preparadas a N_2OR de *Pseudomonas nautica* na forma "purple", na qual o CuZ está no estado redox oxidado $2Cu^{2+}$-$2Cu^{+}$. Esta espécie é redox activa, mas não é cataliticamente competente, uma vez que a sua actividade específica é menor que a da enzime no estado activo, totalmente reduzido.

Finalmente, é apresentada uma abordagem biomimética ao centro catalítico CuZ. A reacção de complexos de cobre(I) mononucleares e binucleares coordenados por diferentes ligantes N-

doadores com enxofre molecular (S_8) foi estudada para mimetizar o cluster tetranuclear de cobre-enxofre presente na N_2OR.

Riassunto

L'enzima multirameico ossido nitroso riduttasi (N_2OR) catalizza la reazione terminale della denitrificazione, cioè la riduzione bielettronica dell'ossido nitroso (N_2O) ad azoto molecolare (N_2). Questo enzima è un dimero funzionale che contiene due siti multi rameici: CuA e CuZ. Il centro CuA è un sito binucleare di rame che trasferisce elettroni al centro catalitico CuZ, un cluster rame-sulfido.

In questa tesi, il citocromo c_{552} isolato da *Pseudomonas nautica* è stato identificato come il donatore di elettroni fisiologico di N_2OR. Lo studio della cinetica enzimatica effettuato in presenza del donatore fisiologico e di un donatore artificiale (citocromo e metilviologeno rispettivamente) presenta notevoli differenze. Per quanto riguarda il citocromo c_{552}, entrambi la caratterizzazione cinetica e lo studio di docking indicano la presenza di una regione idrofobica sulla superficie dell'enzima in prossimità del centro CuA, che costituisce il punto di ingresso degli elettroni. L'analisi della reazione di trasferimento elettronico è stata estesa alla N_2OR isolata da altre fonti batteriche, *Paracoccus denitrificans* and *Achromobacter cycloclastes,* le quali presentano un tipo di interazione principalmente di tipo elettrostatico con i rispettivi donatori di elettroni (citocromi *c* o pseudoazzurrine). Un gruppo di residui amminoacidici conservati svolge un ruolo chiave per il trasferimento elettronico dal partner redox alla ossido nitroso riduttasi. E' stato quindi proposto un modello strutturale per la N_2OR da *Wolinella succinogenes*, che si differisce dalle N_2OR da altre fonti in quanto presenta una regione C-terminale che contiene un dominio di tipo citocromo *c*.

La reazione tra l'enzima N_2OR in forma attivata e una quantità stechiometrica di N_2O ha permesso di identificare una nuova specie reattiva nel turnover enzimatico del centro catalitico, denominata CuZ° e caratterizzata da un assorbimento a 680 nm, differente dalla forma inattiva definita "resting" precedentemente osservata. Questo specie, se mantenuta in assenza di agenti riducenti, tende a riformare la specie inattiva "resting". In quest'ottica, nuovi aspetti del ciclo catalitico e delle reazioni di attivazione/inattivazione del enzima sono presentati in questa tesi.

Inoltre, è noto che è possibile ottenere il centro catalitico CuZ in differenti stati redox a partire da diverse condizioni di purificazione dell'enzima. E' presentata la purificazione dell'enzima nella forma "purple", nella quale il centro CuZ si trova nello stato redox $2Cu^{2+}$-$2Cu^{+}$. Questa forma del centro catalitico è attiva dal punto di vista redox, ma non rientra nel ciclo catalitico, siccome l'attività specifica correlata è minore rispetto alla forma completamente ridotta e comparabile con l'attività del forma "resting" non attiva.

Infine, è stato usato un approccio biomimetico per lo studio del centro catalitico CuZ. La reazione di complessi di Cu^{I} mononucleari e binucleari supportati da differenti leganti N-donatori con zolfo molecolare S_8 è stata studiata con il fine di ottenere modelli simili al cluster tetranucleare rame-zolfo presente nell'enzima N_2OR.

Abbreviations

Ac – Achromobacter cycloclastes

Asc – ascorbate

BH cyt *c* – Bovine Heart cytochrome *c*

COX – cytochrome c oxidase

CT – charge transfer

CV – Cyclic voltammetry

DFT – density field theory

DMF – dimethylformamide

DT – sodium dithionite

EPR – electron paramagnetic resonance

ET – electron transfer

HH cytochrome *c* – horse heart cytochrome *c*

MCD – magnetic circular dichroism

MV – methylviologen

NMR – nuclear magnetic resonance

N_2OR – nitrous oxide reductase

NOR – nitric oxide reductase

Pd – Paracoccus denitrificans

PHYRE – Protein Homology/analogY Recognition Engine

PG – pyrolytic graphite

Pn – Pseudomonas nautica

Pp – Paracoccus pantotrophus

SHE – standard hydrogen electrode

TMS – tetramethylsilane

UV – Ultra-violet

Ws – Wolinella succinogenes

Table of contents

List of figures

Figure 2.2 – Kinetic activity of *Pn* N_2OR as function of electron donor concentration: reduced methylviologen (open circles) or *Pn* cytochrome c_{552} (solid squares). The assays were performed in 0.1 M Tris-HCl at pH 7.6, 70 nM activated N_2OR, 1.25 mM N_2O-saturated water and 6.2 to 155.6 μM MV or 3.6 to 36 μM *Pn* cytochrome c_{552}. The experimental data was fitted with Michaelis-Menten equation, using a K_m of (11.5 ± 3.6) μM and V_{max} of (157 ± 13) U/mg, or a K_m of (50.2 ± 9.0) μM and and V_{max} of (1.8 ± 0.6) U/mg for methylviologen or *Pn* cytochrome c_{552}, respectively.

Figure 2.3 – Kinetic activity of *Pn* N_2OR as function of N_2O concentration with methylviologen (open circles) and cytochrome c_{552} (solid squares) as electron donor. The assays were performed in 0.1 M Tris-HCl at pH 7.6, 35 nM activated N_2OR, 5, 10, 12.5, 25, 37.5, 62.5, 125 and 500 μM N_2O-saturated water, 91 μM MV and 7.5 μM *Pn* cytochrome c_{552}. The experimental data was fitted with Michaelis-Menten equation, using a K_m of (14.0 ± 2.9) μM and V_{max} of (128 ± 17) U/mg, for methylviologen.

Figure 2.4 – pH dependence of the kinetic activity of *Pn* N_2OR using *Pn* cytochrome c_{552} (solid squares) or MV (open circles) as electron donors. The assays were performed adding 35 nM activated N_2OR to a solution containing 9 μM *Pn* cytochrome c_{552} or 91 μM MV, 1.25 mM N_2O-saturated water, in different buffer systems between pH 6.2 and 8.7. The data was non-linear fitted using the equation described in Materials and Methods and pK_a of 8.3 and 6.6 were calculated for cytochrome c_{552} and MV, respectively.

Figure 2.5 – Direct electron transfer between fully oxidised nitrous oxide reductase and reduced electron donors (A) MV and (B) *Pn* cytochrome c_{552}, monitored by visible spectra. (A) The reduction of N_2OR by MV was observed at 480 nm, 540 nm and 800 nm. (A-i) fully oxidised *Pn* N_2OR, (A-ii) N_2OR after addition of reduced MV and (A-iii) difference spectrum between (A-i) and (A-ii). (B) The reduction of *Pn* N_2OR by *Pn* cytochrome c_{552} was observed at 800 nm, while the oxidation of the cytochrome was observed at 552 nm. (B-i) N_2OR spectrum immediately after addition of reduced cytochrome c_{552} (t=0), (B-ii) N_2OR spectrum after addition of reduced cytochrome c_{552} (after t=30s), (B-iii) fully oxidised *Pn* N_2OR and (B-iv) difference spectrum between (B-ii) and (B-i).

Figure 2.6 – ^1H NMR titration of *Pn* cytochrome c_{552} with nitrous oxide reductase. In panel A the low-field spectral region (40 – 12 ppm) containing the cytochrome M1, M2, M3 and M4 heme methyl resonances is shown. The experiment was performed as described in Materials and Methods, and the protein samples were (A, i) R=0, 472 μM cytochrome c_{552}; (A, ii) R=0.5, 440 μM cytochrome c_{552} and 220 μM N_2OR; (A, iii) R=1.0, 410 μM cytochrome c_{552} and 410 μM N_2OR; (A, iv) R=2.0, 365 μM cytochrome c_{552} and 730 μM N_2OR; (A, v) R=3.6, 308 μM cytochrome c_{552} and 1109 μM N_2OR. Panel B shows the chemical shift variation of cytochrome c_{552} heme methyl M4 with increasing molar ratios of nitrous oxide reductase. Panel C shows the fitting curve simulated for a single binding site with K_d = 5.0 μM and δ_{max} = 0.014 ppm, until a ratio of 1:1.

Figure 2.7 – A) 500 top model complexes ranked by Global Score of the docking of N_2OR dimer with cytochrome c_{552} dimer. B) 500 top model complexes ranked by the Hydrophobic Scored of the docking of N_2OR dimer with cytochrome c_{552} dimer. In Panel A and B the geometric center of the cytochrome c_{552} of the 500 putative model complexes is represented as a yellow spheres, while the top 50 are represented as bigger red-coloured spheres. The two copper atoms of the CuA center are red, while the catalyitic center is blue, and the polypeptide of each nitrous oxide reductase monomer is coloured in lighter or darker grey.

Figure 2.8 – Top putative docking positions obtained after analysis of the docking between *Pn* cytochrome c_{552} dimer and *Pn* N_2OR dimer. Only the heme group of 6 out of the top 8 models are displayed: model 1 in grey, model 2 in black, model 5 in green, model 6 in yellow, model 7 in red and model 8 in blue. These numbers correspond to the numbering in Table 1. Model 3 and 4 are not displayed, because they are located near the CuA of the other N_2OR monomer. The two copper atoms of the CuA center are coloured red, while the catalytic center is coloured dark blue, and the polypeptide chain of each nitrous oxide reductase monomer is coloured in lighter or darker grey.

Figure 2.S1 - Simulated kinetic activity of N_2OR as a function of N_2O concentration with cytochrome c_{552} as electron donor. The curves are simulated using equation 17 and [cytochrome c_{552}] of 10, 50, 150 and 250 μM. The upper curve is the reaction with a fully saturated (with cytochrome c_{552}) N_2OR, which is indicated as simulated MM. In panel A, the [N_2O] range is the same as the one used in the experiment described in the manuscript (5 – 500 μM), while panel B shows an inset with [N_2O] between 0 and 30 μM.

Figure 2.S2 - Simulated kinetic activity of N_2OR as function of N_2O concentration with cytochrome c_{552} as electron donor. The curves are simulated using equation 18 and [cytochrome c_{552}] of 10, 50, 150 and 250 μM. The upper curve is the reaction with a fully saturated (with cytochrome c_{552}) N_2OR, which is indicated as simulated MM. In panel A, the [N_2O] range is the same as the one used in the experiment described in the manuscript (5 – 500 μM), while panel B shows an inset with [N_2O] between 0 and 30 μM.

Chapter 3:

Figure 3.1 – Cyclic voltammograms (40 mVs^{-1}) of 50 μM cytochrome c_{552} entrapped in a membrane electrode with 2.5 μM activated *Pseudomonas nautica* N_2OR, in 0.1 M phosphate buffer, pH 7. The black-line is the CV in the absence of substrate and the red-line is the CV after addition of 1 mM N_2O.

Figure 3.2 – Catalytic current from electrochemical assays of *Pn* N_2OR using cytochrome c_{552} as mediator *versus* N_2O concentration. The assays were performed with 2.5 μM activated N_2OR and 50 μM cytochrome c_{552} entrapped in the membrane electrode, in 0.1 M phosphate buffer at pH 7, and in the presence of 8, 17, 25, 33, 48, 125, 330, and 1000 μM N_2O-saturated water. The experimental data were fitted with the Michaelis-Menten equation, using a K_m of (16 ± 2) μM and a $i_{cat\max}$ of (3.9 ± 0.1) × 10^{-7} A.

Figure 3.3 – Intermolecular rate constants of *Pseudomonas nautica* N_2OR *versus* pH, determined by electrochemical assays using cytochrome c_{552} as mediator. The assays were performed with 2.5 μM activated N_2OR and 50 μM cytochrome c_{552} entrapped in the membrane electrode, 1 mM N_2O-saturated water, in different buffer systems with pH between 5,9 and 8.8. The data were nonlinearly fitted using Equation 3, and pK_a values of 8.0 ± 0.7 and 5.5 ± 1.0 (solid line). The dashed line shows the pH dependence fit for the steady-state kinetic study [18], with a pK_a of 8.3.

Figure 3.4 – Rate constant of the inactivation process detected by electrochemical experiments *versus* pH. The *k* values were obtained by fitting the catalytic current decay with an exponential equation. The data were nonlinearly fitted using Equation 3 adapted for one pk_a of 7.1.

Figure 3.5 – (A) Selected spectra of 35 μM *Pseudomonas nautica* N_2OR after reaction with equimolar amount of N_2O at the following times: 0.5 min (black), 1 min (blue), 1.5 min (red), 2 min (green), 4.5 min (grey), 11 min (orange), 45 min (yellow). Inset*:* spectra obtained after subtraction of oxidised CuA contribution at the following times: 0.5 min (black), 1 min (blue), 1.5 min (red), 2 min (green), 4.5 min (grey), 11 min (orange), 45 min (yellow).
(B) N_2OR activity (black squares) *versus* time (100 % corresponds to 133 μmols N_2O-reduced min^{-1} mg^{-1} of enzyme) and 640-nm band intensity (blue squares) *versus* time (100% corresponds to the final spectra at t = 48 min and 0% corresponds to the first spectrum at t = 1 min). Solid lines are exponential fits and a k = 0.3 min^{-1} was used for both fits. Red circles represent the percentage of electrocatalytic activity *versus* time (100 % corresponds to the maximum activity, characterized by an intermolecular rate constant for electron transfer, k', of 1.4 s^{-1}). Yellow circles represent the 680–nm band intensity.

Figure 3.6 – EPR spectra of the different CuZ forms. EPR spectrum of the 680-nm band, CuZ° form (black line), and of the 640-nm band, resting CuZ form (red line). The CuA contribution was subtracted from both spectra. The blue line is the difference between the spectrum of the CuZ° form and that of the resting, inactive CuZ form. Instrumental parameters: modulation amplitude, 5 G; microwave frequency, 9.66 GHz; temperature 30 K.

Figure 3.7 – Potentiometric redox titration of fully reduced *Pseudomonas nautica* N_2OR following the characteristic absorption bands of CuA and CuZ centre in the oxidation and reduction direction. CuA centre was monitored by following the absorption at 540 nm in the oxidative (black squares) and in the reductive titrations (red squares). The titration curve was fitted with E°' = + 240 mV (solid line). CuZ centre was monitored by following the absorption at 640 nm in the oxidative (yellow circles) and in the reductive titrations (blue circles).

Chapter 4:

Legend of Figure 4.1 – Structures and electrostatic surface potential of *Pn* N_2OR (A-B), *Ac* N_2OR (C-D) and *Pd* N_2OR (E-F). In panel A, C and E the CuA and CuZ of the same monomer are represented in blue and light green, respectively. The two monomers are magenta and green coloured, respectively. Electrostatic surface potential is represented between −3 and 3 kT/e (B, D, F). Images were prepared using WebLab Viewer (Accelrys) (Panel A, C abd E) and USCF Chimera program (*panel B, D and F*) [54]. The electrostatic potential was calculated from Chimera using the Coulombic Law and partial charges from the Amber 99SB force field for all residues.

Figure 4.2 – Amino acid sequence comparison of N_2ORs. Comparison was performed using the program CLUSTALW (*41*) on the EBI Web site.

Figure 4.3 – Structures and electrostatic surface potential of *Pn* cytochrome c_{552} (A-B), *Pd* cytochrome c_{550} (C-D), *Pp* pseudoazurin (E-F), *Ac* pseudoazurin (G-H), HH cytochrome *c* (I-J). In panel A, C, E, G and I the heme group is black coloured, while the copper atom is blue. The electrostatic potential was calculated from Chimera using the Coulombic Law and partial charges from the Amber 99SB force field for all residues except for hemes, where the charges were calculated by the Gasteiger method.

Figure 4.4 – The electron transfer complexes between N_2OR and its physiological electron donors. (A) 200 best electron transfer complexes ranked by hydrophobic ranking of *Pn* N_2OR with *Pn* cytochrome c_{552}. (B) 200 best electron transfer complexes ranked by electrostatic

ranking of *Ac* N_2OR with *Ac* pseudoazurin. (C) 200 best electron transfer complexes ranked by electrostatic ranking of *Pd* N_2OR with *Pd* cytochrome c_{550}. (D) 200 best electron transfer complexes ranked by electrostatic ranking of *Pd* N_2OR with *Pp* pseudoazurin. The geometric centre for cytochrome c_{552}, the copper atom for pseudoazurin and the iron atom for cytochrome c_{550} are represented as a yellow sphere. The two copper atoms of CuA are coloured red, while the catalytic centre is coloured blue.

Figure 4.5 – Residues involved in the electron transfer pathways in *Pn* N_2OR structure. Ala495, Asp519, Val524, His566 and Leu568 are shown in dark green. The two copper atoms of CuA are coloured red, while the catalytic centre is coloured blue.

Figure 4.6 – Proposed model for the N_2OR from *Wolinella Succinogenes* with an additional C-terminal domain containing a cytochrome *c*. The heme domain (the heme group is coloured black) is shown to interact with the surface of the N_2OR domain surrounding the CuA site, the supposed entry site for the electron transfer. The two copper atoms of CuA are coloured red, the catalytic centre is coloured blue and the two domains of N_2OR are respectively green and orange coloured.

Figure 4.S-1.1 N_2OR *Ac* – Cytochrome c_{550} *Pd* – 200 top model complexes ranked by global score; 200 top model complexes ranked by electrostatic score; 200 top model complexes ranked by hydrophobic score

Figure 4.S-1.2 N_2OR *Ac* – Cytochrome c_{552} *Pn* – 200 top model complexes ranked by global score; 200 top model complexes ranked by electrostatic score; 200 top model complexes ranked by hydrophobic score

Figure 4.S-1.3 N_2OR *Ac* – BH Cytochrome *c* – 200 top model complexes ranked by global score; 200 top model complexes ranked by electrostatic score; 200 top model complexes ranked by hydrophobic score

Figure 4.S-1.4 N_2OR *Ac* – Pseudoazurin *Ac* – 200 top model complexes ranked by global score; 200 top model complexes ranked by electrostatic score; 200 top model complexes ranked by hydrophobic score

Figure 4.S-1.5 N_2OR *Ac* – Pseudoazurin *Pp* – 200 top model complexes ranked by global score; 200 top model complexes ranked by electrostatic score; 200 top model complexes ranked by hydrophobic score

Figure 4.S-2.1 N_2OR *Pd* – Cytochrome c_{550} *Pd* – 200 top model complexes ranked by global score; 200 top model complexes ranked by electrostatic score; 200 top model complexes ranked by hydrophobic score

Figure 4.S-2.2 N_2OR *Pd* – Cytochrome c_{552} *Pn* – 200 top model complexes ranked by global score; 200 top model complexes ranked by electrostatic score; 200 top model complexes ranked by hydrophobic score

Figure 4.S-2.3 N_2OR *Pd* – HH Cytochrome *c* – 200 top model complexes ranked by global score; 200 top model complexes ranked by electrostatic score; 200 top model complexes ranked by hydrophobic score

Chapter 5:

Chapter 6:

Chapter 7:

List of tables and schemes

Chapter 1

Introduction to nitrous oxide reductase (N_2OR)

1.1 Copper in biological systems

Copper-containing metalloproteins play crucial roles in several cellular processes in animal and bacterial metabolism, such as aerobic and anaerobic respiration (*1-4*). Some unique chemical characteristics allow the presence of copper as a metal cofactor of many proteins and enzymes:

i) stereochemical flexibility and excellent binding capacity of both Cu^{+} and Cu^{2+} make the Cu^{2+}/Cu^{+} couple, coordinated by the biological ligand, to be particularly versatile in the range of oxidizing redox potentials between +0.2 and +0.8 V, in a complementary range to the Fe^{3+}/Fe^{2+}couple;

ii) the Cu^{+} ion is a good π-donor and can bind small inorganic molecules, such as O_2 and CO molecules, which have π-acidic features.

Copper centres are present in several proteins and enzymes playing different functions, such as: electron transport (plastocyanin, azurin, stellacyanin, cytochrome *c* oxidase) (*5-7*), in oxygen transport in arthropods and molluscs by hemocyanin (*8, 9*), in the reduction of O_2 to H_2O (cytochrome *c* oxidase, laccase, ascorbate oxidase) (*10*), in the reduction of O_2 to H_2O_2 (amine oxidase, galactose oxidase) (*11, 12*), in the oxidation of various substrates (tyrosinase, methane monooxygenase, dopamine β-hydroxylase) (*12, 13*), or in the reduction of small inorganic molecules (nitrite reductase, nitrous oxide reductase, superoxide dismutase) (*14-16*). Copper centres in proteins were divided for several years into three classes (type-1, type-2 and type-3) according to their structural and spectroscopic features (*17-19*).

Type-1 copper sites are mononuclear Cu centres, characterized by an intense absorption ($\varepsilon \approx$ 5000 $M^{-1}cm^{-1}$) at around 600 nm in the oxidised state. This absorption is responsible for the intense blue colour of proteins containing (at least) one of these centres and it is due to a cysteine S $\rightarrow$ Cu^{2+} LMCT transition. The EPR spectra exhibit an unusually small parallel hyperfine splitting and a low g factor (*20*). This type of copper centre acts usually as an electron transfer centre, since it exhibits high rates of long-range, outer-sphere electron transfer (*21*). Crystal structures of "blue" copper proteins have shown that the metal centre presents a very irregular "distorted" tetrahedral coordination geometry (*22*). In the equatorial plane the copper ion is coordinated by two histidines and a cysteine, while the axial ligand is a methionine in plastocyanin and amicyanin (*23, 24*), a glutamine in stellacyanin (*25*), or, in the case of azurin, besides a methionine there is a second axial ligand, the backbone carbonyl of a glycine (*26*) (Figure 1.1A).

Type-2 or "normal" copper sites are mononuclear centres that exhibit low extinction coefficients in the optical bands (ε = 100-1000 $M^{-1}cm^{-1}$) that reveal weak ligand-field transitions and EPR spectrum of its oxidised form is similar to the one of "normal" tetragonal Cu^{2+} complex, with $g_{\parallel} > g_{\perp} > 2$ and $A_{\parallel} \geq 120$ G (*21, 27*). Examples of proteins containing type-2 copper centres are Cu-Zn superoxide dismutase, dopamine β-monooxygenase and galactose oxidase, in which the copper ion is coordinated by the side-chain of four histidine residues (Figure 1.1B).

Type-3 copper sites are binuclear Cu centres, identified by an EPR-silent state in the oxidised form due to the strong antiferromagnetic coupling between the copper ions (*19, 21*). Binuclear copper centres are able to bind oxygen reversibly in hemocyanin and in tyrosinase (Figure 1.1C). In tyrosinase, as in hemocyanin, each copper ion is coordinated by the side chain of three histidine residues, which are able to activate oxygen for hydroxylation of phenol to *ortho*-diphenol and further oxidise this compound to *ortho*-quinone (*28*). Catechol oxidase, also known as *ortho*-diphenol oxidase, is a less known member of the type-3 copper protein family (*12*).

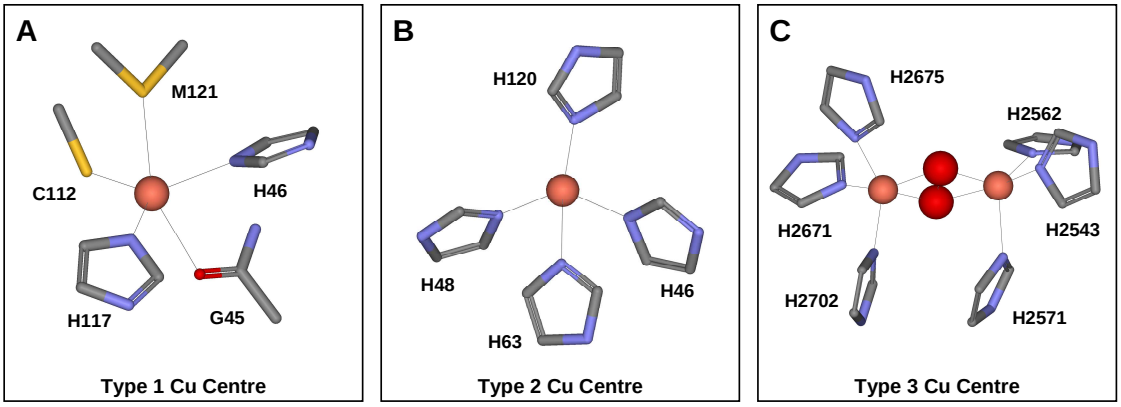

Figure 1.1 – Type 1, type 2 and type 3 copper centres. The coppers are represented as spheres with the protein ligands being represented as sticks and coloured by element. A) Type 1 copper of *Pseudomonas aeruginosa* azurin (1E5Z.pdb), B) Type 2 copper centre of human Cu, Zn – superoxide dismutase (2C9V.pdb), C) Type 3 copper centre of hemocyanin (1JS8.pdb).

Recently, more protein structures and spectroscopic data became available, which revealed new copper sites that cannot be classified into the initial division. The multi-copper oxidases contain, in addition to a type-1 Cu centre, a trinuclear copper site (*12*). The CuA site is a binuclear Cu centre, different from binuclear type-3 sites, that play an electron transfer role, accepting electrons from small electron transfer proteins and transferring them to the catalytic site, usually in another domain of the enzyme (*7*). The CuA centres have been identified in the enzymes cytochrome *c* oxidase and nitrous oxide reductase (N_2OR). In COX, each of the two copper ions is coordinated by two cysteine and two histidine residues, while the third ligand is the carbonyl oxygen of a methionine or a glutamate residue.

The last novel biological copper centre to be identified and characterized is the tetranuclear copper centre CuZ, the catalytic site of nitrous oxide reductase, which catalyses the two-electron reduction of nitrous oxide to nitrogen and water.

Before focusing more deeply on the enzyme nitrous oxide reductase and in particular on its novel copper-catalytic centre, a brief introduction regarding the role of nitrogen for biological systems and in particular about the denitrification is required.

1.2 The nitrogen cycle

Nitrogen is an essential element for living organisms since it is contained in all biomolecules, such as proteins and nucleic acids. In nature, nitrogen is present in different species that can assume formal charges from +5 to –3 and that constitute the biogeochemical cycle of nitrogen (N-cycle). The interconversion of these nitrogen species involves a number of redox reactions in which prokaryotes play the main role since only these organisms are able to carry out these processes (*29*) (Figure 1.2).

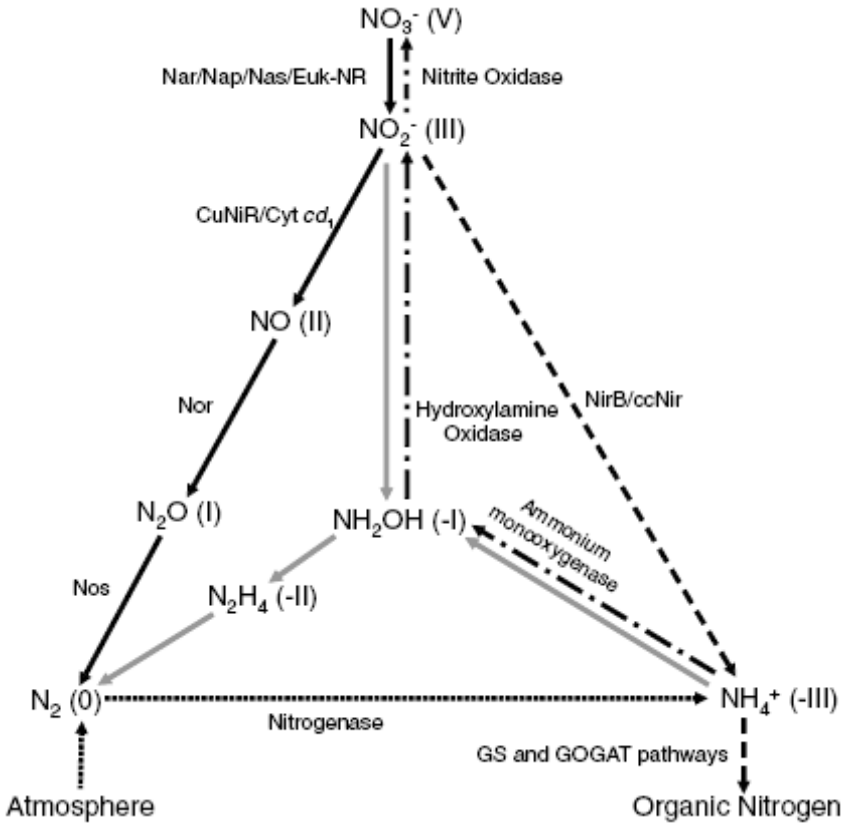

Figure 1.2 - The inorganic nitrogen cycle including the enzymes responsible for each step. The oxidation state of each compound is indicated between parentheses. The pathways are identified as follow: black solid line, respiratory pathway (denitrification); dashed line, dissimilatory and assimilatory ammonification (note that nitrate reduction is indicated only as solid arrow); dotted line, nitrogen fixation; dash-dot line, nitrification; grey solid line, ANAMOX. (Figure adapted from ref. (*30*)).

The dissimilatory processes involve the respiration, where nitrate is converted into N_2 (denitrification), and the ammonification that also starts with the reduction of nitrate to nitrite, but then nitrite is reduced to ammonia (*3, 29, 31-33*).

The nitrification is the only process that is attributed exclusively to bacteria from the *Nitrosomonas* and *Nitrobacter* genus (*34*).

The N-cycle is completed with nitrogen fixation, in which the enzyme nitrogenase reduces nitrogen from both the atmosphere and the respiration process to ammonia (*35*).

A fifth less characterized process named ANAMOX (anaerobic ammonium oxidation), which involves both oxidative and reductive reactions, is used for bacteria to grow in chemolithoautotrophic conditions using ammonia as electron donor and nitrite as electron acceptor (*29, 36, 37*).

1.3 Denitrification

The denitrification is part of the bioenergetic metabolism of bacterial cells, where the nitrogen-oxyanions nitrate and nitrite and the gaseous nitrogen oxides, nitric oxide and nitrous oxide, are used as terminal acceptors for electron transport phosphorylation (*3*). The

denitrification process occurs in oxygen depleted environments or in the presence of low oxygen tension (such as in some soils and groundwater, wetlands, poorly ventilated ocean sites or seafloor sediments), since oxygen is a more favourable electron acceptor than nitrate. This process is carried out by gram-negative bacteria that can be found in a variety of environments, such as soil, water or the human intestine (*38*).

Globally, the reduction of nitrate to molecular nitrogen requires four reactions each one catalyzed by four different metallo-enzymes (*15*):

$$NO_3^- + 2e^- + 2H^+ \rightarrow NO_2^- + H_2O \ (E'° = + 0.42 \text{ V}) \ (1)$$

$$NO_2^- + e^- + 2H^+ \rightarrow NO + H_2O \ (E'° = + 0.34 \text{ V}) \ (2)$$

$$2NO + 2e^- + 2H^+ \rightarrow N_2O + H_2O \ (E'° = + 1.18 \text{ V}) \ (3)$$

$$N_2O + 2e^- + 2H^+ \rightarrow N_2 + H_2O \ (E'° = +1.35 \text{ V}) \ (4)$$

The first step (eq. (1)), the reduction of nitrate to nitrite is catalyzed by mononuclear molybdenum-containing enzymes sub-grouped as respiratory nitrate reductases (Nar), periplasmic nitrate reductases (Nap) and assimilatory nitrate reductases (Nas) (*30*).

Nar is a membrane-bound complex that contains 3 different subunits: NarI, completely immersed in the membrane and containing 2 *b*-type hemes; NarH, containing 4 iron-sulfur clusters; NarG, containing one Fe-S cluster and the Mo-catalytic site.

Nap is a monomeric periplasmatic enzyme containing an iron-sulfur cluster of the type [4Fe–4S], and the molybdenum catalytic site.

Nas is a soluble cytoplasmatic enzyme that has a typical assimilatory function, allowing the utilization of nitrate as nitrogen source. All the Nas isolated so far have an active site containing a Mo- cofactor at the active site but the molecular properties and the number and type of electron transfer centres are diverse and vary in the different organisms.

The second step of denitrification, in which nitrite is further reduced to NO (eq. (2)), is catalyzed by nitrite reductase either cythocrome cd_1 (cd_1-Nir) or copper-containing enzymes (Cu-Nir). Cytochrome cd_1 is a periplasmic homodimer, with an electron transfer centre, a *c*-type heme *c* and a non-covalently bound d_1 –type heme, the catalytic site (*39-42*). The copper-containing nitrite reductases, are also periplasmic enzymes and have a trimeric structure (*43, 44*), with each subunit containing both a type 1 copper (T1Cu) centre, that is involved in the electron transfer, and type 2 copper (T2Cu) center, that constitutes the catalytic site (*43*).

The enzyme that catalyzes the reduction of nitric oxide (NO) to nitrous oxide (N2O) (eq. (3)), the bacterial nitric oxide reductase (NOR), is a heterodimeric membrane-bound enzyme (*45*). Structural information about this enzyme is lacking, since a tridimensional structure has yet to be obtained. However, three classes of NOR have been identified in bacteria (cNOR, qNOR and qCuNOR) that differ in the electron transfer centres, while the catalytic centre is homologous

in all the three groups (*38*). The active site is constituted by binuclear iron-centre, composed by one high-spin *b*-type heme (heme b_3) and a non-heme iron (FeB) (*46-48*). This site can be compared to the heme-copper oxidades, since the FeB centre is also coordinated by three histidine residues, as the copper CuB in cytochrome *c* oxidase. In all three classes a low-spin *b*-type heme acts as an electron provider to the catalytic site.

cNOR presents an extra-subunit with a *c*-type heme centre that receives electrons from a soluble cytochrome *c* or a cupredoxin, while qNOR is an enzyme with a single subunit that receives electrons directly from quinols. The third type, qCuNOR, presents an extra subunit with a binuclear copper CuA centre as electron acceptor from a periplasmic electron donor.

The last step of the denitrification pathway is the reduction of nitrous oxide to molecular nitrogen (eq. (4)) catalyzed by the periplasimic nitrous oxide reductase. This is a copper-containing protein and its properties will be discussed in the next paragraph.

1.4 Nitrous oxide reductase

The conversion of N_2O to N_2 is the final step of the denitrification pathway and can be regarded as a respiratory process (*3, 38*) (eq. (5)).

$N_2O + 2H^+ + 2\ e^- \rightarrow N_2 + H_2O$ [E'° (pH 7.0) = +1.35 V; $\Delta G° = -339.5$ kJ/mol] (5)

The key role of copper in the respiration of N_2O became apparent from the studies of Iwasaki and collaborators (*49, 50*), who demonstrated for the first time the role of this metal as being essential for anaerobic growth with N_2O and in the biosynthesis of N_2OR in denitrifying bacteria.

The first report of a ≈120 kDa Cu-containing protein isolated from denitrifying pseudomonads came from Matsubara and Zumft (*51*). The same authors later reported for the first time the identification of nitrous oxide reductase from *Pseudomonas stutzeri* as a molecular species and the first assay in which the isolated protein reduced N_2O to N_2 using methylviologen, hydrogen, and clostridial hydrogenase as the electron-donating system (*52*).

Since the isolation of N_2OR from *Pseudomonas stutzeri* (formerly *Pseudomonas perfectomarina*), the enzyme has been purified and characterized from the same organism (*53, 54*), as well as from other bacterial sources: *Rhodobacter capsulatus* (formerly *Rhodopseudomonas capsulate*) (*55*), *Rhodobacter sphaeroides f. sp. denitrificans* (*56*), *Paracoccus denitrificans* (*57*), *Wolinella succinogenes* (*58*), *Flexibacter canadensis* (*59*), *Achromobacter cycloclastes* (*60*), *Pseudomonas aeruginosa* (*61*), *Paracoccus pantotrophus* (formely *Thiosphaera pantotropha*) (*62*), *Thiobacillus denitrificans* (*63*), *Alcaligenes xylosoxidans* (*64, 65*), *Pseudomonas nautica* (*66*) and *Hyphomicrobium denitrificans* (*67*).

1.5 History of CuA and CuZ

Even if the history of CuA and CuZ is very recent, the discovery and the study of these two copper-clusters represents a fascinating chapter in the bioinorganic area.

The presence of two distinct copper sites in N_2OR was clear from the first isolation of the enzyme in 1982 (*52*). At that time CuA was already identified as a binuclear copper site, able to accept electrons from small electron donor protein, in cytochrome *c* oxidase (COX) (*68*).

The similarity between the CuA centres in COX and N_2OR was first shown by Kroneck *et al.* (*69, 70*) using a multifrequency EPR approach. Soon after, Jin *et al.* (*71*) studied the copper sites in N_2OR by electron spin echo (ESE) spectroscopy and presented further evidence for the similarity between the CuA in the two enzymes. This similarity was also shown by magnetic circular dichroism (MCD) (*72, 73*) and EXAFS studies, as the Cu EXAFS curve-fitting results for N_2OR are strikingly similar to those of COX (*73, 74*). Finally, the identification of a set of potential Cu ligands in the C-terminal domain of N_2OR that correspond to those of the CuA in COX was also crucial to establish that the CuA site, initially believed to be unique to COX, is clearly also present in N_2OR (*75, 76*) (Figure 1.3).

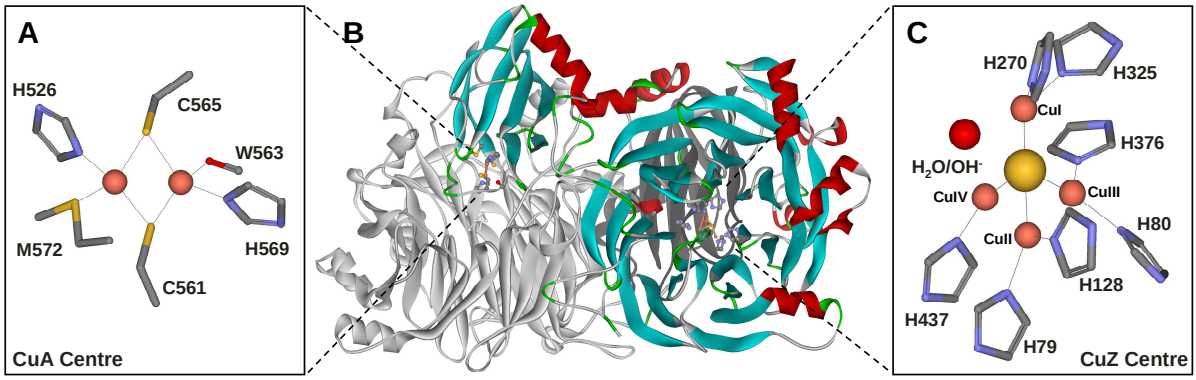

Figure 1.3 – Representation of *Paracoccus denitrificans* nitrous oxide reductase functional dimer. The dimer of nitrous oxide reductase is coloured according to subunit. One monomer is coloured in light gray, while in the other is coloured by secondary structure (B). The CuA (A) and CuZ (C) centres have their copper ligands coloured according to element and the coppers ions in CuZ centre are numbered I, II, III and IV. The figures were created with DSViewer Pro 5.0 (Accelrys) using 1FWX.pdb.

However, the reduction of the enzyme with dithionite produced a species that was clearly different from both CuA and type-1 Cu signals, since it was characterized by a 640 band in the UV-visible spectrum and by a typical EPR signal, with g-values at 2.18 and 2.06 (*53*). This second copper centre was proposed to be the catalytic centre. It was named for the first time by Farrar *et al*. as CuZ (*77*) and was proposed to be an additional binuclear site.

Resonance Raman (RR) studies indicated that there is a highly covalent thiolate site (Cu^{2+}-S^{-} ↔ Cu^{+}-$S^{\bullet}$) in the dithionite reduced enzyme (*72, 78*), the form of the enzyme that will be defined as “resting” state (see below). Moreover, optical, EPR and MCD spectroscopy studies led to

propose that CuZ would have a thiolate coordination supported by cysteines residues, similarly to CuA. However, in the N_2OR sequence, there are no conserved cysteine residues outside the C-terminal CuA domain, which would be able to support two-thiolate binuclear centres. Nevertheless, Zumft noted the presence of 8 conserved histidine residues in the primary sequence of N_2ORs (*3*). This observation, coupled with spectroscopic and mutagenesis data, led to revise the nature of CuZ with the proposal of a multiple histidines coordination (*79*). This study also pointed out that the total number of copper atoms in the active N_2OR was (at the time) uncertain and suggested that the catalytic site of this enzyme may be more complex than a simple binuclear type-3 site. Indeed, the crystal structure of the catalytic site demonstrated that this prediction was correct, showing that the CuZ centre of N_2OR is a unique centre in bioinorganic chemistry (Figure 1.3).

The new structure of CuZ opens a new chapter in the biological clusters study (*80*), giving a structural basis for the interpretation of the spectroscopic data, and also giving the opportunity to implement this analysis with theoretical calculation. The solution of the first crystal structure was solved ten years ago, and many progresses have been occurred in this field, but many questions are still open, like the full comprehension of the catalytic mechanism and the full characterization of the active species in the turnover cycle.

1.6 X-ray structure of N_2OR

The fascinating and unexpected tetranuclear copper cluster CuZ was revealed after the resolution of the three-dimensional structure of N_2OR from *Pseudomonas nautica* at 2.4 Å resolution in the year 2000 (*80*). As predicted, the CuA structure in N2OR can be superimposed with the CuA centre in COX (*6, 81, 82*). The CuA centre is located in the C-terminal domain, with the two copper ions linked by the Cys 561 and Cys 565 Sγ atoms, the His 526 and His 569 Nε2 atoms, the Met 572 Sγ atom and the Trp 563 carbonyl group.

The new copper centre, the catalytic CuZ site, is located in the N-terminal domain that adopts a seven-blade β-propeller fold. The structure of N_2OR shows that CuZ is a novel mixed-valence copper centre (Cu_4S) with a sulphide ion bridging a distorted tetrahedron of copper atoms, in a unique structure in biology. The four copper ions are labelled Cu_I, Cu_{II}, Cu_{III} and Cu_{IV} as shown in Figure 2. The Cu_4S core is bound to the protein via the N atoms of seven well-conserved histidine residues. Five histidine residues bind to the copper ions through their Nε2 atoms (His 80, His 128, His 270, His 325, and His 376 in *Pseudomonas nautica*), whereas two use their Nδ1 atoms (His 79 and His 437).

In the first structure of N_2OR, it was initially considered that an oxygen was bridging the four copper ions in the tetrahedron, which was afterwards replaced by an inorganic sulphur ion after the high resolution structure (1.6 Å) of *Paracoccus denitrificans* N_2OR (*83, 84*), elemental analysis and resonance Raman spectroscopic studies (*85*).

The structure also revealed the functional homodimeric conformation of N_2OR, because the distance between the electron transfer centre CuA and CuZ within the same monomer is ≈ 40 Å, which is inappropriate for an efficient electron transfer (*86*), while the CuA-CuZ distance within the dimer is approximately 10 Å. The structure of N_2OR was further solved from *Achromobacter cycloclastes* at 1.9 Å (*87*), confirming the structural features of the precedent structures and presenting the first observation of an inhibitor species, the iodide ion, bound at the catalytic site (see below).

The Cu_4S core from all the available structures is very similar both in symmetry and interatomic distances (Figure 1.4). This cluster has an approximate *Cs* symmetry with Cu_I-S-Cu_{II} defining the mirror plane. The average distance of the Cu-S bonds is ≈ 2.3 Å and the Cu-Cu distances vary from 2.6 to 3.4 Å. The Cu_I-S-Cu_{II} angle is close to 160°, while all other Cu-S-Cu angles are approximately orthogonal.

The nature of the bridging ligand between Cu_I and Cu_{IV}, the proposed binding site for the substrate N_2O, is otherwise still unclear and object of debate. In the first structure from *Pn* the presence of two hydroxyl groups between Cu_I and Cu_{IV} was proposed (*80*), whereas after a revision of the same structure the bridging ligand was proposed to be an oxygen (*83*). In *Pd* N_2OR structure the ligand proposed is a water molecule or an hydroxyl group (*84*), while in the *Ac* N_2OR structure the pocket between Cu_I and Cu_{IV} can accommodate both a water molecule and an hydroxyl group (*87*).

The structure of CuZ from the three different organisms is shown in Figure 1.4.

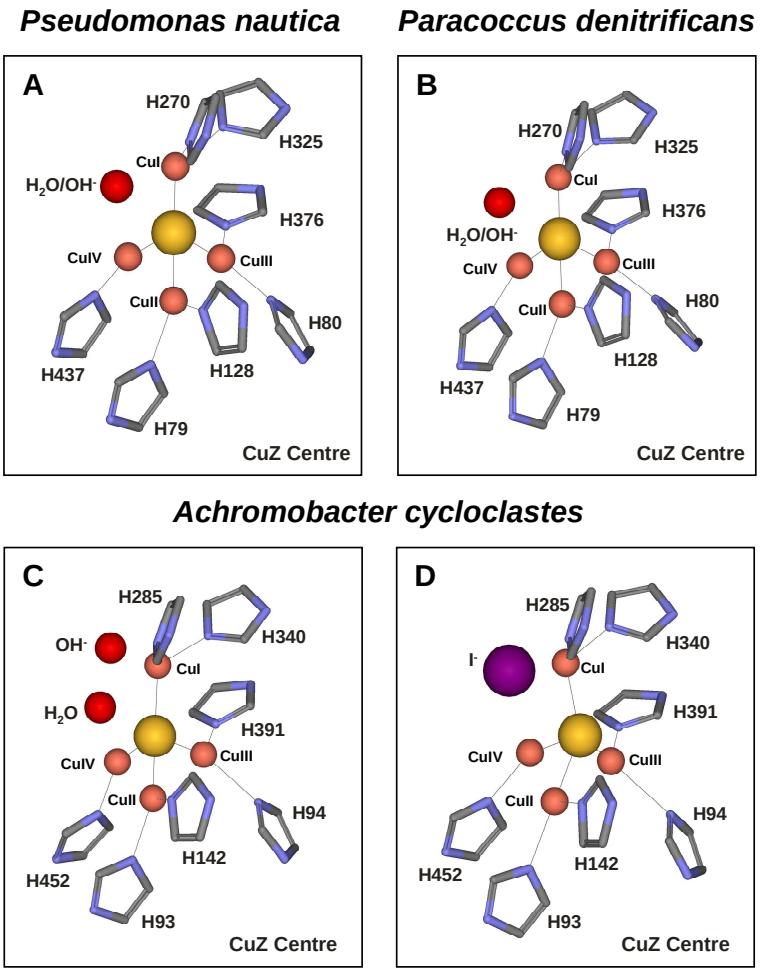

Figure 1.4 – Comparison between the CuZ centre from the *Pseudomonas nautica* (A), *Paracoccus denitrificans* (B) and *Achromobacter cycloclastes* (C, D) nitrous oxide reductase. An oxygen atom, represented as a red sphere, is located in-between CuI and CuIV of the *Pn* and *Pd* CuZ centre. In the CuZ centre of a pink form of *Achromobacter cycloclastes* nitrous oxide reductase (C), it is present a water molecule and a hydroxide in-between CuI and CuIV, and in (D) it is represented the inhibited form of this enzyme with an iodide ion bridging CuI and CuIV. The ligands of the copper atoms are coloured according to element. The figures were created with DSViewer Pro 5.0 (Accelrys) using 1QNI.pdb (A), 1FWX.pdb (B), 2IWF.pdb (C) and 2IWK.pdb (D).

The latter study also presents a structure with the inhibitor iodide bound to the Cu_I-Cu_{IV} edge (Figure 1.4D). This flexibility of the catalytic centre allows the coordination of a bent N_2O molecule with O and terminal N in the same positions as the two observed oxygen atoms in the native *Ac* N_2OR (Figure 1.4C), and the remaining O upon release of N_2 can bind in a bridged position similar to the iodide in the inhibitor-bound complex.

1.7 Spectroscopy of N_2OR

In order to understand the electronic structure of the metal centres in N_2OR, a large amount of spectroscopic data have been published before and after the first crystal structure was determined. The overlapping of some of the spectroscopic bands of the two copper centres in N_2OR, CuA and CuZ, hinders the deconvolution of the spectroscopic features, as CuA in the oxidised state has absorption bands at 480 nm, 550 nm, and 780 nm (but none in the reduced state). The spectroscopic and electronic characteristic of CuA, however, have been exhaustively investigated, not only in N_2OR, but also in cytochrome *c* oxidase (*70, 88, 89*) and, more recently in azurin containing biosynthetic models of this centre (*7*).

As already mentioned, the first spectroscopic characterization of CuZ was performed using the dithionite-reduced form of the enzyme that has the CuA reduced in the spectroscopic silent state (Cu^{+}-Cu^{+}) (S=0), producing the state called "blue" or lately defined as "resting CuZ" (Scheme 1.1-C or E). This "resting CuZ" state is characterized by an absorption band at 640 nm and by a broad EPR signal, with g-values at 2.16-2.18 and 2.04-2.06 and 4-line hyperfine splitting (*53*) (Table 1.1).

Scheme 1.1 – Different redox forms of nitrous oxide reductase.

		CuA	CuZ	
Anaerobic	A	$[Cu^{1.5+}\text{-}Cu^{1.5+}]^{3+}$	$[2Cu^{2+}\text{-}2Cu^{+}S]^{4+}$	as-isolated purple form
	B	$[Cu^{1+}\text{-}Cu^{1+}]^{2+}$	$[2Cu^{2+}\text{-}2Cu^{+}S]^{4+}$	"semi-reduced" ascorbate reduced
	C	$[Cu^{1+}\text{-}Cu^{1+}]^{2+}$	$[1Cu^{2+}\text{-}3Cu^{+}S]^{3+}$	dithionite reduced blue form / "resting state"
Aerobic	D	$[Cu^{1.5+}\text{-}Cu^{1.5+}]^{3+}$	$[1Cu^{2+}\text{-}3Cu^{+}S]^{3+}$	as-isolated pink form
	E	$[Cu^{1+}\text{-}Cu^{1+}]^{2+}$	$[1Cu^{2+}\text{-}3Cu^{+}S]^{3+}$	dithionite reduced blue form / "resting state"
	F	$[Cu^{1+}\text{-}Cu^{1+}]^{2+}$	$[4Cu^{+}S]^{2+}$	Fully reduced Activated form

However, in the early purifications from *Pseudomonas stutzeri*, it became clear that the enzyme can be isolated with CuZ in different redox states depending on the procedure followed during the purification. In particular, the N_2OR purified anaerobically from *Pseudomonas stutzeri*, *Alcaligenes xylosoxidans*, *Paracoccus denitrificans*, *Paracoccus pantotrophus* (*53, 57, 65, 90*) exhibits an intense absorption at 540 nm and a less intense band around 800 nm. This state, that has been defined as "purple" form (Scheme 1.1-A), presents the CuA in the oxidised state, since the EPR spectra presents the typical seven-line hyperfine pattern in the $g_{\|}$ region, and CuZ also in an oxidised state considered to be $[2Cu^{2+}\text{-}2Cu^{+}]$. On the other hand, the N_2OR, isolated aerobically from these bacterial sources, is in a different form, named "pink" (Scheme 1.1-D), which is characterized by a different visible spectrum, with absorption maxima at 480 nm, 550 nm, 640 nm and a shoulder at 800 nm. The pink form has also CuA in the oxidised state but CuZ is in a different oxidation state than the one found in

the purple form, [$3Cu^{2+}$-$1Cu^{+}$]. Therefore, since CuA exhibits absorption maxima at 480 nm, 550 nm and 780 nm, the CuZ in this form is characterized by an absorption band at 640 nm.

The reduction of N_2OR in the purple form (Scheme 1.1-A) by sodium dithionite proceeds in two kinetic steps: a fast phase in which the absorbance at 540 nm decreases almost within seconds (concomitant with the disappearance of the shoulder at 800 nm), due to the reduction of CuA (Scheme 1.1-B), while in the slower phase the "blue" form is generated in the course of minutes (Scheme 1.1-C).

Thus, the enzyme when anaerobically purified can exist in an "as-isolated" (Scheme 1.1-A), a "semi-reduced" (Scheme 1.1-B) and a "dithionite-reduced" (Scheme 1.1-C) state. The EPR spectrum of the "as-isolated" – purple form (Scheme 1.1-A) exhibits a well-defined 7-line hyperfine splitting whereas that of the dithionite-reduced form (Scheme 1.1-C) has a broad and poorly solved 4-line hyperfine splitting signal (*77*). However, the "semi-reduced" form (Scheme 1.1-B), obtained by reducing the purple form with sodium ascorbate, shows an extremely weak EPR signal and must be considered EPR-silent, but still has an absorption band at 540 nm and a small shoulder at 640 nm.

MCD data confirmed that the"semi-reduced" form (Scheme 1.1-B) is not a ferromagnetically coupled (S=1) centre but must be antiferromagnetically coupled (S=0) (*79*). Farrar *et al.* suggested the presence of two distinct forms of CuZ, named CuZ and CuZ*. In particular the catalytic centre could exist in a redox active, CuZ [$2Cu^{2+}$-$2Cu^{+}$], and in a redox inactive form, CuZ* [$1Cu^{2+}$-$3Cu^{+}$] (here after indicated as "resting CuZ"). It was also noticed that the amount of the "resting CuZ" species was dependent on the isolation procedure of N_2OR, and it was shown that the proportion of "resting CuZ" is minimal in the N_2OR from *P. stutzeri* isolated under anaerobic conditions (*77*). *Paracoccus pantotrophus* N_2OR isolated under anaerobic conditions has a "resting CuZ"/CuZ_{total} of 0.29, while the in the aerobic preparation the ratio is 0.66 (*90*). Dooley and co-workers presented the first example of a recombinantly produced N_2OR from *Achromobacter cycloclastes* anaerobically purified (*91*). Interestingly, in contrast to preparations from other microorganism, the anaerobic purification enables the isolation of a "blue" form of the protein with intense band absorption at 625 nm and a shoulder at 500 nm. Presumably, this form presents the CuA in the reduced state, as testified by the oxidation with ferricyanide that shows the reoxidation of CuA detected by its characteristic UV-visible spectrum.

In conclusion, the complete spectroscopic and structural characterization of the purple form of the enzyme is still underway, due to the interference and overlapping of the CuA spectroscopic features and thus more spectroscopic or structural data of this form is required.

On the other hand, the "resting" blue state, obtained from reduction of CuA with dithionite, was very well characterized in the last years by Solomon and co-workers. MCD spectroscopy shows that the paramagnetic state of the resting CuZ in *Pseudomonas nautica* N_2OR have an S = 1/2 rather than S = 3/2 spin state (*92*). Furthermore, Cu K-edge XAS was used to distinguish between the two possible configurations for the tetranuclear centre, [$1Cu^{2+}$-$3Cu^{+}$] or [$3Cu^{2+}$-$1Cu^{+}$], with the experimental data being better fitted considering a [$1Cu^{2+}$-$3Cu^{+}$] oxidation state. Q-band and X-band EPR spectroscopies were used to determine the unpaired electron spin distribution of this CuZ centre in the "resting"-dithionite reduced state. The experimental data and DFT calculations showed that the spin density is mostly distributed between Cu_I (42 %) and Cu_{II} (16 %), with a small contribution also from the last two copper ions (Cu_{III} 8 % and Cu_{IV} 3 %) and a significant contribution from the bridging sulfide (14%) (*92*). A similar EPR study on *Paracoccus pantotrophus* N_2OR indicated a similar result, but with the spin density being even more widely distributed over the CuZ cluster (Cu_I 20.1 %, Cu_{II} 9.5 %, Cu_{III} 4.8 %, Cu_{IV} 9.2 % and S 17.9 %) (*93*).

Other spectroscopic methods, such as resonance Raman and low-temperature absorption spectroscopies, coupled with density functional calculations reveal that the spectral features of the resting CuZ form (Scheme 1.1 – E) by resonance Raman are dominated by the S → Cu_I charge-transfer transition (*94, 95*). In particular the three main contributions in the Raman spectra, at 14300, 15700 and 16500 cm^{-1}, are associated to Cu-S vibrations and contribute to the broad CT absorption band at approximately 640 nm (≈ 15650 cm^{-1}). Since only Cu_I is dominantly oxidised in the "resting" CuZ state (Scheme 1.1 – E), only this ion shows d-d transitions, which have a large MCD/absorption intensity ratio (*94*).

The oxidation states available for CuZ, the correspondent main spectroscopic features and their role in the catalytic cycle are summarized in Table 1.1.

Table 1.1 – The different oxidation states of CuZ centre and their catalytic and spectroscopic properties.

Oxidation states	Definition	Catalytic properties	Visible Absorption	EPR	Ref.
$[4Cu^{2+}S]^{6+}$	*Not observed*	--	--	--	
$[3Cu^{2+}$-$1Cu^{+}S]^{5+}$	*Not observed*	--	--	--	
$[2Cu^{2+}$-$2Cu^{+}S]^{4+}$	2-hole	redox active (E'°=60mV) Not catalytically active	540 nm	EPR silent	(*79, 90*)
$[1Cu^{2+}$-$3Cu^{+}S]^{3+}$	Resting	not active	640 nm	$g_{\|\|}$=2.160; $g_{\perp}$=2.040	(*92, 95*)
$[4Cu^{+}S]^{2+}$	Fully reduced	highly active		EPR silent	(*96, 97*)

1.8 Activation and catalytic properties of N_2OR

The reduction of N_2O is a thermodynamically favourable but kinetically inert reaction, which is reflected in the approximately 59 kcalmol^{-1} activation barrier for its thermal decomposition, consisting with a spin-forbidden process (*98*).

In biological systems, the ability of denitrifying bacteria to reduce N_2O to N_2 was known even before the isolation and purification of N_2OR. Several assays were developed to test the enzyme activity, such as gas-chromatography methodologies (*99*) and Clark-type electrodes (*100*), but the most used assay was the one developed by Kristjansson and Hollocher, that follows the oxidation of methyl or benzyl-viologen cation radical upon reduction of N_2O to N_2 (*101*). The specific activity is typically expressed in μmol of $N_2O \times min^{-1} \times mg^{-1}$ or abbreviated in U/mg. One of the important aspects in the understanding of the catalytic cycle and activity of N_2OR is the identification and characterization of active species that are able to bind and reduce N_2O. As already mentioned the resting or "blue" form (Scheme 1.1 – C or E) cannot be further reduced or oxidised (using dithionite or ferricyanide), thus being redox inactive. In the other hand, the activity assay with reduced methylviologen suggested that a negative potential and long incubation time are necessary to reduce the non-active resting CuZ state to the fully active CuZ state (Scheme 1.1, F). Indeed, it was latter shown that a prolonged reduction with excess of reduced methylviologen allows to fully reduce the resting CuZ to the super-reduced form ($4Cu^{+}$), characterized by a spectroscopic silent form (no EPR signal is detected and no contributions are also observed in the visible region). Parallel activity tests at the same incubation times showed that the enzyme activity increases with increasing incubation time and the increase of activity is directly correlated with the decrease of the intensity of the resting CuZ EPR or UV-vis features (*96, 97*). In conclusion, these studies demonstrated that the electron-rich site of CuZ is required to bind and catalyse the two-electron reduction of N_2O to N_2. Anaerobic purification of N_2OR from *Pseudomonas stutzeri* (*79, 102*) and *Paracoccus pantotrophus* (*90*) produce redox active forms of CuZ centre in the redox state of $2Cu^{2+}$-$2Cu^{+}$ (two-hole form) in the purple form of the enzyme. In particular, in the "anaerobic" *Paracoccus pantotrophus* N_2OR the CuZ centre can be reduced or oxidised with a single electron step at a midpoint reduction of E'° = 60 mV, which is the unique value available up-to-date for the redox potential of CuZ centre between [$2Cu^{2+}$-$2Cu^{+}$] and [$1Cu^{2+}$-$3Cu^{+}$]. Even if this CuZ form can be easily reduced and oxidised between the two-hole to the one-hole form of CuZ, its catalytic activity is very low, similarly to the one of the enzyme in the resting dithionite-reduced state (*90*). Moreover, the activity of the "anaerobic" N_2OR from *Achromobacter cycloclastes* increases from 8 to 125 U/mg after incubation with MV, which means that also this form must be with the CuZ centre in the fully reduced state to attain the maximum activity (*97*). In

conclusion, N_2OR isolated either anaerobically or aerobically always requires an activation process, to fully reduce CuZ and it is the fully reduced form of the enzyme (Scheme 1.1 – F) that presents the maximum specific activity. A protonation step was detected and associated with this process. The pK_a observed at 9.2 was assigned to a lysine close to CuZ (Lys 397 in *Pseudomonas nautica*) that in the protonated state can facilitate the CuZ reduction from the resting Cuz form to the fully reduced CuZ form (*103*).

In order to clarify the catalytic mechanism of N_2O reduction, several kinetic studies were performed in order to clarify the mechanism of the N_2O reduction and calculate its kinetic parameters, in the presence of either physiological or artificial electron donors. In the presence of methylviologen or benzylviologen the K_m for the substrate is found to be in the low micromolar range, while the V_{max} varies between the bacterial sources (Table 2.2).

Table 1.2 – Summary of the kinetic properties of the different N_2O reductases.

N_2OR	Enzyme form	Electron Donor (ED)	K_m for ED (μM)	K_m for N_2O	V_{max} (U/mg)	pK_a / Optimal pH	Ref.
Ps. aeruginosa	As prepared	BV			0.5		(*61*)
	Activated (incubated)	BV	4	2	27		
Ps. stutzeri	Purple ("anaerobic")	BV			4 (60 at pH 9.8)	Optimal pH: 9-10	(*53*)
	Pink ("aerobic")	BV			2		
Ps. denitrificans	Purple ("anaerobic")	MV		7	122		(*57*)
Ac. cycloclastes	Anaerobic (pink)	MV			86		(*60*)
	Anaerobic (blue) not incubated	MV			7		(*91*)
	Anaerobic (blue) incubated	MV		25	124		
Al. xyloxidans	As-isolated (purple)	MV			6		(*65*)
Pa. pantotropus	Anaerobic	MV			3		(*90*)
	Aerobic	MV			9		
		HH cyt *c*	6		0.03		(*62*)
Rd. sphaeroides	Aerobic (pink)	BV	26		63	Optimal pH: 9	(*104*)
H. denitrificans	A (violet)	BV			45	Optimal pH: 8.8	(*67*)
	B (Blue)	BV			29		
W. succinogenes	Additional cyt *c* domain	BV	4	8	160		(*58*)

Abbreviations: *Ps*. – *Pseudomonas*, *Ac*. – *Achromobacter*, *Al*. – *Alcaligenes*, *Pa*. – *Paracoccus*, *Rd*. – *Rhodobacter*, *H*. – *Hyphomicrobium*, and *W*. – *Wolinella*, MV – methylviologen, BV – benzylviologen, HH horse heart.

However, a comparison between earlier values is difficult because it was recently shown that the maximum activity is strongly dependent on the time of incubation (*96, 97*), which was not always completely stated (N_2OR was in intermediate states of activation – not fully activated).

c-type cytochromes, either physiological and non-physiological, were used to donate electrons to the enzyme, as the mitochondrial cytochrome *c* is able to donate electrons to N_2OR from *Paracoccus pantotrophus* (*105*). Cytochrome c_2, that is similar to mitochondrial cytochrome *c*, is the electron donor of N_2OR from *Rhodobacter capsulatus* (*106*), and in *Rhodobacter sphaeroides f. sp. denitrificans* a periplasmic cytochrome *c* is also the redox partner of N_2OR (*107*). N_2OR from *Paracoccus pantotrophus* accepts electron from both cytochrome c_{550} and pseudoazurin from the same microorganism, and also from horse heart cytochrome *c* (*62*). Bovine heart cytochrome *c* is able to reduce N_2OR from *Achromobacter cycloclastes* (*91*), and its physiological electron donor is pseudoazurin (*108*).

N_2OR from *Wolinella succinogenes* shows a peculiar structure, with an extra cytochrome *c* domain present in the C-terminal region of the enzyme (*58, 109, 110*), and a monohemic cytochrome *c* from the same bacterial source was shown to be a putative electron donor to this enzyme.

An optimum activity was found in the range of pH 8.0-9.5 when MV was used as electron donor, for N_2OR from different sources (*53, 62, 67*).

Further insights were obtained on the binding mode of the substrate based on computational studies. For the lowest energy conformation of the fully reduced state, the most favourable binding mode for the substrate is bridging between Cu_I and Cu_{IV}, with a μ-1,3 coordination (*96*). The N_2O molecule after binding assumes a bent conformation, that facilitates the coordination of N_2O, by shifting the π^* orbital of N_2O close to the fully occupied d orbitals of the fully reduced CuZ and turning the substrate into a good electron acceptor. The backbonding interaction between Cu d → N_2O π^* enables the elongation of the N-N and N-O bonds and increases the electron density of the oxygen atom activating it for electrophilic attack by a proton. The transition state is stabilized by the charge transfer, which leads to a strong Cu_{IV}-O bond. The d^{10} configuration of all the copper atoms in the fully reduced form facilitates the back-bonding by maximising the charge transfer CuZ → N_2O. The protein structure provides the structural support for the CuZ cluster, providing the hydrogen bonding and non-covalent interactions that lower the activation barrier of the N-O bond cleavage (*111*).

The reaction of the fully reduced CuZ, in the absence of reductants, with the substrate was studied in order to identify other species or intermediates in the turnover reaction. The reaction with an excess of N_2O gives raise to an oxidised state with CuZ in the oxidised resting state and CuA oxidised, that implies an electron donation from each redox centres (*97*).

1.9 Biomimetic chemistry of CuZ

The difficulty connected to the direct study of copper containing enzymes has stimulated an enormous amount of research activity in the field of coordination chemistry over the years. By this approach it is possible to design structural models for the metal active sites, understand the spectroscopic characteristics and the mechanism of formation of Cu_nO_n and Cu_nS_n complexes, build up biomimetic catalysts that promote chemical transformations of potential synthetic and industrial interest (*112*). Site analogues have contributed significantly to correlate structural properties of the metal sites to spectroscopic and magnetic observables and to characterize intermediates involved in the catalytic cycles.

The CuZ cluster, with its fascinating and unique structure in biology and the capability to perform the difficult chemistry required for N_2O reduction, represents a challenging field for the biomimetic inorganic chemistry. In the last decade, the Tolman's and Karlin's groups tried to explore the sulphur chemistry of copper complexes supported by N-donor ligands (*113, 114*).

The reaction of Cu^+ with molecular sulphur (S_8) and tetradentate N-donor ligands allows to prepare a class of complexes in which two sulphur atoms are bridging two copper atoms in a (μ-η^2:η^2-disulfido)dicopper(II) geometry (*115-119*). These complexes are EPR silent, because of the antiferromagnetic coupling between the two copper ions and exhibit an intense $S_2^{2-} \rightarrow$ Cu(II) charge transfer transition at ≈ 395 nm ($\varepsilon \approx 15\,000\ M^{-1}cm^{-1}$).

A trinuclear complex was synthetized in which the copper-sulfur cluster is $[Cu_3(\mu\text{–}S)_2]^{3+}$, obtained from the reaction of Cu^+ complex with S_8 (*120*) or from $Cu^{2+}(O_3SCF_3)_2$ and Li_2S or Na_2S_2 (*121*).

Recently, the first complex able to bind and react with N_2O was described (*122*). The complex presents a $[Cu_3S_2]^{2+}$ core having a localized mixed-valence cluster, supported by tertiary amine ligands. This complex presents a contribution at 395 nm that is a $S_2^{2-} \rightarrow Cu^{2+}$ charge transfer transition also present in the Cu_2-μ-S_2 and an additional band at 630 nm that is similar only in appearance to the typical CuZ resting spectroscopic feature. In this case, the transition can be attributed to a metal-to-ligand charge transfer (MLCT) from the Cu^+ centres into a π^* orbital of the S-S bond, while for the CuZ in the resting state, the transition is due to a $S \rightarrow Cu_I$ charge-transfer, as already mentioned. The experimental data, supported by DFT calculations, indicate that the cluster dissociates in a Cu^+ fragment and a dicopper(I,II) species that binds N_2O by a μ-1,1-O coordination that promotes the N-O cleavage. This mechanism is different from the μ-1,3-O,N coordination proposed for the CuZ active site in the enzyme (*95, 111*).

1.10 Future perspectives and object of the thesis

From the discovery of N_2OR up to now, several properties of this enzyme were elucidated, however many questions still remain to be answered, in particular regarding the mechanism of the catalytic centre CuZ, a cluster unique in biology for its structure and reactivity.

Following the work performed in Prof. Isabel and José Moura' research groups in the last decade on *P. nautica* N_2OR, the main aims of this thesis are to investigate several aspects that are still obscure in this enzyme. From the introduction section it became clear that a complete study of the interaction of the enzyme with its physiological electron donor is still missing, since the activity test and most of the catalytic data available were obtained in the presence of artificial electron donors, such as methylviologen. The first objective was to identify the physiological electron donor, which is supposed to be a small electron carrier protein from the same microorganism, and study its interaction with the enzyme using kinetic, electrochemical, spectroscopic and docking approaches.

As described above, N_2OR can be purified in different forms depending on the purification conditions. However, the as-isolated form of N_2OR, including the "blue" resting and the "purple" form shows a very low activity compared with the high activity of fully reduced state. The strong reducing conditions required for the activation, which are also not available in the periplasm of a Gram-negative bacterium, suggests that MV can interact directly with CuZ centre over-passing the electron donation through the CuA centre.

The characterization of the intermediates of CuZ involved in the catalytic centre and the study of the reaction of the enzyme with the substrate in absence of artificial electron donors is necessary to understand the unique properties of this challenging enzyme and identify possible intermediates involved in the catalytic cycle.

Moreover, a biomimetic approach to CuZ centre was developed in the Prof. Luigi Casella's bioinorganic laboratory, in Pavia, as part of the mixed fellowship between Portugal and Italy.

Finally, it is important to mention that the full understanding of the CuZ centre structure and mechanism of reduction of N_2O will have a high impact due to the fact that N_2O is a greenhouse gas and plays a serious role in stratospheric ozone depletion (*123-125*).

1.11 References

1. Ramirez, B. E., Malmstrom, B. G., Winkler, J. R., and Gray, H. B. (1995) The Currents of Life: The Terminal Electron-Transfer Complex of Respiration, *PNAS 92*, 11949-11951.
2. Ferguson-Miller, S., and Babcock, G. T. (1996) Heme/Copper Terminal Oxidases, *Chem Rev 96*, 2889-2908.
3. Zumft, W. G. (1997) Cell biology and molecular basis of denitrification, *Microbiol. Mol. Biol. Rev. 61*, 533-616.
4. Kaim, W., and Rall, J. (1996) Copper - A "Modern" Bioelement, *Angew Chem Int Ed Engl 35*, 43-60.
5. Malmström, B. G., and Leckner, J. (1998) The chemical biology of copper, *Current Opinion in Chemical Biology 2*, 286-292.
6. Tsukihara, T., Aoyama, H., Yamashita, E., Tomizaki, T., Yamaguchi, H., Shinzawa-Itoh, K., Nakashima, R., Yaono, R., and Yoshikawa, S. (1996) The Whole Structure of the 13-Subunit Oxidized Cytochrome c Oxidase at 2.8 A, *Science 272*, 1136-1144.
7. Savelieff, M. G., and Lu, Y. Cu(A) centers and their biosynthetic models in azurin, *J Biol Inorg Chem 15*, 461-483.
8. van Holde, K. E., and Miller, K. I. (1995) Hemocyanins, *Adv Protein Chem 47*, 1-81.
9. Solomon, E. I., Tuczek, F., Root, D. E., and Brown, C. A. (1994) Spectroscopy of Binuclear Dioxygen Complexes, *Chemical Reviews 94*, 827-856.
10. Kosman, D. Multicopper oxidases: a workshop on copper coordination chemistry, electron transfer, and metallophysiology, *Journal of Biological Inorganic Chemistry 15*, 15-28.
11. Dooley, D. M., McGuirl, M. A., Brown, D. E., Turowski, P. N., McIntire, W. S., and Knowles, P. F. (1991) A Cu(I)-semiquinone state in substrate-reduced amine oxidases, *Nature 349*, 262-264.
12. Solomon, E. I., Sundaram, U. M., and Machonkin, T. E. (1996) Multicopper Oxidases and Oxygenases, *Chem Rev 96*, 2563-2606.
13. Balasubramanian, R., and Rosenzweig, A. C. (2007) Structural and mechanistic insights into methane oxidation by particulate methane monooxygenase, *Acc Chem Res 40*, 573-580.
14. Aboelella, N. W., Reynolds, A. M., and Tolman, W. B. (2004) BIOPHYSICS: Catching Copper in the Act, *Science 304*, 836-837.
15. Moura, I., and Moura, J. J. (2001) Structural aspects of denitrifying enzymes, *Curr Opin Chem Biol 5*, 168-175.
16. Tainer, J. A., Getzoff, E. D., Richardson, J. S., and Richardson, D. C. (1983) Structure and mechanism of copper, zinc superoxide dismutase, *Nature 306*, 284-287.
17. Malkin, R., and Malmstrom, B. G. (1970) The state and function of copper in biological systems, *Adv Enzymol Relat Areas Mol Biol 33*, 177-244.
18. Adman, E. T. (1991) Copper protein structures, *Adv Protein Chem 42*, 145-197.
19. Solomon, E. I., Lowery, M. D., LaCroix, L. B., and Root, D. E. (1993) Electronic absorption spectroscopy of copper proteins, *Methods Enzymol 226*, 1-33.
20. Solomon, E. I., Baldwin, M. J., and Lowery, M. D. (1992) Electronic structures of active sites in copper proteins: contributions to reactivity, *Chemical Reviews 92*, 521-542.
21. Solomon, E. I., and Lowery, M. D. (1993) Electronic structure contributions to function in bioinorganic chemistry, *Science 259*, 1575-1581.
22. Guss, J. M., Bartunik, H. D., and Freeman, H. C. (1992) Accuracy and precision in protein structure analysis: restrained least-squares refinement of the structure of poplar plastocyanin at 1.33 A resolution, *Acta Crystallographica Section B 48*, 790-811.
23. Díaz-Quintana, A., Navarro, J., Hervás, M., Molina-Heredia, F., De la Cerda, B., and De la Rosa, M. (2003) A comparative structural and functional analysis of cyanobacterial plastocyanin and cytochrome c 6 as alternative electron donors to Photosystem I, *Photosynthesis Research 75*, 97-110.
24. Dennison, C., Vijgenboom, E., de Vries, S., van der Oost, J., and Canters, G. W. (1995) Introduction of a CuA site into the blue copper protein amicyanin from Thiobacillus versutus, *FEBS Lett 365*, 92-94.
25. DeBeer George, S., Basumallick, L., Szilagyi, R. K., Randall, D. W., Hill, M. G., Nersissian, A. M., Valentine, J. S., Hedman, B., Hodgson, K. O., and Solomon, E. I. (2003) Spectroscopic Investigation of Stellacyanin Mutants:â€‰ Axial Ligand Interactions at the Blue Copper Site, *Journal of the American Chemical Society 125*, 11314-11328.

26. Nar, H., Messerschmidt, A., Huber, R., van de Kamp, M., and Canters, G. W. (1991) X-ray crystal structure of the two site-specific mutants His35Gln and His35Leu of azurin from Pseudomonas aeruginosa, *Journal of Molecular Biology 218*, 427-447.
27. Solomon, E. I., Chen, P., Metz, M., Lee, S. K., and Palmer, A. E. (2001) Oxygen Binding, Activation, and Reduction to Water by Copper Proteins, *Angew Chem Int Ed Engl 40*, 4570-4590.
28. Matoba, Y., Kumagai, T., Yamamoto, A., Yoshitsu, H., and Sugiyama, M. (2006) Crystallographic Evidence That the Dinuclear Copper Center of Tyrosinase Is Flexible during Catalysis, *J. Biol. Chem. 281*, 8981-8990.
29. Richardson, D. J., and Watmough, N. J. (1999) Inorganic nitrogen metabolism in bacteria, *Curr Opin Chem Biol 3*, 207-219.
30. Gonzalez, P. J., Correia, C., Moura, I., Brondino, C. D., and Moura, J. J. (2006) Bacterial nitrate reductases: Molecular and biological aspects of nitrate reduction, *J Inorg Biochem 100*, 1015-1023.
31. Berks, B. C., Ferguson, S. J., Moir, J. W., and Richardson, D. J. (1995) Enzymes and associated electron transport systems that catalyse the respiratory reduction of nitrogen oxides and oxyanions, *Biochim Biophys Acta 1232*, 97-173.
32. Moreno-Vivian, C., and Ferguson, S. J. (1998) Definition and distinction between assimilatory, dissimilatory and respiratory pathways, *Mol Microbiol 29*, 664-666.
33. Moreno-Vivian, C., Cabello, P., Martinez-Luque, M., Blasco, R., and Castillo, F. (1999) Prokaryotic Nitrate Reduction: Molecular Properties and Functional Distinction among Bacterial Nitrate Reductases, *J. Bacteriol. 181*, 6573-6584.
34. Richardson, D. J. (2000) Bacterial respiration: a flexible process for a changing environment, *Microbiology 146*, 551-571.
35. Cabello, P., Roldan, M. D., and Moreno-Vivian, C. (2004) Nitrate reduction and the nitrogen cycle in archaea, *Microbiology 150*, 3527-3546.
36. van de Graaf, A. A., Mulder, A., de Bruijn, P., Jetten, M. S., Robertson, L. A., and Kuenen, J. G. (1995) Anaerobic oxidation of ammonium is a biologically mediated process, *Appl. Envir. Microbiol. 61*, 1246-1251.
37. Jetten, M. S., Strous, M., van de Pas-Schoon, K. T., Schalk, J., van Dongen, U. G., van de Graaf, A. A., Logemann, S., Muyzer, G., van Loosdrecht, M. C., and Kuenen, J. G. (1998) The anaerobic oxidation of ammonium, *FEMS Microbiol Rev 22*, 421-437.
38. Tavares, P., Pereira, A. S., Moura, J. J., and Moura, I. (2006) Metalloenzymes of the denitrification pathway, *J Inorg Biochem 100*, 2087-2100.
39. Einsle, O., Messerschmidt, A., Stach, P., Bourenkov, G. P., Bartunik, H. D., Huber, R., and Kroneck, P. M. (1999) Structure of cytochrome c nitrite reductase, *Nature 400*, 476-480.
40. Williams, P. A., Fulop, V., Garman, E. F., Saunders, N. F., Ferguson, S. J., and Hajdu, J. (1997) Haem-ligand switching during catalysis in crystals of a nitrogen-cycle enzyme, *Nature 389*, 406-412.
41. Nurizzo, D., Silvestrini, M. C., Mathieu, M., Cutruzzola, F., Bourgeois, D., Fulop, V., Hajdu, J., Brunori, M., Tegoni, M., and Cambillau, C. (1997) N-terminal arm exchange is observed in the 2.15 A crystal structure of oxidized nitrite reductase from Pseudomonas aeruginosa, *Structure 5*, 1157-1171.
42. Baker, S. C., Saunders, N. F., Willis, A. C., Ferguson, S. J., Hajdu, J., and Fulop, V. (1997) Cytochrome cd1 structure: unusual haem environments in a nitrite reductase and analysis of factors contributing to beta-propeller folds, *J Mol Biol 269*, 440-455.
43. Dodd, F. E., Van Beeumen, J., Eady, R. R., and Hasnain, S. S. (1998) X-ray structure of a blue-copper nitrite reductase in two crystal forms. The nature of the copper sites, mode of substrate binding and recognition by redox partner, *J Mol Biol 282*, 369-382.
44. Godden, J. W., Turley, S., Teller, D. C., Adman, E. T., Liu, M. Y., Payne, W. J., and LeGall, J. (1991) The 2.3 angstrom X-ray structure of nitrite reductase from Achromobacter cycloclastes, *Science 253*, 438-442.
45. Watmough, N. J., Field, S. J., Hughes, R. J., and Richardson, D. J. (2009) The bacterial respiratory nitric oxide reductase, *Biochem Soc Trans 37*, 392-399.
46. Hendriks, J., Warne, A., Gohlke, U., Haltia, T., Ludovici, C., Lubben, M., and Saraste, M. (1998) The active site of the bacterial nitric oxide reductase is a dinuclear iron center, *Biochemistry 37*, 13102-13109.

47. van Wonderen, J. H., Knight, C., Oganesyan, V. S., George, S. J., Zumft, W. G., and Cheesman, M. R. (2007) Activation of the Cytochrome cd1 Nitrite Reductase from Paracoccus pantotrophus: REACTION OF OXIDIZED ENZYME WITH SUBSTRATE DRIVES A LIGAND SWITCH AT HEME c, *J. Biol. Chem. 282*, 28207-28215.
48. Cheesman, M. R., Zumft, W. G., and Thomson, A. J. (1998) The MCD and EPR of the heme centers of nitric oxide reductase from Pseudomonas stutzeri: evidence that the enzyme is structurally related to the heme-copper oxidases, *Biochemistry 37*, 3994-4000.
49. Iwasaki, H., Saigo, T., and Matsubara, T. (1980) Copper as a controlling factor of anaerobic growth under N2O and biosynthesis of N2O reductase in denitrifying bacteria, *Plant. Cell. Physiol. 21*, 1573-1584.
50. Iwasaki, H., and Terai, H. (1982) Analysis of N2 and N2O produced during growth of denitrifying bacteria in copper-depleted and -supplemented media, *J. Gen. Appl. Microbiol. Tokyo 28*, 189-193.
51. Matsubara, T., and Zumft, W. G. (1982) Identification of a copper protein as part of the nitrous oxide-reducing system in nitrite-respiring (denitrifying) pseudomonads, *Arch. Microbiol. 132*, 322-328.
52. Zumft, W. G., and Matsubara, T. (1982) A novel kind of multi-copper protein as terminal oxidoreductase of nitrous oxide respiration in Pseudomonas perfectomarinus, *FEBS Letters 148*, 107-112.
53. Coyle, C. L., Zumft, W. G., Kroneck, P. M., Korner, H., and Jakob, W. (1985) Nitrous oxide reductase from denitrifying Pseudomonas perfectomarina. Purification and properties of a novel multicopper enzyme, *Eur J Biochem 153*, 459-467.
54. Riester, J., Zumft, W. G., and Kroneck, P. M. (1989) Nitrous oxide reductase from Pseudomonas stutzeri. Redox properties and spectroscopic characterization of different forms of the multicopper enzyme, *Eur J Biochem 178*, 751-762.
55. McEwan, A. G., Greenfield, A. J., Wetzstein, H. G., Jackson, J. B., and Ferguson, S. J. (1985) Nitrous oxide reduction by members of the family Rhodospirillaceae and the nitrous oxide reductase of Rhodopseudomonas capsulata, *J. Bacteriol. 164*, 823-830.
56. Sato, K., Okubo, A., and Yamazaki, S. (1998) Characterization of a Multi-Copper Enzyme, Nitrous Oxide Reductase, from Rhodobacter sphaeroides f. sp. denitrificans, *J. Biochem. (Tokyo) 124*, 51-54.
57. Snyder, S. W., and Hollocher, T. C. (1987) Purification and some characteristics of nitrous oxide reductase from Paracoccus denitrificans, *J. Biol. Chem. 262*, 6515-6525.
58. Teraguchi, S., and Hollocher, T. C. (1989) Purification and some characteristics of a cytochrome c-containing nitrous oxide reductase from Wolinella succinogenes, *J. Biol. Chem. 264*, 1972-1979.
59. Jones, A. M., Hollocher, T. C., and Knowles, R. (1992) Nitrous oxide reductase of Flexibacter canadensis: a unique membrane-bound enzyme, *FEMS Microbiology Letters 92*, 205-209.
60. Hulse, C. L., and Averill, B. A. (1990) Isolation of a high specific activity pink, monomeric nitrous oxide reductase from Achromobacter cycloclastes, *Biochem Biophys Res Commun 166*, 729-735.
61. SooHoo, C. K., and Hollocher, T. C. (1991) Purification and characterization of nitrous oxide reductase from Pseudomonas aeruginosa strain P2, *J. Biol. Chem. 266*, 2203-2209.
62. Berks, B. C., Baratta, D., Richardson, J., and Ferguson, S. J. (1993) Purification and characterization of a nitrous oxide reductase from Thiosphaera pantotropha. Implications for the mechanism of aerobic nitrous oxide reduction, *Eur J Biochem 212*, 467-476.
63. Hole, U. H., Vollack, K. U., Zumft, W. G., Eisenmann, E., Siddiqui, R. A., Friedrich, B., and Kroneck, P. M. (1996) Characterization of the membranous denitrification enzymes nitrite reductase (cytochrome cd1) and copper-containing nitrous oxide reductase from Thiobacillus denitrificans, *Arch Microbiol 165*, 55-61.
64. Matsubara, T., and Sano, M. (1985) Isolation and some properties of a novel violet copper protein from a denitrifying bacterium, Alcaligenes sp., *Chem. Lett. 14*, 1053-1056.
65. Ferretti, S., Grossmann, J. G., Hasnain, S. S., Eady, R. R., and Smith, B. E. (1999) Biochemical characterization and solution structure of nitrous oxide reductase from Alcaligenes xylosoxidans (NCIMB 11015), *Eur J Biochem 259*, 651-659.
66. Prudencio, M., Pereira, A. S., Tavares, P., Besson, S., Cabrito, I., Brown, K., Samyn, B., Devreese, B., Van Beeumen, J., Rusnak, F., Fauque, G., Moura, J. J., Tegoni, M., Cambillau, C., and Moura,

I. (2000) Purification, characterization, and preliminary crystallographic study of copper-containing nitrous oxide reductase from Pseudomonas nautica 617, *Biochemistry 39*, 3899-3907.

67. Yamaguchi, K., Kawamura, A., Ogawa, H., and Suzuki, S. (2003) Characterization of Nitrous Oxide Reductase from a Methylotrophic Denitrifying Bacterium, Hyphomicrobium denitrificans A3151, *J. Biochem. (Tokyo) 134*, 853-858.
68. Beinert, H., Griffiths, D. E., Wharton, D. C., and Sands, R. H. (1962) Properties of the Copper Associated with Cytochrome Oxidase as Studied by Paramagnetic Resonance Spectroscopy, *J. Biol. Chem. 237*, 2337-2346.
69. Kroneck, P. M., Antholine, W. A., Riester, J., and Zumft, W. G. (1988) The cupric site in nitrous oxide reductase contains a mixed-valence [Cu(II),Cu(I)] binuclear center: a multifrequency electron paramagnetic resonance investigation, *FEBS Lett 242*, 70-74.
70. Kroneck, P. M., Antholine, W. A., Riester, J., and Zumft, W. G. (1989) The nature of the cupric site in nitrous oxide reductase and of CuA in cytochrome c oxidase, *FEBS Lett 248*, 212-213.
71. Jin, H., Thomann, H., Coyle, C. L., and Zumft, W. G. (1989) Copper coordination in nitrous oxide reductase from Pseudomonas stutzeri, *Journal of the American Chemical Society 111*, 4262-4269.
72. Dooley, D. M., McGuirl, M. A., Rosenzweig, A. C., Landin, J. A., Scott, R. A., Zumft, W. G., Devlin, F., and Stephens, P. J. (1991) Spectroscopic studies of the copper sites in wild-type Pseudomonas stutzeri N2O reductase and in an inactive protein isolated from a mutant deficient in copper-site biosynthesis, *Inorganic Chemistry 30*, 3006-3011.
73. Scott, R. A., Zumft, W. G., Coyle, C. L., and Dooley, D. M. (1989) Pseudomonas stutzeri N2O Reductase Contains CuA-Type Sites, *PNAS 86*, 4082-4086.
74. SooHoo, C. K., Hollocher, T. C., Kolodziej, A. F., Orme-Johnson, W. H., and Bunker, G. (1991) Extended x-ray absorption fine structure and electron paramagnetic resonance of nitrous oxide reductase from Pseudomonas aeruginosa strain P2, *J. Biol. Chem. 266*, 2210-2218.
75. Viebrock, A., and Zumft, W. G. (1988) Molecular cloning, heterologous expression, and primary structure of the structural gene for the copper enzyme nitrous oxide reductase from denitrifying Pseudomonas stutzeri, *J. Bacteriol. 170*, 4658-4668.
76. Zumft, W. G., Dreusch, A., Lochelt, S., Cuypers, H., Friedrich, B., and Schneider, B. (1992) Derived amino acid sequences of the nosZ gene (respiratory N₂O reductase) from Alcaligenes eutrophus, Pseudomonas aeruginosa and Pseudomonas stutzeri reveal potential copper-binding residues, *European Journal of Biochemistry 208*, 31-40.
77. Farrar, J. A., Thomson, A. J., Cheesman, M. R., Dooley, D. M., and Zumft, W. G. (1991) A model of the copper centres of nitrous oxide reductase (Pseudomonas stutzeri). Evidence from optical, EPR and MCD spectroscopy, *FEBS Lett 294*, 11-15.
78. Dooley, D. M., Moog, R. S., and Zumft, W. G. (1987) Characterization of the copper sites in Pseudomonas perfectomarina nitrous oxide reductase by resonance Raman spectroscopy, *Journal of the American Chemical Society 109*, 6730-6735.
79. Farrar, J. A., Zumft, W. G., and Thomson, A. J. (1998) CuA and CuZ are variants of the electron transfer center in nitrous oxide reductase, *PNAS 95*, 9891-9896.
80. Brown, K., Tegoni, M., Prudencio, M., Pereira, A. S., Besson, S., Moura, J. J., Moura, I., and Cambillau, C. (2000) A novel type of catalytic copper cluster in nitrous oxide reductase, *Nat Struct Biol 7*, 191-195.
81. Iwata, S., Ostermeier, C., Ludwig, B., and Michel, H. (1995) Structure at 2.8 A resolution of cytochrome c oxidase from Paracoccus denitrificans, *Nature 376*, 660-669.
82. Williams, P. A., Blackburn, N. J., Sanders, D., Bellamy, H., Stura, E. A., Fee, J. A., and McRee, D. E. (1999) The CuA domain of Thermus thermophilus ba3-type cytochrome c oxidase at 1.6 A resolution, *Nat Struct Biol 6*, 509-516.
83. Brown, K., Djinovic-Carugo, K., Haltia, T., Cabrito, I., Saraste, M., Moura, J. J. G., Moura, I., Tegoni, M., and Cambillau, C. (2000) Revisiting the Catalytic CuZ Cluster of Nitrous Oxide (N2O) Reductase. EVIDENCE OF A BRIDGING INORGANIC SULFUR, *J. Biol. Chem. 275*, 41133-41136.
84. Haltia, T., Brown, K., Tegoni, M., Cambillau, C., Saraste, M., Mattila, K., and Djinovic-Carugo, K. (2003) Crystal structure of nitrous oxide reductase from Paracoccus denitrificans at 1.6 A resolution, *Biochem J 369*, 77-88.

85. Rasmussen, T., Berks, B. C., Sanders-Loehr, J., Dooley, D. M., Zumft, W. G., and Thomson, A. J. (2000) The catalytic center in nitrous oxide reductase, CuZ, is a copper-sulfide cluster, *Biochemistry 39*, 12753-12756.
86. Winkler, J. R. (2000) Electron tunneling pathways in proteins, *Curr Opin Chem Biol 4*, 192-198.
87. Paraskevopoulos, K., Antonyuk, S. V., Sawers, R. G., Eady, R. R., and Hasnain, S. S. (2006) Insight into catalysis of nitrous oxide reductase from high-resolution structures of resting and inhibitor-bound enzyme from Achromobacter cycloclastes, *J Mol Biol 362*, 55-65.
88. Farrar, J. A., Lappalainen, P., Zumft, W. G., Saraste, M., and Thomson, A. J. (1995) Spectroscopic and mutagenesis studies on the CuA centre from the cytochrome-c oxidase complex of Paracoccus denitrificans, *Eur J Biochem 232*, 294-303.
89. Antholine, W. E., Kastrau, D. H., Steffens, G. C., Buse, G., Zumft, W. G., and Kroneck, P. M. (1992) A comparative EPR investigation of the multicopper proteins nitrous-oxide reductase and cytochrome c oxidase, *Eur J Biochem 209*, 875-881.
90. Rasmussen, T., Berks, B. C., Butt, J. N., and Thomson, A. J. (2002) Multiple forms of the catalytic centre, CuZ, in the enzyme nitrous oxide reductase from Paracoccus pantotrophus, *Biochem J 364*, 807-815.
91. Fujita, K., Chan, J. M., Bollinger, J. A., Alvarez, M. L., and Dooley, D. M. (2007) Anaerobic purification, characterization and preliminary mechanistic study of recombinant nitrous oxide reductase from Achromobacter cycloclastes, *J Inorg Biochem 101*, 1836-1844.
92. Chen, P., DeBeer George, S., Cabrito, I., Antholine, W. E., Moura, J. J., Moura, I., Hedman, B., Hodgson, K. O., and Solomon, E. I. (2002) Electronic structure description of the mu(4)-sulfide bridged tetranuclear Cu(Z) center in N(2)O reductase, *J Am Chem Soc 124*, 744-745.
93. Oganesyan, V. S., Rasmussen, T., Fairhurst, S., and Thomson, A. J. (2004) Characterisation of [Cu4S], the catalytic site in nitrous oxide reductase, by EPR spectroscopy, *Dalton Trans 7*, 996-1002.
94. Chen, P., Cabrito, I., Moura, J. J., Moura, I., and Solomon, E. I. (2002) Spectroscopic and electronic structure studies of the mu(4)-sulfide bridged tetranuclear Cu(Z) cluster in N(2)O reductase: molecular insight into the catalytic mechanism, *J Am Chem Soc 124*, 10497-10507.
95. Chen, P., Gorelsky, S. I., Ghosh, S., and Solomon, E. I. (2004) N2O reduction by the mu4-sulfide-bridged tetranuclear CuZ cluster active site, *Angew Chem Int Ed Engl 43*, 4132-4140.
96. Ghosh, S., Gorelsky, S. I., Chen, P., Cabrito, I., Moura, J. J., Moura, I., and Solomon, E. I. (2003) Activation of N2O reduction by the fully reduced micro4-sulfide bridged tetranuclear Cu Z cluster in nitrous oxide reductase, *J Am Chem Soc 125*, 15708-15709.
97. Chan, J. M., Bollinger, J. A., Grewell, C. L., and Dooley, D. M. (2004) Reductively activated nitrous oxide reductase reacts directly with substrate, *J Am Chem Soc 126*, 3030-3031.
98. Vaughan, G. A., Rupert, P. B., and Hillhouse, G. L. (1987) Selective O-atom transfer from nitrous oxide to hydride and aryl ligands of bis(pentamethylcyclopentadienyl)hafnium derivatives, *J Am Chem Soc 109*, 5538-5539.
99. St John, R. T., and Hollocher, T. C. (1977) Nitrogen 15 tracer studies on the pathway of denitrification in Pseudomonas aeruginosa, *J. Biol. Chem. 252*, 212-218.
100. Alefounder, P. R., and Ferguson, S. J. (1982) Electron transport-linked nitrous oxide synthesis and reduction by Paracoccus denitrificans monitored with an electrode, *Biochem Biophys Res Commun 104*, 1149-1155.
101. Kristjansson, J. K., and Hollocher, T. C. (1980) First practical assay for soluble nitrous oxide reductase of denitrifying bacteria and a partial kinetic characterization, *J. Biol. Chem. 255*, 704-707.
102. Alvarez, M. L., Ai, J., Zumft, W., Sanders-Loehr, J., and Dooley, D. M. (2001) Characterization of the copper-sulfur chromophores in nitrous oxide reductase by resonance raman spectroscopy: evidence for sulfur coordination in the catalytic cluster, *J Am Chem Soc 123*, 576-587.
103. Ghosh, S., Gorelsky, S. I., George, S. D., Chan, J. M., Cabrito, I., Dooley, D. M., Moura, J. J., Moura, I., and Solomon, E. I. (2007) Spectroscopic, computational, and kinetic studies of the mu4-sulfide-bridged tetranuclear CuZ cluster in N2O reductase: pH effect on the edge ligand and its contribution to reactivity, *J Am Chem Soc 129*, 3955-3965.
104. Michalski, W. P., Hein, D. H., and Nicholas, D. J. D. (1986) Purification and characterization of nitrous oxide reductase from Rhodopseudomonas sphaeroides f.sp. denitrificans, *Biochimica et Biophysica Acta - Protein Structure and Molecular Enzymology 872*, 50-60.

105. Rasmussen, T., Brittain, T., Berks, B. C., Watmough, N. J., and Thomson, A. J. (2005) Formation of a cytochrome c-nitrous oxide reductase complex is obligatory for N2O reduction by Paracoccus pantotrophus, *Dalton Trans*, 3501-3506.
106. Richardson, D. J., Bell, L. C., McEwan, A. G., Jackson, J. B., and Ferguson, S. J. (1991) Cytochrome c2 is essential for electron transfer to nitrous oxide reductase from physiological substrates in Rhodobacter capsulatus and can act as an electron donor to the reductase in vitro. Correlation with photoinhibition studies, *Eur J Biochem 199*, 677-683.
107. Itoh, M., Matsuura, K., and Satoh, T. (1989) Involvement of cytochrome bc1 complex in the electron transfer pathway for N2O reduction in a photodenitrifier, Rhodobacter sphaeroides f. s. denitrificans, *FEBS Letters 251*, 104-108.
108. Fujita, K., Ijima, F., Obara, Y., Hirasawa, M., Brown, D. E., Kohzuma, T., and Dooley, D. M. (2009) Direct electron transfer from pseudoazurin to nitrous oxide reductase in catalytic N2O reduction, *J Biol Inorg Chem 14 (Suppl 1)*, S11-S20.
109. Zhang, C. S., and Hollocher, T. C. (1993) The reaction of reduced cytochromes *c* with nitrous oxide reductase ot *Wolinella succinogenes*, *Biochim. Biophys. Acta 1142*, 253-261.
110. Zhang, C., Jones, A. M., and Hollocher, T. C. (1992) An apparently allosteric effect involving N2O with the nitrous oxide reductase from Wolinella succinogenes, *Biochem Biophys Res Commun 187*, 135-139.
111. Gorelsky, S. I., Ghosh, S., and Solomon, E. I. (2006) Mechanism of N2O reduction by the mu4-S tetranuclear CuZ cluster of nitrous oxide reductase, *J Am Chem Soc 128*, 278-290.
112. Tolman, W. B. (2006) Using synthetic chemistry to understand copper protein active sites: a personal perspective, *J Biol Inorg Chem 11*, 261-271.
113. York, J. T., Bar-Nahum, I., and Tolman, W. B. (2008) Copper-Sulfur Complexes Supported by N-Donor Ligands: Towards Models of the Cu(Z) Site in Nitrous Oxide Reductase, *Inorganica Chim Acta 361*, 885-893.
114. Sarangi, R., York, J. T., Helton, M. E., Fujisawa, K., Karlin, K. D., Tolman, W. B., Hodgson, K. O., Hedman, B., and Solomon, E. I. (2008) X-ray absorption spectroscopic and theoretical studies on (L)2[Cu2(S2)n]2+ complexes: disulfide versus disulfide(*1-) bonding, *J Am Chem Soc 130*, 676-686.
115. Chen, P., Fujisawa, K., Helton, M. E., Karlin, K. D., and Solomon, E. I. (2003) Spectroscopy and bonding in side-on and end-on Cu2(S2) cores: comparison to peroxide analogues, *J Am Chem Soc 125*, 6394-6408.
116. Helton, M. E., Chen, P., Paul, P. P., Tyeklar, Z., Sommer, R. D., Zakharov, L. N., Rheingold, A. L., Solomon, E. I., and Karlin, K. D. (2003) Reaction of elemental sulfur with a copper(I) complex forming a trans-mu-1,2 end-on disulfide complex: new directions in copper-sulfur chemistry, *J Am Chem Soc 125*, 1160-1161.
117. Helton, M. E., Maiti, D., Zakharov, L. N., Rheingold, A. L., Porco, J. A., and Karlin, K. D. (2006) A mu-eta2:eta2-disulfide dicopper(II) complex from reaction of S8 with a copper(I) precursor: reactivity of the bound disulfur moiety, *Angew Chem Int Ed Engl 45*, 1138-1141.
118. Brown, E. C., Aboelella, N. W., Reynolds, A. M., Aullon, G., Alvarez, S., and Tolman, W. B. (2004) A new class of (mu-eta2:eta2-disulfido)dicopper complexes: synthesis, characterization, and disulfido exchange, *Inorg Chem 43*, 3335-3337.
119. York, J. T., Brown, E. C., and Tolman, W. B. (2005) Characterization of a complex comprising a [Cu2(S2)2]2+ core: bis(mu-S2 2-)dicopperIII or bis(mu-S2).-)dicopperII?, *Angew Chem Int Ed Engl 44*, 7745-7748.
120. Brown, E. C., York, J. T., Antholine, W. E., Ruiz, E., Alvarez, S., and Tolman, W. B. (2005) [Cu3(mu-S)2]3+ clusters supported by N-donor ligands: progress toward a synthetic model of the catalytic site of nitrous oxide reductase, *J Am Chem Soc 127*, 13752-13753.
121. York, J. T., Bar-Nahum, I., and Tolman, W. B. (2007) Structural diversity in copper-sulfur chemistry: synthesis of novel Cu/S clusters through metathesis reactions, *Inorg Chem 46*, 8105-8107.
122. Bar-Nahum, I., Gupta, A. K., Huber, S. M., Ertem, M. Z., Cramer, C. J., and Tolman, W. B. (2009) Reduction of nitrous oxide to dinitrogen by a mixed valent tricopper-disulfido cluster, *J Am Chem Soc 131*, 2812-2814.
123. Richardson, D., Felgate, H., Watmough, N., Thomson, A., and Baggs, E. (2009) Mitigating release of the potent greenhouse gas N2O from the nitrogen cycle - could enzymic regulation hold the key?, *Trends in Biotechnology 27*, 388-397.

124. Ravishankara, A. R., Daniel, J. S., and Portmann, R. W. (2009) Nitrous Oxide (N2O): The Dominant Ozone-Depleting Substance Emitted in the 21st Century, *Science 326*, 123-125.
125. Prather, M. J. (1998) Time Scales in Atmospheric Chemistry: Coupled Perturbations to N2O, NOy, and O3, *Science 279*, 1339-1341.

Chapter 2

Cytochrome c_{552} is the electron donor of N_2OR from *Pseudomonas nautica* – Kinetic, NMR and docking studies

2.1 Abstract

The multicopper enzyme nitrous oxide reductase (N_2OR) catalyses the final step of denitrification, the two-electron reduction of N_2O to N_2. This enzyme is a functional homodimer containing two different multicopper sites: CuA and CuZ. CuA is a binuclear copper site that transfers electrons to the tetranuclear copper-sulfide CuZ, the catalytic site. In this study, *Pseudomonas nautica* cytochrome c_{552} was identified as the physiological electron donor. The kinetic data presents differences when comparing physiological with artificial electron donors (cytochrome versus methylviologen). In the presence of cytochrome c_{552} the reaction rate is dependent on the ET reaction and independent of the N_2O concentration. With MV, the electron donation is faster than the substrate reduction. From the study of cytochrome c_{552} concentration dependence we estimate the kinetic parameters: K_{mc552}=(50.2 ± 9.0) μM and $V_{maxc552}$=(1.8 ± 0.6) U/mg, respectively. The N_2O concentration dependence indicates a K_{mN2O}=(14.0 ± 2.9) μM using MV as electron donor. The pH effect on the kinetic parameters is different when MV or cytochrome c_{552} are used as electron donors (pK_a=6.6 and 8.3, respectively). The kinetic study also revealed the hydrophobic nature of the interaction and direct electron transfer studies showed that CuA is the center that receives electrons from the physiological electron donor. The formation of the electron-transfer complex was

observed by ^{1}H-NMR protein-protein titrations and was modeled with a molecular docking program (BiGGER). The proposed docked complexes corroborated the ET studies giving a large number of solutions in which cytochrome c_{552} is placed nearby a hydrophobic patch located around the CuA center.

This chapter has been published in Biochemistry, 47, 10852-10862 (2008), *Electron Transfer Complex Between Nitrous Oxide Reductase (N_2OR) and Cytochrome c552 from Pseudomonas Nautica: Kinetic, NMR and Docking Studies.* S. Dell'Acqua, S.R. Pauleta, E. Monzani, A.S. Pereira, L. Casella, J.J G. Moura, I. Moura.

2.2 Introduction

Nitrous oxide reductase (N_2OR), is a copper containing enzyme that catalyses the two electron reduction of N_2O to N_2 ($N_2O + 2\ H^+ + 2\ e^- \rightarrow N_2 + H_2O$) (*1, 2*), the last step of the denitrification process ($2\ NO_3^- \rightarrow 2\ NO_2^- \rightarrow 2\ NO \rightarrow N_2O \rightarrow N_2$), which is coupled to ATP generation.

This enzyme has been isolated from several denitrifying bacteria, but only recently its crystal structure has been reported for three different bacterial species, *Pseudomonas nautica* (*Pn*) (*3*), *Paracoccus denitrificans* (*Pd*) (*4*) and *Achromobacter cycloclastes* (*Ac*) (*5*). N_2OR is a functional homodimeric enzyme containing two different multicopper sites: CuA and CuZ. In the functional dimer the CuA-CuZ distance is approximately 10 Å, while within the monomer is around 40 Å (*3, 4*), a distance considered to be inappropriate for an efficient electron transfer (*6*).

The electronic structure of the CuA has been extensively studied, while the one of the catalytic site CuZ has only recently been the object of several studies. The CuA site is located in the C-terminal cupredoxin-like domain and is constituted by a binuclear copper site similar to the CuA from cytochrome oxidases (*1, 7*). In both enzymes this center is involved in long-range electron-transfer due to the low energy of reorganization between the reduced Cu^{+}--Cu^{+} state and the mixed-valence oxidized $Cu^{1.5+}$--$Cu^{1.5+}$ state. The peculiar spectroscopic and electronic properties of this center have been exhaustively investigated, especially in cytochrome *c* oxidase (*8, 9*).

The catalytic CuZ site is located in the N-terminal domain that is constituted by a seven-bladed β-propeller fold. CuZ is a novel mixed-valence copper center (Cu_4S) with a sulfide ion bridging a distorted tetrahedron of copper atoms, in a unique structure in biology. The Cu_4S core is bound to the protein via the N-atoms of seven histidine residues. Five histidine residues bind to the copper ions through their Nε2 atom (His 80, His 128, His 270, His 325 and His 376), whereas two use their Nδ1 atom (His 79 and His 437) (*3*). A water-derived ligand is proposed to bridge the two copper atoms Cu_ICu_{IV}, where the N_2O is proposed to bind.

N_2OR can be isolated in different forms depending on the procedure followed during the purification (*8, 10, 11*). *Pn* N_2OR can be isolated in two forms (*Blue* and *Purple*) (*10*) that differ in the redox state of the CuA center. Both forms are intermediate oxidation states between an oxidized ($Cu^{1.5+}$--$Cu^{1.5+}$) state and one-electron reduced (Cu^{+}--Cu^{+}) state, but the *Purple* form is more oxidized than the *Blue* form, in which CuA is mainly in the (Cu^{+}--Cu^{+}) state.

It has been spectroscopically demonstrated that the aerobically isolated *Pn* N_2OR used for the crystallographic study, described by Brown *et al*. (*3*), contains a $1Cu^{II}/3Cu^{I}$ redox state with a total spin of ½ where the unpaired electron appears to be delocalized between two or more Cu atoms via sulfide ion bridging (*12, 13*), while the CuA is in the reduced (Cu^{+}--Cu^{+}) state.

The CuZ cluster can only be reduced to a fully-reduced state (4 Cu^{I}) after a prolonged incubation with reduced methylviologen (MV), a powerful reductant (E'° = – 0.44 V *vs* NHE (*14*)). Recently, this form has been shown to be catalytically active (*15, 16*), with a k_{cat} of 162.9 s^{-1}, per monomer, when MV is used as electron donor (*17*).

This slow activation process does not appear to be catalytically relevant, which makes more imperative the need to study the interaction of the enzyme with its putative physiological electron donor to clarify both the activation process and the enzyme catalytic cycle.

Although it has been demonstrated that a cytochrome *c* could transfer electrons to nitrous oxide reductase (*18, 19*), the only detailed kinetic characterization was reported for the N_2OR isolated from *Wolinella succinogenes*, where cytochrome *c* was used as an electron donor. However, this enzyme has the unique feature of presenting an additional domain containing a *c*-type heme, which is not found in any other isolated bacterial N_2OR (*20*).

Recently, Rasmussen and co-workers (*21*) reported a pre-steady-state kinetic study on *Paracoccus pantotrophus* N_2OR, using horse heart cytochrome *c* as a non-physiologic electron donor. Moreover, Dooley and co-workers (*17*) were able to activate the *Ac* N_2OR using reduced bovine heart cytochrome *c*.

In *Paracoccus denitrificans*, under denitrifying conditions, two small redox proteins are expressed, a cytochrome *c*, cytochrome c_{550}, and a type I copper protein, pseudoazurin (*22*). Although, none of these proteins were tested as electron donors to this enzyme, a structural model for the electron transfer complex has been proposed based on a theoretical docking study using the structure of *Paracoccus denitrificans* N_2OR (*23*). The model structure shows that both proteins interact with a well defined and conserved region of the enzyme surface, in the C-terminal domain near the CuA center.

Pseudomonas nautica contains at least five monohemic cytochrome *c* in the periplasm: cytochrome c_{552}, cytochrome c_{553}, cytochrome c_{549}, cytochrome $c_{553(548)}$ and cytochrome *c*', which are putative candidates for the role of physiological redox partners of N_2OR. In this work

we have identified cytochrome c_{552} as the physiologic electron donor of nitrous oxide reductase and a kinetic study was carried out. A model of the electron transfer complex was also obtained using protein docking simulation and the formation of this complex was observed by NMR spectroscopy.

2.3 Materials and Methods

2.3.1 Purification of the proteins

Pseudomonas nautica nitrous oxide reductase was purified as previously described (*10*), with some minor modifications. Enzyme concentration was determined using the Lowry method (*24*). *Pn* cytochromes were purified from the soluble extract as previously described, with some minor modifications: cytochrome c_{552} (*25*), cytochrome c_{549} (*25*), cytochrome c_{553} (*26*) and cytochrome *c*' (*26*). Horse heart cytochrome *c* (HH cytochrome *c*), was purchased from Sigma and used without further purification. The concentration of the cytochromes was determined spectrophotometrically using the extinction coefficient at 552 nm, ε = 19.3 mM^{-1} cm^{-1} (*27*); 549 nm, ε = 47.3 mM^{-1} cm^{-1} (*28*); 553 nm, ε = 20.8 mM^{-1} cm^{-1} (*26*); 399 nm, ε = 70 mM^{-1} cm^{-1}, and 550 nm, ε = 29.5 mM^{-1} cm^{-1} (*29*) for the reduced forms of cytochrome c_{552}, cytochrome c_{549}, cytochrome c_{553}, cytochrome *c*' and HH cytochrome *c*, respectively.

2.3.2 Enzyme Activation

Nitrous oxide reductase was activated anaerobically, in a glove box, using reduced methylviologen, as previously described (*30*). The enzyme (1.4 μM) was incubated at room temperature in a degassed solution containing 3.0 mM methylviologen (MV) and 1.5 mM sodium dithionite (DT) in 100 mM Tris-HCl, pH 7.6, for 180 min. The excess of reductants was removed using a PD10 Sephadex G25 column (Amersham Bioscences), equilibrated with 100 mM Tris-HCl at pH 7.6. The eluted solution (1 ml) was collected and stored at –30 °C until further use. After this step, the enzyme concentration (0.7 μM) was determined separately by the Lowry method.

2.3.3 Activity assay

The activity assays were performed using different reduced cytochromes or MV as electron donors to the enzyme. Concentrated solutions of each cytochrome *c* (typically 100 -150 μM) were reduced by addition of 2.5 mM sodium ascorbate, incubated for 5 min, and then desalted into 100 mM Tris-HCl at pH 7.6, using a PD10 Sephadex G25 column (Amersham Bioscences).

Activity assays were started by adding activated N_2OR (70 nM of dimer) to a cuvette containing 100 mM Tris-HCl at pH 7.6, 1.25 mM nitrous oxide (N_2O) and 20 – 25 μM of each cytochrome (cytochrome c_{552}, cytochrome c_{553}, cytochrome c_{549}, cytochrome *c*' or HH cytochrome *c*) or MV (Figure 2.1). The enzymatic activity was determined by monitoring the decreased of the α-band and the shift of the Soret band of each cytochrome *c*, using a TIDAS diode array spectrophotometer. In the case of MV, the assays were monitored at 600 nm. The concentration of the N_2O-saturated solution was assumed to be 25 mM (*30*). The enzyme specific activity is expressed in U/mg units, corresponding to μmol N_2O reduced • min^{-1} • (mg of N_2OR dimer)$^{-1}$.

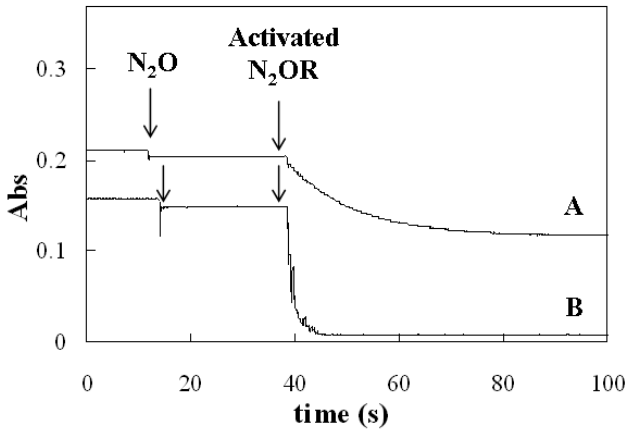

Figure 2.1 – Kinetic trace of the modified enzymatic assay using (A) *Pn* cytochrome c_{552} or (B) methylviologen as electron donors. The assays were initiated by the addition of activated *Pn* N_2OR (70 nM) to a solution containing 1 mM N_2O-saturated water, 0.1 M Tris-HCl at pH 7.6 and 10 μM reduced *Pn* cytochrome c_{552} or 12 μM reduced methylviologen. The absorbance change was followed at 552 nm for cytochrome c_{552} (A) and at 600 nm for MV (B).

For the determination of the cytochrome c_{552} concentration dependence of the reaction rates, the conditions of the assay were 100 mM Tris-HCl, pH 7.6, 1.25 mM nitrous oxide (N_2O) and, 3.6, 6, 12, 18 or 36 μM cytochrome c_{552}. Each kinetic assay was initiated by the addition of activated N_2OR (70 nM of dimer) to the cuvette. The ionic strength dependence was studied by varying the concentration of NaCl in the cuvette containing 100 mM Tris-HCl at pH 7.6, 1.25 mM nitrous oxide (N_2O) and 9 μM cytochrome c_{552}, and 0, 225, 450 or 650 mM NaCl, and initiated with 35 nM activated N_2OR dimer.

For the determination of the MV concentration dependence of the reaction rates, the kinetic assays were started by adding 35 nM activated-N_2OR dimer to a cuvette containing 100 mM Tris-HCl at pH 7.6, 1.25 mM nitrous oxide (N_2O) and, 6.2, 9.3, 28.0, 56.0, 93.4 or 155.6 μM reduced MV. Dithionite was present at stoichiometric amounts relatively to MV.

For the determination of the N_2O concentration dependence of the reaction rates, the kinetic assays were started by adding 35 nM activated-N_2OR dimer to a cuvette containing 100 mM Tris-HCl at pH 7.6, 91 μM MV or 7.5 μM *Pn* cytochrome c_{552}, 5, 10, 12.5, 25, 37.5, 62.5, 125 and 500 μM N_2O, added as N_2O-saturated water, respectively.

In order to determine the pH dependence of the reaction rates with both MV and cytochrome c_{552} as electron donors, the kinetic assays were started by adding 35 nM activated-N_2OR dimer to a cuvette containing 91 μM MV or 9 μM *Pn* cytochrome c_{552}, respectively, 1.25 mM nitrous oxide (N_2O), in 0.1 M buffer system at the desired pH. The following buffers were used: 0.1 M potassium phosphate buffer at pH 6.2, 6.7 and 7.0, or 0.1 M Tris-HCl at pH 7.6, 8.2 and 8.7.
All assays were repeated at least three times. Initial rate constants were determined by linear fitting of the initial region of each progress curve. The values of K_m and V_{max} were obtained from direct fits of the experimental data with the Michaelis-Menten equation. The pH profiles were fitted with the following equation: $Act = (Act_{max})/(1+10^{(pKa-pH)})$ and $Act = (Act_{max})/(1+10^{(pH-pKa)})$ when MV and cytochrome c_{552} were used as electron donor, respectively.

2.3.4 Direct electron transfer studies

Pn N_2OR was fully oxidised by addition of 10 mM ferricyanide, incubated for 5 minutes, and then desalted into 100 mM Tris-HCl at pH 7.6, with a PD10 Sephadex G25 column (Amersham Bioscences). *Pn* cytochrome c_{552} was fully reduced by addition of 2.5 mM sodium ascorbate during 5 min; the excess of reductant was removed using a PD10 Sephadex G25 column (Amersham Bioscences) in 100 mM Tris-HCl at pH 7.6. The MV was reduced by addition of sodium dithionite under anaerobic conditions. The direct electron transfer was studied by adding a stoichiometric amount of reduced electron donor (cytochrome c_{552} or MV) to a cuvette containing fully oxidised enzyme. The UV – visible spectrum of the sample was monitored before and after the addition of the reduced electron donor.

2.3.5 ^{1}H NMR titration

Protein samples were exchanged to 20 mM sodium phosphate buffer at pH 7.6, using a Sephadex G25 column and concentrated above a Vivaspin membrane with a 30 kDa *Mr* cut off for N_2OR or a 5 kDa *Mr* cut off for cytochrome c_{552}. The titration was carried out using a solution of 0.475 mM oxidised cytochrome c_{552} in 20 mM sodium phosphate buffer at pH 7.6, 50 mM NaCl, and 10 % D_2O. Increasing amounts of oxidised N_2OR were added, until a 3.5 molar monomer-monomer ratio was reached. ^{1}H NMR spectra were recorded on a Bruker Avance 600 spectrometer at 288 K with a spectral width of 90 ppm for 32k data points and 512 scans were accumulated. Spectra were obtained presaturating the water signal and processed with the software TOPSPIN 2.0b provided by Bruker. The chemical shifts were referenced to the H_2O resonance (4.86 ppm at 288 K).

2.3.6 Molecular docking simulation

Docking was performed as described in ref. (*31*) using the algorithm BiGGER developed by Palma *et al.* (*32*). The target protein was the functional dimer of *Pn* nitrous oxide reductase. The coordinates for the enzyme (1QNI.pdb), *Pn* cytochrome c_{552} (1CNO.pdb) and HH cytochrome *c* (1HRC.pdb) were obtained from the RCSB Protein data Bank (http://www.rcsb.org). The BiGGER algorithm provides a complete and systematic search of the rotational space of one protein relative to the other, generating a large number of candidate docking geometries based on the complementarity of the molecular surfaces. The 5000 best solutions thus generated were evaluated and ranked according to a combination of additional interaction criteria that include electrostatic energy of interaction, relative solvation energy, and the relative propensity of side chains to interact. For each solution, this combination process produces a "Global Score". In this particular case, the best solutions were ranked according to Global Score and hydrophobic score. We then applied a filter to the results based on the distance between Cu_A center in N_2OR and the iron ions in cytochrome c_{552} heme groups. This procedure is described in the Results section. The top solutions were evaluated individually using the http://www.biochem.ucl.ac.uk/bsm/PP/server/index.html site in order to determine the size of the interface of the complex, the gap volume index (as defined by Jones and Thornton (*33*)) as well as the hydrophobicity.

2.4 Results

2.4.1 Activation and kinetic assay of N_2OR

The as-purified *Pn* N_2OR (mixture between *Blue* and *Purple* forms described by Prudêncio *et al.* (*10*)) showed very low activity, 0.090 ± 0.005 U/mg, when used in a kinetic assay without pre-activation with reducing agent and using MV as the electron donor (without the usual prolonged incubation). In addition, the incubation of this enzyme form with reduced cytochrome c_{552} (the putative physiological redox partner – see below) was not able to activate the enzyme since no activity was detected. Indeed, enzyme activation is only achieved through prolonged incubation (about 1 h) with sodium dithionite and methylviologen, which fully reduce both CuA and CuZ centers, as previously reported (*15*). This activated N_2OR remains active for several hours in anaerobic conditions, even after the complete removal of the reductants (the profile of the activity *vs*. time is not shown).

The activity assay has been slightly changed from the one previously reported (*30*), that was initiated by the addition of N_2O. Actually, contrary to the previous assay, the one described here is designed to separate the effective activity of the enzyme from its activation process (Figure 2.1). In this new assay the activated enzyme (fully reduced enzyme from which

reductants were removed) is added after the substrate to the reduced electron donor. This procedure allows comparison between the behaviour of artificial electron donors, such as methylviologen, with the one of putative physiologic redox partners, such as *Pn* cytochromes.

2.4.2 MV as an electron donor to N_2OR

The catalytic activity of N_2OR was studied using methylviologen as electron donor. The profile of the activity versus concentration of methylviologen can be fitted to Michaelis-Menten equation (Figure 2.2), with a K_{mMV} of (11.5 ± 3.6) μM and a V_{maxMV} of (157 ± 13) U/mg. The k_{cat} value calculated for *Pn* N_2OR (321 ± 27) s^{-1} per monomer of enzyme is larger than the one calculated for *Ac* N_2OR (k_{cat} = 162.9 s^{-1} per monomer (*17*)).

The rate dependence of the activity of *Pn* N_2OR (35 nM) with MV on N_2O concentration (5 – 500 μM) was evaluated while keeping the MV concentration constant at the saturating value (91 μM). The rates follow a hyperbolic behaviour, which can be fitted through the Michaelis-Menten equation. The kinetic parameters for the reaction with different N_2O concentrations are (14.0 ± 2.9) μM and (128 ± 17) U/mg for K_{mN2O} and V_{maxN2O} respectively (Figure 2.3). The k_{cat} in this case is (275 ± 33) s^{-1} per monomer of enzyme.

The ionic strength dependence of the activity was studied at pH 7.6, showing that there is a 20 % decrease in activity when the ionic strength is raised from 0 mM to 650 mM (data not shown). The catalytic activity has a maximum between pH 7.5 and 9 and a pK_a = 6.6, when the ionic strength is 100 mM (Figure 2.4).

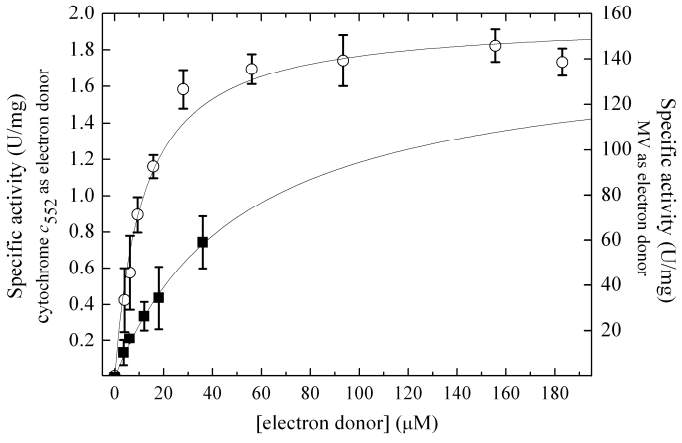

Figure 2.2 – Kinetic activity of *Pn* N_2OR as function of electron donor concentration: reduced methylviologen (open circles) or *Pn* cytochrome c_{552} (solid squares). The assays were performed in 0.1 M Tris-HCl at pH 7.6, 70 nM activated N_2OR, 1.25 mM N_2O-saturated water and 6.2 to 155.6 μM MV or 3.6 to 36 μM *Pn* cytochrome c_{552}. The experimental data was fitted with Michaelis-Menten equation, using a K_m of (11.5 ± 3.6) μM and V_{max} of (157 ± 13) U/mg, or a K_m of (50.2 ± 9.0) μM and and V_{max} of (1.8 ± 0.6) U/mg for methylviologen or *Pn* cytochrome c_{552}, respectively.

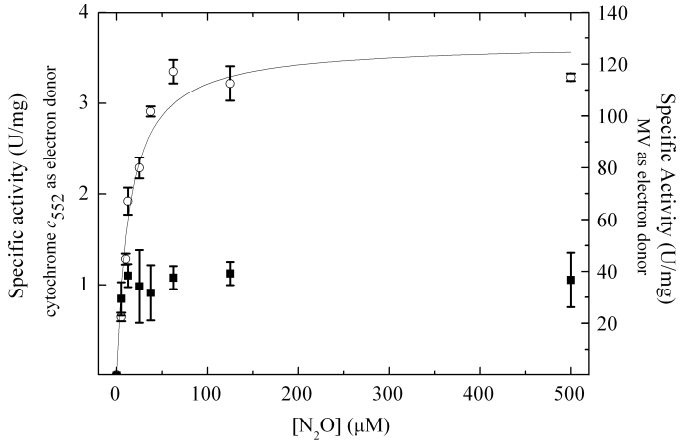

Figure 2.3 – Kinetic activity of *Pn* N_2OR as function of N_2O concentration with methylviologen (open circles) and cytochrome c_{552} (solid squares) as electron donor. The assays were performed in 0.1 M Tris-HCl at pH 7.6, 35 nM activated N_2OR, 5, 10, 12.5, 25, 37.5, 62.5, 125 and 500 μM N_2O-saturated water, 91 μM MV and 7.5 μM *Pn* cytochrome c_{552}. The experimental data was fitted with Michaelis-Menten equation, using a K_m of (14.0 ± 2.9) μM and V_{max} of (128 ± 17) U/mg, for methylviologen.

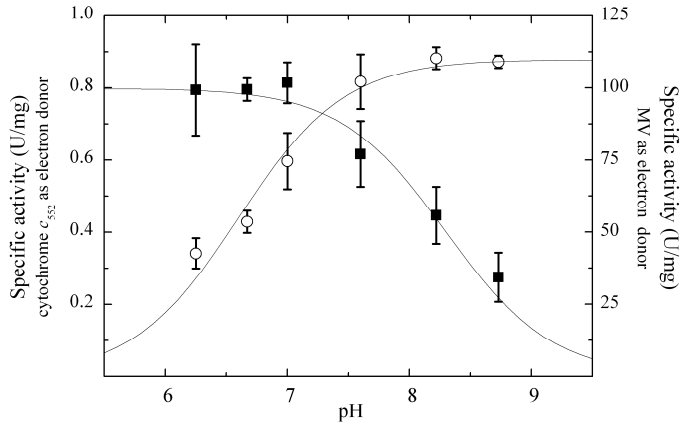

Figure 2.4 – pH dependence of the kinetic activity of *Pn* N_2OR using *Pn* cytochrome c_{552} (solid squares) or MV (open circles) as electron donors. The assays were performed adding 35 nM activated N_2OR to a solution containing 9 μM *Pn* cytochrome c_{552} or 91 μM MV, 1.25 mM N_2O-saturated water, in different buffer systems between pH 6.2 and 8.7. The data was non-linear fitted using the equation described in Materials and Methods and pK_a of 8.3 and 6.6 were calculated for cytochrome c_{552} and MV, respectively.

2.4.3 Cytochrome c_{552} as an electron donor to N_2OR

In order to identify the putative physiologic electron donor of N_2OR, different *Pn* cytochromes *c* (cytochrome c_{552}, cytochrome c_{553}, cytochrome c_{549} and cytochrome *c*') were used as electron donors in the activity assay described before. The only cytochrome that was able to transfer electrons to the activated enzyme was *Pn* cytochrome c_{552} (Figure 2.1). In addition, horse heart cytochrome *c* was also tested as a non-physiological electron donor, but it was also unable to donate electrons to the activated enzyme.

The kinetic parameters K_m and V_{max} for cytochrome c_{552} could not be determined with accuracy due to the difficulty in collecting data at high cytochrome concentrations. Nevertheless, K_{mc552} and $V_{maxc552}$ were estimated to be (50.2 ± 9.0) μM and (1.8 ± 0.6) U/mg, respectively (Figure 2).

Although it is an estimate, the K_m value is of the same magnitude as the ones obtained for other physiological electron transfer complexes, such as the one determined for *Paracoccus pantotrophus* pseudoazurin as an electron donor to cytochrome *c* peroxidase (50 μM) (*34*).

The ionic strength and pH effect on the catalytic activity were studied. The N_2O reduction, catalysed by N_2OR with cytochrome c_{552} as electron donor, is independent on the ionic strength up to 0.65 M (data not shown). In addition, the catalytic activity is constant at acidic pH, until pH 7, and decreases at basic pH, with an apparent pK_a estimated to be 8.3 (Figure 2.4). The rate dependence of the activity of *Pn* N_2OR (35 nM) with cytochrome c_{552} on N_2O concentration (5 – 500 μM) was evaluated while keeping the cytochrome c_{552} concentration constant (7.5 μM). The rates are constant within the experimental error, indicating that the variation of N_2O concentration does not influence the reaction rate (Figure 2.3). Considering that the k_{cat} for N_2O is an intrinsic characteristic of the enzyme, and that it was possible to determine its value using MV as electron donor (k_{cat} = 275 s^{-1}), it is reasonable that the rates do not change with N_2O concentration when cytochrome c_{552} is used as electron donor, since k_{cat} for this electron donor is much lower (k_{cat} = (3.8 ± 1.3) s^{-1} per monomer of enzyme).

2.4.4 Direct electron transfer studies

The direct electron transfer between fully oxidised *Pn* N_2OR and stoichiometric amounts of reduced electron donors (MV and *Pn* cytochrome c_{552}) was studied in the absence of substrate, N_2O. The UV-visible spectrum shows that the CuA center is rapidly reduced by both the artificial (MV) and the physiological electron donor (cytochrome c_{552}). In the case of MV, the bands at 480, 540 and 800 nm disappear. Due to the absorption overlap with cytochrome c_{552}, just the variation at 800 nm could be analysed, while it is possible to follow reoxidation of the cytochrome by the decrease of the band at 552 nm. In both experiments, the CuZ center remains oxidized since there is no change in the absorbance band at 640 nm (Figure 2.5).

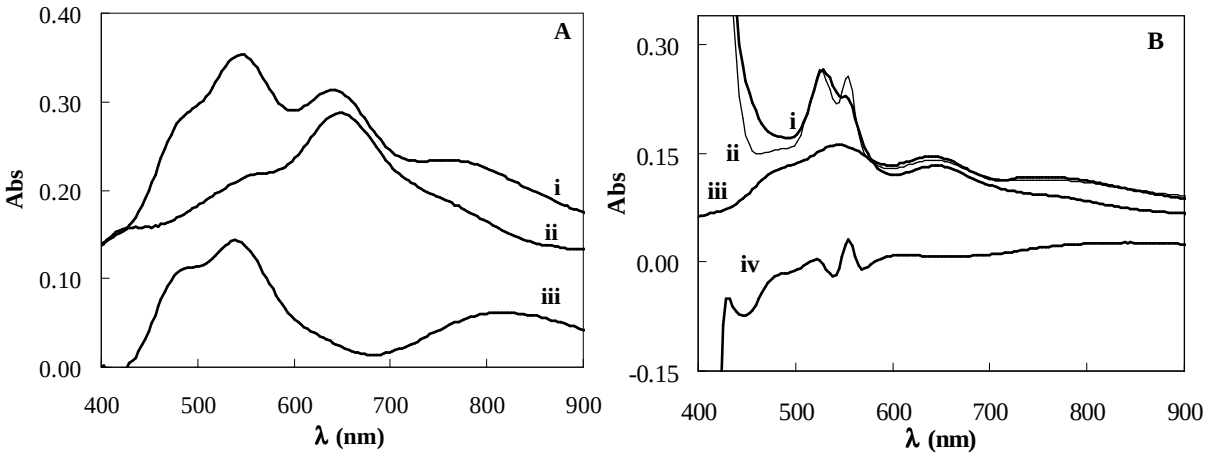

Figure 2.5 – Direct electron transfer between fully oxidised nitrous oxide reductase and reduced electron donors (A) MV and (B) *Pn* cytochrome c_{552}, monitored by visible spectra. (A) The reduction of N_2OR by MV was observed at 480 nm, 540 nm and 800 nm. (A-i) fully oxidised *Pn* N_2OR, (A-ii) N_2OR after addition of reduced MV and (A-iii) difference spectrum between (A-i) and (A-ii). (B) The reduction of *Pn* N_2OR by *Pn* cytochrome c_{552} was observed at 800 nm, while the oxidation of the cytochrome was observed at 552 nm. (B-i) N_2OR spectrum immediately after addition of reduced cytochrome c_{552} (t=0), (B-ii) N_2OR spectrum after addition of reduced cytochrome c_{552} (after t=30s), (B-iii) fully oxidised *Pn* N_2OR and (B-iv) difference spectrum between (B-ii) and (B-i).

2.4.5 ^{1}H NMR titration

As previously reported, the oxidised form of cytochrome c_{552} has a ^{1}H-NMR spectrum typical of a low-spin cytochrome *c* (*27*). The four intense downfield resonances, from 13 to 36 ppm, were assigned to the four-methyl groups of the porphyrin ring (Figure 2.6-A). Upon addition of N_2OR, cytochrome c_{552} heme methyl resonance M3 and M4 undergo a small downfield shift (–0.010 and –0.016 ppm, respectively) with a multiphase behaviour, while the resonances M1 and M2 do not change (Figure 2.6-B). This chemical shift variation shows that the complex between the two proteins is in fast exchange regime on the NMR time-scale.

The chemical shift variation can be simulated with a K_d of 5 μM (Figure 2.6-C), up to the addition of 1 equivalent of monomer N_2OR to cytochrome c_{552}. However, at a 1:1 ratio there is a clear inflection in the curve, and instead of attaining a plateau, there is an increase in both chemical shift variation and line width (data not shown), which does not reach any plateau even at a ratio of 3:1 (Figure 6-B). The line width of methyl M1 increases 234 Hz (0.39 ppm) from a 1:1 ratio to a 3:1 ratio of N_2OR to cytochrome c_{552}. At this ratio, all the heme methyl resonances have an increased chemical shift variation: 0.054 ppm, 0.032 ppm, 0.100 ppm and 0.113 ppm for M1, M2, M3 and M4, respectively.

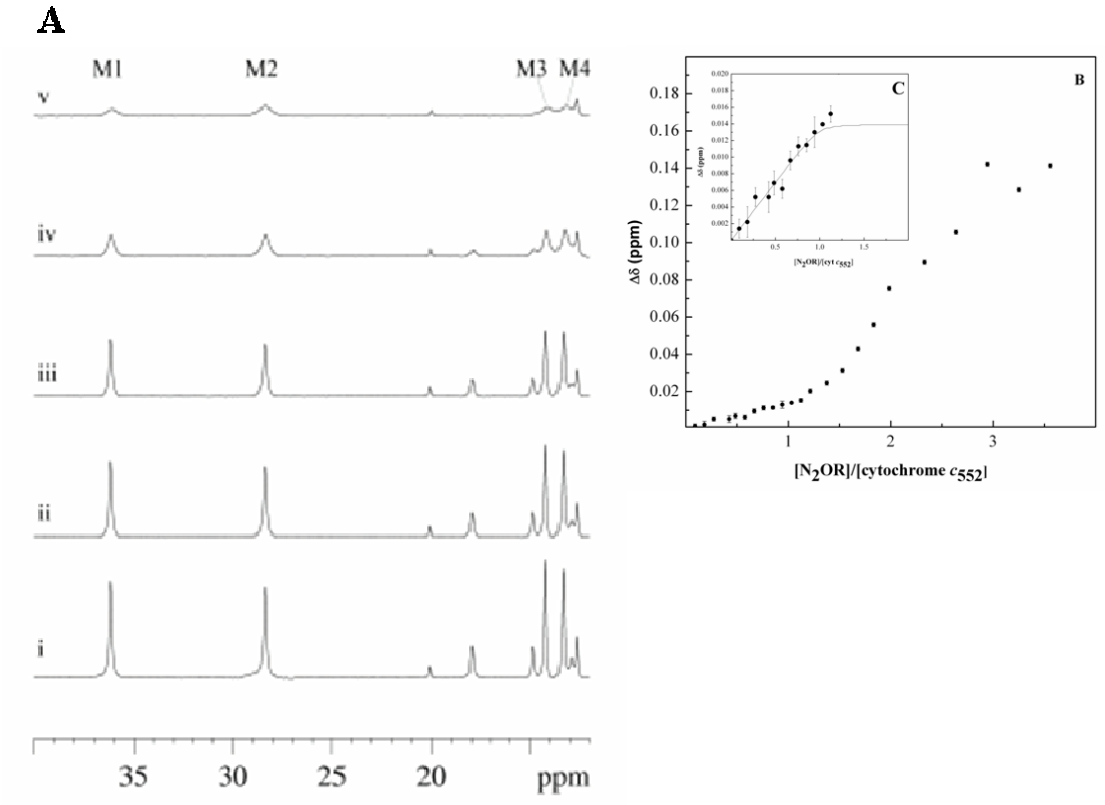

Figure 2.6 – ^{1}H NMR titration of *Pn* cytochrome c_{552} with nitrous oxide reductase. In panel A the low-field spectral region (40 – 12 ppm) containing the cytochrome M1, M2, M3 and M4 heme methyl resonances is shown. The experiment was performed as described in Materials and Methods, and the protein samples were (A, i) R=0, 472 µM cytochrome c_{552}; (A, ii) R=0.5, 440 µM cytochrome c_{552} and 220 µM N_2OR; (A, iii) R=1.0, 410 µM cytochrome c_{552} and 410 µM N_2OR; (A, iv) R=2.0, 365 µM cytochrome c_{552} and 730 µM N_2OR; (A, v) R=3.6, 308 µM cytochrome c_{552} and 1109 µM N_2OR. Panel B shows the chemical shift variation of cytochrome c_{552} heme methyl M4 with increasing molar ratios of nitrous oxide reductase. Panel C shows the fitting curve simulated for a single binding site with K_d = 5.0 µM and δ_{max} = 0.014 ppm, until a ratio of 1:1.

2.4.6 Docking of cytochrome c_{552} to Pn N_2OR

In the first stage of the docking algorithm BiGGER, a set of 5000 models were selected from all possible configurations generated by rotating cytochrome c_{552} (probe) around the surface of nitrous oxide reductase (target protein) in steps of 1 Å and a translation at each 15°-step rotation. The second stage of the docking is called the "Scoring and Ranking", in which these 5000 models were evaluated and ranked according to a Global Score (see Materials and Methods), or to each criterion individually. In the top 500 solutions, ranked either by Global or Hydrophobic Score, the cytochrome c_{552} binds at a particular location of the enzyme surface, near the CuA center (Figure 2.7-A, B).

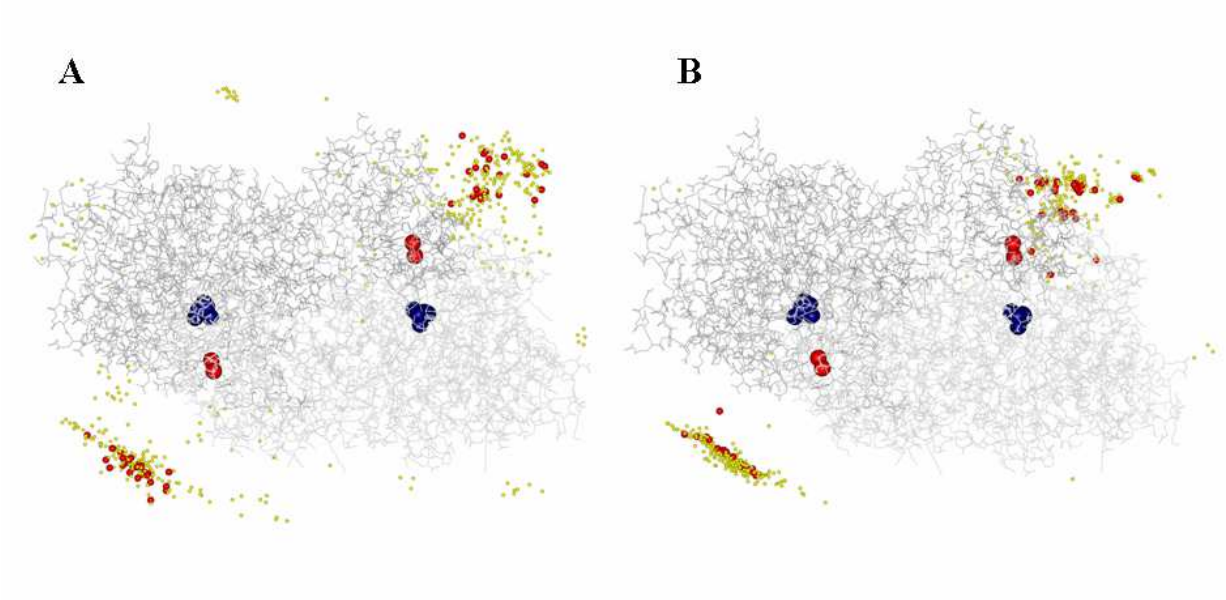

Figure 2.7 – A) 500 top model complexes ranked by Global Score of the docking of N_2OR dimer with cytochrome c_{552} dimer. B) 500 top model complexes ranked by the Hydrophobic Scored of the docking of N_2OR dimer with cytochrome c_{552} dimer. In Panel A and B the geometric center of the cytochrome c_{552} of the 500 putative model complexes is represented as a yellow spheres, while the top 50 are represented as bigger red-coloured spheres. The two copper atoms of the CuA center are red, while the catalyitic center is blue, and the polypeptide of each nitrous oxide reductase monomer is coloured in lighter or darker grey.

The intersection of this two groups of solutions gives 8 solutions (Table 2.1 – Figure 2.8) that have a distance between one of the heme iron of cytochrome c_{552} and the CuA center of N_2OR smaller than 20 Å, appropriate for the electron transfer (*6*).

Table 2.1 – Characteristics of the 8 top model complexes obtained by molecular docking simulation of *Pn* cytochrome c_{552} to *Pn* N_2OR.

Probe	Global Score	Hydrophobicity (kcal/mol)	Interface area (Å^2)	Gap Volume Index (Å)	Apolar Residues[a] (%)	CBC – Cu distance (Å)	CBC – AA Distance (Å)	Closest AA to CBC
1	9.2	-7.0	938	3.1	75	10.7	1.5	Gln497
2	10.4	-6.1	1064	2.6	80	10.3	2.4	Asp519
3	3.3	-5.7	868	3.9	57	11.4	3.0	Ala495
4	3.0	-5.3	995	3.5	64	14.1	1.6	Gly499
5	4.3	-5.0	961	4.0	86	13.8	3.8	His566
6	10.4	-4.8	871	4.0	84	14.0	4.7	Pro496
7	5.9	-4.6	1002	3.4	74	13.9	2.8	Ile340
8	3.1	-4.4	980	2.9	82	11.8	2.2	Val421

[a] The percentage of the interface area of N_2OR composed of apolar atoms.

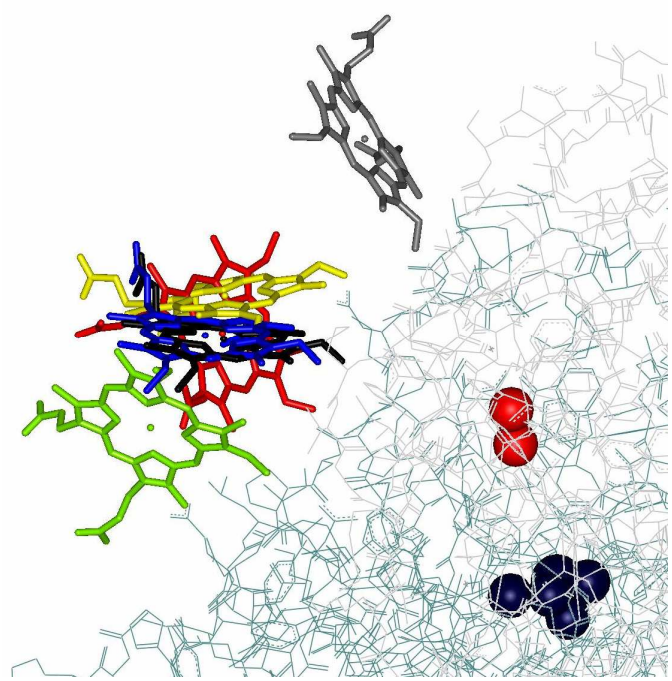

Figure 2.8 – Top putative docking positions obtained after analysis of the docking between *Pn* cytochrome c_{552} dimer and *Pn* N_2OR dimer. Only the heme group of 6 out of the top 8 models are displayed: model 1 in grey, model 2 in black, model 5 in green, model 6 in yellow, model 7 in red and model 8 in blue. These numbers correspond to the numbering in Table 1. Model 3 and 4 are not displayed, because they are located near the CuA of the other N_2OR monomer. The two copper atoms of the CuA center are coloured red, while the catalytic center is coloured dark blue, and the polypeptide chain of each nitrous oxide reductase monomer is coloured in lighter or darker grey.

These top solutions have an interface accessible area between 868 and 1064 $Å^2$ (Table 2.1), that is typical for small complexes following the criteria of Lo Conte *et al.* (*35*). The gap volume index was also calculated, as defined by Jones and Thornton (*33*), in order to estimate the complementarity in the complex interface. An average gap index of 3.4 ± 0.5 Å was obtained for the chosen 8 solutions (Table 2.1). In these docking models, 64 to 86 % apolar residues compose the interface area, which is consistent with a hydrophobic interaction (Table 2.1). Different residues on the N_2OR surface can be identified as the putative entry point for the electron, according to different possible orientations of cytochrome c_{552} in these electron transfer complexes (Table 2.1 and Figure 2.8).

Horse cytochrome *c* was also used as a probe in a docking study with *Pn* nitrous oxide reductase as target, and the results show that this small cytochrome binds at the groove formed between the two monomers of the enzyme, far from the proposed electron entry site, CuA (data not shown).

2.5 Discussion

2.5.1 Establishment of the physiological electron donor of N_2OR

Cytochrome c_{552}, cytochrome c_{553}, cytochrome c_{549} and cytochrome *c*' isolated from the soluble extract of *Pn*, were tested as putative electron donors to *Pn* N_2OR in an assay performed using activated enzyme, as described in Materials and Methods. Cytochrome $c_{553(548)}$ is present in much smaller amounts in the periplasm of this bacterium, in comparison with the other

cytochromes, and at this point was excluded as a physiological redox partner. Cytochrome c_{553}, cytochrome c_{549} or cytochrome *c*' did not exhibit any catalytic oxidation, within the experimental conditions, upon addition of activated N_2OR, and only when reduced cytochrome c_{552} was used as electron donor, a detectable catalytic oxidation of the electron donor was observed.

The data suggests that cytochrome c_{552} is the physiological electron donor to nitrous oxide reductase. Actually, this cytochrome had already been shown to be the physiological redox partner of other enzymes isolated from the periplasm of *Pseudomonas nautica* and involved either in denitrification, as electron donor to cytochrome cd_1 nitrite reductase (*36*) and nitric oxide reductase (*37*), or in detoxification of hydrogen peroxide, as electron donor to cytochrome *c* peroxidase (*38*).

Moreover, HH cytochrome *c*, that was previously used as electron donor to *Paracoccus pantotrophus* N_2OR (*21*), was unable to donate electrons to *Pn* N_2OR, similarly to what had already been observed for another enzyme isolated form this organism, cytochrome *c* peroxidase (*38*).

It should be noted that *Pseudomonas nautica* is a marine organism, living in a high ionic strength environment, and therefore it is expected that its periplasmic enzymes had evolved to provide high turnover rates under these conditions. The surface of the enzymes so far studied (or from which three-dimensional structure has been determined) is mostly hydrophobic in nature in contrast to horse heart cytochrome *c*, which has a relatively high dipole moment, with a ring of positive charges around the exposed heme edge. This difference in charge surface complementary might be the reason for the result observed in the kinetic study. This also provides an explanation for the fact that no putative electron transfer orientations were obtained in the docking study using HH cytochrome *c* as a probe.

Direct electron transfer studies, performed in the absence of substrate, also give strong evidence for electron donation from *Pn* cytochrome c_{552} to *Pn* N_2OR (Figure 5). These studies show that both cytochrome c_{552} and MV, an artificial electron donor, are able to donate electrons directly to CuA center of nitrous oxide reductase, making CuA center a point of entrance of the electrons needed for the catalysis that occurs at the CuZ center, as previously proposed (*23*).

2.5.2 Kinetic characterization – Cytochrome c_{552} as the electron donor to Pn N_2OR

The detailed kinetic characterization of the N_2OR activity must consider that the reaction depends on both N_2O and reducing agent concentration. This multi-substrate enzymatic reaction could proceed in two general cases that are described in detail in Supporting Information. In particular the reaction could require the binding of two substrates to give a ternary adduct or the reaction could occur in a sequence of two separate steps involving each substrate. Our experimental data obtained when cytochrome c_{552} is used as the electron donor perfectly agree with the latter case, as shown by the simulation provided in the Supporting Information (Figure S1 and Figure S2). Therefore, we conclude that the rates do not depend on N_2O concentration (Figure 2.3), indicating that this substrate is involved in a fast step of the catalytic cycle. However, the rates depend on cytochrome c_{552} concentration, indicating that its reaction (including the formation of the complex between the two proteins, the electron transfer reaction and the dissociation of the complex) is slower than the reduction of N_2O and this is the rate-limiting step of the enzyme turnover. Data analysis allowed determination of the kinetic parameters K_{mc552}, (50.2 ± 9.0) μM, and $V_{maxc552}$, (1.8 ± 0.6) U/mg, at pH 7.6 (Figure 2.2).

Comparing to the non-physiologic HH cytochrome *c* tested with N_2OR from *Paracoccus pantotrophus* (*Pp*) (K_m = 6 ± 3 μM and V_{max} = 0.034 ± 0.002 U/mg (*18*)), *Pn* cytochrome c_{552} is shown to be a more efficient electron donor, although in those studies the *Pp* enzyme was not activated, as in the present work.

The reactivity pattern observed with MV as electron donor is different. The reaction rates depend on both N_2O and MV concentration showing apparent saturation behaviour (Figures 2 and 3). It should be noted that the global rates are much higher with MV than those observed when cytochrome c_{552} is used as electron donor (Figure 2.2). This is in agreement with a much faster electron transfer with the non-physiologic reducing agent. The enzyme reduction becomes a fast pre-equilibrium with the N_2O reduction as the slow step of the turnover cycle.

The K_m value for cytochrome c_{552} is higher than the one calculated for MV, indicating a lower affinity of N_2OR for the cytochrome, and the k_{cat} for cytochrome is much lower. In fact, MV is the reductive agent necessary to turn the inactive as-isolated N_2OR into the active fully reduced form and the kinetic data shows a stronger affinity towards the enzyme. However, there is no evidence about the site of interaction of MV to the enzyme surface, while for the cytochrome the contact takes place in the region surrounding the CuA center, as described below.

Overall, as already suggested by Wunsch *et al.* (*39*), the activity assay with MV may not probe the internal electron flow between CuA and CuZ of N_2OR. Nevertheless, both the artificial and

the physiologic electron donor were able to reduce the CuA, as shown in the direct electron transfer experiment (Figure 5). This evidence suggests that MV might donate electrons to both CuA and CuZ sites, justifying the high turnover number obtained and the different behaviour in the pH dependent and the low but not negligible dependence on ionic strength for MV. Being a small molecule, the binding of MV to the enzyme is just diffusion controlled, and the k_{off} rate affects the overall reaction rate at a lesser extent.

On the other hand, the negligible influence of the activity over a wide range of ionic strength suggests an interaction between cytochrome c_{552} and N_2OR mainly driven by hydrophobic effects. Moreover, this cytochrome has been previously shown to be the redox partner of *Pn* cytochrome *c* peroxidase and a similar effect of ionic strength on the activity was observed (*38*).

The pH effect also pointes out for a different behaviour of the two molecules as electron donors. MV-mediated catalysis shows a maximum activity at pH higher than 8, with a pK_a of about 6.6, as already observed in past studies on N_2OR from different sources (*18, 40*). Instead, the activity promoted by cytochrome c_{552} as electron donor decreases at pH above pH 7, presenting a pK_a of 8.3. A similar behaviour has already been observed for *Pp* N_2OR (*18*), where the reaction rate with HH cytochrome *c* is faster at lower pH. This different pH dependence and the slower reaction rate for the cytochrome-mediated reaction (two orders of magnitude lower than the MV-donor system) might suggest that the electron transfer between cytochrome and N_2OR is the rate-limiting step and the pH dependence of the reaction can be attributed to the protein-protein interaction or to the reduction process of the CuZ site (*vide infra*), as already proposed for the N_2O concentration dependence kinetic studies.

In contrast, Rasmussen *et al*. (*21*) found that when non-physiologic HH cytochrome *c* is used as electron donor, not the electron donation but the N_2O-reduction is the rate-limiting step in the catalysis even if the internal ET (in particular intra-ET between CuA and CuZ) is slow. These authors also suggested that the rapid turnover promoted by MV-donor system could bypass the electron transfer path used by the cytochrome, as seems to be evident in the results presented here.

2.5.3 Characterization of the electron transfer complex between cytochrome c_{552} and N_2OR

(i) ^{1}H NMR titration

The chemical shift variation observed for methyl M4 and M3 (M1 and M2 have almost negligible variations - data not shown) upon addition of increasing amounts of N_2OR up to 1:1 ratio ([N_2OR] monomer to [c_{552}] monomer) is small (Figure 2.6-A). The possibility that the small shift variation observed could be due to a non-specific complex formation can be ruled out

since just two of the heme methyl resonances are affected, until a ratio of 1:1. Moreover, as cytochrome c_{552} is the electron donor to N_2OR, the complex between these two proteins is expected to be specific.

Until this 1:1 ratio, the chemical shift variation could be simulated with a K_d of 5 μM, an estimate that is not very reliable due to the high concentrations of protein used in the NMR experiments.

The small chemical shift variation is then attributed to a weak perturbation of the heme vicinity surrounding upon cytochrome c_{552} binding. Cytochrome c_{552} structure shows that methyl M4, in the porphyrin ring, is the most solvent exposed heme methyl in a favorable position for electron transfer. Moreover, heme methyl M4 is close to the CBC methyl group, the most probable point for electron transfer in our docking simulation (see below), while the other heme methyls are not exposed and may not take an active part in the electron transfer process.

It should be noted that the chemical shift variation and the observed line broadening are not due to a paramagnetic effect related to the increasing amount of N_2OR which contains several paramagnetic centers (in this experiment N_2OR presents CuA center in the mixed-valance state $Cu^{1.5+}$--$Cu^{1.5+}$, while CuZ is in the oxidized state $1Cu^{2+}$--$3Cu^{1+}$). In fact, the paramagnetic effect on resonance shift and broadening could be due to two contributions: contact mechanism and dipolar contribution (or Curie). The contact mechanism is excluded since there are no covalent bonds between the porphyrin in cytochrome c_{552} and the paramagnetic centers of N_2OR. The dipolar contribution is very sensitive to the distance between the protons and the paramagnetic center (with a r^{-6} dependence) and to the correlation time for the spin inversion in the metal center (τ_s) (*41*). Both the large distance obtained in the docking simulation, where the CuA is at least 10.4 Å far from the methyl M4 (see below), and the very low τ_S observed in coupled copper clusters (*41*) suggests that the dipolar contribution is negligible.

The larger chemical shift variations observed at protein ratios higher than 1:1 can be attributed to the formation of larger complexes, in which there might be non-specific binding of N_2OR to the complex. The high molecular weight (> 150 kDa – 1 dimer of cytochrome c_{552} and 2 dimers of N_2OR) of these complexes implies a dramatic broadening of the resonances of cytochrome and a concomitant shift related to the slow tumbling of the large aggregate. The line width is a function of the correlation time (molecular tumbling time), which depends on the molecular size. The presence of aggregates would explain the broadening of the heme methyls resonances observed at higher ratios, but may not explain the further chemical shift observed unless it is an induced effect due to the formation of the high molecular weight complex, but not directly due to the binding of the protein at the contact surface. This hypothesis is further

supported by the equivalent chemical shift variation and broadening observed for all the methyl groups independently of their spatial arrangement in the adduct between the two proteins.

(ii) Docking of Pn cytochrome c_{552}

In agreement with the kinetic data, the interface analysis of the modelled complexes shows that the interaction between N_2OR and cytochrome c_{552} is mainly hydrophobic. In fact, in our docking models, the composition of N_2OR surface involved in the ET complex contains 64 % to 86% apolar residues (Table 1). This has already been observed for other electron transfer complexes, but these values are higher than the average reported for *c*-type cytochromes (*42*). Moreover, the hydrophobic interface has a low dielectric constant, which is favourable for electron transfer (*43*).

The small interface area of the complexes indicated in Table 1 (868 to 1064 $Å^2$) is also a characteristic found in short-lived complexes (< 1200 $Å^2$) (*35*), and the average gap index of 3.4 ± 0.5 Å is close to the one found for redox protein complexes (4.7 ± 1.5 Å) (*42*), which is consistent with low geometric fitting and poorly packed interfaces in this type of complexes.

The hydrophobic and poorly packed interfaces enable the interaction with different redox partners. This does not seem to be the case for N_2OR that is proposed to have only one redox partner, but on the other hand, can explain the ability of cytochrome c_{552} in donating electrons to at least two other *Pn* periplasmic enzymes, cytochrome *c* peroxidase (*38*) and nitrite reductase *cd*1 (*36*). As described by Williams *et al.* (*43*), that introduce the concept of "pseudospecific" docking, hydrophobic interactions are less specific and less directional than electrostatic ones.

Regarding the HH cytochrome *c* – N_2OR docking study, the absence of interaction may provide an explanation for the fact that no electron-transfer was observed between reduced horse cytochrome *c* and activated N_2OR, in the kinetic assay. Although, this is a single example, it shows that this docking program can also be used to discriminate between putative electron donors, prior to acquiring experimental data, as long as the three-dimensional structure of the intervenient proteins is known.

Although, our 8 top model complexes were not energy minimized it is possible to compare them with the ones obtained for *Pd* N_2OR and cytochrome c_{550}: the distance between the heme ring and one of the coppers of CuA in the models of the present study is the same range (10.3 to 14.1 Å) (Table 1) as the one found for *Pd* N_2OR complexes (12.8 to 14.3 Å) (*23*); in both cases the interface has a hydrophobic patch in the central area; and the same residues are

found in close contact with the redox partner (A495, P496, H566 and D519), that comprise a conserved surface region near CuA center.

2.5.4 Suggested electron transfer pathway and reduction process of CuZ

The interface of the modelled complexes can be analysed in order to identity putative residues involved in the electron transfer pathway. Cytochrome *c* oxidase (COX) presents the same binuclear copper center, CuA and the amino acid chain in proximity of the CuA site is similar for both COX and N_2OR. Recent structural studies assert that in cytochrome *c* oxidase a tryptophan exposed on the surface is essential for the electron transfer from a cytochrome to the center CuA (*44*). In N_2OR, isolated either from *Pd* or *Pn*, there is no Trp residue in the expected position that could be implied in the electron transfer. Mattila *et al.* (*23*), that performed a docking study on N_2OR from *Pd* and two putative electron donors, pseudoazurin and cytochrome c_{550}, proposed that residues Pro565 and His635 for *Pd*, occupying an analogous position to Trp121 in cytochrome *c* oxidase, are involved in the electron transfer pathway. In fact, Pro565 occupies the same position of Trp121 in the polypeptide chain, while the imidazolic ring of His635 replaces the indolic ring of the tryptophan. In other small copper proteins, like pseudoazurins also a histidine (that coordinates the copper ion) and a proline residue that is located adjacent to this histidine are proposed to be the point of entry or leaving of the electron (*34, 45*).

As this region is well conserved, these amino acids correspond to Pro496 and His566 in *Pn*, and were found in the interface of the top 8 solutions. Moreover, residue Asp519 (corresponding to Asp 558 in *Pd*) appears to be exposed on the surface and available for the electron transfer. The homologous of this amino acid in cytochrome *c* oxidase from *Pd,* Asp178, has been shown to be important for the binding of cytochrome *c* (*44*). This is the only residue that is common to all known N_2OR and COX structures and in all these the Asp carboxylic group is hydrogen bonded to His526, the terminal ligand of CuA center.

At the moment, it is not possible to define a unique ET pathway and binding interface. The 8 best solutions chosen have different heme orientations and involve slightly different interfaces, but in all of them, those three conserved residues (Pro496, Asp519 and His566) are present in the complex interface (data not shown). These docking models also support the view that electrons from cytochrome c_{552} must be delivered to CuA and then to CuZ.

The electron transfer from cytochrome c_{552} to N_2OR necessary to complete the catalytic cycle that occurs in the CuZ center controls the enzymatic activity and pH dependence suggested that a group with a pK_a of 8.3 must be in the protonated form to enable the reaction to occur. It is known that cytochrome c_{552} potential is higher at acidic pH and decreases at basic pH (with

a pK_{ox} = 7.3 ± 0.1 and a pK_{red} = 9.0 ± 0.2) (*27*), indicating that electron donation from the cytochrome becomes less favourable in this range. As the kinetic studies gave an opposite result and this pK_a cannot be correlated to any residue on the protein-protein interface, the attention is then turned to the reduction process of CuZ center in N_2OR.

As within CuZ the pair of Cu_ICu_{IV} atoms is the site of N_2O binding and reduction, we propose that the protonation of a water molecule that bridges these two copper atoms (with a pK_a of 8.3), controls the electron transfer process. Though, this Cu pair cycles between three states during turnover: $Cu^{II}Cu^{II}$, $Cu^{II}Cu^{I}$, and $Cu^{I}Cu^{I}$, according to the accepted mechanism of N_2O reduction (*46*), and the fully oxidised form of the enzyme Cu_ICu_{IV} pair is achieved upon N_2 release. From a variety of model studies on binuclear copper complexes containing N-donor ligands, it is known that deprotonation of a bridging water molecule bound to a couple of Cu^{II} ions typically occurs in the range between pH 7 and 8 (*47*). Perhaps more important is that deprotonation of the Cu^{2+}-H_2O-Cu^{2+} species to the Cu^{2+}-OH-Cu^{2+} form systematically leads to a large reduction in the $E°(Cu^{II}/Cu^{I})$ values (*48, 49*).

However, in the stepwise reduction of the CuZ center during catalysis, it is the second reduction step, from Cu^{2+}-H_2O-Cu^{+} to Cu^{+}-H_2O-Cu^{+}, which is expected to be more difficult and probably rate limiting (*48*). For this mixed valent sate, one-hole Cu^{2+}-H_2O-Cu^{+} species, we also expect that the redox potential will be lowered upon deprotonation to the corresponding hydroxo species, Cu^{2+}-OH-Cu^{+}.

Considering the second one-electron reduction by cytochrome c_{552} as the rate-limiting step of the catalytic cycle, that hypothesis would also explain the determined pK_a of 8.3 found in the experiment, as it is expected that a bound water will be slightly less acidic in the mixed-valent Cu^{2+}-H_2O-Cu^{+} species then in the Cu^{2+}-H_2O-Cu^{2+} species. Thus, the activity of N_2OR at pH above 9 is completely inhibited because the bridge between Cu_I and Cu_{IV} within the CuZ cluster is fully deprotonated and CuA (i.e. cytochrome c_{552}) cannot reduce CuZ. This problem does not exist when methylviologen is used as the electron source, because it is a strong reductant and can directly reduce CuZ, without the need to deliver electrons to this site through CuA. The activity of N_2OR mediated by this non-physiological electron donor is controlled by the protonation state of a group with pK_a of about 6.6, which could be reasonably associated with His566. A schematic picture of the key reduction pathway of the Cu_ICu_{IV} pair in CuZ is shown in Scheme 2.1.

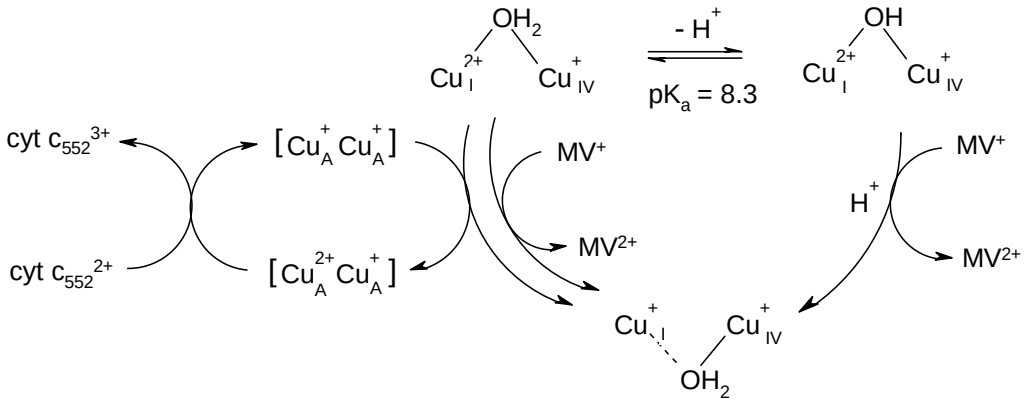

Scheme 2.1 – Proposed electron transfer pathways: cytochrome c_{552} and MV reduce CuA and CuZ with different mechanism. Only CuI and CuIV of CuZ are represented.

According to a recent study (*50*), the water molecule acting as a bridging ligand of the Cu_ICu_{IV} pair remains in the deprotonated state in a pH range, from 6 to 10, and reduction of CuZ by methylviologen is controlled by a group with a pK_a of 9.2 (likely to be K397 in *Pn* N_2OR). The latter data refers to the bimolecular reaction between methylviologen and the as-isolated N_2OR, while in the present work the pH effect was studied for the turnover of the activated enzyme, and different profiles were obtained whether methylviologen or cytochrome c_{552} are used as electron donors. Therefore, the interaction of the enzyme with both the substrate and the electron donor is important. As we know from the present study, the interaction of cytochrome c_{552} with N_2OR is specific, while in the case of methylviologen it may occur in more than one site, with the most effective one being different in the absence or presence of bound N_2O. Moreover, it is also possible that during turnover the other Cu atoms of the CuZ cluster, Cu_{II} and Cu_{III}, take a more active part than is currently hypothesized.

In any case, the reduction process of N_2O, after binding to the fully reduced Cu_ICu_{IV} pair, could be facilitated by the presence of a protonated water ligand within the CuZ site, as this could be the source of the proton assisting the cleavage of the N-O bond and release of N_2 (*46*).

2.6 Conclusion

In conclusion, a new activity assay is presented here that separates the activation of N_2OR from the catalytic reduction of N_2O and allows the comparison between different electron donors. Cytochrome c_{552} from *Pn* was recognized to be the electron donor of N_2OR and the first kinetic characterization of N_2OR with its physiological partner was carried out. The artificial electron donor, methylviologen, the reductive agent that is required to activate the enzyme, showed to be a more efficient electron donor. Nevertheless, differences in the mechanism and interaction with the enzyme are pointed out. In particular, the electron

transfer reaction is the rate-limiting step when cytochrome c_{552} is the electron donor, while the reduction of N_2O is the slower reaction when reduced MV is used as electron donor. The determined pK_as and the different ionic strength dependence suggests that MV might not interact only with CuA center (which was observed in the direct electron transfer experiments) but also directly with CuZ center through a different reduction pathway for the physiological electron donor. The pH dependence of the enzymatic activity when using cytochrome c_{552}, as the electron donor, also suggests the presence of a water bridging ligand at the CuZ center. For cytochrome c_{552}, both the kinetic and the docking studies indicate the presence of a hydrophobic patch near the CuA, which is the electron entry site.

2.7 Supplementary materials

Kinetic treatment for N_2O reduction catalyzed by N_2OR and promoted by electron donor

2.7.1 Steady state kinetic equations for enzymatic reactions requiring two substrates

Case A

The reaction requires the binding of the two substrates to give a ternary adduct in order to have product formation; i.e., only in the presence of both substrates bound to the enzyme the reaction occurs. The reaction scheme is as follows:

$$E \underset{K_{ER}}{\overset{R}{\rightleftarrows}} ER \underset{K_{ERS}}{\overset{S}{\rightleftarrows}} ERS \xrightarrow{k} E + product$$

where E represents the enzyme and R and S are the two substrates; ER and ERS indicate the enzyme with a bound a R molecule and both S and R molecules, respectively; ERS is a ternary complex; K_{ER} and K_{ERS} are the binding constants of R to the native enzyme and S to the intermediate ER, respectively; k is the first order rate constant for the transformation of ERS into the native enzyme and product. In developing the equation we consider the steady state approximation, therefore the concentration of each intermediate is considered constant during catalysis. Here we also consider the binding processes very fast, so that the concentration of the intermediates is ruled by the substrate concentrations. Considering initial rates, it is possible to neglect consumption of the substrates, i.e. we consider [S] and [R] ≈ constant.

$$\begin{cases} 1) & \text{rate} = \dfrac{d[\text{product}]}{dt} = k \times [ERS] \\ 2) & K_{ER} = \dfrac{[ER]}{[E] \times [R]} \\ 3) & K_{ERS} = \dfrac{[ERS]}{[ER] \times [S]} \\ 4) & [E_0] = [E] + [ER] + [ERS] \end{cases}$$

Equations 2) and 3) are the definitions of the binding constants and 4) represents the mass balance on the enzyme, where $[E_0]$ is the total enzyme concentration.

Equations 2) and 3) can be rearranged and combined to:

$$5) \quad [ER] = K_{ER} \times [E] \times [R]$$

$$6) \quad [ERS] = K_{ERS} \times [ER] \times [S] = K_{ER} \times K_{ERS} \times [E] \times [R] \times [S]$$

Introducing [ER] and [ERS] into equation 4) gives:

$$7) \qquad [E_0] = [E] + K_{ER} \times [E] \times [R] + K_{ER} \times K_{ERS} \times [E] \times [R] \times [S]$$
$$= [E] + K_{ER} \times [E] \times [R] \times (1 + K_{ERS} \times [S])$$

Thus:

$$8) \qquad [E] = \frac{[E_0]}{1 + K_{ER} \times [R] \times (1 + K_{ERS} \times [S])}$$

$$9) \qquad [ERS] = \frac{K_{ER} \times K_{ERS} \times [E_0] \times [R] \times [S]}{1 + K_{ER} \times [R] \times (1 + K_{ERS} \times [S])}$$

The global rate equation can be obtained by substituting equation 9) into equation 1):

$$10) \qquad \text{rate} = \frac{k \times K_{ER} \times K_{ERS} \times [E_0] \times [R] \times [S]}{1 + K_{ER} \times [R] \times (1 + K_{ERS} \times [S])}$$

$$11) \qquad \text{rate} = \frac{k \times [E_0] \times [R] \times [S]}{\frac{1}{K_{ER} \times K_{ERS}} + \frac{1}{K_{ERS}} \times [R] + [R][S]}$$

A similar equation could be obtained considering a reverse order of binding of the two substrates.

The global rate depends on the concentration of both the substrates and the binding constants.

<u>Case B</u>

The reaction occurs in a sequence of two steps. The first one involves reversible binding of one substrate molecule which reacts with the enzyme giving the first intermediate. This species, in turn, binds reversibly a second substrate molecule; this complex reacts giving the product and restoring the enzyme in the native form. Here simultaneous binding of the two substrates to the enzyme is not required. The reaction scheme is:

$$E \underset{k_{-1}}{\overset{k_1 \times [R]}{\rightleftharpoons}} ER \xrightarrow{k_2} I \underset{k_{-3}}{\overset{k_3 \times [S]}{\rightleftharpoons}} IS \xrightarrow{k_4} E + \text{products}$$

where E represents the enzyme and R and S are the two substrates; ER indicates the native enzyme with a bound S molecule; I is the first enzyme intermediate and IS is its complex with the substrate S; the k constants linked to the arrows are the rate constants for the individual steps; k_1 and k_3 are second order rate constants, while k_{-1}, k_2, k_{-3}, and k_4 are first order rate constants.

In developing the equation we consider the steady state approximation, therefore the concentration of each intermediate is considered constant during catalysis. Considering initial

rates, it is possible to neglect the consumption of the substrates, i.e. we consider [S] and [R] ≈ constant.

$$\begin{cases} 1) & \text{rate} = \dfrac{d[\text{product}]}{dt} = k_4 \times [IS] \\ 2) & [E_0] = [E] + [ER] + [I] + [IS] \\ 3) & \dfrac{d[ER]}{dt} = k_1 \times [R] \times [E] - k_{-1} \times [ER] - k_2 \times [ER] \approx 0 \\ 4) & \dfrac{d[IS]}{dt} = k_3 \times [S] \times [I] - k_{-3} \times [IS] - k_4 \times [IS] \approx 0 \\ 5) & \dfrac{d[E]}{dt} = k_4 \times [IS] + k_{-1} \times [ER] - k_1 \times [E] \times [R] \approx 0 \end{cases}$$

Equation 2) represents the mass balance on the enzyme, while equations 3), 4) and 5) are the steady state approximations on the enzyme species ER, IS and E, respectively.

The addition of equations 3) and 5) gives:

$$6) \qquad k_4 \times [IS] = k_2 \times [ER]$$

i.e. in steady state, the two irreversible reactions occur at the same rate. Substituting equation 6) into equation 5) gives:

$$7) \qquad k_2 \times [ER] + k_{-1} \times [ER] - k_1 \times [E] \times [R] = 0$$

$$8) \qquad [E] = \frac{k_2 + k_{-1}}{k_1} \times \frac{[ER]}{[R]} = K_{MR} \times \frac{[ER]}{[R]}$$

Where $K_{MR} = \dfrac{k_2 + k_{-1}}{k_1}$ is the Michaelis constant for the reaction of substrate R with the native enzyme in the first step of the catalytic cycle. Similarly, equation 4) gives:

$$9) \qquad [I] = \frac{k_4 + k_{-3}}{k_3} \times \frac{[IS]}{[S]} = K_{MS} \times \frac{[IS]}{[S]}$$

Where $K_{MS} = \dfrac{k_4 + k_{-3}}{k_3}$ is the Michaelis constant for the reaction of substrate S with intermediate I in the second step of the catalytic cycle.

Equations 6), 8) and 9) can be introduced into the mass balance 2), in order to obtain all concentrations as a function of [IS]:

10) $$[E_0] = \frac{k_4}{k_2} \times [IS] + \frac{K_{MS}}{[S]} \times [IS] + \frac{K_{MR}}{[R]} \times \frac{k_4}{k_2} \times [IS] + [IS]$$

11) $$[E_0] = \left(\frac{k_4}{k_2} + \frac{K_{MS}}{[S]} + \frac{K_{MR}}{[R]} \times \frac{k_4}{k_2} + 1 \right) \times [IS]$$

Isolating [IS] from equation 11 gives:

12) $$[IS] = \frac{[E_0]}{1 + \frac{k_4}{k_2} + \frac{K_{MS}}{[S]} + \frac{K_{MR}}{[R]} \times \frac{k_4}{k_2}}$$

The rate equation can be obtained after introducing equation 12) into equation 1):

13) $$\text{rate} = \frac{k_4 \times [E_0]}{1 + \frac{k_4}{k_2} + \frac{K_{MS}}{[S]} + \frac{K_{MR}}{[R]} \times \frac{k_4}{k_2}}$$

It can be noted that the rate depends on both the substrate concentrations and the catalytic constants.

But two limit conditions can be considered.

i) <u>The first step is very fast</u>. When the first process is much faster than the second one, i.e. $k_2 >> k_4$ and [R] is not much lower than K_{MR}, equation 13) can be simplified to:

14) $$\text{rate} = \frac{k_4 \times [E_0]}{1 + \frac{K_{MS}}{[S]}}$$

Equation 14) is a simple Michaelis-Menten type equation depending on [S]. The second step of the cycle is called the “slow step” of the catalysis.

[R] does not affect the observed rate unless it is in a very low concentration, where in equation 13) in the term $\frac{K_{MR}}{[R]} \times \frac{k_4}{k_2}$ the high value of the first fraction could compensate the low value of the second fraction.

ii) <u>The second step is very fast</u>. When the second process is much faster than the first one, i.e. $k_2 << k_4$ and [S] is not much lower than K_{MS}, equation 13) can be simplified to:

15) $$\text{rate} = \frac{k_4 \times [E_0]}{\frac{k_4}{k_2} + \frac{K_{MR}}{[R]} \times \frac{k_4}{k_2}} = \frac{k_2 \times [E_0]}{1 + \frac{K_{MR}}{[R]}}$$

Equation 15) is a simple Michaelis-Menten type equation depending on [R]. The fist step of the cycle is called the "slow step" of the catalysis.

[S] does not affect the observed rate unless it is in a very low concentration ($\frac{K_{MS}}{[S]} >> \frac{k_4}{k_2}$).

A particular case, that applies to our study on N_2OR. If we consider in the mechanism proposed that the second phase is much faster with respect of the first, i.e. $k_2 << k_4$ as in ii), but with [S] which could span also values below K_{MS}. Simplification of equation 13) gives:

16) $$\text{rate} \approx \frac{k_4 \times [E_0]}{\frac{k_4}{k_2} + \frac{K_{MS}}{[S]} + \frac{K_{MR}}{[R]} \times \frac{k_4}{k_2}} = \frac{k_2 \times [E_0]}{1 + \frac{K_{MS}}{[S]} \times \frac{k_2}{k_4} + \frac{K_{MR}}{[R]}}$$

Even in the presence of a saturating R concentration ([R]>>K_{MR}), the maximum observed rate in the presence of large concentration of S gives k_2 and not the rate constant of the fast step k_4. Furthermore, the hyperbolic behaviour observed upon changing [S] is not simply connected to K_{MS} but to an ensemble of constants which can not be determined separately. Here, high turnover rates, close to k_2, are observed even when [S] is lower than K_{MS}; this means that the enzyme reaches maximum activity also when S is not saturating.

In steady state measurements, the kinetic parameters of the fast phases of the catalytic cycle are hidden by the "dominating" slow phase.

This case applies to the catalytic reduction of N_2O by iron(II) cytochrome c_{552} catalysed by N_2OR where, as N_2O reacts with the enzyme in the reduced form, in the reaction scheme N_2O represents S and cytochrome c_{552} is R.

This can be deduced by comparison of the catalytic activity of the enzyme with MV or cytochrome c_{552} as reducing agents. Both substrates require reduction of the enzyme to activate it for the reaction with nitrous oxide. But with the second substrate the rates are much lower. The observed turnover numbers are independent of [N_2O], but this happens not because [S]>>K_{MS}, i.e. not because this substrate is in a saturating concentration, but because it reacts in a fast step ($k_2 << k_4$). The reaction rate depends only on the concentration of cytochrome c_{552}, i.e. substrate R, the substrate reacting in the rate determining step of the process.

In order to observe a rate dependence on N_2O, i.e. substrate S, its concentration must be reduced down to a value much lower than K_{MS}, so that the term $\frac{K_{MS}}{[S]} \times \frac{k_2}{k_4}$ in equation 16) can approach 1. Anyway, even if in this case the rate depends on [N_2O], from the rate dependence on the concentration of this substrate, the plateau that is reached at high values does not indicate that the enzyme is saturated with N_2O but only that $\frac{K_{MS}}{[S]} \times \frac{k_2}{k_4}$ (and not $\frac{K_{MS}}{[S]}$, as it would happen in the case of saturation) could be neglected in equation 16).

2.7.2 Simulation of the catalytic activity of N_2OR with cytochrome c_{552} and N_2O

Experimental data:

- In the catalytic reaction with MV as reducing agents the enzyme follows a Michaelis Menten rate profile with both the substrates. The kinetic parameters are as follows:

For MV:

K_M = (11.5 ± 3.6) μM

k_{cat} = (321 ± 27) s^{-1}

For N_2O

K_M = (14.0 ± 2.9) μM

k_{cat} = (275 ± 33) s^{-1}

- When cytochrome c_{552} is used as reducing agent the reaction rates follow a Michaelis Menten profile with the substrate cytochrome c_{552}, while no rate dependence on [N_2O] was observed in the range 5 – 500 μM.

For cytochrome c_{552}:

K_M = (50.2 ± 9.0) μM

k_{cat} = (3.8 ± 1.3) s^{-1}

In the simulation of the rate dependence on substrate concentration two mechanisms (A and B) could be taken into consideration according to the mechanism followed in the catalytic cycle (see above for details).

Case A:

$$E \underset{K_{B-c552}}{\overset{c552}{\rightleftharpoons}} ER \underset{K_{B-N2O}}{\overset{N_2O}{\rightleftharpoons}} ERS \xrightarrow{k_{cat}} E + product$$

17) $$\frac{rate}{[N_2OR]} = \frac{k_{cat} \times [c_{552}] \times [N_2O]}{\frac{1}{K_{B-c552} \times K_{B-N2O}} + \frac{1}{K_{B-N2O}} \times [c_{552}] + [c_{552}] \times [N_2O]}$$

Where E is N_2OR, ER is the reduced enzyme after reaction with the reducing substrate, ERS is the reduced enzyme with N_2O bound in the active site. $K_{B\text{-}c552}$ is the binding constant for cytochrome $_{c552}$ to the enzyme and could be approximated with the reciprocal of the Michaelis constant experimentally obtained for this substrate ($K_{B\text{-}c552} \approx 1/ K_M$).

$K_{B\text{-}N2O}$ is the binding constant of N_2O to the reduced enzyme and k_{cat} is the maximum reaction rate for the reduction of nitrous oxide. The data for N_2O are not experimentally available but they can be assumed to be similar to those obtained in the experiments with MV as reducing agent. Here again the binding constant can be approximated as the reciprocal of the Michaelis constant.

Introducing the experimental rate constants into the rate equation, the value of rate/$[N_2O]$ can be obtained for different $[c_{552}]$ and $[N_2O]$. The figure S1 shows simulated results for different nitrous oxide concentrations and with $[c_{552}]$ of 10, 50, 150 and 250 μM. The graph also reports, in the upper trace, the simulated profile for the reaction with a fully saturated (with cytochrome c_{552}) N_2OR, which is indicated as simulated Michaelis Menten (simulated MM). All the graphs are Michaelis Menten-like, and increasing the reducing agent concentration the rate value must approach the very high values obtained with MV as reducing agent.

This behaviour is completely different from that experimentally observed with cytochrome c_{552}, where low and constant rates were observed in the $[c_{552}]$ range studied.

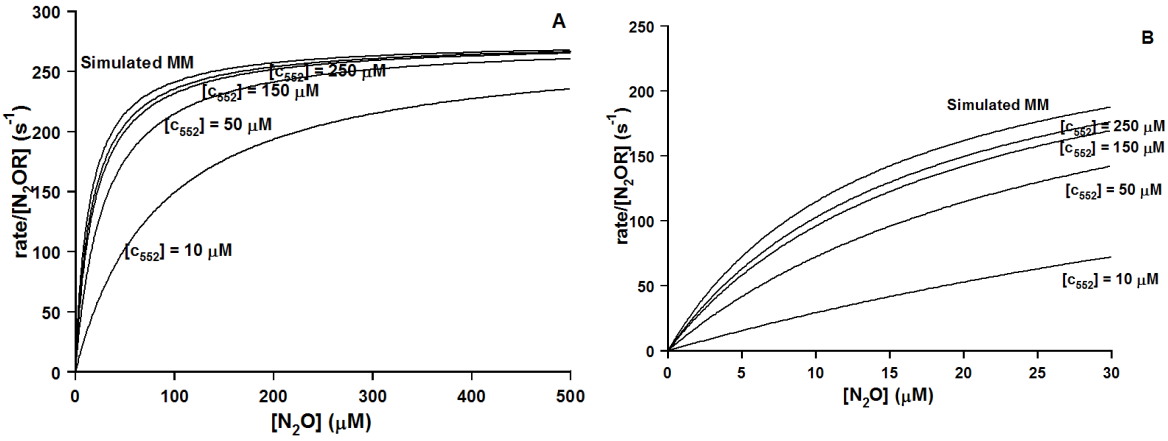

Figure 2.S1 - Simulated kinetic activity of N_2OR as a function of N_2O concentration with cytochrome c_{552} as electron donor. The curves are simulated using equation 17 and [cytochrome c_{552}] of 10, 50, 150 and 250 μM. The upper curve is the reaction with a fully saturated (with cytochrome c_{552}) N_2OR, which is indicated as simulated MM. In panel A, the $[N_2O]$ range is the same as the one used in the experiment described in the manuscript (5 – 500 μM), while panel B shows an inset with $[N_2O]$ between 0 and 30 μM.

Case B)

$$E \underset{k_{-1}}{\overset{k_1\times[c552]}{\rightleftarrows}} ER \xrightarrow{k_{cat-c552}} I \underset{k_{-3}}{\overset{k_3\times[S]}{\rightleftarrows}} IS \xrightarrow{k_{cat-N2O}} E + products$$

18) $$\frac{rate}{[N_2OR]} = \frac{k_{cat-N2O}}{1+\frac{k_{cat-N2O}}{k_{cat-c552}}+\frac{K_{M-N2O}}{[N_2O]}+\frac{K_{M-c552}}{[c_{552}]}\times\frac{k_{cat-N2O}}{k_{cat-c552}}}$$

where E represents N_2OR the enzyme; ER indicates the native enzyme with a bound c_{552} molecule; I is the reduced enzyme and IS is its complex with the substrate N_2O; the k constants linked to the arrows are the rate constants for the individual steps.

$K_{M\text{-}c552}$ and $k_{cat\text{-}c552}$ are the Michaelis constant and the turnover number for cytochrome c_{552}, respectively, which have been experimentally obtained for this substrate.

$K_{M\text{-}N2O}$ and $k_{cat\text{-}N2O}$ are not experimentally available but they can be assumed to be similar to those obtained in the experiments with MV as reducing agent.

Introducing the experimental rate constants into the rate equation, the value of rate/$[N_2O]$ can be obtained for different $[c_{552}]$ and $[N_2O]$. The figure S2 shows simulated results for different nitrous oxide concentrations and with $[c_{552}]$ of 10, 50, 150 and 250 μM. The graph also reports, in the steepest trace, the simulated profile for a hypothetical reaction in which the reduction

process with cytochrome c_{552}, is fast ($k_{cat\text{-}c552}$ >> $k_{cat\text{-}N2O}$); this trace has been indicated as simulated Michaelis Menten (simulated MM).

The graphs simulated with the equation above show a hyperbolic behaviour localised at very low N_2O concentrations and a plateau at [N_2O] above 1 µM. The reaction rates are always very low and do not approach the maximum activity the enzyme could reach for the reduction of N_2O (simulated MM trace).

This behaviour perfectly agrees with that experimentally observed with cytochrome c_{552}, where low and constant rates were observed in the [c_{552}] range studied.

It should be noted that extending the observation range to a region in which the rates depend on [N_2O] would require a very low substrate concentration. Furthermore, these data would be useless for the characterization of the activity of the enzyme toward N_2O.

The graphs also show that using higher concentrations of cytochrome c_{552} would only slightly increase the observed rates but the rate will remain always much lower compared with the simulated MM.

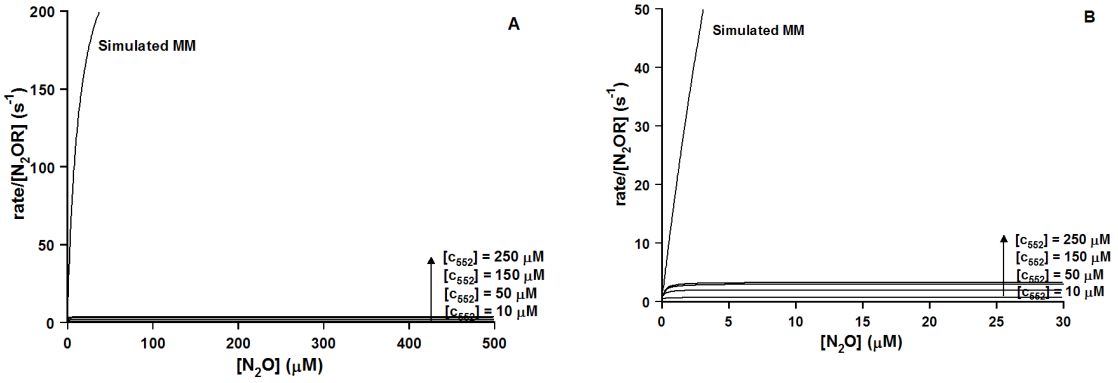

Figure 2.S2 - Simulated kinetic activity of N_2OR as function of N_2O concentration with cytochrome c_{552} as electron donor. The curves are simulated using equation 18 and [cytochrome c_{552}] of 10, 50, 150 and 250 µM. The upper curve is the reaction with a fully saturated (with cytochrome c_{552}) N_2OR, which is indicated as simulated MM. In panel A, the [N_2O] range is the same as the one used in the experiment described in the manuscript (5 – 500 µM), while panel B shows an inset with [N_2O] between 0 and 30 µM.

2.8 References

1. Zumft, W. G., and Kroneck, P. M. (2007) Respiratory transformation of nitrous oxide (N2O) to dinitrogen by Bacteria and Archaea, *Adv Microb Physiol 52*, 107-227.
2. Tavares, P., Pereira, A. S., Moura, J. J., and Moura, I. (2006) Metalloenzymes of the denitrification pathway, *J Inorg Biochem 100*, 2087-2100.
3. Brown, K., Tegoni, M., Prudencio, M., Pereira, A. S., Besson, S., Moura, J. J., Moura, I., and Cambillau, C. (2000) A novel type of catalytic copper cluster in nitrous oxide reductase, *Nat Struct Biol 7*, 191-195.
4. Haltia, T., Brown, K., Tegoni, M., Cambillau, C., Saraste, M., Mattila, K., and Djinovic-Carugo, K. (2003) Crystal structure of nitrous oxide reductase from Paracoccus denitrificans at 1.6 A resolution, *Biochem J 369*, 77-88.
5. Paraskevopoulos, K., Antonyuk, S. V., Sawers, R. G., Eady, R. R., and Hasnain, S. S. (2006) Insight into catalysis of nitrous oxide reductase from high-resolution structures of resting and inhibitor-bound enzyme from Achromobacter cycloclastes, *J Mol Biol 362*, 55-65.
6. Winkler, J. R. (2000) Electron tunneling pathways in proteins, *Curr Opin Chem Biol 4*, 192-198.
7. Kroneck, P. M., Antholine, W. A., Riester, J., and Zumft, W. G. (1989) The nature of the cupric site in nitrous oxide reductase and of CuA in cytochrome c oxidase, *FEBS Lett 248*, 212-213.
8. Farrar, J. A., Zumft, W. G., and Thomson, A. J. (1998) CuA and CuZ are variants of the electron transfer center in nitrous oxide reductase, *PNAS 95*, 9891-9896.
9. Farrar, J. A., Lappalainen, P., Zumft, W. G., Saraste, M., and Thomson, A. J. (1995) Spectroscopic and mutagenesis studies on the CuA centre from the cytochrome-c oxidase complex of Paracoccus denitrificans, *Eur J Biochem 232*, 294-303.
10. Prudencio, M., Pereira, A. S., Tavares, P., Besson, S., Cabrito, I., Brown, K., Samyn, B., Devreese, B., Van Beeumen, J., Rusnak, F., Fauque, G., Moura, J. J., Tegoni, M., Cambillau, C., and Moura, I. (2000) Purification, characterization, and preliminary crystallographic study of copper-containing nitrous oxide reductase from Pseudomonas nautica 617, *Biochemistry 39*, 3899-3907.
11. Rasmussen, T., Berks, B. C., Butt, J. N., and Thomson, A. J. (2002) Multiple forms of the catalytic centre, CuZ, in the enzyme nitrous oxide reductase from Paracoccus pantotrophus, *Biochem J 364*, 807-815.
12. Chen, P., Cabrito, I., Moura, J. J., Moura, I., and Solomon, E. I. (2002) Spectroscopic and electronic structure studies of the mu(4)-sulfide bridged tetranuclear Cu(Z) cluster in N(2)O reductase: molecular insight into the catalytic mechanism, *J Am Chem Soc 124*, 10497-10507.
13. Chen, P., Gorelsky, S. I., Ghosh, S., and Solomon, E. I. (2004) N2O reduction by the mu4-sulfide-bridged tetranuclear CuZ cluster active site, *Angew Chem Int Ed Engl 43*, 4132-4140.
14. Clark, W. M. (1960) Oxidation-Reduction Potentials of Organic Systems, *Williams and Wilkins, Baltimore*.
15. Ghosh, S., Gorelsky, S. I., Chen, P., Cabrito, I., Moura, J. J., Moura, I., and Solomon, E. I. (2003) Activation of N2O reduction by the fully reduced micro4-sulfide bridged tetranuclear Cu Z cluster in nitrous oxide reductase, *J Am Chem Soc 125*, 15708-15709.
16. Chan, J. M., Bollinger, J. A., Grewell, C. L., and Dooley, D. M. (2004) Reductively activated nitrous oxide reductase reacts directly with substrate, *J Am Chem Soc 126*, 3030-3031.
17. Fujita, K., Chan, J. M., Bollinger, J. A., Alvarez, M. L., and Dooley, D. M. (2007) Anaerobic purification, characterization and preliminary mechanistic study of recombinant nitrous oxide reductase from Achromobacter cycloclastes, *J Inorg Biochem 101*, 1836-1844.
18. Berks, B. C., Baratta, D., Richardson, J., and Ferguson, S. J. (1993) Purification and characterization of a nitrous oxide reductase from Thiosphaera pantotropha. Implications for the mechanism of aerobic nitrous oxide reduction, *Eur J Biochem 212*, 467-476.
19. Richardson, D. J., Bell, L. C., McEwan, A. G., Jackson, J. B., and Ferguson, S. J. (1991) Cytochrome c2 is essential for electron transfer to nitrous oxide reductase from physiological substrates in Rhodobacter capsulatus and can act as an electron donor to the reductase in vitro. Correlation with photoinhibition studies, *Eur J Biochem 199*, 677-683.
20. Zhang, C. S., and Hollocher, T. C. (1993) The reaction of reduced cytochromes *c* with nitrous oxide reductase ot *Wolinella succinogenes*, *Biochim. Biophys. Acta 1142*, 253-261.

21. Rasmussen, T., Brittain, T., Berks, B. C., Watmough, N. J., and Thomson, A. J. (2005) Formation of a cytochrome c-nitrous oxide reductase complex is obligatory for N2O reduction by Paracoccus pantotrophus, *Dalton Trans*, 3501-3506.
22. Pearson, I. V., Page, M. D., van Spanning, R. J. M., and Ferguson, S. J. (2003) A Mutant of Paracoccus denitrificans with Disrupted Genes Coding for Cytochrome c550 and Pseudoazurin Establishes These Two Proteins as the In Vivo Electron Donors to Cytochrome cd1 Nitrite Reductase, *J. Bacteriol. 185*, 6308-6315.
23. Mattila, K., and Haltia, T. (2005) How does nitrous oxide reductase interact with its electron donors?--A docking study, *Proteins 59*, 708-722.
24. Lowry, O. H., Rosebrough, N. J., Farr, A. L., and Randall, R. J. (1951) PROTEIN MEASUREMENT WITH THE FOLIN PHENOL REAGENT, *J. Biol. Chem. 193*, 265-275.
25. Fauque G, M. J., Besson S, Saraiva L, Moura I (1992) Caractérisation préliminaire du système cytochromique de la bactérie marine dénitricante Pseudomonas nautica 617, *Oceanis 18*, 211-216.
26. Saraiva, L. M., Besson, S., Moura, I., and Fauque, G. (1995) Purification and preliminary characterization of three c-type cytochromes from Pseudomonas nautica strain 617, *Biochem Biophys Res Commun 212*, 1088-1097.
27. Saraiva, L. M., Fauque, G., Besson, S., and Moura, I. (1994) Physico-chemical and spectroscopic properties of the monohemic cytochrome C552 from Pseudomonas nautica 617, *Eur J Biochem 224*, 1011-1017.
28. Saraiva, L. M., Besson, S., Fauque, G., and Moura, I. (1994) Characterization of the dihemic cytochrome c549 from the marine denitrifying bacterium Pseudomonas nautica 617, *Biochem Biophys Res Commun 199*, 1289-1296.
29. Van Gelder, B. F., and Slater, E. C. (1962) The extinction coefficient of cytochrome c, *Biochim. Biophys. Acta 58*, 593-595.
30. Kristjansson, J. K., and Hollocher, T. C. (1980) First practical assay for soluble nitrous oxide reductase of denitrifying bacteria and a partial kinetic characterization, *J. Biol. Chem. 255*, 704-707.
31. Pettigrew, G. W., Pauleta, S. R., Goodhew, C. F., Cooper, A., Nutley, M., Jumel, K., Harding, S. E., Costa, C., Krippahl, L., Moura, I., and Moura, J. (2003) Electron transfer complexes of cytochrome c peroxidase from Paracoccus denitrificans containing more than one cytochrome, *Biochemistry 42*, 11968-11981.
32. Palma, P. N., Krippahl, L., Wampler, J. E., and Moura, J. J. (2000) BiGGER: a new (soft) docking algorithm for predicting protein interactions, *Proteins 39*, 372-384.
33. Jones, S., and Thornton, J. M. (1996) Principles of protein-protein interactions, *PNAS 93*, 13-20.
34. Pauleta, S. R., Guerlesquin, F., Goodhew, C. F., Devreese, B., Van Beeumen, J., Pereira, A. S., Moura, I., and Pettigrew, G. W. (2004) Paracoccus pantotrophus pseudoazurin is an electron donor to cytochrome c peroxidase, *Biochemistry 43*, 11214-11225.
35. Lo Conte, L., Chothia, C., and Janin, J. (1999) The atomic structure of protein-protein recognition sites, *J Mol Biol 285*, 2177-2198.
36. Lopes, H., Besson, S., Moura, I., and Moura, J. J. (2001) Kinetics of inter- and intramolecular electron transfer of Pseudomonas nautica cytochrome cd1 nitrite reductase: regulation of the NO-bound end product, *J Biol Inorg Chem 6*, 55-62.
37. Martins, C. E., Pereira, A. S., Tavares, P., Cordas, C. M., Folgosa, F., Timóteo, C. G., Naik, S., Huynh, B. H., Moura, J. J. G., and Moura, I. (2007) Redox states of Nitric Oxide Reductase from Pseudomonas nautica: Kinetic and Spectroscopic characterization, *J Biol Inorg Chem 12*, S53-98.
38. Alves, T., Besson, S., Duarte, L. C., Pettigrew, G. W., Girio, F. M., Devreese, B., Vandenberghe, I., Van Beeumen, J., Fauque, G., and Moura, I. (1999) A cytochrome c peroxidase from Pseudomonas nautica 617 active at high ionic strength: expression, purification and characterization, *Biochim Biophys Acta 1434*, 248-259.
39. Wunsch, P., Korner, H., Neese, F., van Spanning, R. J., Kroneck, P. M., and Zumft, W. G. (2005) NosX function connects to nitrous oxide (N2O) reduction by affecting the Cu(Z) center of NosZ and its activity in vivo, *FEBS Lett 579*, 4605-4609.
40. Yamaguchi, K., Kawamura, A., Ogawa, H., and Suzuki, S. (2003) Characterization of Nitrous Oxide Reductase from a Methylotrophic Denitrifying Bacterium, Hyphomicrobium denitrificans A3151, *J. Biochem. (Tokyo) 134*, 853-858.

41. Bertini, I., and Luchinat, C. (1996) Hyperfine shift and relaxation in the presence of chemical exchange, *Coord. Chem. Rev. 150*, 111-130.
42. Crowley, P. B., and Carrondo, M. A. (2004) The architecture of the binding site in redox protein complexes: implications for fast dissociation, *Proteins 55*, 603-612.
43. Williams, P. A., Fulop, V., Leung, Y. C., Chan, C., Moir, J. W., Howlett, G., Ferguson, S. J., Radford, S. E., and Hajdu, J. (1995) Pseudospecific docking surfaces on electron transfer proteins as illustrated by pseudoazurin, cytochrome c550 and cytochrome cd1 nitrite reductase, *Nat Struct Biol 2*, 975-982.
44. Witt, H., Malatesta, F., Nicoletti, F., Brunori, M., and Ludwig, B. (1998) Tryptophan 121 of Subunit II Is the Electron Entry Site to Cytochrome-c Oxidase in Paracoccus denitrificans. INVOLVEMENT OF A HYDROPHOBIC PATCH IN THE DOCKING REACTION, *J. Biol. Chem. 273*, 5132-5136.
45. Kukimoto, M., Nishiyama, M., Ohnuki, T., Turley, S., Adman, E. T., Horinouchi, S., and Beppu, T. (1995) Identification of interaction site of pseudoazurin with its redox partner, copper-containing nitrite reductase from Alcaligenes faecalis S-6, *Protein Eng. 8*, 153-158.
46. Gorelsky, S. I., Ghosh, S., and Solomon, E. I. (2006) Mechanism of N2O reduction by the mu4-S tetranuclear CuZ cluster of nitrous oxide reductase, *J Am Chem Soc 128*, 278-290.
47. Granata, A., Monzani, E., and Casella, L. (2004) Mechanistic insight into the catechol oxidase activity by a biomimetic dinuclear copper complex, *J Biol Inorg Chem 9*, 903-913.
48. Casella, L., Carugo, O., Gullotti, M., Garofani, S., and Zanello, P. (1993) Hemocyanin and tyrosinase models. Synthesis, azide binding, and electrochemistry of dinuclear copper(II) complexes with poly(benzimidazole) ligands modeling the met forms of the proteins, *Inorg. Chem. 32*, 2056-2067.
49. Torelli, S., Belle, C., Gautier-Luneau, I., Pierre, J. L., Saint-Aman, E., Latour, J. M., Le Pape, L., and Luneau, D. (2000) pH-Controlled Change of the Metal Coordination in a Dicopper(II) Complex of the Ligand H-BPMP: Crystal Structures, Magnetic Properties, and Catecholase Activity, *Inorg. Chem. 39*, 3526-3536.
50. Ghosh, S., Gorelsky, S. I., George, S. D., Chan, J. M., Cabrito, I., Dooley, D. M., Moura, J. J., Moura, I., and Solomon, E. I. (2007) Spectroscopic, computational, and kinetic studies of the mu4-sulfide-bridged tetranuclear CuZ cluster in N2O reductase: pH effect on the edge ligand and its contribution to reactivity, *J Am Chem Soc 129*, 3955-3965.

Chapter 3

A new CuZ active form in the catalytic reduction of N_2O by N_2OR

3.1 Abstract

The final step of bacterial denitrification, the two-electron reduction of N_2O to N_2, is catalyzed by a multi-copper enzyme named nitrous oxide reductase. The catalytic centre of this enzyme is a tetranuclear copper site called CuZ, unique in biological systems. The *in vitro* reconstruction of the activity requires a slow activation in the presence of the artificial electron donor, reduced methylviologen, necessary to reduce CuZ from the resting non-active state ($1Cu^{II}/3Cu^{I}$) to the fully reduced state ($4\ Cu^{I}$), in contrast to the turnover cycle that is very fast. In the present work, the direct reaction of the activated form of *Pseudomonas nautica* nitrous oxide reductase with stoichiometric amounts of N_2O allowed the identification of a new reactive intermediate of the catalytic centre, CuZ°, in the turnover cycle, characterized by an intense absorption band at 680 nm. Moreover, the first mediated electrochemical study of *Pseudomonas nautica* nitrous oxide reductase with its physiological electron donor, cytochrome c_{552}, was performed. The intermolecular electron transfer was analysed by cyclic voltammetry, under catalytic conditions, and a second-order rate constant (k) of $(5.5 \pm 0.9) \times 10^5\ M^{-1}s^{-1}$ was determined. Both the reaction of stoichiometric amounts of substrate and the electrochemical studies show that the active CuZ° species, generated in the absence of

reductants, can rearrange to the resting non-active CuZ state. In this light, new aspects of the catalytic and activation/inactivation mechanism of the enzyme are discussed.

This chapter has been published in J. Biol. Inorg. Chem, **15**, 967-976 (2010), *"A New CuZ Active Form in the Catalytic Reduction of N_2O by Nitrous Oxide Reductase from Pseudomonas Nautica"* S. Dell'Acqua, S.R. Pauleta, P.M. Paes de Sousa, E. Monzani, L. Casella, J.J.G. Moura, I. Moura

3.2 Introduction

The multi-copper enzyme nitrous oxide reductase (N_2OR) catalyzes the final step of bacterial dissimilatory denitrification ($2\ NO_3^- \rightarrow 2\ NO_2^- \rightarrow 2\ NO \rightarrow N_2O \rightarrow N_2$), namely the two-electron reduction of the kinetically inert molecule nitrous oxide (N_2O) to dinitrogen (N_2) and water (*1, 2*).

Recently the structure of N_2OR was solved from *Pseudomonas nautica* (*Pn*) (*3*), *Paracoccus denitrificans* (*Pd*) (*4*) and *Achromobacter cycloclastes* (*Ac*) (*5*). The crystal structure revealed that N_2OR is a functional homodimer containing two different multicopper centres per subunit, called CuA and CuZ.

The binuclear copper centre, CuA, is an electron transfer centre similar to the CuA found in cytochrome oxidases and its properties have been extensively studied (*6-9*). CuZ is a novel mixed-valence copper center (Cu_4S) with a sulfide ion bridging a distorted tetrahedron of copper atoms, a unique structural feature in biology. This cluster is coordinated by seven histidines, while a water-derived ligand is proposed to bridge the two copper ions (CuI and CuIV), where the substrate binds to the enzyme.

The CuZ from *Pn* N_2OR, in the as-isolated state, contains a $1Cu^{II}/3Cu^{I}$ redox state with a total spin of ½, where the unpaired electron is delocalized between two or more copper atoms through the bridging sulfide ion (*10-12*). This state, which has a typical electronic spectral band at 640 nm and a 4-line splitting EPR signature (*13, 14*), cannot be easily reduced or oxidized. The catalytically active, fully reduced form ($4Cu^{I}$) can be obtained only after a prolonged incubation with reduced methylviologen (MV) (*15, 16*).

In contrast, the catalytic centre, CuZ, of *Pd* N_2OR has been identified in two forms, named CuZ and CuZ*, with the relative proportion between them depending on the purification conditions (*17*). In particular the CuZ* form, characterized by an intense absorption band at 650 nm, is more abundant in the 'aerobic' preparation, while the CuZ form, with an absorption band at 670 nm, is predominant in the 'anaerobic' purification. CuZ* is redox inert while the CuZ midpoint potential was calculated to be E°' = 60 mV (vs NHE). Despite this feature, the 'aerobic' preparation shows a slightly higher steady-state activity compared to the 'anaerobic'

preparation. In addition, the CuZ form shows an EPR spectrum similar to the CuZ* form, suggesting a $1Cu^{II}/3Cu^{I}$ redox state for both species (*17*).

In the previous chapter of this thesis, the catalytic parameters of *Pn* N_2OR activity were determined to compare the physiological (*Pn* cytochrome c_{552}) and artificial (MV) electron donors (*18*). This study revealed that these two electron donors have a distinct mechanism of interaction towards the enzyme, when cytochrome c_{552} was used as electron donor a k_{cat} = 3.8 s^{-1}, a K_m = 50.2 μM and a pK_a = 8.3 were estimated, while when an artificial electron donor, MV, was used a k_{cat} = 320 s^{-1}, a K_m = 11.5 μM and a pK_a = 6.6 were obtained.

We present here the first mediated electrochemical study of N_2OR with its physiological electron donor, cytochrome c_{552}. The electrochemical behaviour of this cytochrome has been well characterized (*19*), and it has already been shown to be the electron donor of other enzymes isolated from *Pn*, cytochrome *c* peroxidase (*20*) and cytochrome cd_1 nitrite reductase (*21*). In the latter case the electron transfer reaction was also investigated using electrochemical techniques.

In order to understand the complex mechanism of activation and catalysis of N_2OR CuZ, we have also studied the properties of the enzyme in the activated form by direct reaction of N_2OR with stoichiometric amounts of substrate in the absence of reductants. The identification of a new active intermediate of the catalytic centre, CuZ°, led us to revise both the catalytic and the activation mechanism of this challenging enzyme.

3.3 Materials and Methods

3.3.1 Protein purification

N_2OR was purified from *Pseudomonas nautica* 617 (also known as *Marinobacter hydrocarbonoclasticus* 617) cellular extract as previously described (*13*), with some minor modifications. Enzyme concentrations were determined by the Lowry method (*22*).

Pn cytochrome c_{552} was purified as previously described (*23*), with some minor modifications. The concentration of cytochrome c_{552} was determined spectrophotometrically using the extinction coefficient at 552 nm, ε = 19.3 $mM^{-1}cm^{-1}$ (*24*), for the fully reduced form.

3.3.2 Enzyme activation and activity assay

Enzyme activation was performed in the glove box as previously described in Chapter 2 (*18*). The activity assay used was the one described previously (*18*), using methylviologen as the electron donor.

3.3.3 Electrochemical methods

Voltammetric measurements were performed using a potentiostat/galvanostat AUTOLAB/PSTAT 12 from ECO Chemie (Utrecht, The Netherlands). Data were analysed with the GPES software package from ECO Chemie. A conventional three-electrode configuration cell was used, with a platinum auxiliary electrode and a SCE reference electrode (+ 244 mV *vs* SHE). The working electrode was a pyrolytic graphite (PG) electrode, with a 3 mm diameter (surface area = 0.07 cm^2), which was used in a membrane configuration (*19*). Throughout the paper, all potentials are referred to the standard hydrogen electrode (SHE).

Before each experiment, the PG electrode was polished by hand on a polishing cloth (Buehler 40-7212) using a water–alumina slurry (0.05 μm, Buehler 40-6365-006), sonicated for 5 min and rinsed carefully with Milli-Q water. The membrane electrode was prepared by dropping a 5 μl drop, containing 2.5 μM pre-activated N_2OR and 50 μM oxidised cytochrome c_{552}, on a small square (10 mm x 10 mm) of negatively charged Spectra/Por MWCO 3500 dialysis membrane. The membrane was fitted tightly to the electrode with a rubber O-ring.

In typical experiments, the working solution contained 0.1 M phosphate buffer pH 7.0, the scan rate was 40 mV/s, and cyclic voltammograms were obtained in the range of + 0.6 V to – 0.25 V *vs* SHE.

For the scan rate dependence of the catalytic current, cyclic voltammograms were performed between 5 and 100 mV/s. In the determination of the N_2O concentration dependence of the catalytic current, 8, 17, 25, 33, 48, 125, 330 and 1000 μM N_2O were added as N_2O-saturated water. In the pH dependence studies of the catalytic current, the following buffers were used: 0.1 M potassium phosphate buffer at pH 5.9, 6.2, 6.4, 6.7 and 7.0, or 0.1 M Tris-HCl at pH 7.3, 7.6, 8.0, 8.4 and 8.8. All the electrochemical experiments were performed inside a glove-box filled with an argon-saturated atmosphere.

3.3.4 Direct reaction of N_2OR with substrate

For the direct reaction of the enzyme with substrate, an equimolar amount of N_2O was added to 35 μM N_2OR pre-activated in 0.1 M Tris-HCl at pH 7.6. The reaction was followed using a TIDAS diode array spectrophotometer. At corresponding incubation times of each UV-visible spectrum, an aliquot of this solution was taken in order to determine the enzyme activity, using MV-reduced with sodium dithionite as electron donor, as previously described (*18*).

3.3.5 EPR spectroscopy

X-band EPR spectra were recorded using a Bruker EMX spectrometer equipped with a rectangular cavity (model ER4102ST) and an Oxford Instruments continuous-flow cryostat. EPR spectra were simulated using the program WINEPR Simfonia version 1.2 from Bruker Instruments.

The sample of the enzyme form characterized by the 680 nm absorption band was prepared under anaerobic conditions (glove box) by mixing 75 μM of pre-activated N_2OR and an equimolar amount of N_2O, in 0.1 M Tris-HCl. The EPR tube was frozen with liquid nitrogen 1 minute after the addition of N_2O. The resting CuZ form, with absorption at 640 nm, was obtained by exposing the previous sample to air for 30 min. Experimental conditions are described in the Figure legend.

3.3.6 Redox titration

Pre-activated N_2OR (35 μM) in 0.1 M Tris-HCl pH 7.6 was titrated in a 1 ml cuvette. The potential was measured with a platinum–silver/silver chloride combined electrode (Crison). The oxidative experiments were performed with addition of potassium ferricyanide (E = + 420 mV *vs* SHE) and the reaction was followed by UV-visible spectra. The following mediators were added each at 2 μM concentration: 1,2-naphthoquinone-4-sulfonic acid, 1,2-naphthoquinone, phenazine methosulphate, resorufin (2,8-dihydroxyphenoxazine), indigodisulfonate, 2-hydroxy-1,4-naphthoquinone and methylviologen. The titration was performed in a glove box.

3.4 Results and discussion

3.4.1 Electrocatalytic activity of Pn N_2OR with cytochrome c_{552} as electron donor

The catalytic activity of *Pn* N_2OR for N_2O reduction was analysed for the first time by mediated electrochemistry using *Pn* cytochrome c_{552}, a small electron transfer protein that was established to be the physiological redox partner of this enzyme (*18*). For this purpose, both redox partners were entrapped between the electrode surface and a dialysis membrane (*25*) and cyclic voltammetry was performed.

In the absence of cytochrome c_{552}, pre-activated or non pre-activated N_2OR do not exhibit any electrochemical signal, probably due to the incompatibility of the negatively charged graphite electrode surface and the negatively charged surface of *Pn* N_2OR (pI = 5.4). Moreover, no catalytic current was observed in these conditions upon addition of nitrous oxide to pre-activated N_2OR within the potential range used.

In previous reports, cytochrome c_{552} was shown to exhibit a well defined direct electrochemical signal at a carbon membrane electrode (*19*). In our experimental conditions, this reversible electrochemical behaviour was also verified and the calculated redox potential, $E^{0'}$ = + (245 ± 5) mV *vs* SHE at pH 7, is in agreement with the one reported on that study. In our work, although the membrane configuration was used, the peak currents of cytochrome c_{552} varied linearly with the square root of the scan rate, as expected for a diffusion controlled process, a behaviour that has also been observed in other studies for this type of proteins with this electrode configuration (*26*).

The cyclic voltammograms of cytochrome c_{552} alone (data not shown) and the ones in the presence of pre-activated N_2OR are identical (Figure 3.1 – continuous line). Upon addition of a saturating amount of substrate, N_2O, the original peak shaped voltammogram transforms into the characteristic sigmoid catalytic wave, with a steady-state current plateau (Figure 3.1 – dashed line).

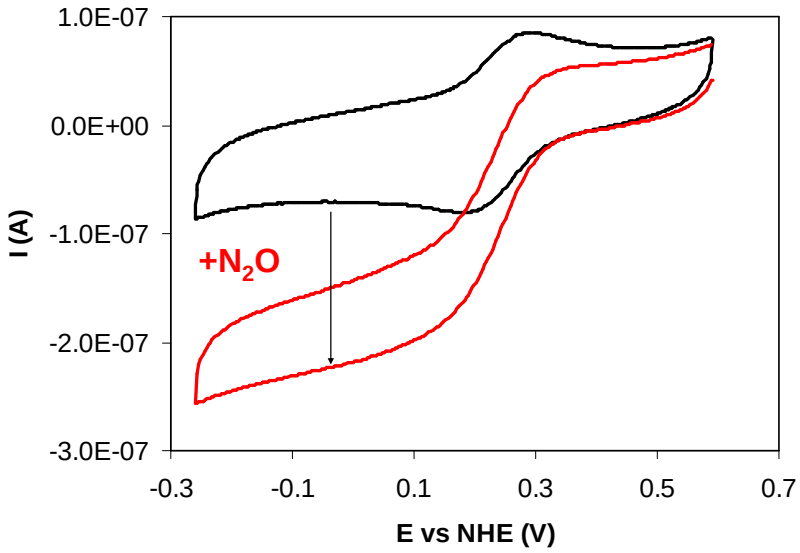

Figure 3.1 – Cyclic voltammograms (40 mVs^{-1}) of 50 µM cytochrome c_{552} entrapped in a membrane electrode with 2.5 µM activated *Pseudomonas nautica* N_2OR, in 0.1 M phosphate buffer, pH 7. The black-line is the CV in the absence of substrate and the red-line is the CV after addition of 1 mM N_2O.

This behaviour can be interpreted with the reaction mechanism shown in Scheme 3.1. An initial heterogeneous electron-transfer reaction at the electrode (Step 1) is followed by two homogeneous chemical reactions: the reduced form of cytochrome c_{552} is oxidised by N_2OR (Step 2) which is then regenerated by N_2O (Step 3).

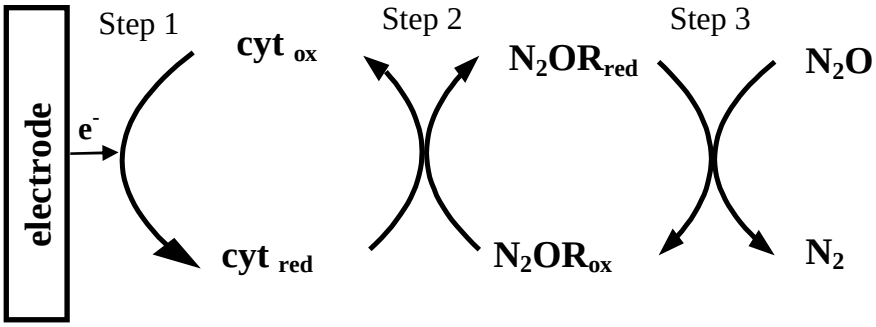

Scheme 3.1 – Mediation scheme for N_2OR: the electrode reduces cytochrome c_{552}, which is immediately reoxidized by N_2OR; the level of oxidized N_2OR is then restored by conversion of N_2O to N_2.

This mechanism can be simplified to

$$\text{Cyt } c_{552ox} + e^- \rightleftharpoons \text{Cyt } c_{552red} \quad (1)$$

$$\text{Cyt } c_{552red} + N_2OR_{ox} \rightarrow \text{Cyt } c_{552ox} + N_2OR_{red} \quad (2)$$

$$N_2OR_{red} + N_2O \rightarrow N_2OR_{ox} + N_2 \quad (3)$$

as long as four conditions are obeyed: (1) the heterogeneous electron transfer (Step 1) is a reversible reaction; (2) the homogeneous chemical reaction (Step 2) is irreversible; (3) the reaction between cytochrome c_{552} and N_2OR is pseudo-first order with the reaction rate constant given by $k' = k\,[N_2OR]$, where k is the second-order rate constant; (4) reaction 3 is fast.

As reported in (*19*) and confirmed in this work, the first condition is verified. The experiments were performed under an excess of the substrate N_2O, thus the enzyme is reoxidized by the catalytic reaction (Step 3), and not by transferring electrons back to cytochrome c_{552}. For this reason, the second condition is obeyed. Condition 3 implies that the enzyme concentration is much higher than that of cytochrome c_{552}. Although this is not the case, the saturating concentration of N_2O guarantees that the oxidized form of the enzyme is quickly restored by Step 3, as long as the latter is not rate-limiting (condition 4). Therefore, N_2OR will always be available to react with cytochrome c_{552} and pseudo-first order conditions are met.

According to the theory of steady-state voltammetric catalysis, the rate constant can only be determined from the steady state catalytic current if the latter is not scan rate dependent (*27, 28*). For the mediated catalysis of N_2OR by cytochrome c_{552}, the catalytic current increases linearly with the scan rate, between 5 and 40 mV/s, and then becomes independent of this parameter, up to 100 mV/s (data not shown). Moreover, the catalytic current decreases after the first scan, until the initial cytochrome c_{552} signal is restored. This behaviour, corroborated

by the fact that further addition of substrate does not restore the catalytic signal, suggests that the enzyme is being inactivated (see below).

The rate constant of the intermolecular electron transfer reaction between cytochrome c_{552} and N_2OR was estimated using two approaches, with the catalytic currents being measured at 40 mV/s. In one of the approaches, the CV data were processed according to the Nicholson and Shain theory (*27*), where the pseudo-first order rate constant, *k*', can be determined plotting the ratio between the catalytic current (the plateau current value, i_{cat}) and the diffusion-controlled currents (the cytochrome c_{552} reduction peak current, i_p) versus the reciprocal of the square root of the scan rate, *v*:

$$i_{cat}/i_p = 2.241(RT/nF)^{1/2}\, k'^{1/2}\, (1/v)^{1/2} \quad \text{(Equation 1)}$$

where *n* is the number of electrons exchanged, and *R*, *T*, and *F* are the universal gas constant, the temperature, and the Faraday constant, respectively. The cytochrome c_{552} redox reaction is a reversible one-electron process, and thus from the slope a *k*' value of 1.4 ± 0.2 s^{-1} was obtained. The intermolecular rate constant, *k*, for the reaction between N_2OR and cytochrome c_{552} at pH 7.0 was determined to be (5.4 ± 0.8) × 10^5 $M^{-1}s^{-1}$, since the enzyme concentration entrapped in the membrane was 2.5 μM.

In the other approach, *k* is calculated from the value of the N_2O-saturated limiting current, i_{cat} (*29-32*):

$$i_{cat} = nFAC_{cyt\,c}\,(D_{cyt\,c}\,k')^{1/2} \quad \text{(Equation 2)}$$

where, $C_{cyt\ c}$ is the concentration of cytochrome c_{552} under the membrane, D is its diffusion coefficient (D = 1.0 × 10^{-6} cm^2s^{-1} (*33*)) and *A* the electrode surface area (see Materials and Methods). Calculations with this equation gave *k* = (5.6 ± 0.4) × 10^5 $M^{-1}s^{-1}$ at pH 7.0, a value identical to the one obtained with the previous approach (Equation 1).

This value compares well with other intermolecular rate constants determined using cyclic voltammetry. Cytochrome c_{552} was used in mediated electrochemical experiments for the reduction of nitrite by *Pn* cytochrome cd_1 nitrite reductase (*21*) and a similar rate constant was calculated in that study (*k* = (4.1 ± 0.1) × 10^5 $M^{-1}s^{-1}$ at pH 6.3). Other examples are the electron transfer from *Ac* pseudoazurin to its electron donor, nitrite reductase, that was determined to have a *k* value of 7.3 × 10^5 $M^{-1}s^{-1}$ (*34*), and also the electron transfer between *Paracoccus pantotrophus* pseudoazurin and cytochrome *c* peroxidase with a *k* = 1.4 × 10^5 $M^{-1}s^{-1}$ (*25*).

This voltammetric theory implies that the catalytic current should be directly proportional to the mediator concentration. This condition is verified because the electrochemical experiments were performed at 50 μM, corresponding to the linear region of the Michaelis-Menten equation (K_{mc552} = 50 μM (Chapter 2 and ref. *18*)). However, investigation of the catalytic current at higher cytochrome c_{552} concentrations revealed a nonlinear behaviour

(data not shown), confirming that also cytochrome c_{552} contributes to the global rate with a Michaelis-Menten term (*18*).

It is possible to compare the second-order kinetic constant, k, calculated with the electrochemical approach (k = (5.5 ± 0.9) × 10^5 $M^{-1}s^{-1}$) with the ratio k_{cat}/K_m determined by the steady-state kinetic study ((7.6 ± 0.7) × 10^4 $M^{-1}s^{-1}$) (see Supplementary Materials). The difference between the two values can be attributed to the limitations of the steady-state kinetic study, where the k_{cat} and K_m were not determined with accuracy due to experimental problems at high cytochrome c_{552} concentrations (*18*).

The dependence of the electrochemical activity on the nitrous oxide concentration was studied using constant concentrations of N_2OR and cytochrome c_{552} entrapped in the membrane. The catalytic currents calculated for each substrate concentration were fitted to the Michaelis-Menten equation (Figure 3.2), using a K_m of (16 ± 2) μM and a i_{catmax} of (3.9 ± 0.1) × 10^{-7} A.

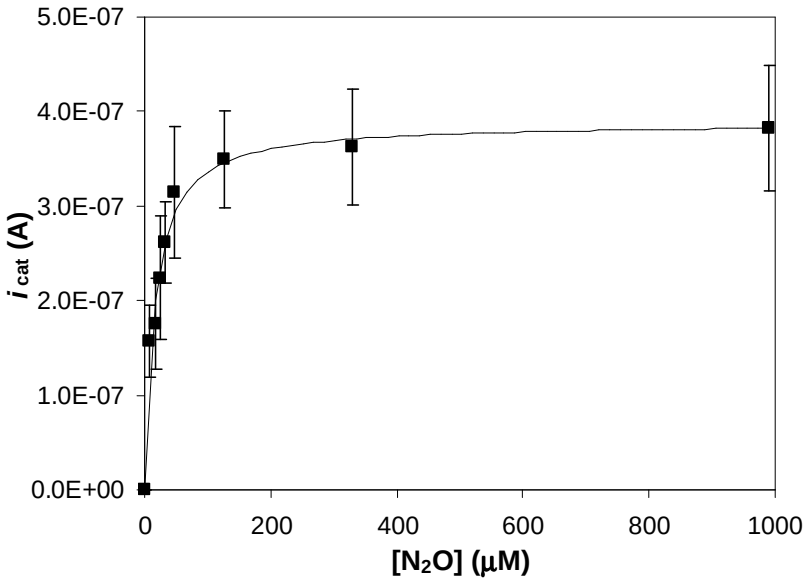

Figure 3.2 – Catalytic current from electrochemical assays of *Pn* N_2OR using cytochrome c_{552} as mediator *versus* N_2O concentration. The assays were performed with 2.5 μM activated N_2OR and 50 μM cytochrome c_{552} entrapped in the membrane electrode, in 0.1 M phosphate buffer at pH 7, and in the presence of 8, 17, 25, 33, 48, 125, 330, and 1000 μM N_2O-saturated water. The experimental data were fitted with the Michaelis-Menten equation, using a K_m of (16 ± 2) μM and a i_{catmax} of (3.9 ± 0.1) × 10^{-7} A.

The K_{mN2O}, with cytochrome c_{552} as an electron donor, could not be estimated in the steady-state activity assay because the N_2O reduction is involved in a fast step compared to the N_2OR reduction by cytochrome c_{552} (*18*). The value obtained in that study using MV as electron donor (K_{mN2O} = 14.0 ± 2.9 μM) is very similar to the one calculated by steady state kinetics, but it must be pointed out that using a stationary electrode, mass transport limitations are not avoided at low substrate concentrations. Therefore, the K_m value estimated from the fitting of

the electrochemical assay should not be regarded as accurate, whereas from the $i_{cat\max}$ value it was possible to calculate a k'_{max} value of (1.4 ± 0.1) s^{-1}. Since the N_2OR concentration used in this study was 2.5 µM, a k of (5.6 ± 0.4) × 10^5 $M^{-1}s^{-1}$ was estimated, a value that is identical to the one calculated using the approaches presented above.

The effect of pH on the intermolecular rate constant was analyzed, revealing a bell shaped curve, that can be simulated using Equation 3 (*35*) and pK_as of 5.5 ± 1.0 and 8.0 ± 0.7 (Figure 3.3).

$$Act = Act_{max}/(1 + 10^{(pKa1-pH)} + 10^{(pH-pKa2)}) \quad \text{(Equation 3)}$$

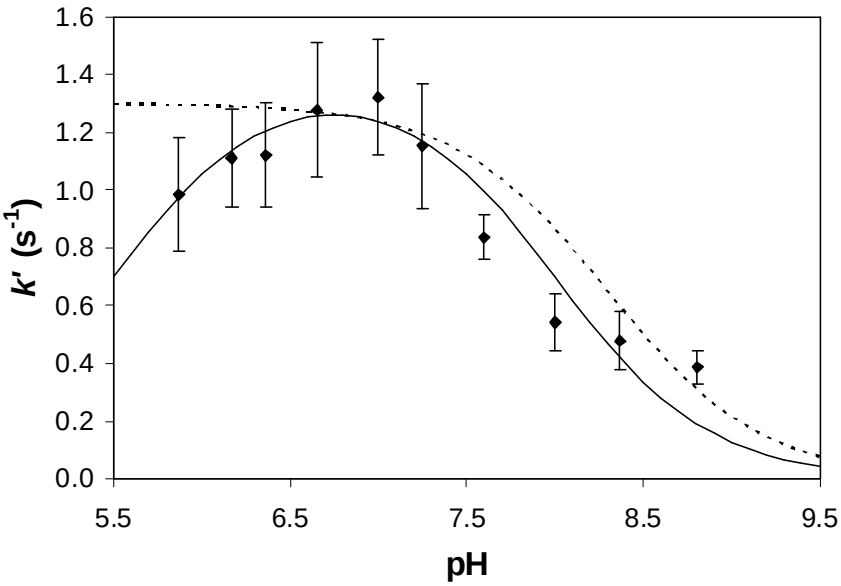

Figure 3.3 – Intermolecular rate constants of *Pseudomonas nautica* N_2OR *versus* pH, determined by electrochemical assays using cytochrome c_{552} as mediator. The assays were performed with 2.5 µM activated N_2OR and 50 µM cytochrome c_{552} entrapped in the membrane electrode, 1 mM N_2O-saturated water, in different buffer systems with pH between 5,9 and 8.8. The data were nonlinearly fitted using Equation 3, and pK_a values of 8.0 ± 0.7 and 5.5 ± 1.0 (solid line). The dashed line shows the pH dependence fit for the steady-state kinetic study [18], with a pK_a of 8.3.

The latter pK_a matches the solution kinetic value (pK_a at 8.3 (Chapter 2 and ref. *18*)), which was attributed to a deprotonation occurring at the catalytic CuZ centre and identified as a key process in the reduction mechanism of CuZ. The more acidic pK_a was not detected in the steady-state kinetic experiment, since it is outside of the pH range studied in that work (pH between 6.2 and 8.7).

As mentioned above, in the electrochemical studies of the mediated activity of N_2OR by cytochrome c_{552} it was observed that the catalytic current, measured at successive scans, decreases after each scan (Figure 5B – black circles). This decay can be attributed to an inactivation process that occurs with time (in between each new scan). Moreover, in the experiments performed at different pH it was observed that this inactivation process is lower at acidic pH than at basic pH (Figure 3.4), and a pK_a of 7.1 ± 0.8 was estimated. This is an

indication that a deprotonation is involved in the inactivation of the enzyme (*vide infra*), as it has been proposed before (*19*).

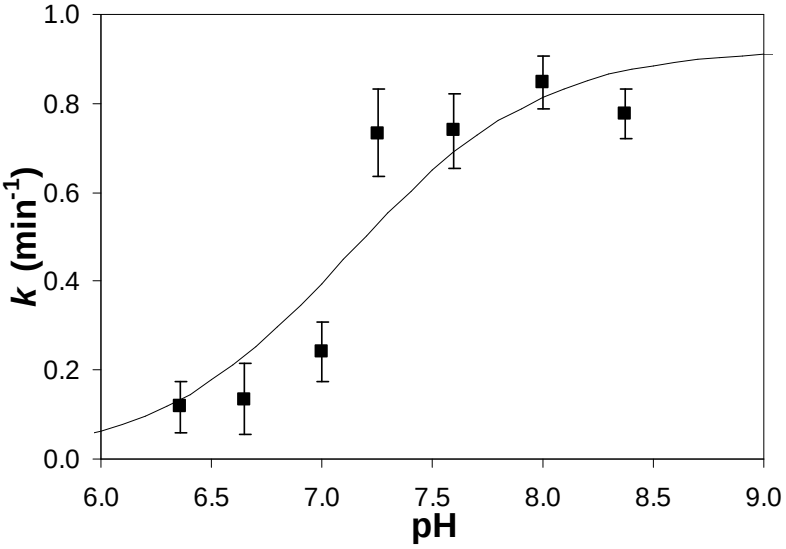

Figure 3.4 – Rate constant of the inactivation process detected by electrochemical experiments *versus* pH. The *k* values were obtained by fitting the catalytic current decay with an exponential equation. The data were nonlinearly fitted using Equation 3 adapted for one pk_a of 7.1.

3.4.2 Direct reaction with substrate N_2O

The reaction between pre-activated-N_2OR and a stoichiometric amount of N_2O, monitored by UV-visible spectroscopy, showed a rapid (within 1 s) oxidation of the CuA centre, through the increase of the two characteristic absorption bands at 480 and 540 nm (*13*), and the development of an absorption band at 680 nm, that has not been previously reported. Then, this 680-nm absorption band slowly (in the order of minutes) shifts to the usual position of 640 nm for the resting enzyme (Figure 5A). At corresponding times to the UV-visible monitoring, the enzyme activity was assayed to understand the contribution to catalysis of the N_2OR forms characterized by the 680-nm absorption band and that featuring the 640-nm absorption band (Figure 3.5B).

The increase of the 640-nm band in the UV-visible spectrum *vs* time (Figure 3.5B, open squares) can be fitted with a rate similar to the decay rate of the enzymatic activity (k = 0.3 min^{-1} for both experimental data sets), suggesting that the two processes are directly correlated.

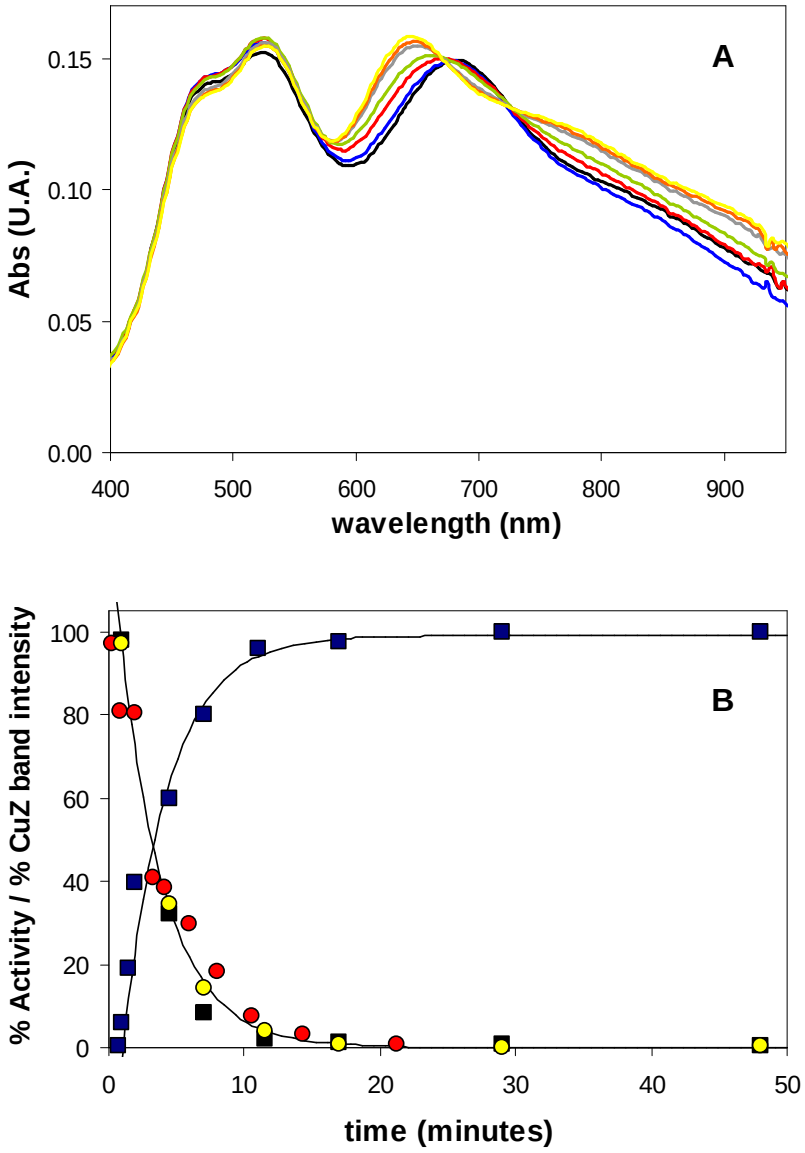

Figure 3.5 – (A) Selected spectra of 35 µM *Pseudomonas nautica* N_2OR after reaction with equimolar amount of N_2O at the following times: 0.5 min (black), 1 min (blue), 1.5 min (red), 2 min (green), 4.5 min (grey), 11 min (orange), 45 min (yellow). Inset*:* spectra obtained after subtraction of oxidised CuA contribution at the following times: 0.5 min (black), 1 min (blue), 1.5 min (red), 2 min (green), 4.5 min (grey), 11 min (orange), 45 min (yellow).
(B) N_2OR activity (black squares) *versus* time (100 % corresponds to 133 µmols N_2O-reduced min^{-1} mg^{-1} of enzyme) and 640-nm band intensity (blue squares) *versus* time (100% corresponds to the final spectra at t = 48 min and 0% corresponds to the first spectrum at t = 1 min). Solid lines are exponential fits and a k = 0.3 min^{-1} was used for both fits. Red circles represent the percentage of electrocatalytic activity *versus* time (100 % corresponds to the maximum activity, characterized by an intermolecular rate constant for electron transfer, k', of 1.4 s^{-1}). Yellow circles represent the 680–nm band intensity.

The maximum activity for this enzyme preparation determined in a separate activity assay was 133 µmolN_2O/min×mgN_2OR. The activity calculated 1 min after the reaction between N_2OR and stoichiometric amount of N_2O is 130 µmolN_2O/min×mgN_2OR (98% with respect to the

initial value). The activity decreases with time, reaching the value of 0.6 µmolN_2O/min×mgN_2OR (0.4% with respect to the initial value) after 48 minutes.

The direct correlation of the enzyme activity with the presence of a N_2OR form exhibiting the 680-nm band (open circles in Figure 4B) indicates that CuZ is in a new redox-active form, that will be represented here as CuZ°. This also rules out that the broad 680 nm absorption band might have a contribution from the 640 nm absorption band.

Therefore, it is the first time that such an enzyme form has been shown to be directly involved in the turnover mechanism of N_2OR. In fact, the two enzyme forms previously identified for *Pd* N_2OR, CuZ and CuZ*, that also present different absorption bands (670 nm and 650 nm, respectively), show very low specific activity when compared to the active CuZ° form (*17*).

The EPR spectrum of the CuZ° form was obtained by direct reaction of fully reduced N_2OR with a stoichiometric amount of N_2O for 1 minute (Figure 3.6). The oxidized CuA centre contributes to the total EPR spectrum with its typical 7-line hyperfine splitting (*7, 36*), so this contribution was subtracted in the spectra shown in Figure 6. The resting, inactive CuZ form characterized by the band at 640 nm in the UV-visible spectrum, exhibits the following EPR parameters: $g_{\|}$ = 2.160 and $g_{\perp}$ = 2.040 and a 4-line hyperfine splitting (*10*) (Figure 3.6b).

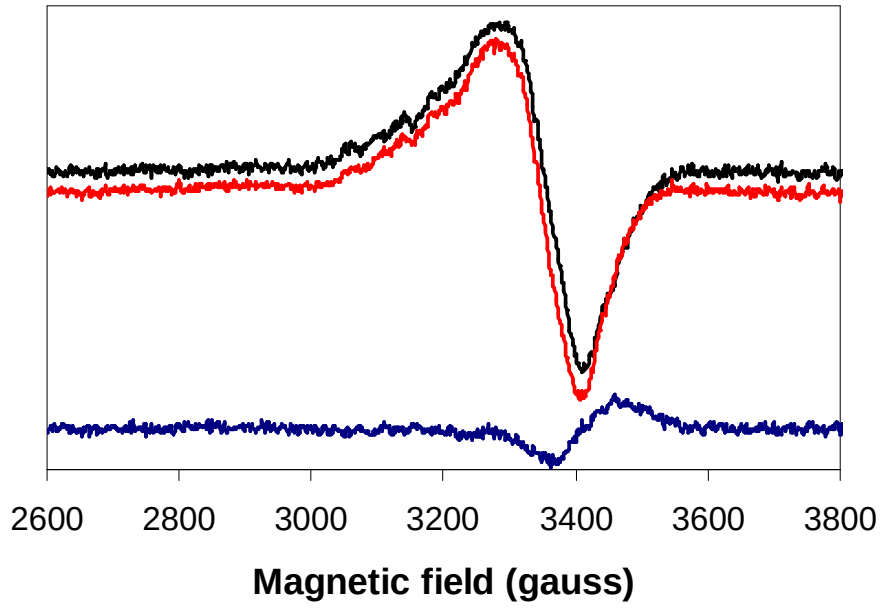

Figure 3.6 – EPR spectra of the different CuZ forms. EPR spectrum of the 680-nm band, CuZ° form (black line), and of the 640-nm band, resting CuZ form (red line). The CuA contribution was subtracted from both spectra. The blue line is the difference between the spectrum of the CuZ° form and that of the resting, inactive CuZ form. Instrumental parameters: modulation amplitude, 5 G; microwave frequency, 9.66 GHz; temperature 30 K.

The EPR signal of the active CuZ° form is very similar, both in shape and intensity (Figure 3.6a), indicating that it has the same paramagnetic state as the resting form ($1Cu^{II}/3Cu^{I}$) with a total spin S = ½. The $g_{\parallel}$ value is unchanged, while $g_{\perp}$ is only slightly lower ($g_{\perp}$ = 2.037) for CuZ°. In the light of this similarity in the EPR spectrum, the coordination environment of the coppers in the two forms has not changed drastically, and in particular we can assume that CuI remains in the formal Cu^{2+} state within the cluster (*10*), while the small change in $g_{\perp}$ may suggest that some minor local rearrangement is occurring at the site. Also the shift of the electronic band from CuZ to CuZ° can be correlated to some minor change in the CuI environment.

The high intensity of the 680-nm band in CuZ° confirms that this absorption band remains a $S^{2-} \rightarrow$Cu LMCT transition, as for the 640-nm band in the resting CuZ, which is actually a multicomponent band with partially overlapping features at higher and lower energy (*11, 12*). Indeed, looking carefully to the difference spectra reported in Figure 3.4A, it seems that the 680-nm absorption of CuZ° results from the overlap between the high-intensity component, which is red-shifted from its original position at 640 nm, and a low-intensity component, blue-shifted from its position near 720 nm, in the CuZ spectrum, which is missing in the CuZ° spectrum. The increased band-width of the 680-nm band with respect to the 640-nm band supports this interpretation. We may therefore interpret the 640-nm to 680-nm shift of the LMCT band as a result of the reduction of the splitting between the components of the complex $S^{2-} \rightarrow$ Cu LMCT band, indicating that in the CuZ° centre, the CuI atom undergoes a small displacement in its relative position *vs* the μ_4-S^{2-} ligand with respect to the resting CuZ cluster.

A possible explanation for the spectral difference between CuZ and CuZ° is a protonation/deprotonation process of the hydroxo-ligand between CuI and CuIV. As a simple proton transfer would be faster than the time scale of conversion of CuZ° to the redox equivalent, inactive form, it is likely that the deprotonation of a bound water molecule in CuZ° (see below) occurs with formation of a μ-hydroxo bridge between CuI and CuIV in the resting form (*18*). This will likely involve some minor structural change in the cluster to meet the geometrical requirement needed to optimize the formation of the bridge.

In the recent crystallographic study of *Ac* N_2OR, it was shown that the CuZ cluster is flexible and can accommodate alternatively one water molecule and one hydroxyl group or even an iodide ion in a bridged mode (*5*). In particular, it was shown that the CuZ cluster can rearrange its structure by changing the Cu-S distances and the orientation of some of the histidines residues. From our data we can suggest that the configuration with the μ-hydroxo bridge between CuI and CuIV prevents the CuZ centre from further catalysis, while a non-bridged

water molecule would be more susceptible to be released, enabling the accommodation of a new substrate molecule at CuZ.

3.4.3 Mechanistic insight involving the new CuZ° active form

On the basis of the identification of the fast-reacting CuZ° N_2OR form, it is possible to formulate a new mechanism of reduction, catalysis and inactivation of the catalytic N_2OR centre, as shown in Scheme 3.2. The resting CuZ state, characterized by the absorption band at 640 nm, does not participate in the catalytic cycle because of the slow reduction (activation process) required to obtain the fully reduced state (*15*). The fast turnover cycle (k_{cat} = 320 s^{-1} and k_{cat} = 3.8 s^{-1} for MV and cytochrome c_{552}, respectively (Chapter 2 and ref. *18*)) implies that the re-reduction of the N_2O-oxidised CuZ centre must be rapid in the enzymatic turnover and excludes the involvement of the resting CuZ state. This is also in agreement with the fact that N_2OR as-purified is not catalytically active, unless it is subjected to prolonged activation with reduced methylviologen.

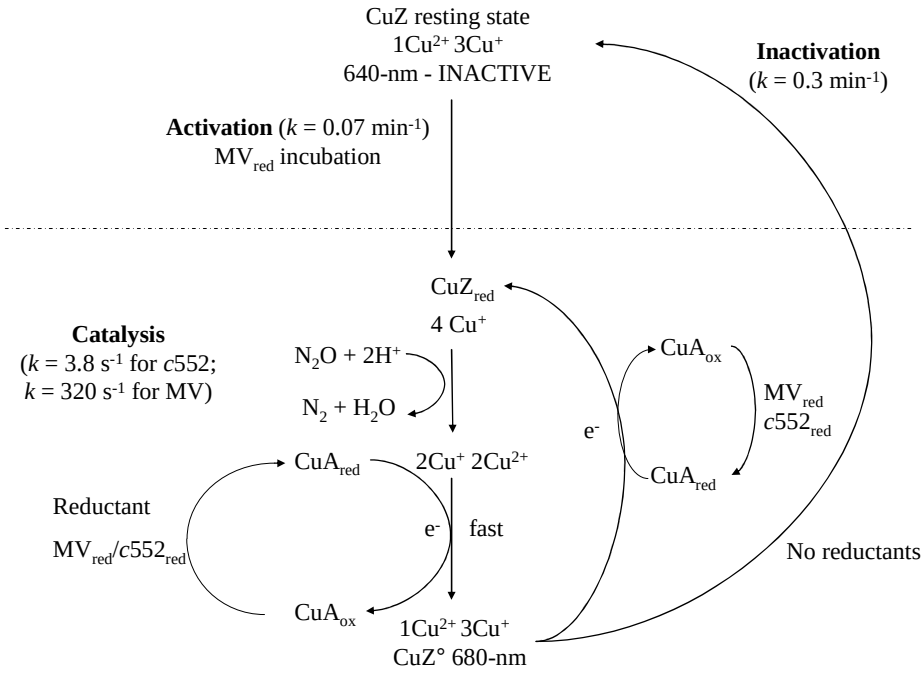

Scheme 3.2 - New mechanism of reduction, inactivation and catalysis of the catalytic N_2OR centre, CuZ centre

Therefore, the two-electron oxidised form of the CuZ is not detectable as it has a very short life and is very rapidly reduced by one electron coming from CuA, yielding the $1Cu^{2+}3Cu^{+}$

intermediate species CuZ° (Scheme 2). The intramolecular electron transfer producing CuZ° cannot be analysed in our conditions but is signalled by the formation of the characteristic optical bands of oxidised CuA (in 0.1 s time-scale). Then, during catalytic turnover, CuZ° is directly reduced back to the fully reduced enzyme by another electron coming from CuA. As the enzymatic reaction produces a water molecule by consumption of two protons, we believe that this water molecule is bound to the oxidized CuI in CuZ°. The fast reduction of the latter species during turnover prevents the rearrangement of CuZ° to the μ-hydroxo-bridged, redox-equivalent resting form. We already noticed that the Cu(II)/Cu(I) redox potential of the μ-hydroxo-bridged dinuclear copper(II) complexes is lower than that of the corresponding aqua complexes (*18*). This is consistent with the formulation of the oxidized CuI-CuIV as a non-bridged $Cu^{2+}Cu^{2+}$-H_2O species, as this would make the subsequent reduction by CuA easier.

In the typical activity assays, the strong absorption of the reductants (reduced MV or cytochrome c_{552}) prevents the detection of the CuZ° intermediate form. Instead, as shown here, in the absence of reductants, this form is slowly converted to the inactive resting state of CuZ. Moreover, the inactivation process does not involve any electron transfer reaction, because CuA remains in the oxidised state ($Cu^{1.5+}/Cu^{1.5+}$) during this process.

The inactivation process that was detected in the electrochemical experiments, where the activity of N_2OR is mediated by cytochrome c_{552}, has the same decay as the one observed in the UV-visible study, which suggests that the process that is occurring is the same in the two situations. In addition, the effect of pH on the inactivation process is consistent with the deprotonation of the water-ligand between CuI and CuIV in the CuZ° species, as the pK_a calculated from the inactivation process (7.1 ± 0.8) is compatible with those calculated through the electrochemical assay and steady-state kinetic (pK_a = 8.0 ± 0.7 and pK_a = 8.3, respectively)

3.4.4 Redox titration

The titration of N_2OR was performed in the oxidation direction since the activated form is in the fully reduced state. The CuA centre shows a midpoint potential at E ≈ 240 mV (Figure 3.7 – full squares in the oxidation direction, open squares in the reduction direction). This midpoint potential is in full agreement with literature values for this centre in N_2OR (*13, 17, 37*). The oxidation of CuZ brings this centre directly to the form characterized by the 640-nm band with no contribution at 680 nm (Figure 3.7 – open circles, spectra not shown).

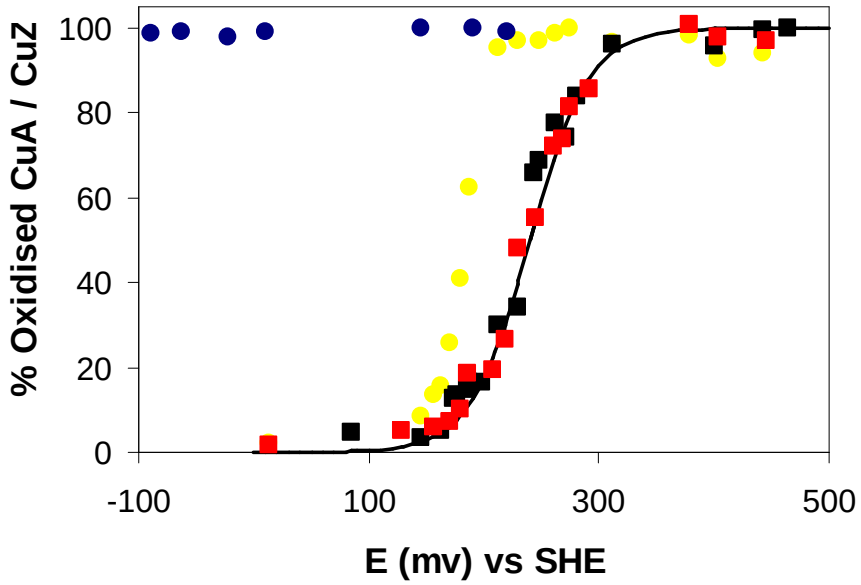

Figure 3.7 – Potentiometric redox titration of fully reduced *Pseudomonas nautica* N_2OR following the characteristic absorption bands of CuA and CuZ centre in the oxidation and reduction direction. CuA centre was monitored by following the absorption at 540 nm in the oxidative (black squares) and in the reductive titrations (red squares). The titration curve was fitted with E°' = + 240 mV (solid line). CuZ centre was monitored by following the absorption at 640 nm in the oxidative (yellow circles) and in the reductive titrations (blue circles).

The impossibility to reduce this form (titrations using either dithionite or Ti^{III}citrate were not successful, Figure 3.7 – full circles) does not allow the application of the Nernst equation that can be used only for a reversible system and does not enable the calculation of the midpoint redox potential for this centre. In fact, this data set does not fit with the Nernst equation for 1 electron.

The oxidation of the fully reduced CuZ promoted by ferricyanide, brings CuZ directly to the inactive form, which is characterized by the 640-nm band. This form cannot be re-reduced again unless through an activation process with reduced methylviologen (Scheme 3.2).

The irreversible oxidation of the CuZ is catalytically unproductive and this behaviour confirms the proposed mechanism in which the CuZ° is the only active form in the turnover cycle, where it is generated by the substrate and it is rapidly reduced by the electron flow from the CuA centre.

3.5 Conclusions

The first example of mediated electrochemistry of N_2OR described here allowed the calculation of the rate constant of the intermolecular electron transfer to the physiological electron donor (k of $(5.5 \pm 0.9) \times 10^5$ $M^{-1}s^{-1}$). The rate constant is similar to the values found for

other intermolecular protein-protein electron transfers determined using cyclic voltammetry. Moreover, the study of the dependence of the rate on N_2O concentration and pH confirms the recent results obtained in the kinetic analysis between N_2OR and cytochrome c_{552} from *Pseudomonas nautica*.

The reaction of the activated form of N_2OR with a stoichiometric amount of substrate enabled the identification of a new active CuZ° form in the turnover cycle, which is characterized by an absorption band at 680 nm and is different from the resting and inactive CuZ form, previously observed. In the absence of reductants to complete the catalytic cycle, the CuZ° form rearranges to restore the resting form in a slow process (k = 0.3 s^{-1}), compared with the turnover rate. This inactivation process was also detected in the electrochemical studies where the catalytic current decreases at a similar rate to the formation of the inactive enzyme form.

A scheme that shows the activation required *in vitro* and the inactivation detected during these experiments was presented. In particular the difference between the resting CuZ and the active CuZ° was discussed in order to clarify the activation mechanism and the catalysis of N_2OR.

3.6 Supplementaty materials

In the electrochemical experiment, the catalytic current is calculated by equation (4) in the text. In this equation, the rate of the process is described as:

(1) $rate = k'[cytc]$

However, the global kinetic of the process can be written as:

(2) $rate = (k_{cat}[cyt]/(K_m + [cyt]))[N_2OR]$

Since we are in the linear part of the Michaelis-Menten equation, we can omit the [cyt] term at the denominator. Equation (2) can be re-written as:

(3) $rate = (k_{cat} / K_m)[cyt][N_2OR]$

Then we can equal equations (1) and (2)

(4) $k'[cyt] = (k_{cat} / K_m)[cyt][N_2OR]$

(5) $k' = (k_{cat} / K_m)[N_2OR]$

In conclusion

(6) $k = k'/[N_2OR] = k_{cat} / K_m$

Kinetic constants:

k_{cat} = 3.8 s^{-1}

K_m = 50 µM

k_{cat}/K_m = 7.6 × 10^4 $M^{-1}s^{-1}$

Electrochemical constant:

k = 5.5 × 10^5 $M^{-1}s^{-1}$

3.7 References

1. Zumft, W. G., and Kroneck, P. M. (2007) Respiratory transformation of nitrous oxide (N2O) to dinitrogen by Bacteria and Archaea, *Adv Microb Physiol 52*, 107-227.
2. Tavares, P., Pereira, A. S., Moura, J. J., and Moura, I. (2006) Metalloenzymes of the denitrification pathway, *J Inorg Biochem 100*, 2087-2100.
3. Brown, K., Tegoni, M., Prudencio, M., Pereira, A. S., Besson, S., Moura, J. J., Moura, I., and Cambillau, C. (2000) A novel type of catalytic copper cluster in nitrous oxide reductase, *Nat Struct Biol 7*, 191-195.
4. Haltia, T., Brown, K., Tegoni, M., Cambillau, C., Saraste, M., Mattila, K., and Djinovic-Carugo, K. (2003) Crystal structure of nitrous oxide reductase from Paracoccus denitrificans at 1.6 A resolution, *Biochem J 369*, 77-88.
5. Paraskevopoulos, K., Antonyuk, S. V., Sawers, R. G., Eady, R. R., and Hasnain, S. S. (2006) Insight into catalysis of nitrous oxide reductase from high-resolution structures of resting and inhibitor-bound enzyme from Achromobacter cycloclastes, *J Mol Biol 362*, 55-65.
6. Scott, R. A., Zumft, W. G., Coyle, C. L., and Dooley, D. M. (1989) Pseudomonas stutzeri N2O Reductase Contains CuA-Type Sites, *PNAS 86*, 4082-4086.
7. Antholine, W. E., Kastrau, D. H., Steffens, G. C., Buse, G., Zumft, W. G., and Kroneck, P. M. (1992) A comparative EPR investigation of the multicopper proteins nitrous-oxide reductase and cytochrome c oxidase, *Eur J Biochem 209*, 875-881.
8. Gorelsky, S. I., Xie, X., Chen, Y., Fee, J. A., and Solomon, E. I. (2006) The two-state issue in the mixed-valence binuclear CuA center in cytochrome C oxidase and N2O reductase, *J Am Chem Soc 128*, 16452-16453.
9. Kroneck, P. M., Antholine, W. A., Riester, J., and Zumft, W. G. (1989) The nature of the cupric site in nitrous oxide reductase and of CuA in cytochrome c oxidase, *FEBS Lett 248*, 212-213.
10. Chen, P., DeBeer George, S., Cabrito, I., Antholine, W. E., Moura, J. J., Moura, I., Hedman, B., Hodgson, K. O., and Solomon, E. I. (2002) Electronic structure description of the mu(4)-sulfide bridged tetranuclear Cu(Z) center in N(2)O reductase, *J Am Chem Soc 124*, 744-745.
11. Chen, P., Cabrito, I., Moura, J. J., Moura, I., and Solomon, E. I. (2002) Spectroscopic and electronic structure studies of the mu(4)-sulfide bridged tetranuclear Cu(Z) cluster in N(2)O reductase: molecular insight into the catalytic mechanism, *J Am Chem Soc 124*, 10497-10507.
12. Chen, P., Gorelsky, S. I., Ghosh, S., and Solomon, E. I. (2004) N2O reduction by the mu4-sulfide-bridged tetranuclear CuZ cluster active site, *Angew Chem Int Ed Engl 43*, 4132-4140.
13. Prudencio, M., Pereira, A. S., Tavares, P., Besson, S., Cabrito, I., Brown, K., Samyn, B., Devreese, B., Van Beeumen, J., Rusnak, F., Fauque, G., Moura, J. J., Tegoni, M., Cambillau, C., and Moura, I. (2000) Purification, characterization, and preliminary crystallographic study of copper-containing nitrous oxide reductase from Pseudomonas nautica 617, *Biochemistry 39*, 3899-3907.
14. Oganesyan, V. S., Rasmussen, T., Fairhurst, S., and Thomson, A. J. (2004) Characterisation of [Cu4S], the catalytic site in nitrous oxide reductase, by EPR spectroscopy, *Dalton Trans 7*, 996-1002.
15. Ghosh, S., Gorelsky, S. I., Chen, P., Cabrito, I., Moura, J. J., Moura, I., and Solomon, E. I. (2003) Activation of N2O reduction by the fully reduced micro4-sulfide bridged tetranuclear Cu Z cluster in nitrous oxide reductase, *J Am Chem Soc 125*, 15708-15709.
16. Chan, J. M., Bollinger, J. A., Grewell, C. L., and Dooley, D. M. (2004) Reductively activated nitrous oxide reductase reacts directly with substrate, *J Am Chem Soc 126*, 3030-3031.
17. Rasmussen, T., Berks, B. C., Butt, J. N., and Thomson, A. J. (2002) Multiple forms of the catalytic centre, CuZ, in the enzyme nitrous oxide reductase from Paracoccus pantotrophus, *Biochem J 364*, 807-815.
18. Dell'acqua, S., Pauleta, S. R., Monzani, E., Pereira, A. S., Casella, L., Moura, J. J., and Moura, I. (2008) Electron transfer complex between nitrous oxide reductase and cytochrome c552 from Pseudomonas nautica: kinetic, nuclear magnetic resonance, and docking studies, *Biochemistry 47*, 10852-10862.
19. Correia dos Santos, M. M., Paes de Sousa, P.M., Simoes Gonçalves, M.L., Krippahl, L., Moura, J.J.G., Lojou, E., Bianco, P. (2003) Electrochemical studies on small electron transfer proteins using membrane electrodes, *J Electroanal Chem 541*, 153-162.

20. Alves, T., Besson, S., Duarte, L. C., Pettigrew, G. W., Girio, F. M., Devreese, B., Vandenberghe, I., Van Beeumen, J., Fauque, G., and Moura, I. (1999) A cytochrome c peroxidase from Pseudomonas nautica 617 active at high ionic strength: expression, purification and characterization, *Biochim Biophys Acta 1434*, 248-259.
21. Lopes, H., Besson, S., Moura, I., and Moura, J. J. (2001) Kinetics of inter- and intramolecular electron transfer of Pseudomonas nautica cytochrome cd1 nitrite reductase: regulation of the NO-bound end product, *J Biol Inorg Chem 6*, 55-62.
22. Lowry, O. H., Rosebrough, N. J., Farr, A. L., and Randall, R. J. (1951) PROTEIN MEASUREMENT WITH THE FOLIN PHENOL REAGENT, *J. Biol. Chem. 193*, 265-275.
23. Fauque, G., Moura, J. J. G., Besson, S., Saraiva, L., and Moura, I. (1992) Caractérisation préliminaire du système cytochromique de la bactérie marine dénitricante Pseudomonas nautica 617, *Oceanis 18*, 211-216.
24. Saraiva, L. M., Besson, S., Fauque, G., and Moura, I. (1994) Characterization of the dihemic cytochrome c549 from the marine denitrifying bacterium Pseudomonas nautica 617, *Biochem Biophys Res Commun 199*, 1289-1296.
25. de Sousa, P. M., Pauleta, S. R., Goncalves, M. L., Pettigrew, G. W., Moura, I., Dos Santos, M. M., and Moura, J. J. (2007) Mediated catalysis of Paracoccus pantotrophus cytochrome c peroxidase by P. pantotrophus pseudoazurin: kinetics of intermolecular electron transfer, *J Biol Inorg Chem 12*, 691-698.
26. Ferapontova, E. E., Ruzgas, T., and Gorton, L. (2003) Direct electron transfer of heme- and molybdopterin cofactor-containing chicken liver sulfite oxidase on alkanethiol-modified gold electrodes, *Anal Chem 75*, 4841-4850.
27. Nicholson, R. S., Shain, I. (1964) Theory of Stationary Electrode Polarography. Single Scan and Cyclic Methods Applied to Reversible, Irreversible, and Kinetic Systems., *Anal Chem 36*, 706-723.
28. Bard, A. J., and Faulkner, L. R. (2001) Electrochemical methods, fundamentals and applications., *Wiley, New York*.
29. Saveant, J. M., Vianello, E. (1965) Potential-sweep chronoamperometry: Kinetic currents for first-order chemical reaction parallel to electron-transfer process (catalytic currents), *Electrochim. Acta 10*, 905-920.
30. Coury, L. A., Oliver, B. N., Egekeze, J. O., Sosnoff, C. S., Brumfield, J. C., Buck, R. P., and Murray, R. W. (1990) Mediated, anaerobic voltammetry of sulfite oxidase, *Anal Chem 62*, 452-458.
31. Coury, L. A., Liu Yang and Murray, R. W. (1993) Electrochemical study of the rate of activation of the molybdoheme protein sulfite oxidase by organic electron acceptors, *Anal Chem 65*, 242-246.
32. Yang, L., Coury, L. A., and Murray, R. W. (1993) Intra-Enzyme and Mediator Cross-Reaction Electron-Transfer Reaction Kinetics of Sulfite Oxidase, *J Phys Chem 97*, 1694-1700.
33. Correia dos Santos, M. M., Paes de Sousa, P.M., Simoes Gonçalves, M.L., Lopes, H., Moura, I., Moura, J.J.G. (1999) Electrochemical studies on c-type cytochromes at microelectrodes, *464*, 76-84.
34. Kataoka, K., Yamaguchi, K., Kobayashi, M., Mori, T., Bokui, N., and Suzuki, S. (2004) Structure-based Engineering of Alcaligenes xylosoxidans Copper-containing Nitrite Reductase Enhances Intermolecular Electron Transfer Reaction with Pseudoazurin, *J. Biol. Chem. 279*, 53374-53378.
35. Cornish-Bowden, A. (2001) Fundamentals of Enzyme Kinetics, *Portland Press, London*, 179-192.
36. Farrar, J. A., Thomson, A. J., Cheesman, M. R., Dooley, D. M., and Zumft, W. G. (1991) A model of the copper centres of nitrous oxide reductase (Pseudomonas stutzeri). Evidence from optical, EPR and MCD spectroscopy, *FEBS Lett 294*, 11-15.
37. Coyle, C. L., Zumft, W. G., Kroneck, P. M., Korner, H., and Jakob, W. (1985) Nitrous oxide reductase from denitrifying Pseudomonas perfectomarina. Purification and properties of a novel multicopper enzyme, *Eur J Biochem 153*, 459-467.

Chapter 4

The electron transfer complex between nitrous oxide reductase and its electron donors

4.1 Abstract

Identifying redox partners and the interaction surfaces is important to fully understand the electron flow in a respiratory chain. In this study, we focus our attention on the interaction of the enzyme nitrous oxide reductase (N_2OR), that catalyzes the final step in bacterial denitrification, with its physiological electron donor, either a cytochrome *c* or a type 1 copper protein, pseudoazurin. The comparison between the interaction of N_2OR from three different microorganisms, *Pseudomonas nautica*, *Paracoccus denitrificans* and *Achromobacter cycloclastes*, with their physiological electron donors was performed through the analysis of their primary sequence alignment, electrostatic surface and by molecular docking simulations using the BiGGER algorithm. The docking results were refined on the basis of experimental data, since the interaction is suggested to have either a hydrophobic, in the case of *Pseudomonas nautica* N_2OR, or an electrostatic nature, in the case of *Paracoccus denitrificans* and *Achromobacter cycloclastes.* The properties of the electron transfer complex were further investigated by focusing on the pathways for the electron transfer. A set of well conserved residues on the N_2OR surface are proposed to be involved in the electron pathway from the

redox partner to nitrous oxide reductase (Ala495, Asp519, Val524, His566 and Leu568 in the case of *Pseudomonas nautica* N_2OR). Moreover, we built a model for *Wolinella succinogenes* N_2OR, an enzyme that presents an additional cytochrome *c* domain. The structure of both N_2OR – domain and cytochrome *c* – domain were modelled and the full length structure was obtained by molecular docking simulation of these two domains.

4.2 Introduction

Electron transfer reactions between proteins are essential for a large number of biological processes involving redox changes, such as some metabolic processes, photosynthesis and both aerobic and anaerobic respiration. The denitrification pathway occurs under anaerobic conditions, and involves the reduction of nitrate to nitrogen (N_2), that is catalyzed by a group of enzymes that contain transition metals as cofactors. The global process requires 10 electrons that must be transfered to the enzymes through small electron donor proteins, such as cytochromes *c* or type 1 copper proteins, as pseudoazurins.

In general, electron transfer complexes are part of a group of protein-protein complexes, the transient complexes, characterized by a short life time (in the millisecond timescale) and a low binding affinity (K_d in the mM to μM range). (*1, 2*) This transient nature distinguishes the electron transfer complexes from more stable long-lived protein-protein complexes, such as inhibitor-enzyme complexes, antigen-antibody and signal transduction complexes.

The short life time and the low binding affinity constant necessary for a rapid electron transfer reaction make these complexes difficult to crystallize. As a consequence, until now only a few three-dimensional structures of this type of complexes have been determined by X-ray crystallography. An alternative to the co-crystallization is offered by protein-protein docking simulations, often coupled with experimental data, such as NMR and other experimental parameters that provide information on the binding interface.

One of these docking algorithms is BiGGER (Bimolecular Complex Generation with Global Evaluation and Ranking) that is included in the Chemera software package (*3*). This algorithm has been used in the last decade to predict the putative interaction between electron donor and acceptor of several electron transfer complexes (*4-10*). BiGGER is a free docking software that can be used to obtain a structural model of protein complexes, as long as the three-dimensional structures of the proteins involved are available. Although the coordinates used are considered as “rigid bodies” the algorithm offers an option called “soft-docking” that takes into account the conformational freedom of some of the residue side-chains, as lysine, located at the surface to assist the prediction of the mode of binding of two proteins. However, for a

complete analysis, the ET complexes obtained need to be validated by experimental data, as mutagenesis studies, kinetic studies of the electron transfer or the mapping of the interaction surface by chemical shift perturbation (using 2D NMR titrations).

In this work, the nitrous oxide reductase from different species, which catalyses the final step of the bacterial denitrification process, the two-electron reduction of nitrous oxide (N_2O) to dinitrogen (N_2) (*11, 12*), will be used as a case study for electron transfer complexes. The recently solved structures (*Pseudomonas nautica* (*Pn*) N_2OR (*13*), *Paracoccus denitrificans* (*Pd*) N_2OR (*14*), *Achromobacter cycloclastes* (*Ac*) N_2OR (*15*)) revealed the presence of two multicopper centres: a binuclear electron transfer centre CuA and a tetranuclear catalytic centre CuZ. The large distance between CuA and CuZ within the same monomer imposes the dimeric conformation of the enzyme, as a functional homodimer, in which the two subunits are oriented "head to tail" bringing CuA and CuZ at approximately 10 Å, a distance appropriate for an efficient electron transfer (*16*).

The binuclear CuA centre in N_2OR is located in a cupredoxin like domain, similar to the one found in cytochrome *c* oxidase and in both cases constitutes the proposed docking and electron entry site from the small electron donor to the catalytic centre (*12, 17, 18*). The low energy of reorganization between the reduced Cu^{+}-Cu^{+} state and the mixed-valence oxidized $Cu^{1.5+}$-$Cu^{1.5+}$ state ensures a rapid electron transfer (*19-21*).

The CuZ centre has a unique structure in biology, consisting in a novel cluster with a sulphide ion bridging a distorted tetrahedron of four copper ions (Cu_4S), coordinated by seven histidines, while a water-derived ligand is proposed to bridge two copper atoms identified as CuI and CuIV, that constitute the substrate binding site. This copper centre is located in the N-terminal domain that adopts a seven-blade β-propeller fold.

In Chapter 2, the physiological electron donor of *Pseudomonas nautica* N_2OR was identified to be cytochrome c_{552} (*22*). In that study it was also shown by steady-state kinetics that the interaction between the two proteins is mainly hydrophobic in nature and that mitochondrial cytochrome *c* is not a competent electron donor to N_2OR (*22*).

In the case of *Paracoccus pantotrophus* (*Pp*), an organism closely related to *Paracoccus denitrificans* (*23*), there are two physiological electron donors of N_2OR, cytochrome c_{550} and pseudoazurin, a type I copper protein (*24-26*), and also mitochondrial cytochrome *c* was demonstrated to be able to donate electrons to this enzyme. A structural model for the electron transfer complex between *Pd* N_2OR and either *Pp* cytochrome c_{550} or *Pp* pseudoazurin was proposed on the basis of a theoretical docking study (*27*).

In the case of *Ac* N_2OR, its electron donor was shown to be only pseudoazurin (*28*), since no small cytochrome *c* was identified in the periplasm of the bacteria growing under denitrifying

conditions (*29*). Nevertheless, it was demonstrated that bovine heart cytochrome *c* was able to reductively activate this enzyme, thus reducing CuA centre (*30*).

The N_2OR from *Wolinella succinogenes* (*Ws*) presents a unique structural feature with an additional C-terminal domain containing a *c*-type heme, which is not found in any other N_2OR isolated up-to-now (*31*). The reduction of N_2O by this cytochrome *c*-N_2OR system shows a second-order kinetic, first order each in cytochrome *c* and enzyme. The second order rate constant is 3×10^6 $M^{-1}s^{-1}$ (*32*).

The purpose of this study is to analyze the electron transfer complexes formed between N_2OR from *Pn*, *Pd* and *Ac* and their respective electron donors using a molecular docking approach, and compare the results obtained with the ones with the non-physiological redox partners. The *ab initio* calculated docking solutions will be filtered using the properties of the electron transfer complexes derived from the kinetic studies. The putative model structures will be discussed in term of selectivity of the binding and electron transfer pathway.

Moreover, we will also build a model for *Ws* N_2OR and compare this structure with the one of a small cytochrome *c* docked to N_2OR.

4.3 Methods

4.3.1 Molecular docking simulation

Molecular docking simulations were performed using the algorithm BiGGER developed by Palma *et al.* (*3*). The target protein was the functional dimer of nitrous oxide reductase. The coordinates for the *Pn* N_2OR (1QNI (*13*)), *Pd* N_2OR (1FWX (*14*)), Ac N_2OR (2IWF (*15*)), *Pn* cytochrome c_{552} (1CNO (*33*)), *Pd* cytochrome c_{550} (1COT (*34*)), *Pp* pseudoazurin (3ERX (*35*)), *Ac* pseudoazurin (1BQK (oxidized) – 1BQR (reduced) (*36*)), horse heart cytochrome *c* (1HRC (*37*)) and bovine heart cytochrome *c* (2B4Z (*38*)) were obtained from the RCSB Protein data Bank (http://www.rcsb.org). The BiGGER algorithm provides a complete and systematic search of the rotational space of one protein relative to the other, generating a large number of putative docking geometries based on the complementarity of the molecular surfaces. The 5000 best solutions thus generated were evaluated and ranked according to a combination of additional interaction criteria that includes electrostatic energy of interaction, relative solvation energy, and the relative propensity of side chains to interact. For each solution, this evaluation process produces a "Global Score". The solutions can be also ranked according to electrostatic or hydrophobic scores. The top solutions were evaluated individually using the http://www.ebi.ac.uk/msd-srv/prot_int/pistart.html site to determine the size of the interface area of the complex and the hydrophobicity.

4.3.2 Analysis of the electrostatic surface

The electrostatic potential of nitrous oxide reductase and small electron donor proteins used in this study was generated in Chimera using the Coulombic Law and partial charges from the Amber 99SB force field for all residues except for hemes, where the charges were calculated by the Gasteiger method.

4.3.3 Analysis of the electron transfer pathways

The donor-acceptor coupling constant and the most probable electron transfer pathway was predicted using the PATHWAYS algorithm (*39, 40*), included in the HARLEM molecular modelling software (http://www.kurnikov.org/harlem_manual/html/index.html).

4.3.4 Sequence analysis and alignment

Sequence alignment was carried out using the program CLUSTALW (*41*) on the EBI Web site.

4.3.5 Model Building for N_2OR from W. succinogenes

Models of the N-terminal N_2OR and C-terminal heme-containing cytochrome *c* domain from *W. succinogenes* were obtained with the Web-based Protein Homology/analogY Recognition Engine (*42*) (PHYRE; http://www.sbg.bio.ic.ac.uk/phyre/), the successor of 3D-PSSM (*43*) with a fully up-to-date fold library and a 10–15% better coverage than 3D-PSSM. The resulting structure-based sequence alignment is presented. Other homology modelling programs were tested, ROBETTA (*44*) and SwissModel (*45*). Plausible conformations of *Ws* N_2OR conformation were predicted by analysis of the complexes obtained from the docking, performed with BiGGER algorithm (*3*) between the N_2OR domain and cytochrome *c* domain described above.

4.4 Results and discussion

4.4.1 Surface and sequence homology analysis

We have started by investigating the charge distribution on the surface of the small electron donor proteins and nitrous oxide reductase with known structure and the primary sequence alignment between those nitrous oxide reductases.

In Figure 4.1, the three structures of nitrous oxide reductases are presented with their surface coloured by electrostatic potential. Although, the total charge of *Pseudomonas nautica* (*Pn*), *Achromobacter cycloclastes* (*Ac*) and *Paracoccus denitrificans* (*Pd*) N_2OR dimer is -40, -43 and -59, respectively, the *Ac* and *Pd* enzymes present a very similar charge distribution around CuA center.

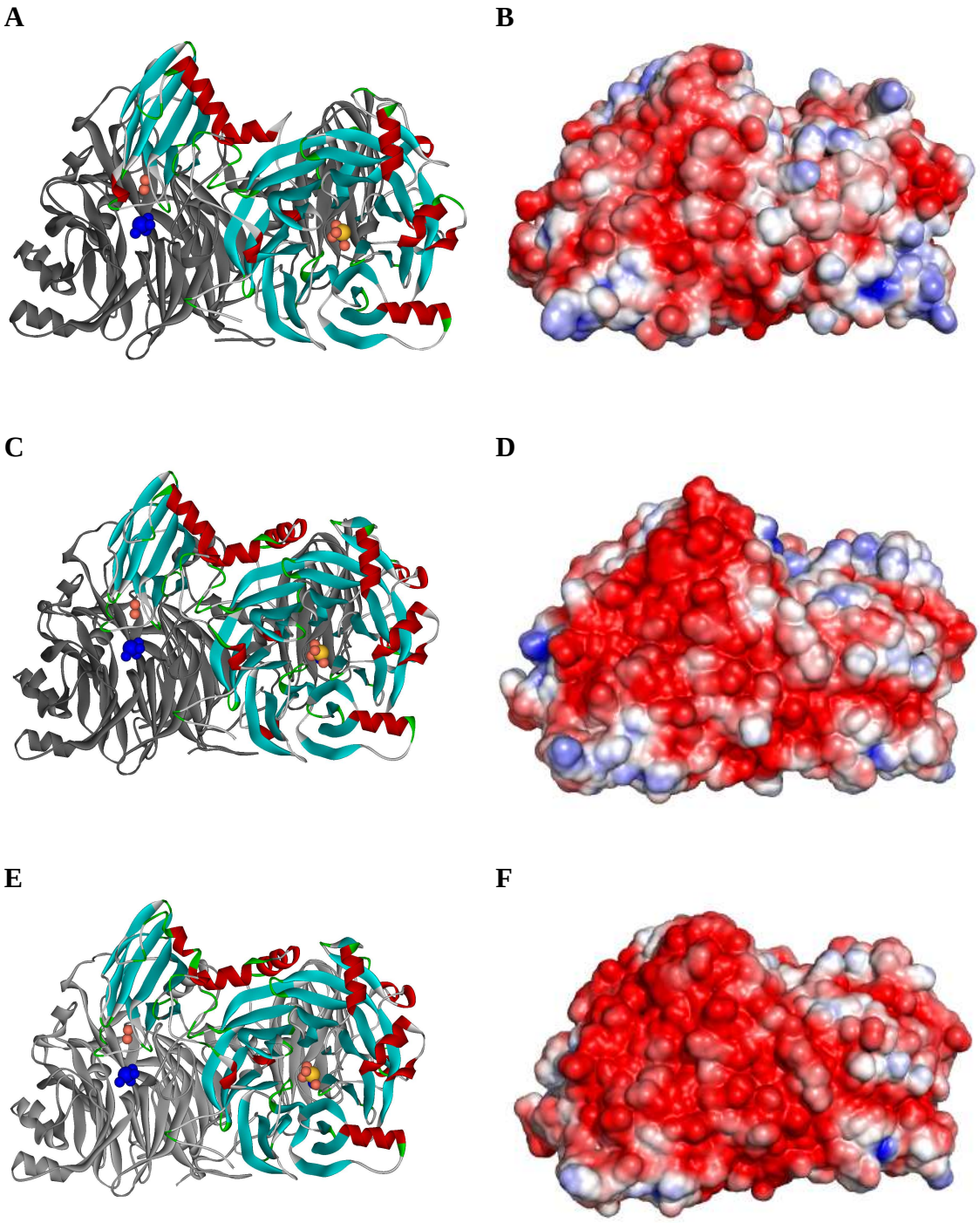

Figure 4.1 – Structures and electrostatic surface potential of *Pn* N_2OR (A-B), *Ac* N_2OR (C-D) and *Pd* N_2OR (E-F). In panel A, C and E the CuA and CuZ of the same monomer are represented in blue and light green, respectively. The two monomers are magenta and green coloured, respectively. Electrostatic surface potential is represented between −3 and 3 kT/e (B, D, F). Images were prepared using WebLab Viewer (Accelrys) (Panel A, C abd E) and USCF Chimera program (*panel B, D and F*) [54]. The electrostatic potential was calculated from Chimera using the Coulombic Law and partial charges from the Amber 99SB force field for all residues.

As already suggested in previous studies (*27, 46*), the sequence alignment shows a high similarity between *Ac* and *Pd* N_2OR, consisting in 87% identity, while *Pn* N_2OR has a lower sequence identity relative to the other two enzymes, with 58 % identity with *Pd* N_2OR and 60 % with *Ac* N_2OR (Figure 4.2). However, N_2OR sequences from different sources shows several very conserved regions, such as the residues that bind CuA and CuZ and the residues at the binding interface (*14*).

The homology is also pointed out in the charge distribution analysis (Figure 4.1), with *Ac* and *Pd* N_2OR having a more negatively charged surface, and also the region around CuA centre presents a predominant negatively charged surface, while in *Pn* N_2OR the charged residues are globally distributed over the protein surface and the CuA patch is characterized by a hydrophobic area.

Regarding the electron donors used in this study, which are represented in Figure 4.3, the global charge is + 3 for *Pn* cytochrome c_{552}, – 2 for *Pd* cytochrome c_{550}, – 5 for *Pp* pseudoazurin, 0 for *Ac* pseudoazurin, and + 8 for both HH and BH cytochrome *c*. Although, there is a relative difference in the global charge of the small electron transfer proteins, they share the feature of having a more or less positive patch around the proposed electron entry/exit point, which is located in a region composed mainly by hydrophobic residues. In the case of cytochrome c_{552} from *Pseudomonas nautica* the number of charged residues is clearly lower when compared with the other small electron transfer proteins.

```
A. cycloclastes          MESKEHKGLSRRALFSATAGSAILAGTVG------PAALSLGAAGLATPA 44
P. denitrificans         MESKQEKGLSRRALLGATAGGAAVAGAFGGRLALGPAALGLGTAGVATVA 50
P. nautica               ------------------------------------------AAAEEA 6
W. succinogenes          ----MQRLLKQSLVVTASLLALGTASLASSDLQTIMKERKLTEKDVLAAA 46
                                                                       *

A. cycloclastes          RA----ATGADGSVAPGKLDDYYGFWSSGQTGEMRILGIPSMRELMRVPV 90
P. denitrificans         GSGAALAASGDGSVAPGQLDDYYGFWSSGQSGEMRILGIPSMRELMRVPV 100
P. nautica               RN--------KAHVAPGELDEYYGFWSGGHQGEVRVLGVPSMRELMRIPV 48
W. succinogenes          KT----------YQPSGRKDEFVVFSSGGQSGQILVYGVPSMRIYKYIGV 86
                                     ..*. *::  * *.*: *:: : *:****    : *

A. cycloclastes          FNRCSATGWGQTNESIRIHQRTMTEKTKKQLAANGKKIHDNGDLHHVHMS 140
P. denitrificans         FNRCSATGWGQTNESLRIHERTMSERTKKFLAANGKRIHDNGDLHHVHMS 150
P. nautica               FNVDSATGWGITNESKEILG-------------GDQQYLNGDCHHPHIS 84
W. succinogenes          FTPEPWQGYGFDDDSKKVLRQ----------GDIRGREINWGDTHHPNFT 126
                         *.  .  *:*  ::* .:                 :    ** ** :::

A. cycloclastes          FTDGKYDGRYLFMNDKANTRVARVRCDVMKTDAILEIPNAKGIHGMRPQK 190
P. denitrificans         FTEGKYDGRFLFMNDKANTRVARVRCDVMKCDAILEIPNAKGIHGLRPQK 200
P. nautica               MTDGRYDGKYLFINDKANTRVARIRLDIMKTDKITHIPNVQAIHGLRLQK 134
W. succinogenes          EKNGEYVGDYLFINDKANPRIAVVNLHDFETTQIVVNPIMKSEHGG-SFV 175
                          .:*.* * :**:*****.*:* :. . ::   *   *  :. **

A. cycloclastes          WPRSNYVFCNGEDEAPLVNDGSTMTDVATYVN-------IFTAVDADKWE 233
P. denitrificans         WPRSNYVFCNGEDETPLVNDGTNMEDVANYVN-------VFTAVDADKWE 243
P. nautica               VPKTNYVFCNAEFVIPQPNDGTDFSLDNSYT--------MFTAIDAETMD 176
W. succinogenes          TPNTEYVIEASQYAAPLDHQYHPIEEYEAVFRGAVTLWKFDYAKGKIDEK 225
                         *.::**:  .:   *  ::   :              .  * .    .

A. cycloclastes          VAWQVKVSGNLDNCDADYEG---KWAFSTSYNSEMGMT---------LEE 271
P. denitrificans         VAWQVLVSGNLDNCDADYEG---KWAFSTSYNSEKGMT---------LPE 281
P. nautica               VAWQVIVDGNLDNTDADYTG---KYATSTCYNSERAVD---------LAG 214
W. succinogenes          ASFSLEFPPYMQDLSDAGKGESFGWAFTNSFNSEMYTGGIEKGLPPFEAG 275
                         .::.: .   ::: .    *    :* :..:***

A. cycloclastes          MTKSEMDHVVVFNIAEIEKAIKAGQYEEING--VKVVDGRKEAKSLFTRY 319
P. denitrificans         MTAAEMDHIVVFNIAEIEKAIAAGDYQELNG--VKVVDGRKEASSLFTRY 329
P. nautica               TMRNDRDWVVVFNVERIAAAVKAGNFKTIGDSKVPVVDGRGESE--FTRY 262
W. succinogenes          MSRNDTDYMHVYNWQMLEKLAQDPKNYKIYHG-HRVISIEAAVKAGALFL 324
                             : * : *:*   :       .   :      *:. .   .

A. cycloclastes          IPIANNPHGCNMAPDRKHLCVAGKLSPTVTVLDVTKFDALFYDN------ 363
P. denitrificans         IPIANNPHGCNMAPDKKHLCVAGKLSPTVTVLDVTRFDAVFYEN------ 373
P. nautica               IPVPKNPHGLNTSPDGKYFIANGKLSPTVSVIAIDKLDDLFEDK------ 306
W. succinogenes          IPEPKSPHGVDVSPDGRYIVVGGKLDTHASVYDFRKIKQLIDKKEFIGAD 374
                         ** .:.*** : :** ::: . ***.. .:*  . ::. :: .:

A. cycloclastes          ------AEPRSAVVAEPELGLGPLHTAFDGR-GNAYTSLFLDSQVVKWNI 406
P. denitrificans         ------ADPRSAVVAEPELGLGPLHTAFDGR-GNAYTSLFLDSQVVKWNI 416
P. nautica               ------IELRDTIVAEPELGLGPLHTTFDGR-GNAYTTLFIDSQVCKWNI 349
W. succinogenes          PYGIPILDMKKTLHGQVELGLGPLHHTYDAQDGIIYTSLYVDSQIVKWDY 424
                               : :.:: .: ******** ::*.: *  **:*::***: **:

A. cycloclastes          DEAIRAYAGEKINPIKDKLDVQYQPGHLKTVMGETLDAANDWLVCLCKFS 456
P. denitrificans         EDAIRAYAGEKVDPIKDKLDVHYQPGHLKTVMGETLDATNDWLVCLSKFS 466
P. nautica               ADAIKHYNGDRVNYIRQKLDVQYQPGHNHASLTESRDADGKWLVVLSKFS 399
W. succinogenes          KNLK----------VLDRVNVHYNIGHLDSMEGKSAKPKGKYALALDKLS 464
                          :            : ::::*:*: ** .:   :: .. ..: : * *:*

A. cycloclastes          KDRFLNVGPLKPENDQLIDISGDKMVLVHDGPT-FAEPHDAIAVSPSILP 505
P. denitrificans         KDRFLNVGPLKPENDQLIDISGDKMVLVHDGPT-FAEPHDAIAVHPSILS 515
P. nautica               KDRFLPVGPLHPENDQLIDISGEEMKLVHDGPT-YAEPHDCILVRRDQIK 448
W. succinogenes          IDRFNPVGPLHPQNHQLIDIGGPKMELIYDLPIPLGEPHDVISIAADKLK 514
                          ***  ****:*:*.*****.* :* *::* *   .**** * :  . :
```

```
A. cycloclastes          NIRSVWDRNDPLWAETRKQAEADEVDIDEWTEAVIRDGNKVRVYMTSVAP 555
P. denitrificans         DIKSVWDRNDPMWAETRAQAEADGVDIDNWTEEVIRDGNKVRVYMSSVAP 565
P. nautica               -TKKIYERNDPYFASCRAQAEKDGVTLES-DNKVIRDGNKVRVYMTSVAP 496
W. succinogenes          -----PQVTYPMGTNSRTGKQHEAMTLAG-QERVERKGNEVKIYGTLIRS 558
                               : . *  :. *   : : : :    : * *.**:*::* : : .

A. cycloclastes          SFSQPSFTVKEGDEVTVIVTNLDEIDDLTHGFTMGNHGVAMEVGPQQTSS 605
P. denitrificans         SFSIESFTVKEGDEVTVIVTNLDEIDDLTHGFTMGNYGVAMEIGPQMTSS 615
P. nautica               QYGMTDFKVKEGDEVTVYITNLDMVEDVTHGFCMVNHGVSMEISPQQTAS 546
W. succinogenes          HINPEHVTVNKGDKVTFYLTNLERAQDETHGFAVSGYNVHASVEPGKTVA 608
                           .   ..*::**:**. :***:  :* **** : .:.*  .: *  * :

A. cycloclastes          VTFVAANPGVYWYYCQWFCHALHMEMRGRMFVEPKGA------------- 642
P. denitrificans         VTFVAANPGVYWYYCQWFCHALHMEMRGRMLVEPKEA------------- 652
P. nautica               VTFTAGKPGVYWYYCNWFCHALHMEMVGRMLVEAA--------------- 581
W. succinogenes          VTFTADEEGVFPYYCTEFCSALHLEMMGYLYVKDPKKKYESVKELKLQKM 658
                         ***.* : **: ***  ** ***:** * : *:

A. cycloclastes          --------------------------------------------------
P. denitrificans         --------------------------------------------------
P. nautica               --------------------------------------------------
W. succinogenes          SKEQLESEYKKVIATNKATDDVIQSVVKFLKDKNYAKYPKVKSLVEDALD 708


A. cycloclastes          --------------------------------------------------
P. denitrificans         --------------------------------------------------
P. nautica               --------------------------------------------------
W. succinogenes          QYGKIGEVKAKADESYKKGDVNGAILWEYQVWQYMVKTADVGLRAKNNLA 758

A. cycloclastes          --------------------------------------------------
P. denitrificans         --------------------------------------------------
P. nautica               --------------------------------------------------
W. succinogenes          KELATPMKPAAQKGEEAYLKGGCNGCHVIGQVSSGPDLTGVLSRHENAEK 808


A. cycloclastes          --------------------------------------------------
P. denitrificans         --------------------------------------------------
P. nautica               --------------------------------------------------
W. succinogenes          WVFDFIKNPASKYEEDYVKTMINYFNLRMPNQHMNDQEIKDIIEYLKWID 858


A. cycloclastes          ------
P. denitrificans         ------
P. nautica               ------
W. succinogenes          ENAGLF 864
```

Figure 4.2 – Amino acid sequence comparison of N_2ORs. Comparison was performed using the program CLUSTALW (*41*) on the EBI Web site.

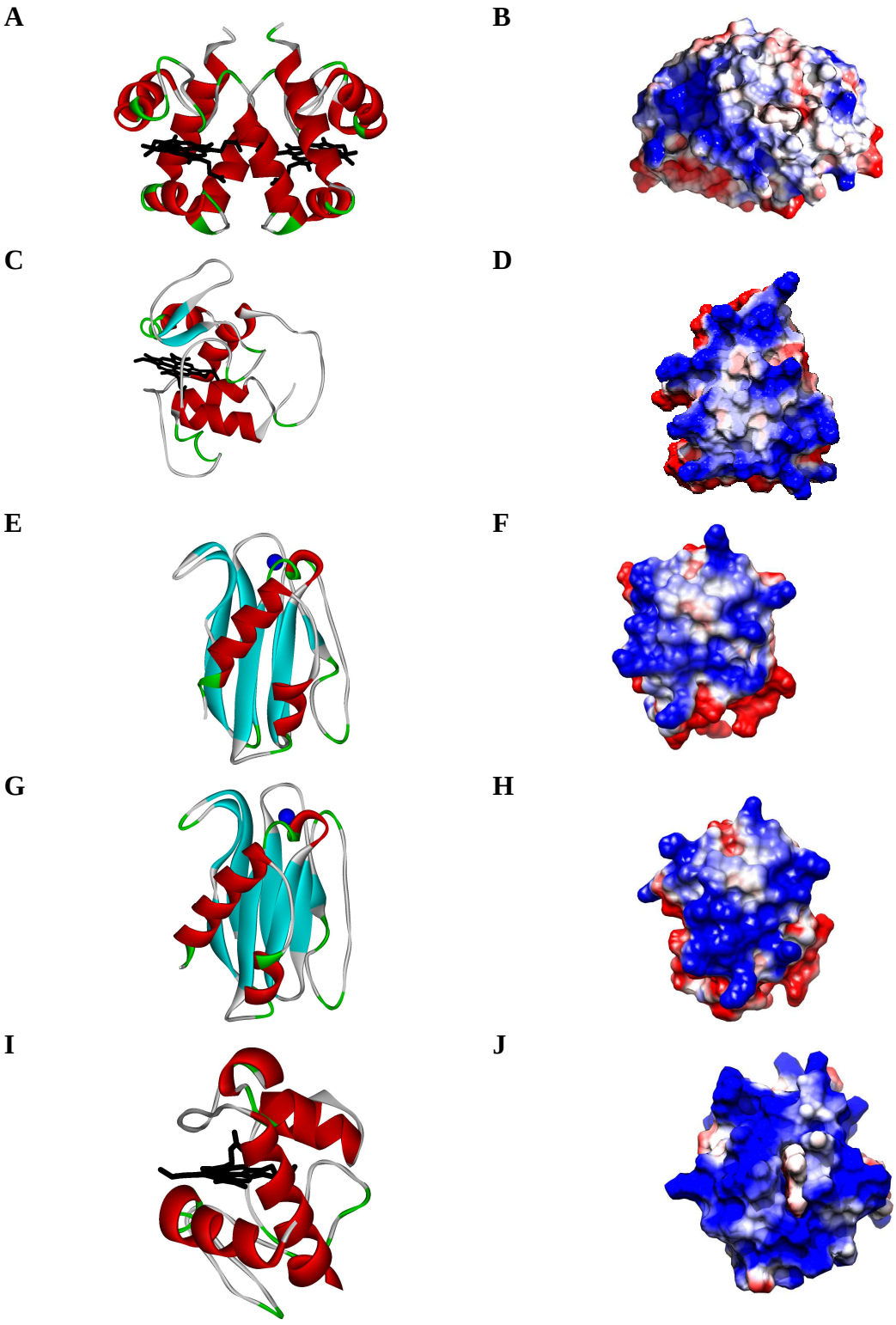

Figure 4.3 – Structures and charge distribution of *Pn* cytochrome c_{552} (A-B), *Pd* cytochrome c_{550} (C-D), *Pp* pseudoazurin (E-F), *Ac* pseudoazurin (G-H), HH cytochrome *c* (I-J). In panel A, C, E, G and I the heme group is black coloured, while the copper atom is blue. In panel B, D and F the aminoacidic residues are represented in order of their electrostatic properties: the negatively charged residues are blue, the positively charged residues are red and the hydrophobic residues are white.

In general, electrostatic interactions are proposed to be instrumental in the pre-orientation of the partners for the formation of a competent electron transfer complex, during the formation of the encounter complex, rather than at the interface of the final electron transfer complex. Moreover, in the "pseudo-specific" docking, when several proteins can act as electron donors to the same enzyme or, on the other hand, one enzyme can receive electrons from different small protein carriers, the hydrophobic patch that surrounds the exposed entry/exit site for the electron has a prominent role (*47*).

The interaction of *Pn* cytochrome c_{552} with the partner proteins is proposed to be driven mainly by hydrophobic effects, while for *Pd* electron transfer complexes the electrostatic forces have been proposed to play a higher role, and similarly mitochondrial cytochrome *c* interactions are also driven by electrostatic forces (*10, 23, 48*).

In pseudoazurin from *Ac* and *Pp*, the contact site close to the Cu centre and centred around the exposed histidine that coordinates this copper ion, is constituted by an hydrophobic surface surrounded by positive charged residues, suggesting an electrostatic interaction with the redox partner (*49, 50*).

4.4.2 Molecular docking simulation

The docking analysis of the complex formed between *Ac*, *Pd* and *Pn* N_2OR and the respective physiological and non-physiological electron donors was performed. In each case, the first stage of the BiGGER algorithm provides a set of 5000 solutions chosen from all the possible orientations generated by rotating the small electron donor (probe) around the surface of each nitrous oxide reductase (target) in steps of 1 Å and translation step of 15°. In the second stage, the docking results were analysed considering the top solutions ranked by Global Score and either hydrophobic or electrostatic Score depending on the nature of the electron transfer complex (see Methods).

Although the primary sequence of *Pp* N_2OR is not known, it is expected to have a high identity to the enzyme from *Pd* attending to the high sequence identity that is found in the other proteins from these two organisms (92% and 95% sequence identity for cytochrome c_{550} and pseudoazurin, respectively). This high homology justifies not only the use of *Pp* pseudoazurin structure, in the docking studies, but also of the biochemical properties of *Paracoccus*

pantotrophus nitrous oxide reductase, as it was reported that the increase in ionic strength decreases the activity of N_2OR in the presence of HH cytochrome *c*, which is an indication that the complex formed has an electrostatic nature (*23*).

In the case of *Pn* N_2OR there is information that in the complex between the enzyme and cytochrome c_{552}, the physiological electron donor, the interaction is hydrophobic (Chapter 2 and ref. *22*). However, in the case of nitrous oxide reductase from *Achromobacter cycloclastes*, there is no evidence in the literature for the complex to be of either electrostatic or hydrophobic nature. Nevertheless, there are several studies that have shown that the copper containing nitrite reductase (CuNiR) and pseudoazurin from this organism form an electrostatic complex (*50, 51*). Thus, we propose that the electron transfer complex formed between pseudoazurin and N_2OR, from this same organism, has a similar nature.

Therefore in the second stage, the docking solutions were analysed taking into account this information about the complex. The top 200 solutions ranked by Global Score and electrostatic score or hydrophobic score were analysed and their representations are shown in Figure 4.4 and in Supplementary Material (Figures 4.S1, 4.S2 and 4.S3).

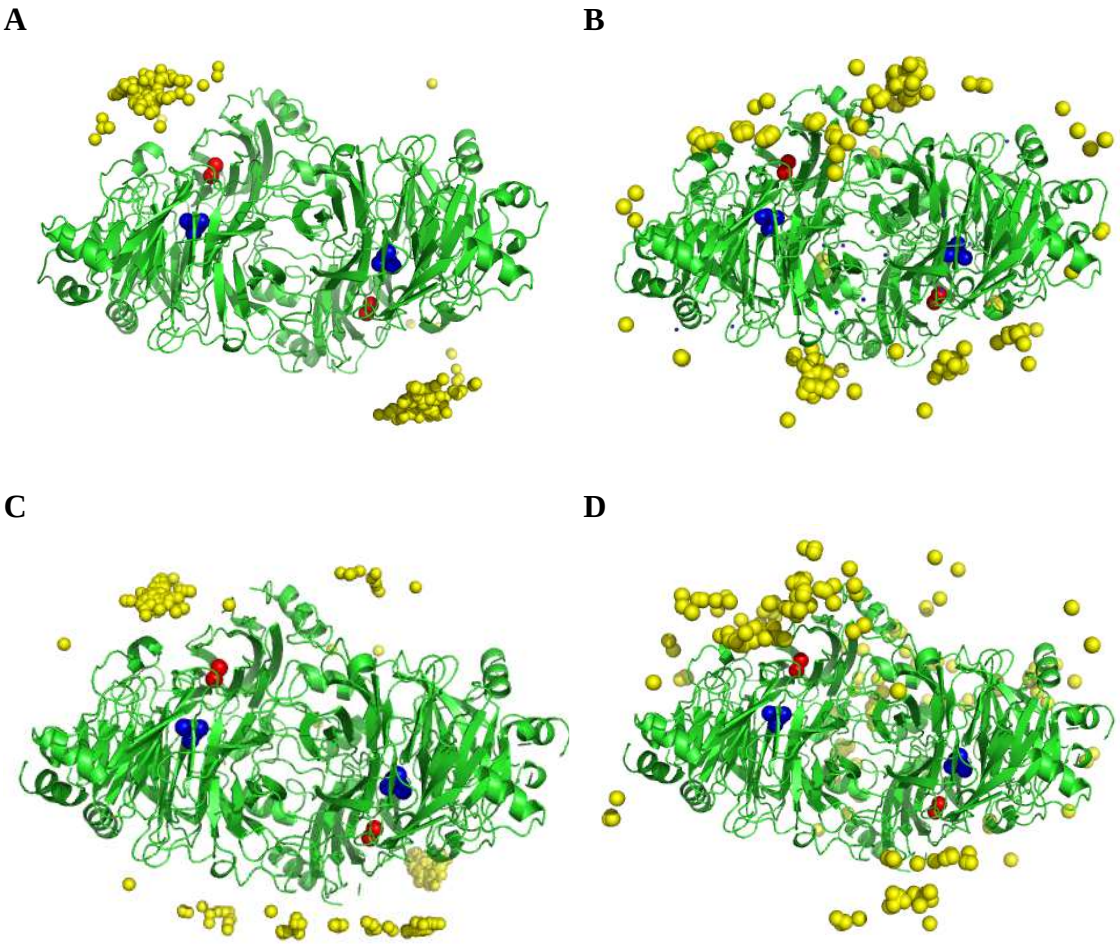

Figure 4.4 – The electron transfer complexes between N_2OR and its physiological electron donors. (A) 200 best electron transfer complexes ranked by hydrophobic ranking of *Pn* N_2OR with *Pn* cytochrome c_{552}. (B) 200 best electron transfer complexes ranked by electrostatic ranking of *Ac* N_2OR with *Ac* pseudoazurin. (C) 200 best electron transfer complexes ranked by electrostatic ranking of *Pd* N_2OR with *Pd* cytochrome c_{550}. (D) 200 best electron transfer complexes ranked by electrostatic ranking of *Pd* N_2OR with *Pp* pseudoazurin. The geometric centre for cytochrome c_{552}, the copper atom for pseudoazurin and the iron atom for cytochrome c_{550} are represented as a yellow sphere. The two copper atoms of CuA are coloured red, while the catalytic centre is coloured blue.

Previously, direct electron transfer studies have shown, for *Pp* and *Pn* N_2OR, that the small electron transfer proteins donate electrons directly to CuA of N_2OR (*22, 23*). Therefore, the solutions were then filtered using the condition that the distance between the redox centres, the binuclear CuA centre of N_2OR, and the Fe ion of cytochrome *c*, or Cu ion of pseudoazurin, should be less than 20 Å, a condition required for efficient electron transfer (*16*).

In order to further analyse the results obtained, and in an attempt to determine whether the docking program can be used to discriminate between effective and non-effective electron donors, the score obtained for each of the top 200 solutions were ranked as a function of the distance between the redox centres (a summary of the results in presented in Table 4.1, and

the representation of these results are in the Supplementary Materials, Figures 4.S1, 4.S2 and 4.S3).

Table 4.1 – Analysis of the molecular docking s between N_2OR from different microorganisms and the electron donors performed with BiGGER algorithm (*3*).

N_2OR *source*	electron donor	Best 200 GB+d<20Å[a]	Best 200 electostatic+d<20Å[b]	Best 200 hydrophobics+d<20Å[c]
Pn	*Pn* cyt c_{552}	23	41	139
Pn	*Pd* cyt c_{550}	/	/	3
Pn	HH cyt *c*	/	/	/
Pn	*Ac* pseudoazurin	1	4	8
Pn	*Pp* pseudoazurin	/	4	4
Pd	*Pd* cyt c_{550}	9	83	80
Pd	*Pp* pseudoazurin	5	20	35
Pd	HH cyt *c*	12	92	108
Pd	*Ac* pseudoazurin	1	27	39
Pd	*Pn* cyt c_{552}	4	34	66
Ac	*Ac* pseudoazurin	6	85	55
Ac	BH cyt *c*	1	44	37
Ac	*Pd* cyt c_{550}	12	126	42
Ac	*Pn* cyt c_{552}	8	79	62
Ac	HH cyt *c*	/	26	27
Ac	*Pp* pseudoazurin	9	26	40

([a]) number of solutions in the top 200 in Global Score ranking with a CuA-Fe/Cu distance lower than 20Å.
([b]) number of solutions in the top 200 in electrostatic ranking with a CuA-Fe/Cu distance lower than 20Å.
([c]) number of solutions in the top 200 in hydrophobic ranking with a CuA-Fe/Cu distance lower than 20Å.

In the case of *Pn* N_2OR, the complex with the electron donor cytochrome c_{552} shows a higher number of putative effective electron transfer complex for N_2OR compared to any of the other non-physiological electron shuttles tested (Table 4.1, Figure 4.4 and Figure 4.S3). The number of solutions with an appropriate distance between the redox centres is maximum considering the hydrophobic score, as predicted taking into account the kinetic studies (*22*). Moreover, it was shown that the positively charged HH cytochrome *c* was not able to donate electrons to *Pn* N_2OR, and this result is well confirmed by the docking analysis, without any solution with the appropriate orientation for electron transfer (Figure 4.S3). On the other hand, this mitochondrial cytochrome was demonstrated to be a competent electron donor to *Pd* N_2OR (*23*), and indeed the docking simulation gives rise to several top putative orientations, in all the ranking scores used, in a geometry that is predicted to enable an effective electron

transfer (Table 4.1), even if the formation of the competent electron transfer complexes is thought to be mainly driven by electrostatic forces.

The physiological electron donors of *Pd* N_2OR have long been established to be cytochrome c_{550} and a pseudoazurin (*25, 26*). In the first case, the docking simulation gave several solutions in the top 200 of each ranking with a good orientation for electron transfer (Figure 4.4C and 4.4D and Table 4.1). The pseudoazurin shows a "lower affinity" (lower number of probable solutions) towards *Pd* N_2OR compared to cytochrome c_{550}. Our results are widely in agreement with a previous docking analysis performed with a different algorithm, FTDOCK (*27*), which supports both the use of the docking algorithm BiGGER and the methodology employed in this work for the analysis of the 5000 solution obtained from the *ab initio* soft-docking calculation.

In the last case study, the molecular docking simulation between *Ac* N_2OR and its physiological electron donor, pseudoazurin, originated several putative solutions with a short distance between the redox centers especially when the solutions were ranked by the electrostatic score (Figure 4.4B and Table 4.1).

The lower number of putative complexes obtained when pseudoazurin, either from *Achromobacter cycloclastes or Paracoccus pantotrophus* are used, can be attributed to the smaller size of protein surface that is expected to interact with nitrous oxide reductase (surface which includes the solvent exposed histidine side-chain that also coordinates the copper center), when compared with the corresponding surface in the case of the cytochromes (surface that includes the exposed heme edge). This smaller protein surface means that there is a smaller interface area involved in the electron transfer complex (below the threshold set in the program), and thus solutions were not kept by BiGGER algorithm during the early steps of the BiGGER algorithm.

It is interesting to note that the mitochondrial BH cytochrome *c*, that was shown to be able to donate electrons to CuA center of *Ac* N_2OR, behaves as potential electron donor, with more putative solutions being found when the complexes were analysed considering the interaction driven mainly by electrostatic forces (Figure 4.S1). Similarly, *Pd* cytochrome c_{550} was also predicted, by BiGGER, to function as putative electron donor to this enzyme, in an interaction with electrostatic properties. This can be explained by the fact these small proteins all have a similar electrostatic surface in the region proposed to interact with its partner, nitrous oxide reductase.

The results of the analysis of the docking simulations combined with the previous experimental data were summarized in Table 4.2.

Table 4.2 – Comparison of the experimental data available for the electron transfer complexes of N_2OR with the electron donor and the docking analysis performed.

N_2OR		*Ac* PAz	*Pp* Paz	*Pd* c_{550}	*Pn* c_{552}	Mit. cyt *c*
Pn	Exp. Data	-	-	-	Yes Hydrophobic (*22*)	No
	Docking < 20Å hydrophobic	8	4	3	139	0
Pd	Exp. Data	-	Yes Electrostatic (*24*)	Yes Electrostatic (*24*)	-	Yes Electrostatic (*23*)
	Docking < 20Å electrostatic	27	20	83	34	92
Ac	Exp. Data	Yes (*28*)	-	-	-	Yes (*30*)
	Docking < 20Å electrostatic	85	25	126	79	44

The interface accessible area of the top solutions for each of the physiologic docking analysis were evaluated; these complexes have an area between 943 to 1368 $Å^2$ (Table 4.3), which is typical for small complexes following the criteria of Lo Conte et al. (*1*). The docking models for cytochrome c_{552} – Pn N_2OR presents the higher percentage of apolar residues in the interface area (average area of 79 %), confirming the hydrophobic nature of the interaction. For Ac N_2OR and Pd N_2OR the average value of apolar residues in the interface is 64 % and 69 %, respectively, which corresponds to an electrostatic interaction between the lysine residues in cytochrome or pseudoazurin surface and glutamate or aspartate residues on N_2OR.

Table 4.3 – Parameters of the top model complex obtained by docking simulation of N_2OR with the respective electron donor

docking	ID	GB (rank)	Ele (rank)	Hydro (rank)	d (Å)	Coupling constant ([a])	Pathway	Interface area (Å^2)	(%) apolar residues [b]
BHcyt*c*–*Ac*N_2OR	4142	1.88 (387°)	-151.71 (56°)	-6.03 (440°)	15.7	2.75 × 10^{-5}	Fe-Ala554	1366	66
*Ac*Ps – *Ac*N_2OR	3203	2.17 (102°)	-91.49 (49°)	-5.36 (918°)	16.9	1.08 × 10^{-4}	Cu-Leu627	1090	63
*Ac*Ps–*Ac*N_2OR	3167	2.12 (140°)	-78.38 (162°)	-6.64 (266°)	18.9	9.35 × 10^{-6}	Cu-Leu627	1115	64
*Pp*Ps–*Pd*N_2OR	3077	2.27 (71°)	-22.65 (298°)	-6.86 (150°)	15.7	1.31 × 10^{-5}	Cu-Leu593	1277	68
Pdc_{550}–*Pd*N_2OR	4851	2.16 (62°)	-101.42 (152°)	-5.48 (1385°)	14.7	4.70 × 10^{-4}	Cu-His635	1368	67
HHcyt*c*–*Pd*N_2OR	2205	1.90 (85°)	-169.69 (145°)	-5.61 (135°)	15.3	7.63 × 10^{-5}	Fe-Ala564	1163	71
HHcyt*c*–*Pd*N_2OR	1712	1.90 (86°)	-175.13 (121°)	-6.68 (38°)	15.5	2.82 × 10^{-4}	Fe-His635	1289	70
HHcyt*c*–*Pd*N_2OR	4004	1.96 (29°)	-197.66 (27°)	-4.41 (310°)	16.4	8.99 × 10^{-6}	Fe-Ala564	1205	69
HHcyt*c*–*Pd*N_2OR	2367	1.89 (132°)	-183.39 (77°)	-5.54 (144°)	16.5	1.33 × 10^{-5}	Fe-His635	1215	68
HHcyt*c*–*Pd*N_2OR	4808	1.99 (22°)	-199.33 (21°)	-4.62 (286°)	17.3	4.63 × 10^{-5}	Fe-His635	1168	70
HHcyt*c*–*Pd*N_2OR	4737	1.91 (67°)	-179.78 (91°)	-4.39 (314°)	17.4	3.79 × 10^{-5}	Fe-His635	1148	72
HHcyt*c*–*Pd*N_2OR	1822	1.89 (133°)	-177.85 (107°)	-5.73 (119°)	17.8	8.49 × 10^{-5}	Fe-His635	1231	64
HHcyt*c*–*Pd*N_2OR	1811	1.90 (88°)	-189.2 (45°)	-7.02 (27°)	18.2	1.73 × 10^{-6}	Fe-His635	1249	69
Pnc$_{552}$–*Pn*N_2OR	105	10.38 (35°)	-22.69 (3545°)	-6.05 (13°)	16.3	3.04 × 10^{-5}	Fe-Asp519	1222	75
Pnc$_{552}$–*Pn*N_2OR	579	9.17 (51°)	-50.7 (312°)	-6.97 (2°)	17.5	3.00 × 10^{-5}	Fe-Gln497	1211	79
Pnc$_{552}$–*Pn*N_2OR	2181	10.36 (36°)	-39.64 (1118°)	-4.83 (175°)	17.9	2.06 × 10^{-6}	Fe-His566	943	84

([a]) Coupling constant is the value for the best electron transfer path from Cu or Fe atoms to CuA centers as analyzed with PATHWAYS

([b]) The percentage of the interface area of N_2OR composed of apolar atoms.

4.4.3 Electron transfer pathway

In order to establish the electron pathway from the small electron donor protein to CuA center of nitrous oxide reductase, the top complexes for each of the dockings simulation were further analysed using the program PATHWAYS. These top complexes that were chosen for further analysis had to have a distance between redox centres (small electron donor and CuA centre of N_2OR) shorter than 20 Å, and be present in the top 200 Global Score and either in hydrophobic

score, for *Pseudomonas nautica*, or in electrostatic score, for *Paracoccus denitrificans* and *Achromobacter cycloclastes* complexes.

In the case of the electron transfer complex between *Pn* cytochrome c_{552} and N_2OR there are 3 solutions that fulfil those conditions (solution with the ID 105, ID 579 and ID 2181). In the case of *Paracoccus denitrificans* N_2OR, there are experimental evidences that it can receive electrons from cytochrome c_{550}, pseudoazurin and HH cytochrome *c*, and the electron pathway was analysed for the top putative complexes between them and *Pd* N_2OR: there are one complex for *Pd* cytochrome c_{550} (ID 4851), one for *Pp* pseudoazurin and *Pd* N_2OR (ID 3077), and for HH cytochrome *c* there are 8 solutions (ID 2205, ID 1712, ID 4004, ID 2367, ID 4808, ID 4737, ID 1822 and ID 114) with d < 20 in the top 200 for Global Score and electrostatic rankings.

Finally, *Ac* pseudoazurin and BH cytochrome *c* were the only small electron transfer proteins shown to be competent in donating electrons to *Ac* N_2OR, thus 2 solutions were analysed for pseudoazurin (ID 3203 and ID 3167) and one for BH cytochrome *c* (ID 4142), which were in the top 200 for Global Score and electrostatic rankings.

As represented in Table 4.4, a conserved histidine residue (*Ac* His625, *Pd* His635 and *Pn* His566) is used as the entry point in the electron transfer path in 8 of the complexes analysed. An alanine (*Ac* Ala554, *Pd* Ala564 and *Pn* Ala495) is present in 3 complexes, a leucine (*Ac* Leu627, *Pd* Leu637 and *Pn* Leu568) in 2 complexes, while an aspartate (*Ac* Asp578, *Pd* Asp588 and *Pn* Asp519), a glutamine (*Pn* Gln497, that corresponds to *Ac* Ser556 and *Pd* Ser566) and a leucine (*Ac* Leu583 and *Pd* Leu593, that corresponds to *Pn* Val524) are each present in 1 complex.

Table 4.4 – Key residues in the electron transfer pathway

N_2OR ([a])	residue ([b])					
Ac (5)	Ala554 (1)	Ser556	Asp 578	Leu583	His625	Leu627 (2)
Pd (12)	Ala564 (2)	Ser566	Asp 588	Leu593 (1)	His635 (7)	Leu637
Pn (3)	Ala495	Gln497 (1)	Asp 519 (1)	Val524	His566 (1)	Leu568

([a]) number of docking analysed

([b]) number of solutions in which the residue is involved in the electron transfer

The sequence alignment shows that all these residues are conserved in the N_2OR from the different microorganisms, suggesting that there is a conserved region located near the CuA centre that functions both as the binding site for the electron donor and entry of the electron to this redox centre of nitrous oxide reductase, which is the electron transferring centre to CuZ centre, the catalytic centre of the enzyme (Figure 4.5).

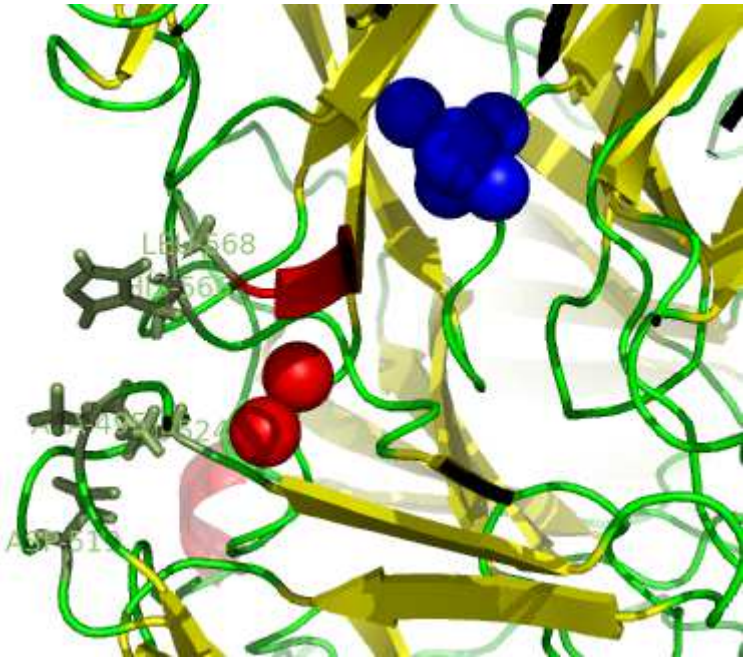

Figure 4.5 – Residues involved in the electron transfer pathways in *Pn* N_2OR structure. Ala495, Asp519, Val524, His566 and Leu568 are shown in dark green. The two copper atoms of CuA are coloured red, while the catalytic centre is coloured blue.

Once more, these results are in agreement with a previous docking study on *Pd* N_2OR with *Pd* cytochrome c_{550} and *Pp* pseudoazurin, in which three residues, His635, Ala564, and Pro565 were proposed to play key roles in electron transfer to the CuA centre (*27*).

In the case of non-physiological complexes *Ac* pseudoazurin with *Pd* N2OR and *Pp* pseudoazurin with *Ac* N_2OR, there is no solution with d <20 Å and present in the top 200 in both Global Score and electrostatic score (Table 4.3). The electron transfer pathways has been analyzed for the 3 shorter redox centre distances solutions present in top 200 electrostatic scores. Cys565 and the neighbour His566, already observed for the physiological electron donor, are involved in the electron transfer.

Nitrous oxide reductase has two domains, one can be considered the electron transferring domain and contains the CuA centre, and the other is the catalytic domain and contains the CuZ centre (*52*). The CuA domain has a cupredoxin fold similar to the one found in cytochrome *c* oxidase (COX), which also contains a similar binuclear copper centre, responsible for receiving electrons from the electron transfer partner. Thus, the electron pathway proposed for cytochrome *c* oxidase can be compared with that proposed here for nitrous oxide reductase. In cytochrome *c* oxidase from *Paracoccus denitrificans* a tryptophan residue exposed on the surface plays a crucial role for the ET (*17*), while in cytochrome *c* oxidase from *Thermus thermophilus* the electron transfer pathway is proposed to involve a phenylanine (Phe88) and a neighbouring alanine residue (Ala87) (*53*). Although, neither a tryptophan nor a

phenylanine residue is present in any of the N_2OR primary sequence in an equivalent position, there is a conserved proline and histidine residue (*27*).

In the present study, the histidine residue (*Ac* His625, *Pd* His635 and *Pn* His566) was proposed by the PATHWAYS analysis to be involved in the electron transfer pathway of several complexes, while the proline residue is the neighbouring residue of the alanine (*Ac* Ala554, *Pd* Ala564 and *Pn* Ala495) that was also proposed to be involved in some of the proposed electron transfer pathways (*27*).

In our proposed model for the electron transfer pathway the electrons will then be transferred from CuA to CuZ, through the histidine (His628 in *Ac*, His638 in *Pd* and His569 in *Pn*) that is one of the two terminal ligands of CuA. In particular, rapid electron-transfer kinetics of cytochrome *c* oxidase mutants studied by flash photolysis has proven the essential role of this residue (*54*).

4.4.4 Building a model for N_2OR from W. succinogenes

The nitrous oxide reductase from *Wolinella succinogenes* is unique in that it presents an additional domain at its C-terminal, which has the canonical sequence to bind a *c*-type cytochrome, -CXXCH-. This enzyme was shown to receive electrons from a small soluble periplasmic cytochrome isolated from the same organism, and to be always active without going to the resting state when there is lack of electrons to complete a catalytic cycle (*32*).

As the structure of this protein has not yet been solved and it can be regarded as the electron transfer complex between a nitrous oxide reductase and a cytochrome *c*, which we have just modelled, we have decided to model its structure and compare with the model complexes obtained before.

A model structure for *Ws* N_2OR was constructed in two steps: first a model of the N-terminal N_2OR domain and the C-terminal cytochrome *c* domain were created, and then the fusion of these domains was performed in order to obtain a model structure for the complete enzyme.

In the first stage of the procedure, regarding the N_2OR domain, the structure of the enzyme from *Pseudomonas nautica* (PDB code 1qni) has the highest score (with an amino acid sequence identity with *Ws* N_2OR of 34%), and was considered to be the most reliable model to be used for the *Ws* N_2OR N-terminal domain, composed by the CuA and CuZ domains. Concerning the C-terminal domain, which presents the canonical sequence of *c*-type cytochromes, CXXCH, the highest-scoring PHYRE model was given by the structure of *Rhodothermus marinus* caa_3 cytochrome *c* domain (1W2L (*55*)), followed by quinohemoprotein alcohol dehydrogenase C-terminal domain from *Pseudomonas putida* HK5 (1KV9 (*56*)), the monohemic cytochrome c_2 from *Rhodopila globiformis* (1HRO (*57*)) and the monohemic cytochrome *c* from *Rhodothermus marinus* (3CP5 (*58*)). These four model structures for the

cytochrome *c* domain were used in molecular docking experiments performed with BiGGER, as probes, while the N_2OR model built on *Pn* enzyme as a target.

However, the aminoacidic sequence alignment shows that there is a region between the N-terminal N_2OR-type domain, and the C-terminal cytochrome c-type domain which has very low homology. This region comprises around 100 residues, which were modelled using ROBETTA, as three α–helices, but this folding is specific for λ N_2OR (*27*), since it is not present in N_2OR from other sources. For this reason we cannot provide a realistic linker connecting N- and C-terminal domains. However, an acceptable docking complex can be selected taking in account that an effective electron transfer distance between the redox centre CuA and heme-iron should be less than 20 Å. In this way we can select the solutions provided by the docking simulation that have the appropriate distance.

The results show that cytochrome *c* from *Rhodothermus marinus* (3CP5) has the larger number of solutions with an appropriate Fe-CuA distance.

In particular, the two solutions with the shorter Fe-CuA distance represent a good model for *Ws* N_2OR, as they position the cytochrome *c* domain in close vicinity of the patch of the N_2OR domain that acts as the electron transfer site. Figure 4.6 shows the probable conformation of the *Ws* N_2OR.

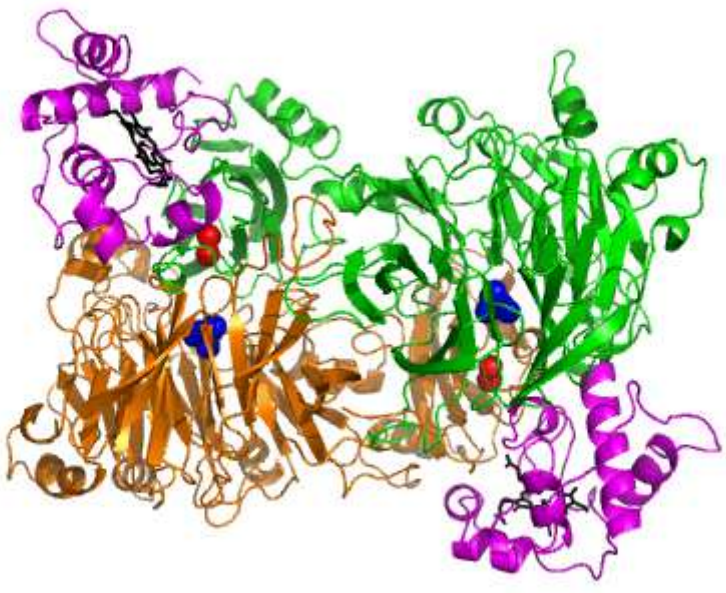

Figure 4.6 – Proposed model for the N_2OR from *Wolinella Succinogenes* with an additional C-terminal domain containing a cytochrome *c*. The heme domain (the heme group is coloured black) is shown to interact with the surface of the N_2OR domain surrounding the CuA site, the supposed entry site for the electron transfer. The two copper atoms of CuA are coloured red, the catalytic centre is coloured blue and the two domains of N_2OR are respectively green and orange coloured.

The PATHWAYS analysis in this case determined a distance of 17.8 and 18.8 Å between the Fe iron and CuA centre, with Arg557 and Cys627 in the N_2OR domain as the key residues for the entry electron. Arg557 corresponds to the conserved alanine in N_2OR from other sources (*Ac* Ala554, *Pd* Ala564 and *Pn* Ala495). Cys627 is the neighbour residue of Ser628, that corresponds to a histidine that is the entry point for several electron transfer complexes (*Ac* His625, *Pd* His635 and *Pn* His566). The involvement of these two residues in the structural model of *Ws* N_2OR gives further evidence that the same small set of conserved residues located in the same surface region of N_2OR is involved in the electron transfer reaction.

4.5 Conclusions

In conclusion, the docking studies offer a good prediction of the interaction between N_2OR and its physiological electron donor when compared to the experimental data available. Moreover, a previous docking study performed with a different algorithm used as a control experiment of our procedure, confirmed the results presented.

A set of well conserved residues is crucial for the electron transfer, suggesting the presence of specific region in both proteins, the donor and the acceptor, that enable the molecular recognition and the electron transfer. However, not one single route has been found, but a multiple set of effective pathways were identified. This comparative study enabled us to propose an electron transfer pathway, in the absence of the possibility to mutating each of the important residues.

We have also constructed a structural model for the *Ws* N_2OR that, unlike the other N_2OR structures known, presents a C-terminal extension containing a *c*-type heme binding motif. The model presents the Fe ion of the cytochrome at a distance of 17 Å from the CuA site of the N_2OR domain, forming a possible electron transfer path. The structure determination is however required to fully understand the structure of this N_2OR.

4.6 Supplementary material

Figure 4.S-1.1 N_2OR *Ac* – Cytochrome c_{550} *Pd*

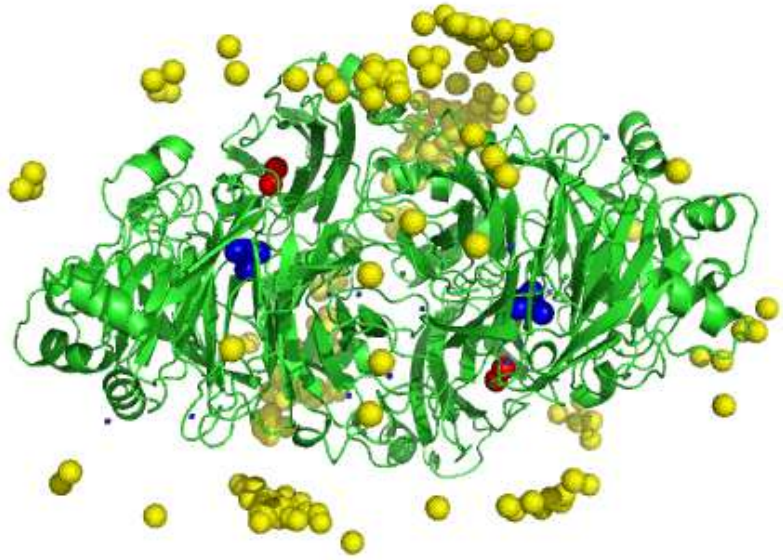

200 top model complexes ranked by global score

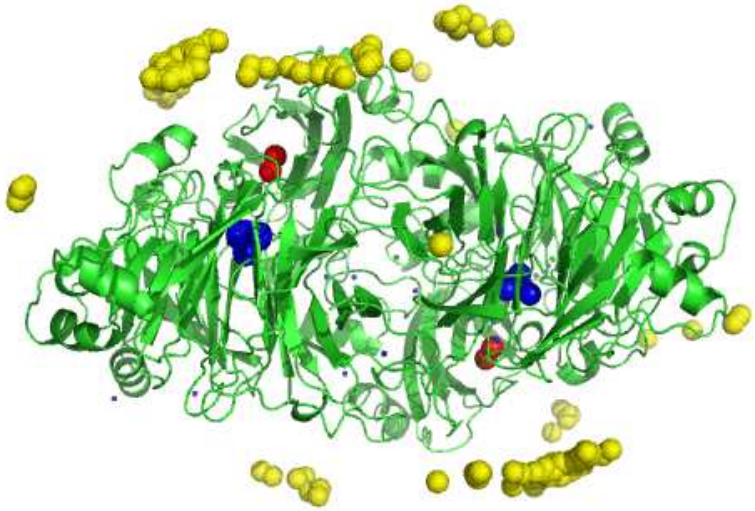

200 top model complexes ranked by electrostatic score

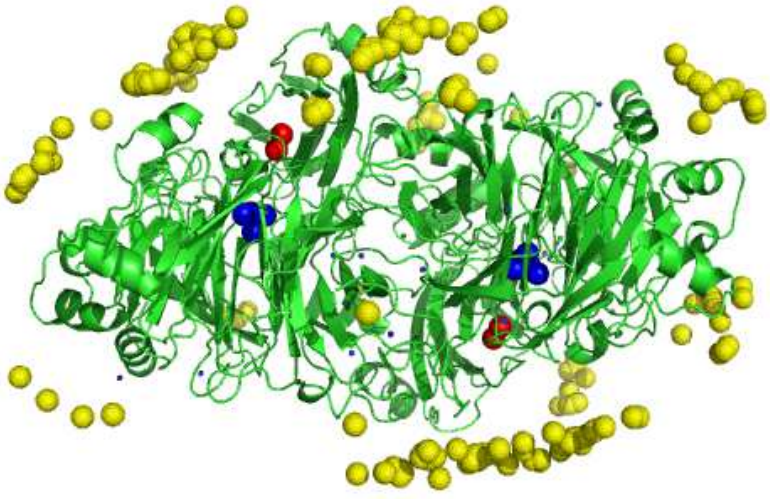

200 top model complexes ranked by hydrophobic score

Figure 4.S-1.2 N_2OR *Ac* – Cytochrome c_{552} *Pn*

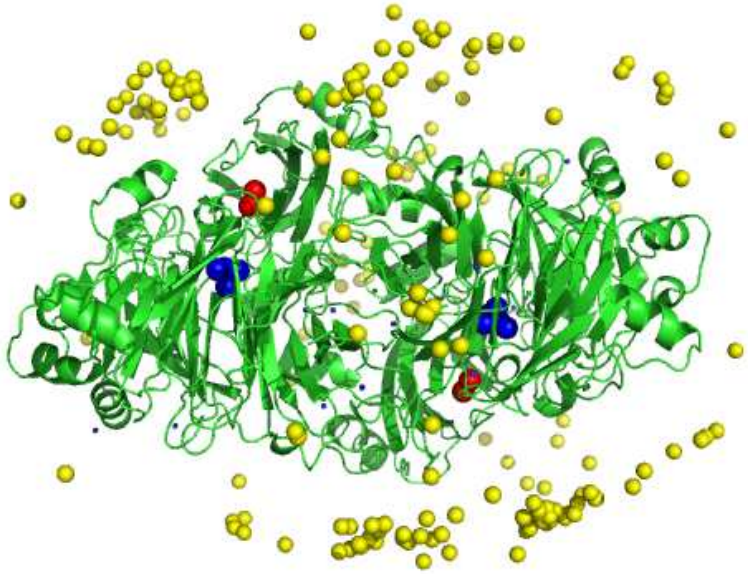

200 top model complexes ranked by global score

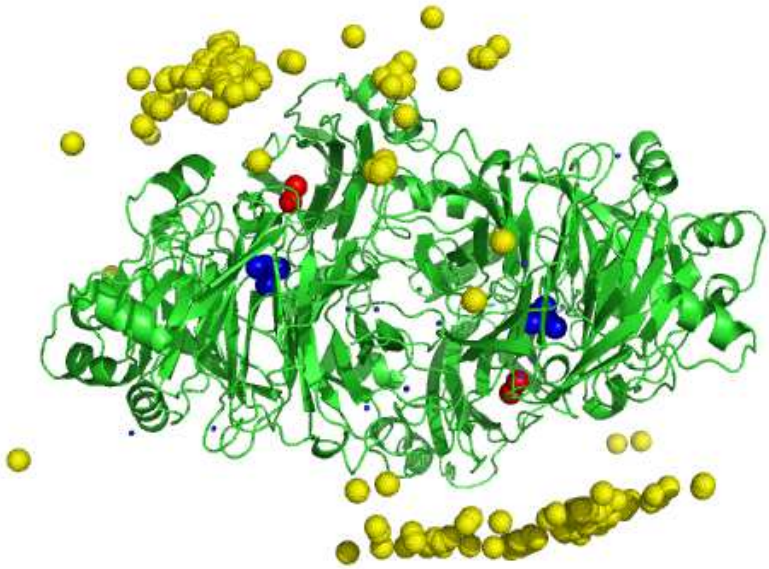

200 top model complexes ranked by electrostatic score

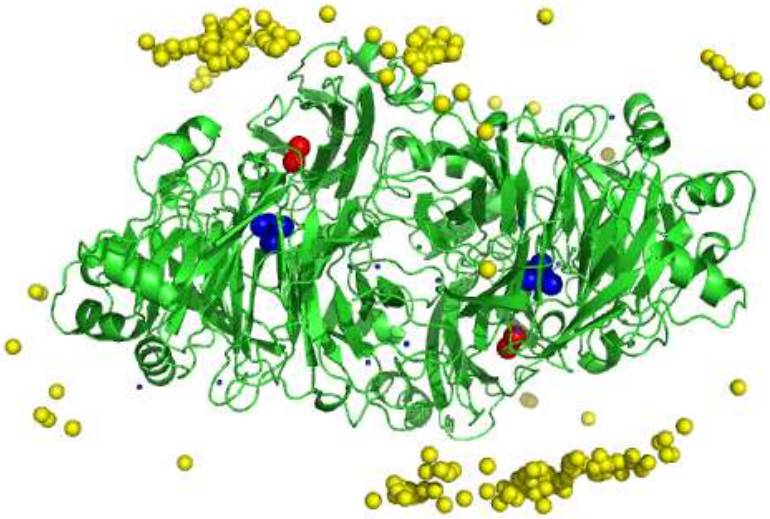

200 top model complexes ranked by hydrophobic score

Figure 4.S-1.3 N_2OR *Ac* – BH Cytochrome *c*

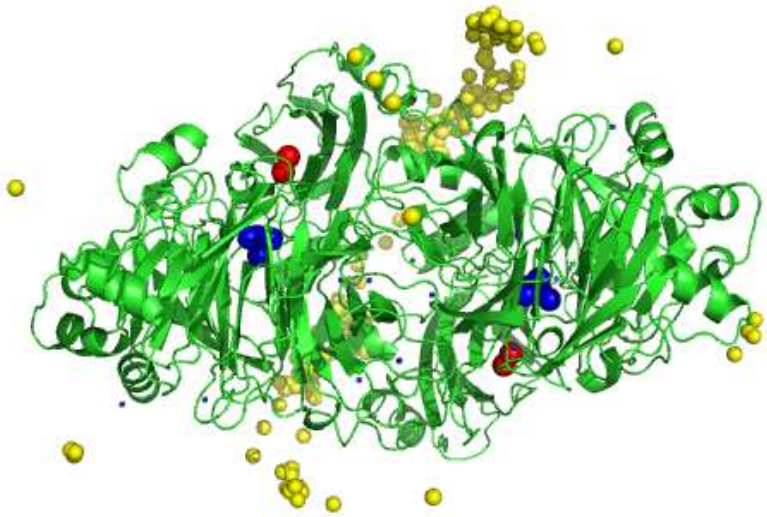

200 top model complexes ranked by global score

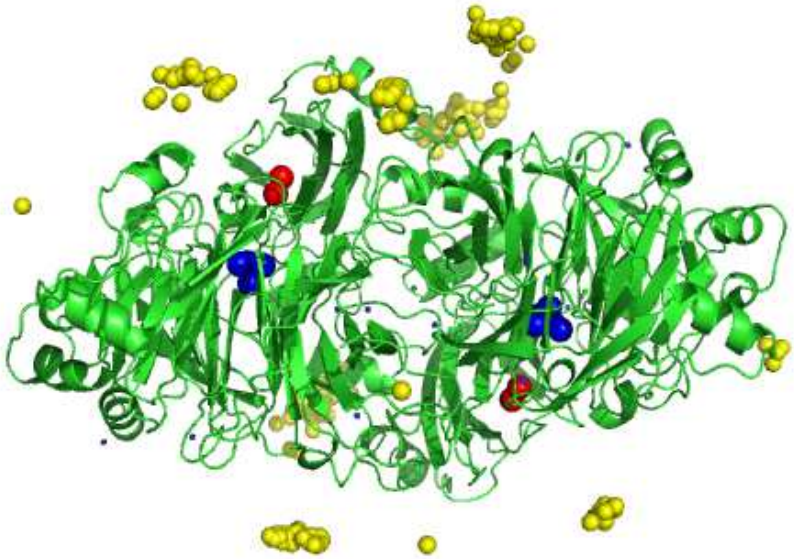

200 top model complexes ranked by electrostatic score

200 top model complexes ranked by hydrophobic score

Figure 4.S-1.4 N_2OR *Ac* – Pseudoazurin *Ac*

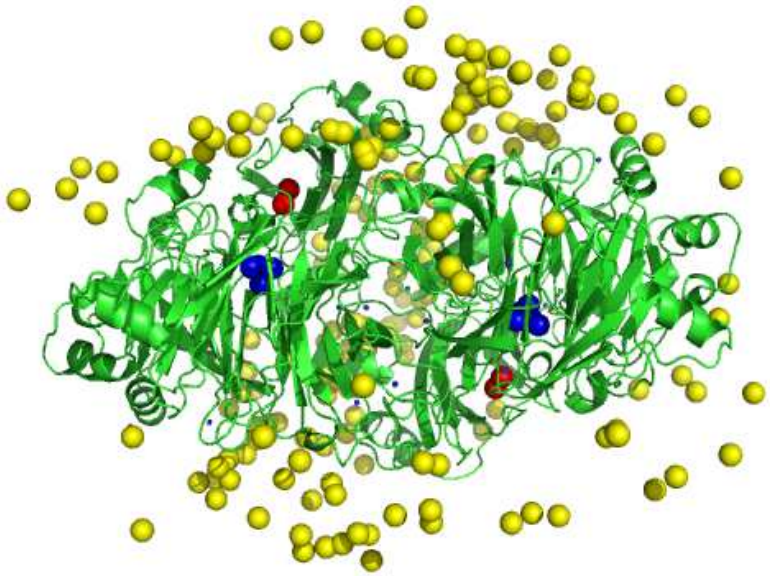

200 top model complexes ranked by global score

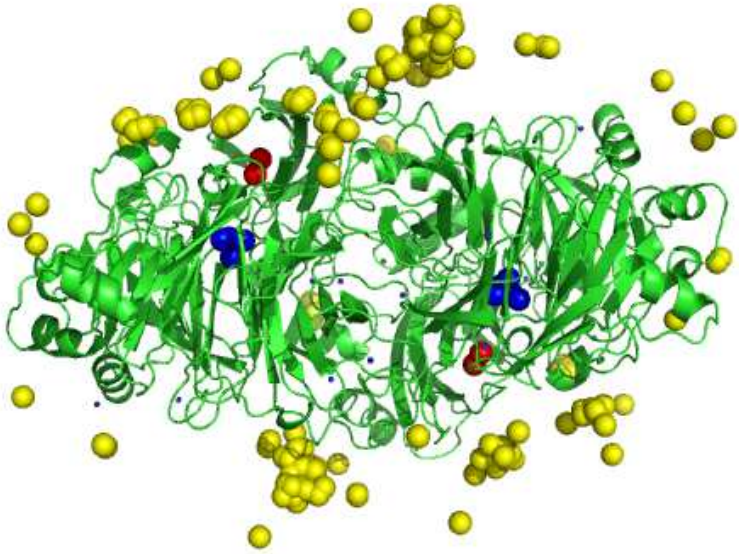

200 top model complexes ranked by electrostatic score

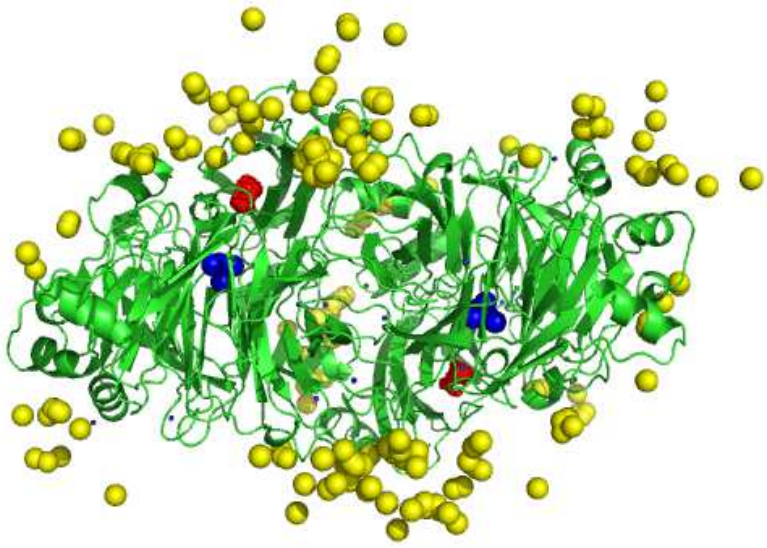

200 top model complexes ranked by hydrophobic score

Figure 4.S-1.5 N_2OR *Ac* – Pseudoazurin *Pp*

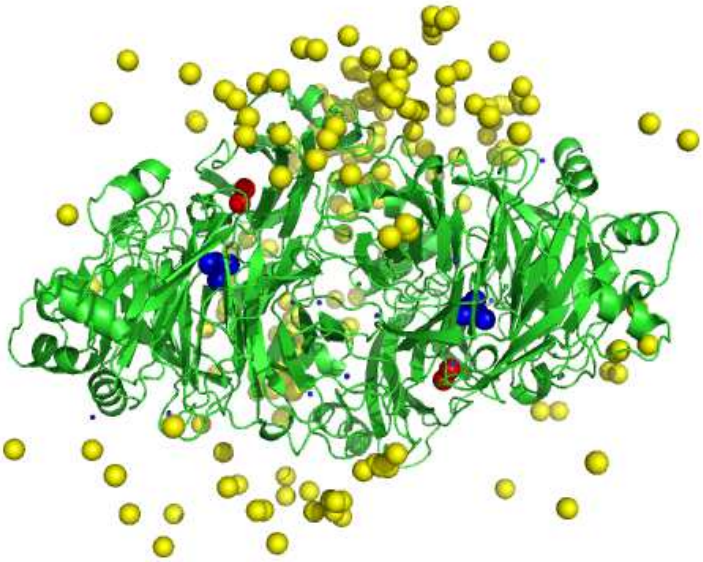

200 top model complexes ranked by global score

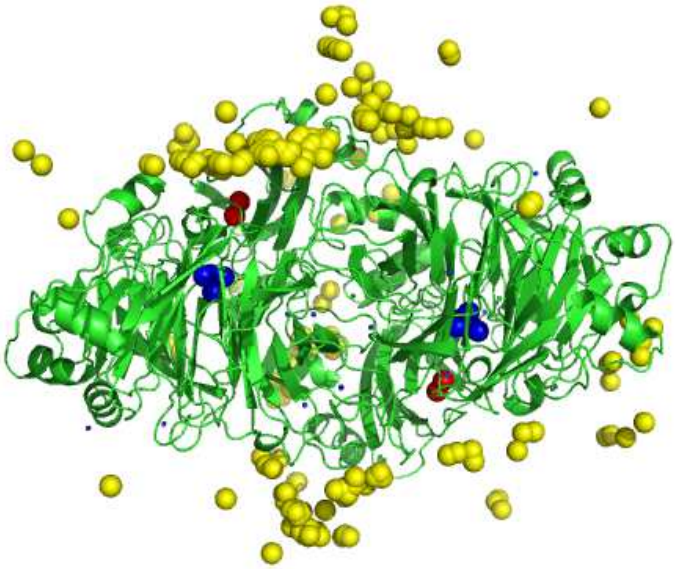

200 top model complexes ranked by electrostatic score

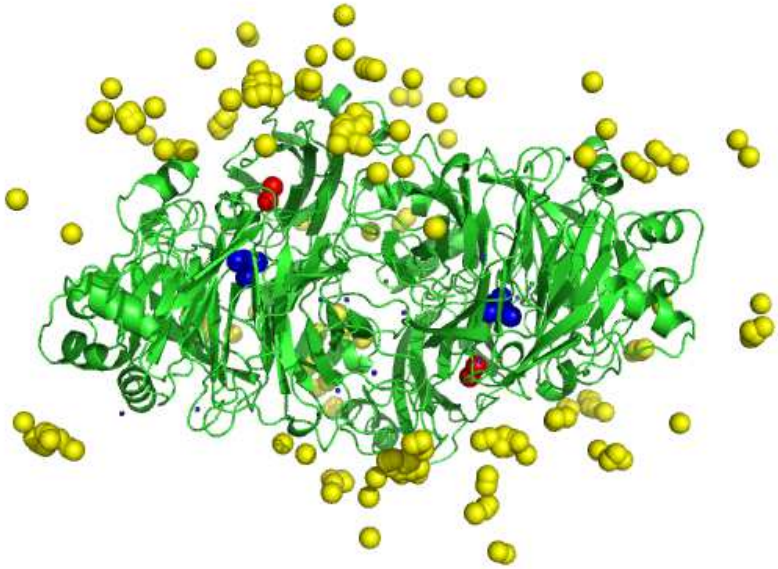

200 top model complexes ranked by hydrophobic score

Figure 4.S-2.1 N_2OR *Pd* – Cytochrome c_{550} *Pd*

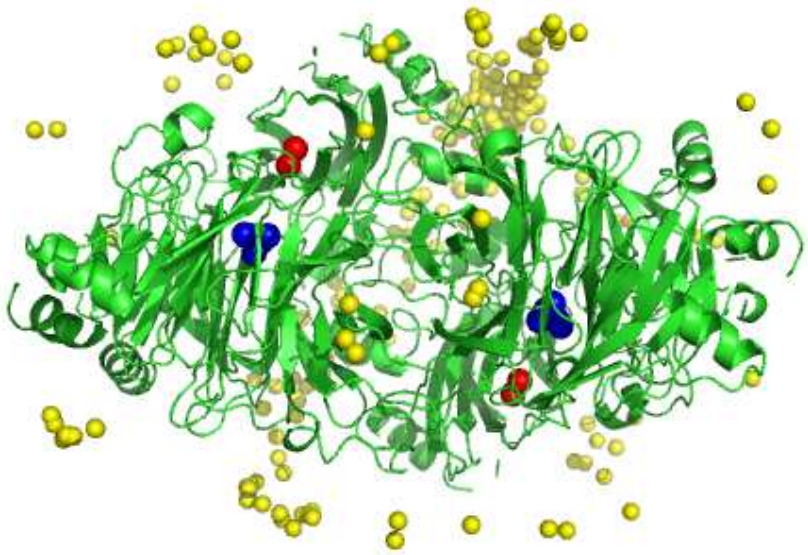

200 top model complexes ranked by global score

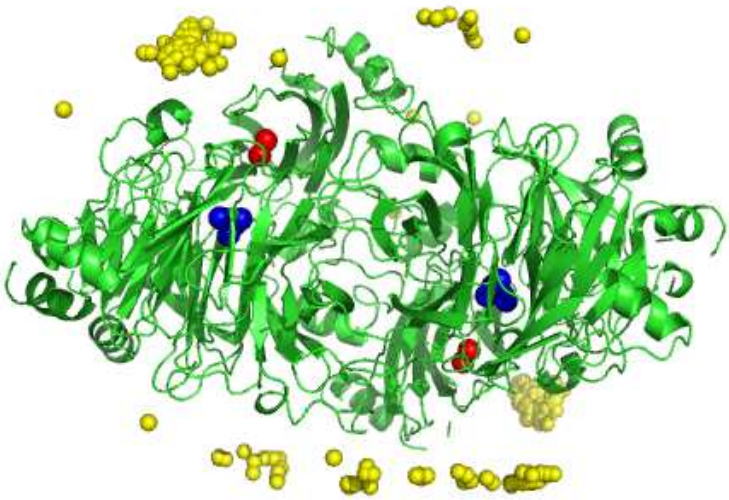

200 top model complexes ranked by electrostatic score

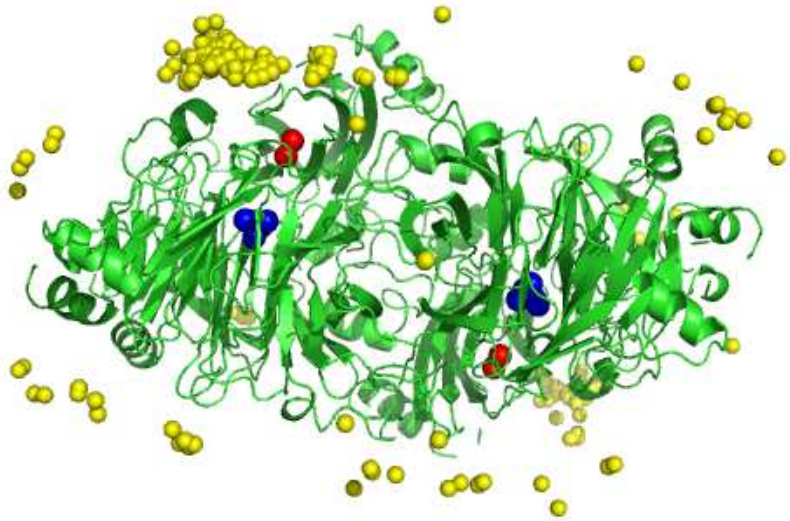

200 top model complexes ranked by hydrophobic score

Figure 4.S-2.2 N_2OR *Pd* – Cytochrome c_{552} *Pn*

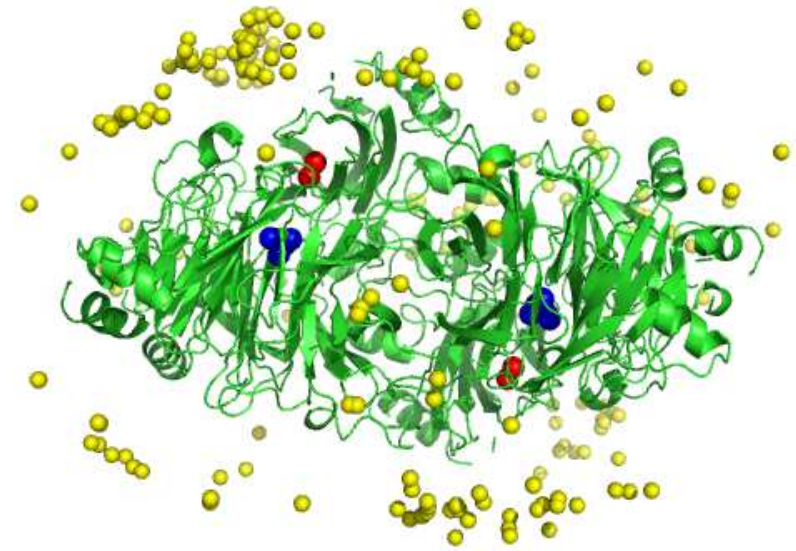

200 top model complexes ranked by global score

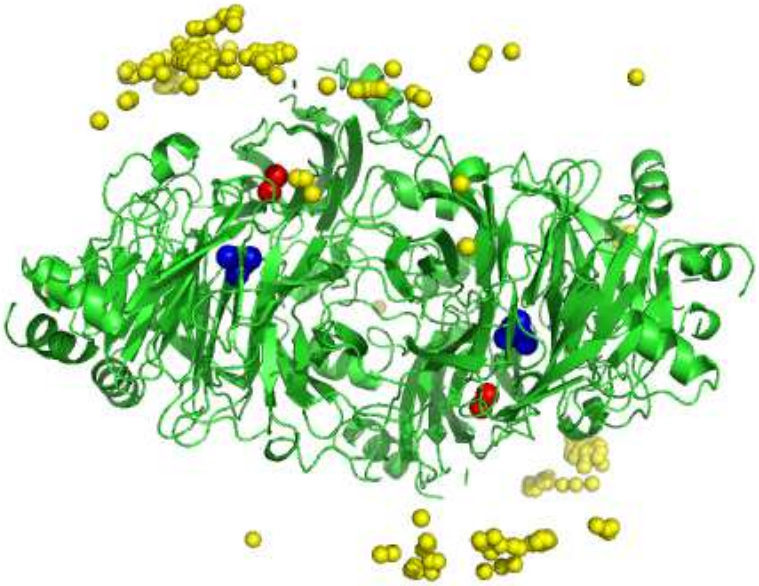

200 top model complexes ranked by electrostatic score

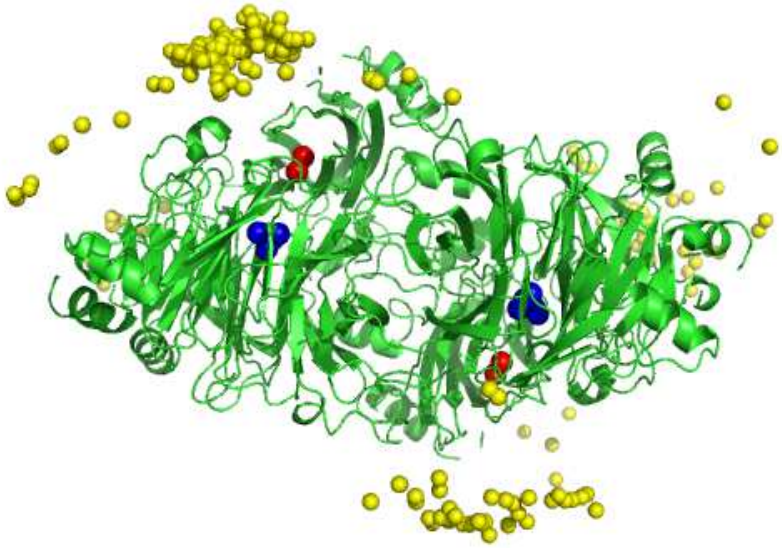

200 top model complexes ranked by hydrophobic score

Figure 4.S-2.3 N_2OR *Pd* – HH Cytochrome *c*

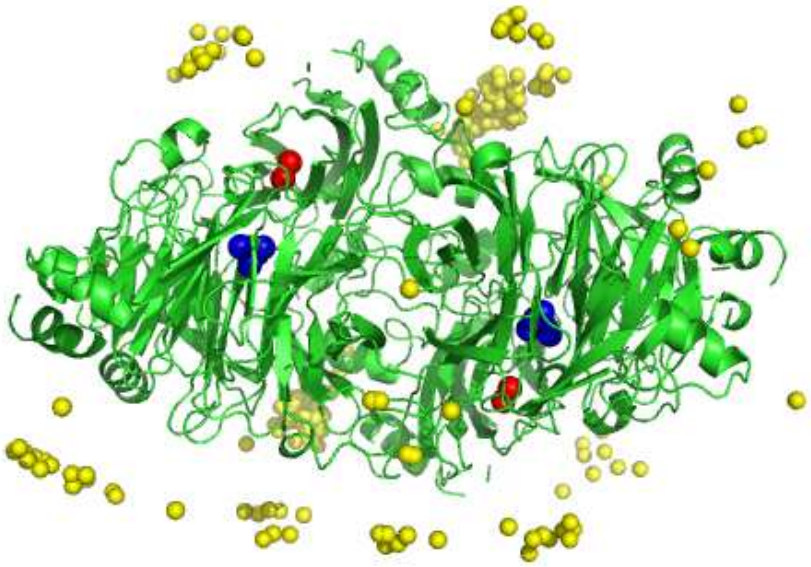

200 top model complexes ranked by global score

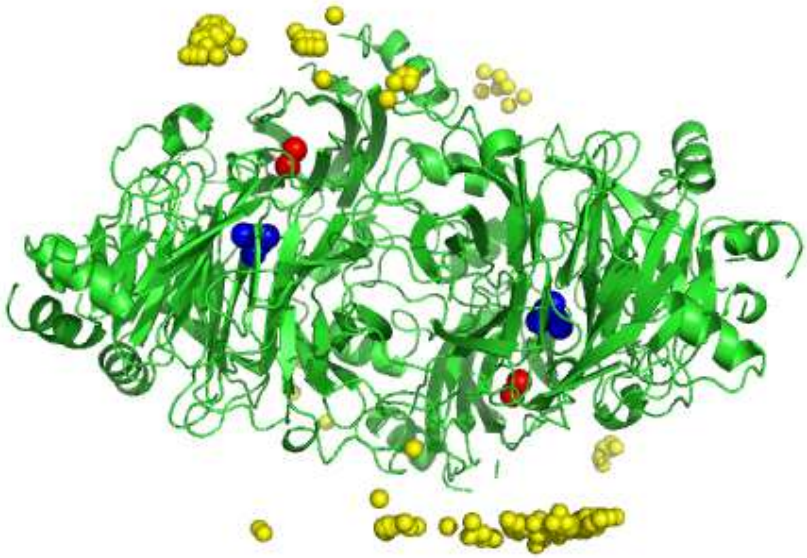

200 top model complexes ranked by electrostatic score

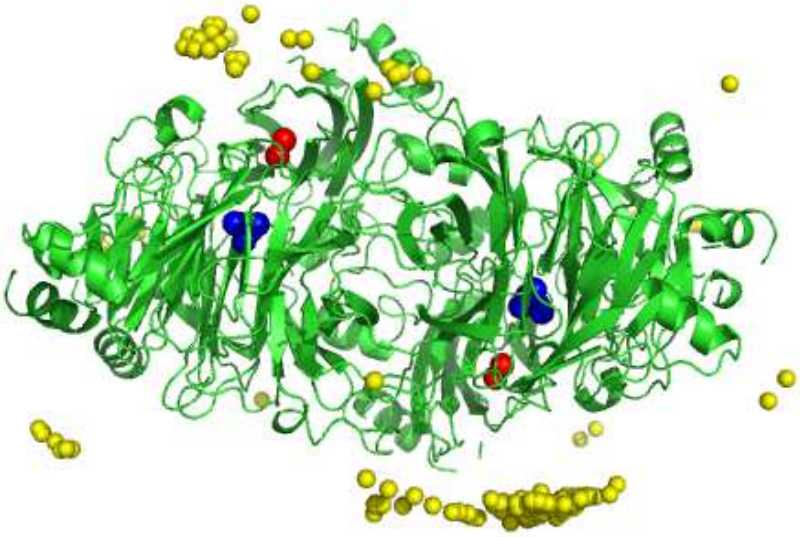

200 top model complexes ranked by hydrophobic score

Figure 4.S-2.4 N_2OR *Pd* – Pseudoazurin *Ac*

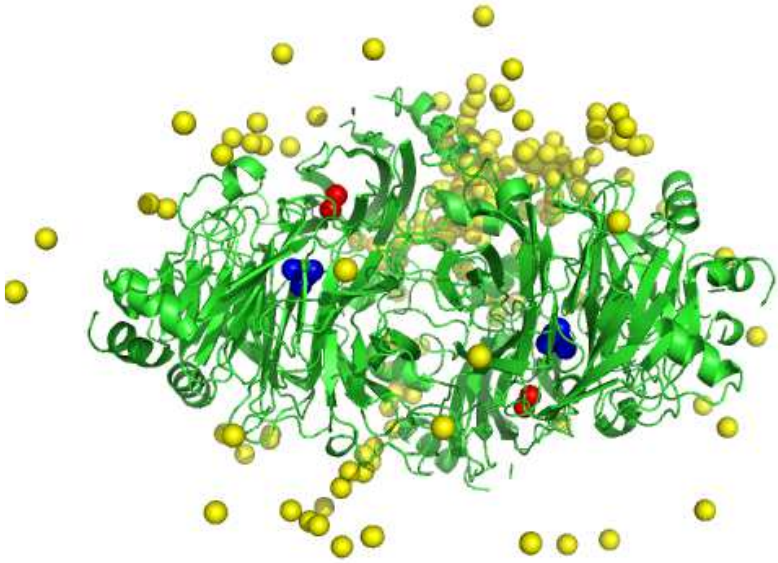

200 top model complexes ranked by global score

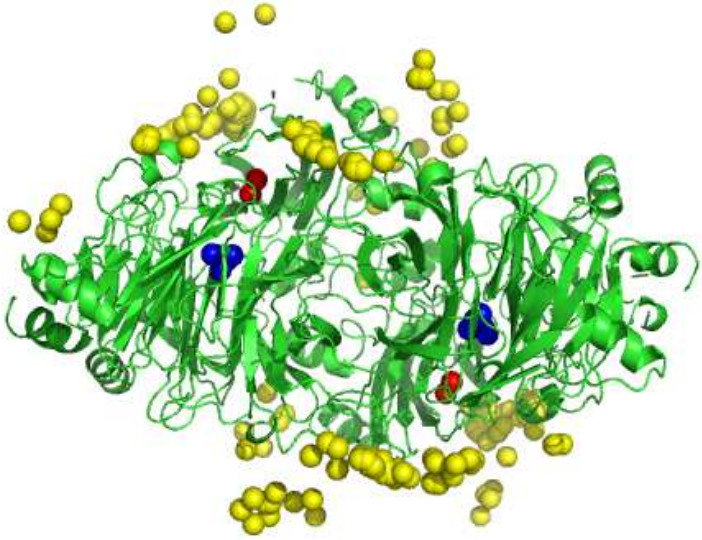

200 top model complexes ranked by electrostatic score

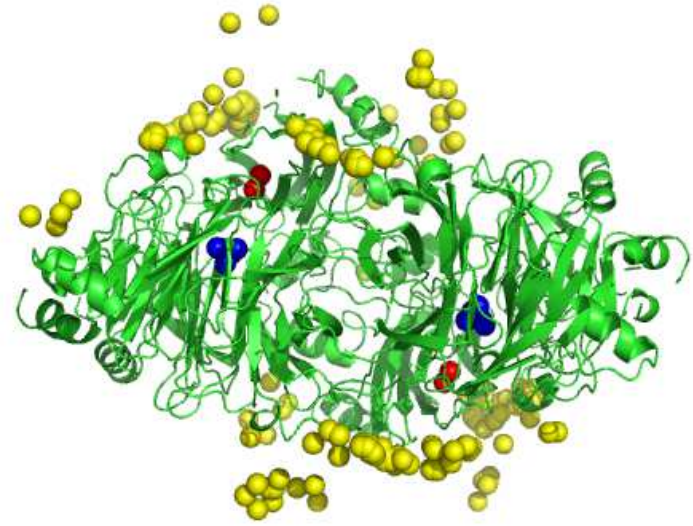

200 top model complexes ranked by hydrophobic score

Figure 4.S-2.5 N_2OR *Pd* – Pseudoazurin *Pp*

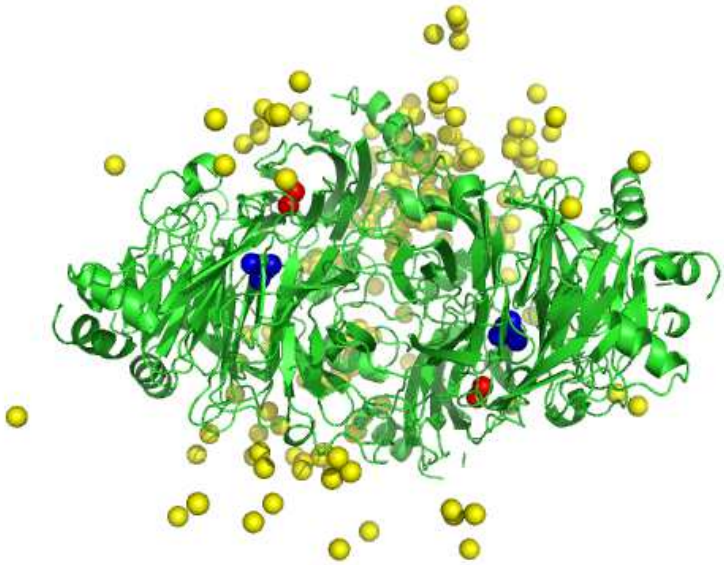

200 top model complexes ranked by global score

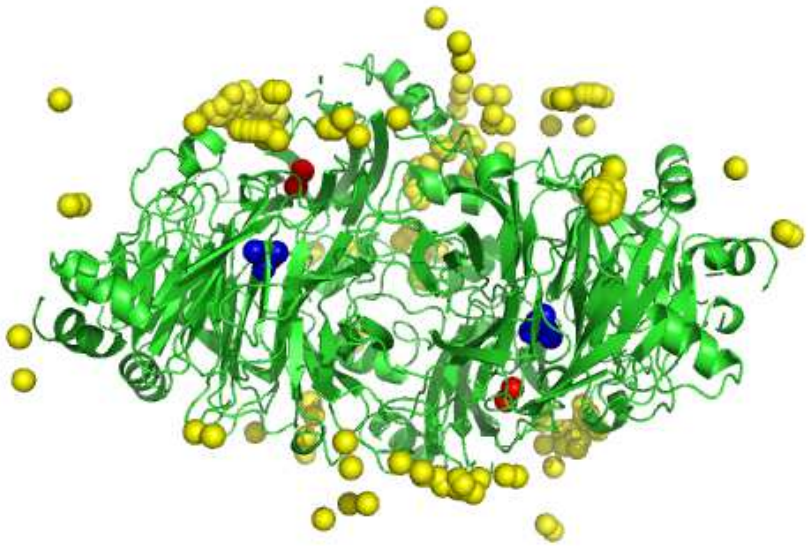

200 top model complexes ranked by electrostatic score

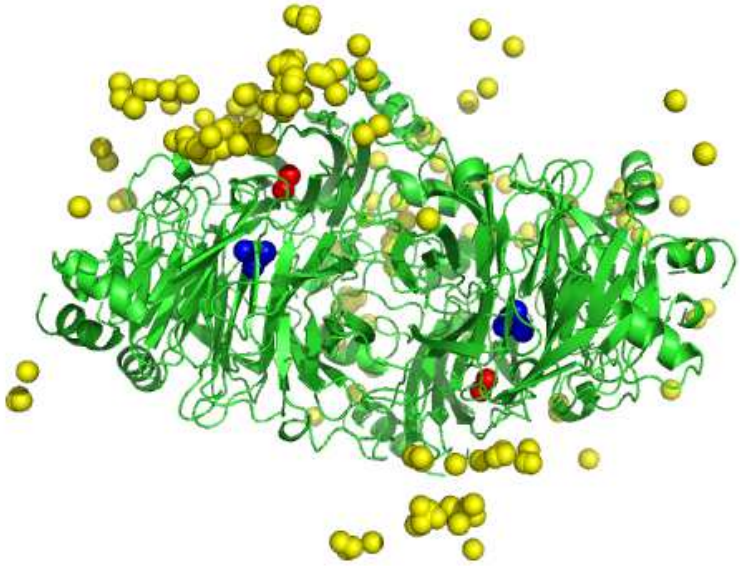

200 top model complexes ranked by hydrophobic score

Figure 4.S-3.1 N_2OR *Pn* – Cytochrome c_{550} *Pd*

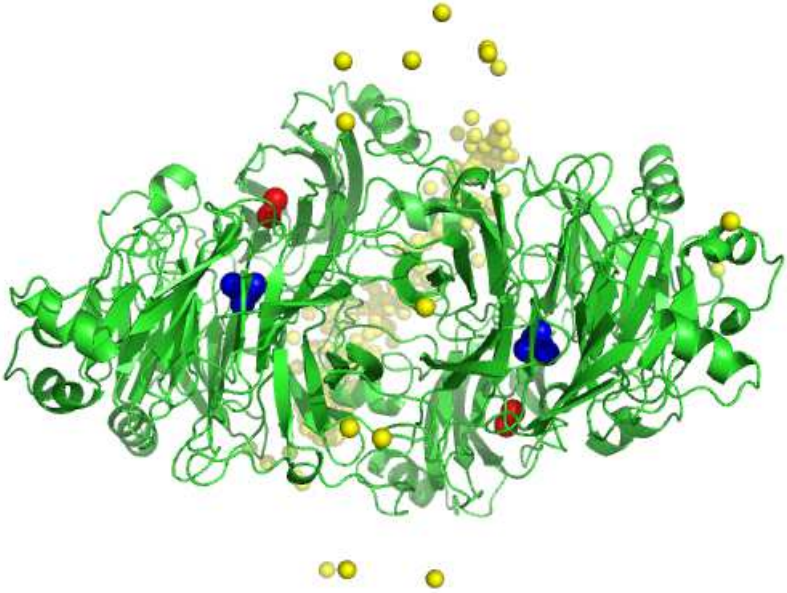

200 top model complexes ranked by global score

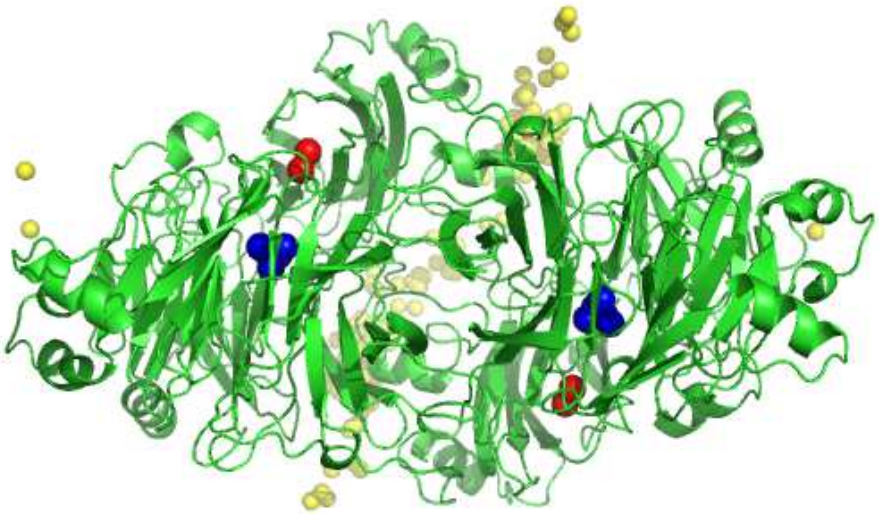

200 top model complexes ranked by electrostatic score

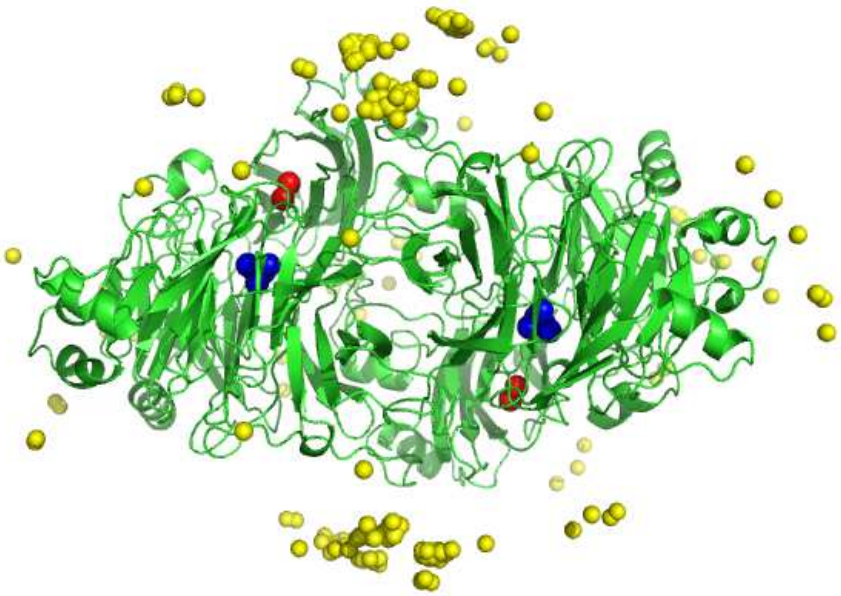

200 top model complexes ranked by hydrophobic score

Figure 4.S-3.2 N_2OR *Pn* – Cytochrome c_{552} *Pn*

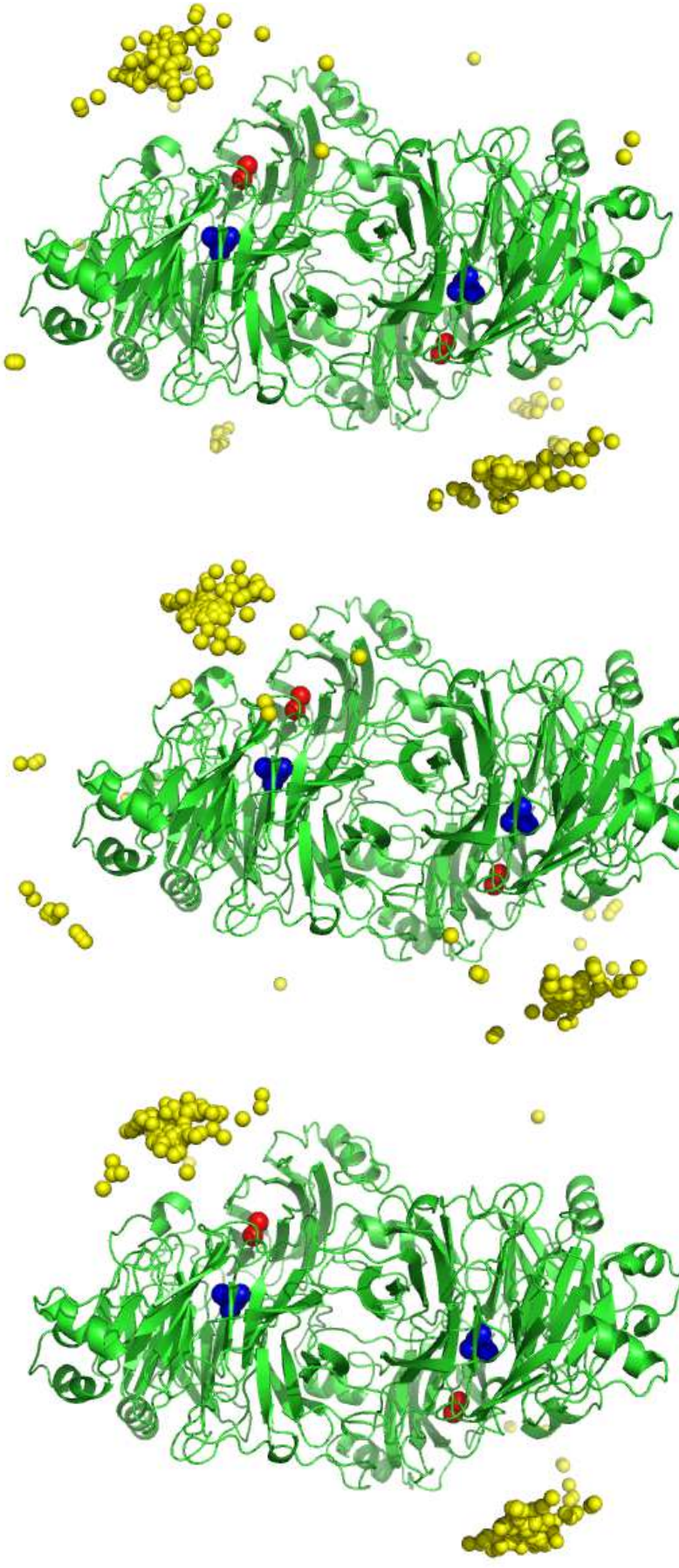

200 top model complexes ranked by global score

200 top model complexes ranked by electrostatic score

200 top model complexes ranked by hydrophobic score

Figure 4.S-3.3 N_2OR *Pn* – HH Cytochrome *c*

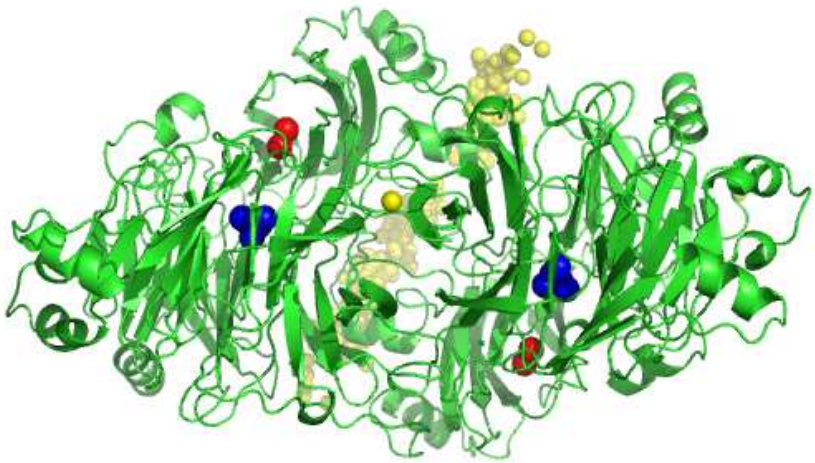

200 top model complexes ranked by global score

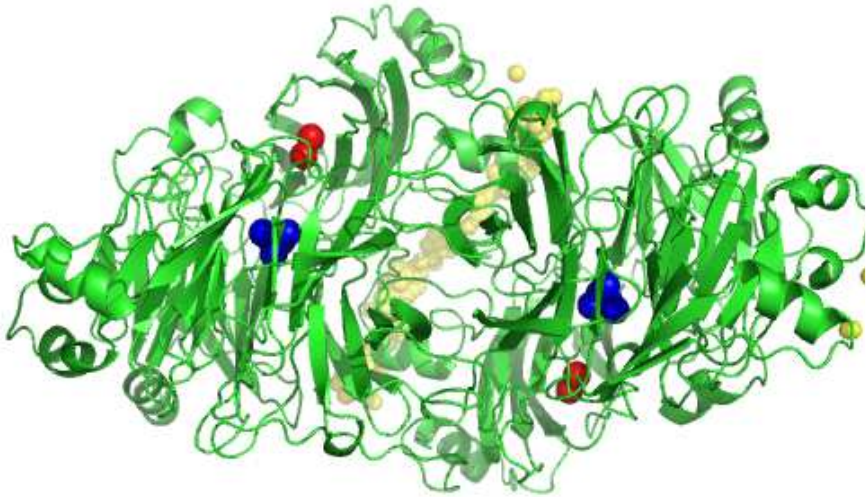

200 top model complexes ranked by electrostatic score

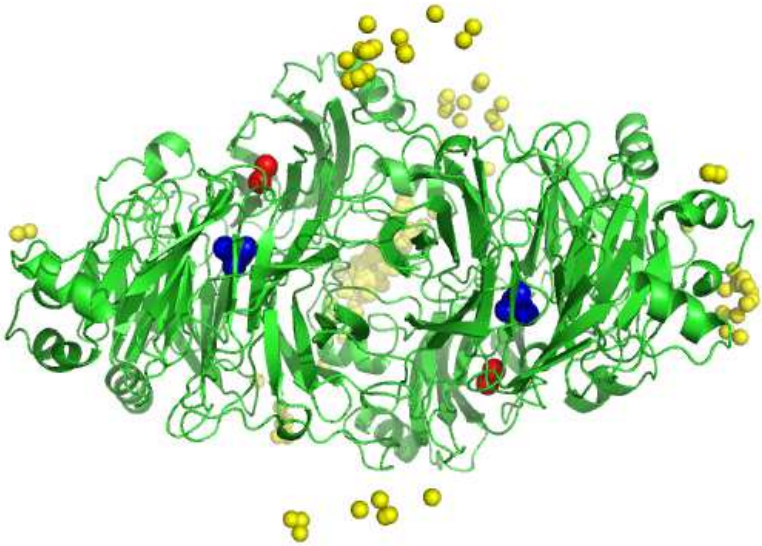

200 top model complexes ranked by hydrophobic score

Figure 4.S-3.4 N_2OR *Pn* – Pseudoazurin *Ac*

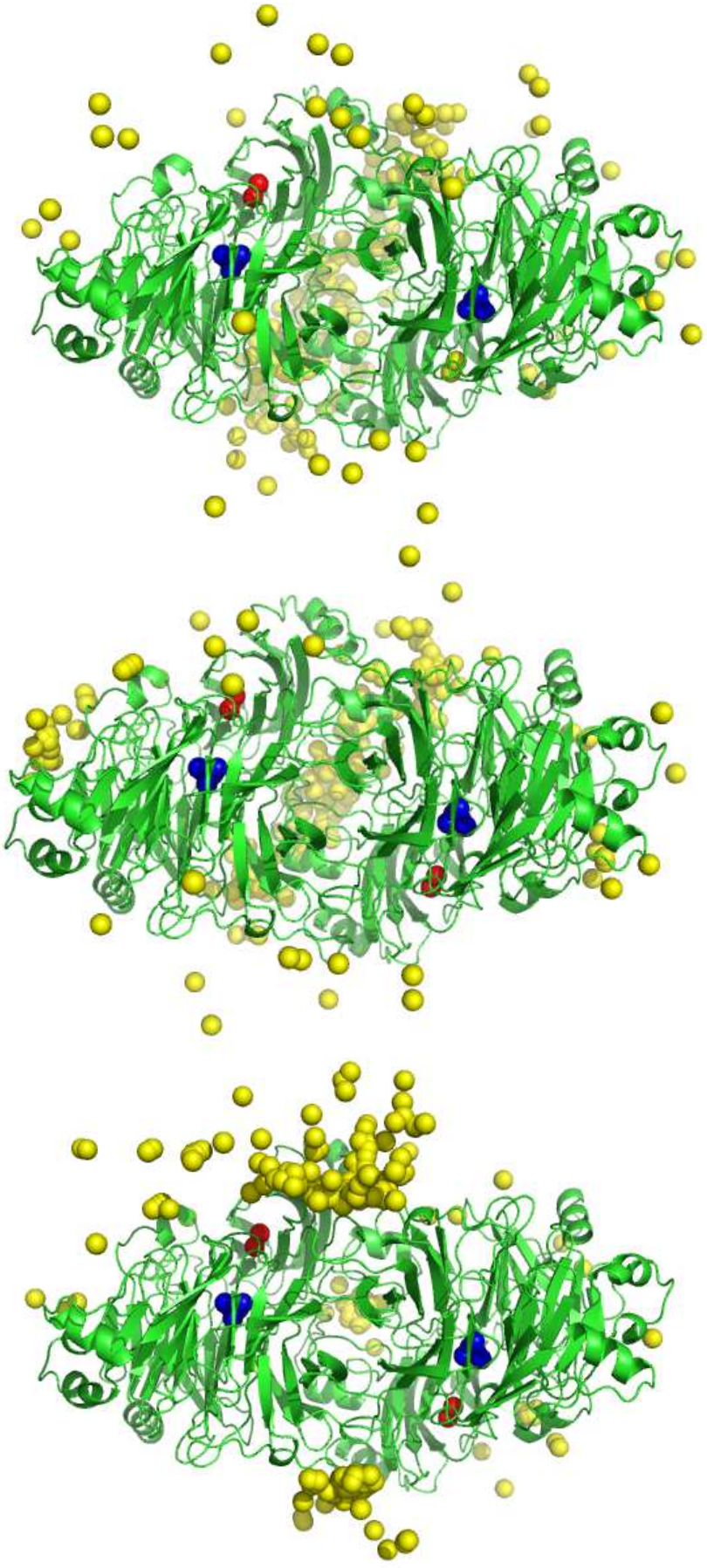

200 top model complexes ranked by global score

200 top model complexes ranked by electrostatic score

200 top model complexes ranked by hydrophobic score

Figure 4.S-3.5 N_2OR *Pn* – Pseudoazurin *Pp*

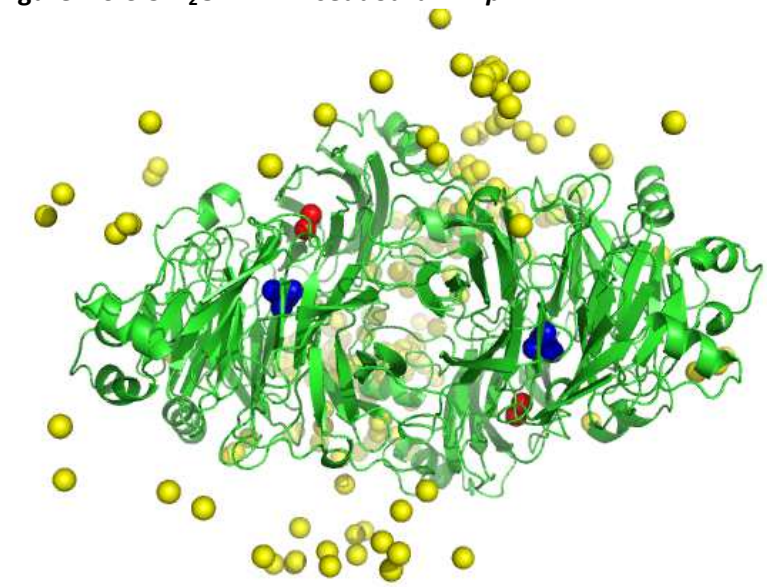

200 top model complexes ranked by global score

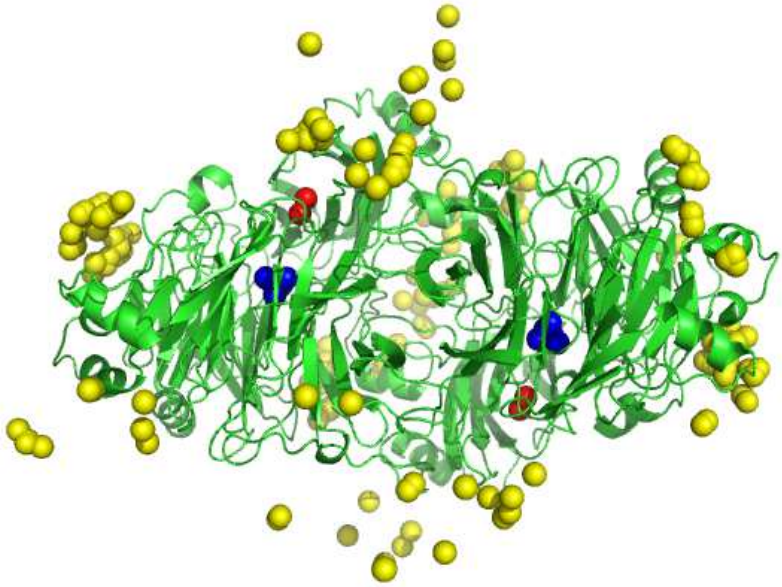

200 top model complexes ranked by electrostatic score

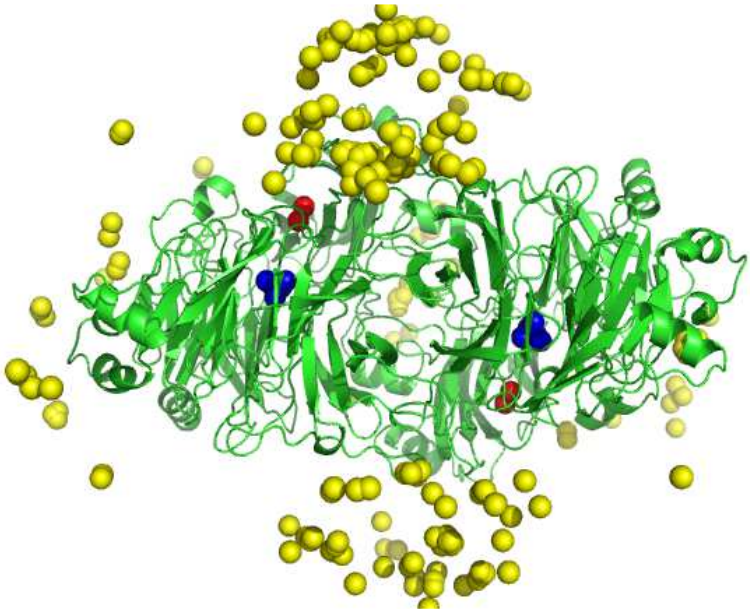

200 top model complexes ranked by hydrophobic score

4.7 References

1. Lo Conte, L., Chothia, C., and Janin, J. (1999) The atomic structure of protein-protein recognition sites, *J Mol Biol 285*, 2177-2198.
2. Prudencio, M., and Ubbink, M. (2004) Transient complexes of redox proteins: structural and dynamic details from NMR studies, *J Mol Recognit 17*, 524-539.
3. Palma, P. N., Krippahl, L., Wampler, J. E., and Moura, J. J. (2000) BiGGER: a new (soft) docking algorithm for predicting protein interactions, *Proteins 39*, 372-384.
4. Fantuzzi, A., Meharenna, Y. T., Briscoe, P. B., Guerlesquin, F., Sadeghi, S. J., and Gilardi, G. (2009) Characterisation of the electron transfer and complex formation between Flavodoxin from D-vulgaris and the haem domain of Cytochrome P450 BM3 from B-megaterium, *Biochimica Et Biophysica Acta-Bioenergetics 1787*, 234-241.
5. Xu, X. F., Schurmann, P., Chung, J. S., Hass, M. A. S., Kim, S. K., Hirasawa, M., Tripathy, J. N., Knaff, D. B., and Ubbink, M. (2009) Ternary Protein Complex of Ferredoxin, Ferredoxin:Thioredoxin Reductase, and Thioredoxin Studied by Paramagnetic NMR Spectroscopy, *Journal of the American Chemical Society 131*, 17576-17582.
6. Almeida, R. M., Pauleta, S. R., Moura, I., and Moura, J. J. G. (2009) Rubredoxin as a paramagnetic relaxation-inducing probe, *Journal of Inorganic Biochemistry 103*, 1245-1253.
7. Pauleta, S. R., Cooper, A., Nutley, M., Errington, N., Harding, S., Guerlesquin, F., Goodhew, C. F., Moura, I., Moura, J. J. G., and Pettigrew, G. W. (2004) A copper protein and a cytochrome bind at the same site on bacterial cytochrome c peroxidase, *Biochemistry 43*, 14566-14576.
8. Crowley, P. B., Diaz-Quintana, A., Molina-Heredia, F. P., Nieto, P., Sutter, M., Haehnel, W., De la Rosa, M. A., and Ubbink, M. (2002) The interactions of cyanobacterial cytochrome c(6) and cytochrome f, characterized by NMR, *Journal of Biological Chemistry 277*, 48685-48689.
9. Morelli, X. J., Palma, P. N., Guerlesquin, F., and Rigby, A. C. (2001) A novel approach for assessing macromolecular complexes combining soft-docking calculations with NMR data, *Protein Sci 10*, 2131-2137.
10. Pettigrew, G. W., Pauleta, S. R., Goodhew, C. F., Cooper, A., Nutley, M., Jumel, K., Harding, S. E., Costa, C., Krippahl, L., Moura, I., and Moura, J. (2003) Electron transfer complexes of cytochrome c peroxidase from Paracoccus denitrificans containing more than one cytochrome, *Biochemistry 42*, 11968-11981.
11. Tavares, P., Pereira, A. S., Moura, J. J., and Moura, I. (2006) Metalloenzymes of the denitrification pathway, *J Inorg Biochem 100*, 2087-2100.
12. Zumft, W. G., and Kroneck, P. M. (2007) Respiratory transformation of nitrous oxide (N2O) to dinitrogen by Bacteria and Archaea, *Adv Microb Physiol 52*, 107-227.
13. Brown, K., Tegoni, M., Prudencio, M., Pereira, A. S., Besson, S., Moura, J. J., Moura, I., and Cambillau, C. (2000) A novel type of catalytic copper cluster in nitrous oxide reductase, *Nat Struct Biol 7*, 191-195.
14. Haltia, T., Brown, K., Tegoni, M., Cambillau, C., Saraste, M., Mattila, K., and Djinovic-Carugo, K. (2003) Crystal structure of nitrous oxide reductase from Paracoccus denitrificans at 1.6 A resolution, *Biochem J 369*, 77-88.
15. Paraskevopoulos, K., Antonyuk, S. V., Sawers, R. G., Eady, R. R., and Hasnain, S. S. (2006) Insight into catalysis of nitrous oxide reductase from high-resolution structures of resting and inhibitor-bound enzyme from Achromobacter cycloclastes, *J Mol Biol 362*, 55-65.
16. Winkler, J. R. (2000) Electron tunneling pathways in proteins, *Curr Opin Chem Biol 4*, 192-198.
17. Witt, H., Malatesta, F., Nicoletti, F., Brunori, M., and Ludwig, B. (1998) Tryptophan 121 of Subunit II Is the Electron Entry Site to Cytochrome-c Oxidase in Paracoccus denitrificans. INVOLVEMENT OF A HYDROPHOBIC PATCH IN THE DOCKING REACTION, *J. Biol. Chem. 273*, 5132-5136.
18. Maneg, O., Ludwig, B., and Malatesta, F. (2003) Different Interaction Modes of Two Cytochrome-c Oxidase Soluble CuA Fragments with Their Substrates, *J. Biol. Chem. 278*, 46734-46740.

19. Winkler, J. R., Malmstrom, B. G., and Gray, H. B. (1995) Rapid electron injection into multisite metalloproteins: intramolecular electron transfer in cytochrome oxidase, *Biophys Chem 54*, 199-209.
20. Gorelsky, S. I., Xie, X., Chen, Y., Fee, J. A., and Solomon, E. I. (2006) The two-state issue in the mixed-valence binuclear CuA center in cytochrome C oxidase and N2O reductase, *J Am Chem Soc 128*, 16452-16453.
21. DeBeer George, S., Metz, M., Szilagyi, R. K., Wang, H., Cramer, S. P., Lu, Y., Tolman, W. B., Hedman, B., Hodgson, K. O., and Solomon, E. I. (2001) A quantitative description of the ground-state wave function of Cu(A) by X-ray absorption spectroscopy: comparison to plastocyanin and relevance to electron transfer, *J Am Chem Soc 123*, 5757-5767.
22. Dell'acqua, S., Pauleta, S. R., Monzani, E., Pereira, A. S., Casella, L., Moura, J. J., and Moura, I. (2008) Electron transfer complex between nitrous oxide reductase and cytochrome c552 from Pseudomonas nautica: kinetic, nuclear magnetic resonance, and docking studies, *Biochemistry 47*, 10852-10862.
23. Rasmussen, T., Brittain, T., Berks, B. C., Watmough, N. J., and Thomson, A. J. (2005) Formation of a cytochrome c-nitrous oxide reductase complex is obligatory for N2O reduction by Paracoccus pantotrophus, *Dalton Trans*, 3501-3506.
24. Berks, B. C., Baratta, D., Richardson, J., and Ferguson, S. J. (1993) Purification and characterization of a nitrous oxide reductase from Thiosphaera pantotropha. Implications for the mechanism of aerobic nitrous oxide reduction, *Eur J Biochem 212*, 467-476.
25. Moir, J. W. B., and Ferguson, S. J. (1994) Properties of a Paracoccus denitrificans mutant deleted in cytochrome c550 indicate that a copper protein can substitute for this cytochrome in electron transport to nitrite, nitric oxide and nitrous oxide, *Microbiology 140*, 389-397.
26. Koutny, M., Kucera, I., Tesarik, R., Turanek, J., and Van Spanning, R. J. (1999) Pseudoazurin mediates periplasmic electron flow in a mutant strain of Paracoccus denitrificans lacking cytochrome c550, *FEBS Lett 448*, 157-159.
27. Mattila, K., and Haltia, T. (2005) How does nitrous oxide reductase interact with its electron donors?--A docking study, *Proteins 59*, 708-722.
28. Fujita, K., Ijima, F., Obara, Y., Hirasawa, M., Brown, D. E., Kohzuma, T., and Dooley, D. M. (2009) Direct electron transfer from pseudoazurin to nitrous oxide reductase in catalytic N2O reduction, *J Biol Inorg Chem 14 (Suppl 1)*, S11-S20.
29. Liu, M. Y., Liu, M. C., Payne, W. J., and Legall, J. (1986) Properties and electron transfer specificity of copper proteins from the denitrifier "Achromobacter cycloclastes", *J. Bacteriol. 166*, 604-608.
30. Fujita, K., Chan, J. M., Bollinger, J. A., Alvarez, M. L., and Dooley, D. M. (2007) Anaerobic purification, characterization and preliminary mechanistic study of recombinant nitrous oxide reductase from Achromobacter cycloclastes, *J Inorg Biochem 101*, 1836-1844.
31. Teraguchi, S., and Hollocher, T. C. (1989) Purification and some characteristics of a cytochrome c-containing nitrous oxide reductase from Wolinella succinogenes, *J. Biol. Chem. 264*, 1972-1979.
32. Zhang, C. S., and Hollocher, T. C. (1993) The reaction of reduced cytochromes *c* with nitrous oxide reductase ot *Wolinella succinogenes*, *Biochim. Biophys. Acta 1142*, 253-261.
33. Brown, K., Nurizzo, D., Besson, S., Shepard, W., Moura, J., Moura, I., Tegoni, M., and Cambillau, C. (1999) MAD structure of Pseudomonas nautica dimeric cytochrome c552 mimicks the c4 Dihemic cytochrome domain association, *J Mol Biol 289*, 1017-1028.
34. Benning, M. M., Meyer, T. E., and Holden, H. M. (1994) X-Ray structure of the cytochrome c2 isolated from Paracoccus denitrificans refined to 1.7-A resolution, *Arch Biochem Biophys 310*, 460-466.
35. Najmudin, S., Pauleta, S. R., Moura, I., and Romao, M. J. (2010) The 1.4 A resolution structure of Paracoccus pantotrophus pseudoazurin, *Acta Crystallogr Sect F Struct Biol Cryst Commun 66*, 627-635.
36. Inoue, T., Nishio, N., Suzuki, S., Kataoka, K., Kohzuma, T., and Kai, Y. (1999) Crystal Structure Determinations of Oxidized and Reduced Pseudoazurins from Achromobacter cycloclastes. CONCERTED MOVEMENT OF COPPER SITE IN REDOX FORMS WITH THE REARRANGEMENT OF HYDROGEN BOND AT A REMOTE HISTIDINE, *J. Biol. Chem. 274*, 17845-17852.
37. Bushnell, G. W., Louie, G. V., and Brayer, G. D. (1990) High-resolution three-dimensional structure of horse heart cytochrome c, *J Mol Biol 214*, 585-595.

38. Mirkin, N., Jaconcic, J., Stojanoff, V., and Moreno, A. (2008) High resolution X-ray crystallographic structure of bovine heart cytochrome c and its application to the design of an electron transfer biosensor, *Proteins 70*, 83-92.
39. Betts, J. N., Beratan, D. N., and Onuchic, J. N. (1992) Mapping electron tunneling pathways: an algorithm that finds the "minimum length"/maximum coupling pathway between electron donors and acceptors in proteins, *Journal of the American Chemical Society 114*, 4043-4046.
40. Regan, J. J., Risser, S. M., Beratan, D. N., and Onuchic, J. N. (1993) Protein electron transport: single versus multiple pathways, *The Journal of Physical Chemistry 97*, 13083-13088.
41. Thompson, J. D., Higgins, D. G., and Gibson, T. J. (1994) CLUSTAL W: improving the sensitivity of progressive multiple sequence alignment through sequence weighting, position-specific gap penalties and weight matrix choice, *Nucleic Acids Res. 22*, 4673-4680.
42. Kelley, L. A., and Sternberg, M. J. (2009) Protein structure prediction on the Web: a case study using the Phyre server, *Nat Protoc 4*, 363-371.
43. Kelley, L. A., MacCallum, R. M., and Sternberg, M. J. (2000) Enhanced genome annotation using structural profiles in the program 3D-PSSM, *J Mol Biol 299*, 499-520.
44. Kim, D. E., Chivian, D., and Baker, D. (2004) Protein structure prediction and analysis using the Robetta server, *Nucleic Acids Res. 32*, W526-531.
45. Arnold, K., Bordoli, L., Kopp, J., and Schwede, T. (2006) The SWISS-MODEL workspace: a web-based environment for protein structure homology modelling, *Bioinformatics 22*, 195-201.
46. Prudencio, M., Pereira, A. S., Tavares, P., Besson, S., Cabrito, I., Brown, K., Samyn, B., Devreese, B., Van Beeumen, J., Rusnak, F., Fauque, G., Moura, J. J., Tegoni, M., Cambillau, C., and Moura, I. (2000) Purification, characterization, and preliminary crystallographic study of copper-containing nitrous oxide reductase from Pseudomonas nautica 617, *Biochemistry 39*, 3899-3907.
47. Williams, P. A., Fulop, V., Leung, Y. C., Chan, C., Moir, J. W., Howlett, G., Ferguson, S. J., Radford, S. E., and Hajdu, J. (1995) Pseudospecific docking surfaces on electron transfer proteins as illustrated by pseudoazurin, cytochrome c550 and cytochrome cd1 nitrite reductase, *Nat Struct Biol 2*, 975-982.
48. Pettigrew, G. W., Prazeres, S., Costa, C., Palma, N., Krippahl, L., Moura, I., and Moura, J. J. G. (1999) The Structure of an Electron Transfer Complex Containing a Cytochrome c and a Peroxidase, *J. Biol. Chem. 274*, 11383-11389.
49. Pauleta, S. R., Guerlesquin, F., Goodhew, C. F., Devreese, B., Van Beeumen, J., Pereira, A. S., Moura, I., and Pettigrew, G. W. (2004) Paracoccus pantotrophus pseudoazurin is an electron donor to cytochrome c peroxidase, *Biochemistry 43*, 11214-11225.
50. Kataoka, K., Yamaguchi, K., Kobayashi, M., Mori, T., Bokui, N., and Suzuki, S. (2004) Structure-based Engineering of Alcaligenes xylosoxidans Copper-containing Nitrite Reductase Enhances Intermolecular Electron Transfer Reaction with Pseudoazurin, *J. Biol. Chem. 279,* 53374-53378.
51. Kukimoto, M., Nishiyama, M., Tanokura, M., Adman, E. T., and Horinouchi, S. (1996) Studies on Protein-Protein Interaction between Copper-containing Nitrite Reductase and Pseudoazurin from Alcaligenes faecalis S-6, *J. Biol. Chem. 271*, 13680-13683.
52. Moura, I., Pauleta, S. R., and Moura, J. J. (2008) Enzymatic activity mastered by altering metal coordination spheres, *J Biol Inorg Chem 13*, 1185-1195.
53. Muresanu, L., Pristovsek, P., Löhr, F., Maneg, O., Mukrasch, M. D., Rüterjans, H., Ludwig, B., and Lücke, C. (2006) The Electron Transfer Complex between Cytochrome c552 and the CuA Domain of the Thermus thermophilus ba3 Oxidase, *Journal of Biological Chemistry 281*, 14503-14513.
54. Wang, K., Geren, L., Zhen, Y., Ma, L., Ferguson-Miller, S., Durham, B., and Millett, F. (2002) Mutants of the CuA Site in Cytochrome c Oxidase of Rhodobacter sphaeroides:â€‰ II. Rapid Kinetic Analysis of Electron Transferâ€ *Biochemistry 41*, 2298-2304.
55. Srinivasan, V., Rajendran, C., Sousa, F. L., Melo, A. M., Saraiva, L. M., Pereira, M. M., Santana, M., Teixeira, M., and Michel, H. (2005) Structure at 1.3 A resolution of Rhodothermus marinus caa(3) cytochrome c domain, *J Mol Biol 345*, 1047-1057.
56. Chen, Z. W., Matsushita, K., Yamashita, T., Fujii, T. A., Toyama, H., Adachi, O., Bellamy, H. D., and Mathews, F. S. (2002) Structure at 1.9 A resolution of a quinohemoprotein alcohol dehydrogenase from Pseudomonas putida HK5, *Structure 10*, 837-849.
57. Benning, M. M., Meyer, T. E., and Holden, H. M. (1996) Molecular structure of a high potential cytochrome c2 isolated from Rhodopila globiformis, *Arch Biochem Biophys 333*, 338-348.

58. Stelter, M., Melo, A. M., Pereira, M. M., Gomes, C. M., Hreggvidsson, G. O., Hjorleifsdottir, S., Saraiva, L. M., Teixeira, M., and Archer, M. (2008) A novel type of monoheme cytochrome c: biochemical and structural characterization at 1.23 A resolution of rhodothermus marinus cytochrome c, *Biochemistry 47*, 11953-11963.

Chapter 5

Multiple forms of N_2OR

5.1 Abstract

Nitrous oxide reductase catalyses the final step of the denitrification pathway, the reduction of nitrous oxide to nitrogen. The catalytic center of this enzyme is a unique cluster in biology, CuZ center, which is a tetranuclear center bridged by inorganic sulfur in a tetrahedron shape. The CuZ center in N_2OR isolated from *Pseudomonas nautica* was previously purified in the $1Cu^{2+}$-$3Cu^{+}$ resting form, which is a redox and catalytically inert state. By changing the growth conditions it was possible to obtain CuZ center in a different redox state.

Here, we have prepared N_2OR from *Ps. nautica* for the first time in the "purple" form, in which CuZ center is in the oxidised $2Cu^{2+}$-$2Cu^{+}$ redox state. This form is proposed to be redox active but it is not catalytically competent, since its specific activity is comparable to the one of enzyme in the non-active resting form and thus much smaller than the one of the fully reduced active form of the enzyme.

5.2 Introduction

CuZ is the catalytic center of nitrous oxide reductase (N_2OR), the enzyme that catalyses the final step of denitrification, the reduction of N_2O to N_2 [1, 2]. This center has a unique structure in biology and is constituted by a tetranuclear copper cluster bridged by a sulfur atom in a tetrahedron arrangment [3]. There is a particular interest in revealing the complex chemistry of CuZ center, which is to understand and identify the different forms of CuZ center, their redox states, and the involvement of these states in the catalytic cycle.

The presence of the electron-transferring center, a binuclear CuA center, makes the interpretation of the spectroscopic properties of these two copper centers difficult. However, the spectral features of CuA have been widely studied in both cytochrome *c* oxidase and N_2OR [4, 5]. The oxidised mixed-valence form of the CuA center ($Cu^{1.5+}$-$Cu^{1.5+}$) presents absorption bands at 480 nm and 540 nm, and a EPR spectrum characterized by a typical 7-line hyperfine coupling [1, 4, 6].

Previously, *Pseudomonas nautica* N_2OR, purified aerobically from a strictly anaerobic growth, presented CuZ center in the resting form ($1Cu^{2+}$-$3Cu^{+}$, some authors name this form as CuZ* [7, 8]), and CuA center as a mixture of the two possible redox states: oxidised ($Cu^{1.5+}$-$Cu^{1.5+}$) and one-electron reduced (Cu^{+}-Cu^{+}). Therefore, the resting form of N_2OR presents an absorption spectrum characterized by an absorption band at 640 nm, characteristic of the resting CuZ center, and contributions at 480 nm, 550 nm and 800 nm from the CuA center [9].

Although the spectroscopic, electronic and structural properties of the resting state of CuZ center have been very well characterized [10], this state is redox inactive, in the sense that it cannot be oxidised or easily reduced. In addition, the resting form of CuZ center is catalytically inactive, as its specific activity is very low when compared with the one of the enzyme with fully reduced CuZ center [11, 12]. However, this resting form of the enzyme can be activated via a prolonged incubation with a strong reductant, such as reduced methylviologen [11]. During this activation CuZ center is completely reduced to 4 Cu^{+}.

It has been hypothesized that this activation is a long process as it corresponds to a change in the coordination sphere of CuZ center, which is required for full activity. Indeed, recently, a form of CuZ, CuZ°, which is proposed to be in the same redox state as the resting form ($1Cu^{2+}$-$3Cu^{+}$), was shown to have full activity but being short lived, with a decay to the resting form of 0.3 min^{-1} (Chapter 3 – [13]).

However, from the earlier purification of N_2OR from *Ps. stutzeri*, it became clear that this enzyme can be isolated with CuZ center in different redox states depending on the purification conditions. Anaerobically purified N_2OR from *Ps. stutzeri*, *Ac. xylosoxidans*, *Pa. denitrificans*, and *Pa. pantotrophus* [7, 14-16] exhibits an intense absorption at 540 nm. This form, named

"purple" (due to its colour), presents the CuA center oxidised since the EPR spectra presents the typical seven-line hyperfine pattern in the $g_{\|}$ region, and the CuZ center in the oxidised [$2Cu^{2+}$-$2Cu^{+}$] state. On the other hand, aerobically purified N_2OR from these bacterial sources is in a different form, named "pink" [17], which is similar to the aerobically isolated enzyme from *Ps. nautica*.

The reduction of N_2OR in the purple form by sodium dithionite proceeds in two kinetic steps: a fast phase in which the absorbance at 540 nm disappears almost within seconds, due to the reduction of CuA (this form is a semi-reduced form, which is also obtained by reduction with sodium ascorbate), and a slower phase, in which the resting form (named "blue") is generated in the course of minutes [1, 18].

The EPR spectrum of the purple form exhibits a well-defined 7-line hyperfine splitting whereas that of the resting form has a broad and poorly resolved 4-line hyperfine splitting signal [19], and the semi-reduced form, shows an extremely weak EPR signal and must be considered EPR-silent, although it still presents an absorption band at 540 nm and a small contribution at 640 nm. MCD data confirmed that the semi-reduced form is not a ferromagnetically coupled (S=1) but must be antiferromagnetically coupled (S=0) [8].

It is also important to mention that the aerobic preparation of *P. pantotrophus* N_2OR presents a ratio of CuZresting/CuZ_{total} of 0.66, while in the anaerobic preparation this ratio is 0.29 [7], thus the resting form of CuZ center has always been present in all enzyme preparations reported.

It has been argued that the oxidised CuZ form is catalytically important, and its redox potential was estimated to be E'° = 60 mV for the reduction of [$2Cu^{2+}$-$2Cu^{+}$] to [$1Cu^{2+}$-$3Cu^{+}$]. However, this is still a subject of discussion and contradictions, as its catalytic activity seems to be very low, and similar to the one of N_2OR with CuZ center in the resting dithionite-reduced state [7]. Moreover, it was reported that the enzymatic activity of the anaerobically purified *Ac. cycloclastes* N_2OR increases from 8 to 125 U/mg after incubation with MV [12].

Another spectroscopic characterization of the different forms of CuZ center has been performed by Dooley *et al*. [18] using resonance Raman spectroscopy, in which an anaerobic "purple" form of N_2OR was compared with an aerobic "pink" form. In this resonance Raman characterization it was pointed out that the resting CuZ center (or 1-hole CuZ or CuZ*, as defined here) is predominant in the aerobic preparation. This form has a strong frequency line at 384 cm^{-1}, which is also observed in the enzyme form obtained after dithionite reduction. The resting CuZ center ([$1Cu^{2+}$-$3Cu^{+}$]) is also present in the anaerobic preparation, as the contribution at 384 cm^{-1} is always present in the Raman spectra. The presence of other contributions at 352 cm^{-1} and 408 cm^{-1} was ascribed to the CuZ center in the [$2Cu^{2+}$-$2Cu^{+}$]

form. They observed that the striking similarities between CuZ and CuZ* when reduced with dithionite (identical absorption maximum at 650 nm, nearly identical MCD features, superimposable broad EPR signals, and resonance Raman spectra with nearly identical frequency lines) indicate that they are the same spectroscopic chromophore rather than independent moieties.

In *Al. xylosoxidans* N_2OR [16], the enzyme was isolated in the "semi-reduced" form (CuA center reduced and CuZ center oxidised), as shown by the optical absorption spectrum, which presents an absorption maximum at 550 nm with a shoulder at 635 nm, and by the shift in the absorption maximum to 540 nm and appearance of new contributions at 800 nm and at 480 nm, with $K_3Fe(CN)_6$ oxidation, corresponding to CuA center oxidation.

The redox active purple form, in which the CuZ center can be oxidised and reduced between the [$2Cu^{2+}$-$2Cu^{+}$] and [$1Cu^{2+}$-$3Cu^{+}$] states, had not been isolated from *Pseudomonas nautica*. Here, we present for the first time isolation, purification and characterization of *Pseudomonas nautica* N_2OR in the purple form. This form of the enzyme was obtained from a microaerobic growth in the presence of nitrate and was aerobically purified, unlike the precedent isolation from other bacterial sources, which has only been accomplished from anaerobic preparations. In this work, a thorough analysis of the spectroscopic and catalytic activity of N_2OR, with CuZ center in the different redox states, was performed.

5.3 Materials and Methods

5.3.1 Preparation of the different N_2OR forms

Pseudomonas nautica 617 (recently renamed as *Marinobacter hydrocarbonoclausticus* [20]) was grown in a 10L fermenter in microaerobic conditions in the presence of nitrate (Ribau, *et al*., unpublished results). The periplasmic extract was obtained by diluting 5x the resuspended cells into 10 mM Tris-HCl, pH 7.6 and 1 mM EGTA and incubating during 1h. The extract was ultracentrifugated at 40000 g (Beckman), and the soluble extract was loaded onto a DE52 fast-flow chromatographic column (GE Healthcare), equilibrated with 10 mM Tris-HCl, pH 7.6. The proteins were eluted with a gradient between 10 mM Tris-HCl, pH 7.6 and 10 mM Tris-HCl, 500 mM NaCl. The fractions containing N_2OR were combined and concentrated in a diaflo apparatus (Millipore) over a 30 kDa cut off membrane. This fraction was then loaded onto a gel filtration column (Superdex 200) equilibrated with 300 mM Tris-HCl, pH 7.6. The fractions containing the pure N_2OR were combined, concentrated, and stored at -80ºC until further use. The purity of the fractions was checked through out the purification by SDS-PAGE, and N_2OR

concentration was determined using 7.1 $mM^{-1}cm^{-1}$ extinction coefficient at 640 nm for the dithionite-reduced form [9]. The total protein content was determined using BCA kit (Sigma).
N_2OR from two different anaerobic growths were prepared and purified as previously described [9].

5.3.2 Spectroscopic methods

UV–visible absorption spectra were recorded with a Shimadzu UV-1800 spectrophotometer using 1 cm quartz cells. X-band EPR spectra were recorded on a Bruker EMX spectrometer equipped with a rectangular cavity (model ER 4102ST) and an Oxford Instruments continuous-flow cryostat at 30 K temperature. EPR spectra were simulated using the program WINEPR Simfonia version 1.2 from Bruker Instruments. Samples for EPR spectroscopy were prepared with 150 μM enzyme in 100 mM Tris-HCl. Spin quantification was performed at the same temperature under nonsaturating conditions, using a sample of dithionite-reduced N_2OR (1 spin). Experimental conditions are described in the Figure legends.

5.3.3 Activity assay

The activity assay was performed using the procedure previously described in Chapter 2 [21], by adding N_2OR in the different forms as the last reactant to a cuvette already containing reduced methylviologen and N_2O. The enzyme specific activity was expressed in U/mg units, corresponding to μmol N_2O reduced • min^{-1} • (mg of N_2OR dimer)$^{-1}$.

5.4 *Results and discussion*

5.4.1 Aerobic growth of Pseudomonas nautica cells

The growth of *Ps. nautica* in microaerobic conditions, in the presence of nitrate, expressed unexpectedly N_2OR, showing that not only strictly anaerobic conditions promote the denitrification pathway in *Ps. nautica*.

5.4.2 Characterization of the Purple form of N_2OR from Ps. nautica

i) Spectroscopic characterization

The "purple" *Pseudomonas nautica* N_2OR form was obtained from a cellular growth of *Ps. nautica* under microaerobic conditions in the presence of nitrate and purified aerobically.
This N_2OR preparation presents a UV-visible spectrum characterized by an absorption maximum at 550 nm with a shoulder at 635 nm (Figure 5.1 A - ii) and a small absorption band at 800 nm. After oxidation with $K_3Fe(CN)_6$ the absorption maximum at 550 nm shifts to 540 nm

and the absorption band at 800 nm (Figure 5.1 A – i) becomes more intense, which is an evidence of CuA center being practically reduced in the as-isolated form (only approximately 10 % of CuA center is oxidised in the as-isolated form), and becoming fully oxidised upon addition of potassium ferricyanide.

The absortion spectrum of CuA center alone can be obtained by subtracting the ascorbate-reduced N_2OR spectrum from the ferricyanide-oxidised N_2OR spectrum (Figure 5.1 D). Thus, the absorption bands observed at 550 nm and 635 nm must correspond to the CuZ center in the $2Cu^{2+}$-$2Cu^{+}$ oxidation state (see below). This form of N_2OR has never been isolated from an aerobic purification and microaerobic growth in the presence of nitrate.

Although, a similar form of the enzyme was previously reported for *Al. xylosoxidans* N_2OR [16], it had been isolated from a growth under denitrifying anaerobic condition and purified anaerobically with two anionic-exchange (DE-52 and Q-sepharose) and one gel-filtration chromatographic steps (Sephacryl S-200).

The reduction of the as-isolated "purple" N_2OR with sodium ascorbate produces a spectrum with absorption bands at 550 nm with a shoulder at 635 nm (Figure 5.1 A – iii), which is similar to the one described for the semi-reduced state of *Ps. stutzeri* N_2OR. The reduction with dithionite brings the enzyme to what has been denominated as the resting state (Figure 5.1 A – iv), with CuZ center in the $1Cu^{2+}$-$3Cu^{+}$ state. However, the shape of the absorption band at 640 nm is broader in this case than the one of the resting state obtained from the anaerobic preparation.

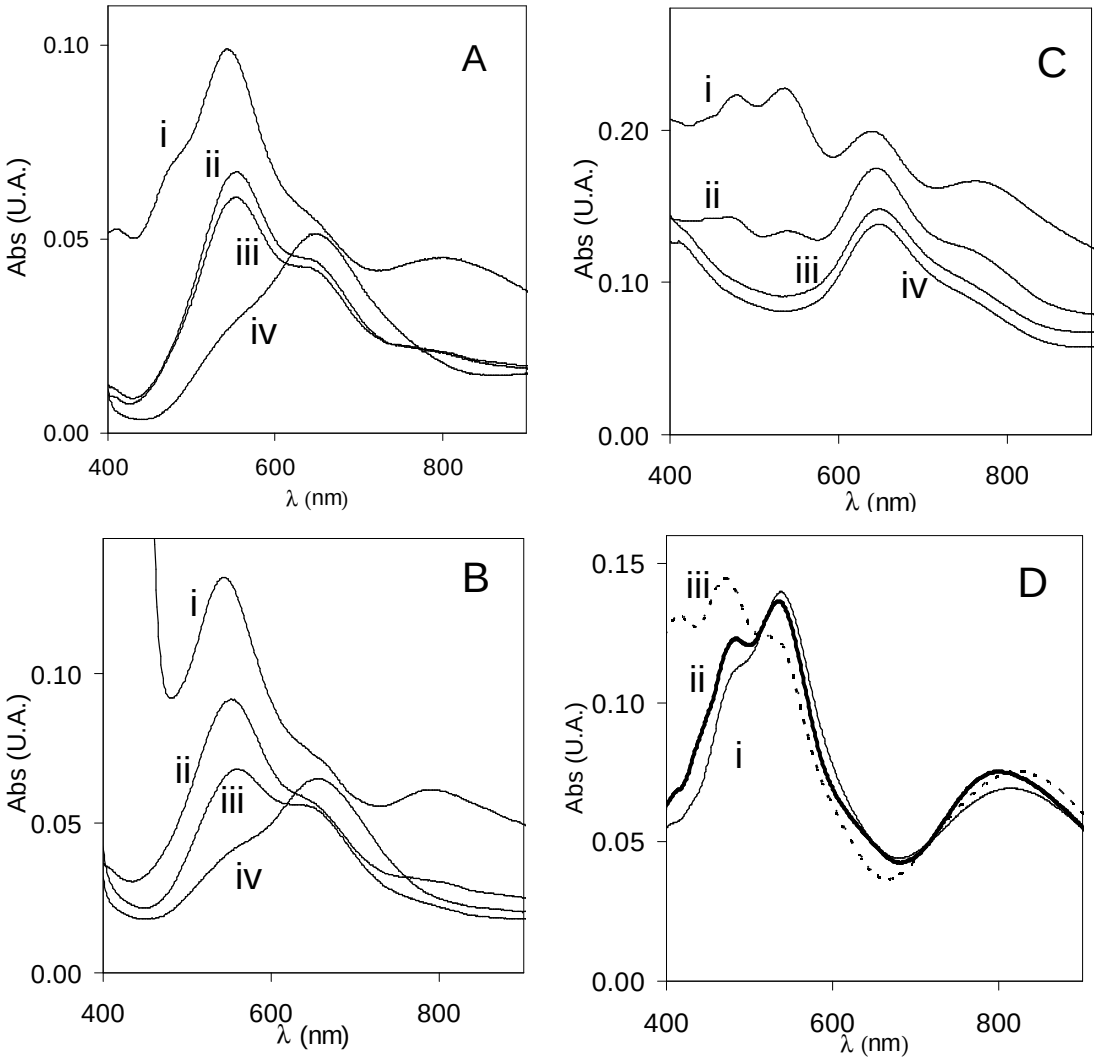

Figure 5.1 – UV-visible spectra of N_2OR purified from (A) an aerobic growth, (B) anaerobic growth 1, (C) anaerobic growth 2. In each panel it is presented the spectrum of the ferricyanide-oxidised (i), as-isolated (ii), ascorbate-reduced (iii) and dithionite-reduced (iv) form of the enzyme. In panel D, the visible difference spectra: ferricyanide oxidised minus ascorbate-reduced samples of N_2OR: (i) continuous line – aerobic; (ii) bold line – anaerobic 1; (iii) dotted line – anaerobic 2.

As previously described by Prudêncio *et al* [9], the N_2OR isolated from an anaerobic growth of *Ps. nautica* and purified aerobically shows absorption bands at 480 nm, 550 nm, 640 nm and 800 nm (Figure 5.1 C – ii). This shows that CuA center is partially oxidised (480 nm, 550 nm and 800 nm absorption bands, see below) and CuZ center is in the resting state (640 nm). This form of N_2OR has been named "pink" due to its color, and will be referred here as "anaerobic 2".

However, there are different preparations of the enzyme in which CuZ center is in a mixture of states, "anaerobic 1", being partially as [$2Cu^{2+}$-$2Cu^{+}$] (the amount in this state can vary from preparation to preparation).

Regarding the redox behavior, ferricyanide is able to fully oxidised CuA (Figure 5.1 C – i) that is not completely oxidised in the as-isolated form, while both sodium ascorbate and dithionite

fully reduce CuA center, with CuZ center remaining unchanged and in the resting state ($1Cu^{2+}$-$3Cu^{+}$) (Figure 5.1 C – iii and iv). It is also important to mention that the degree of oxidation of CuA center varies between different preparations, while CuZ center has been found mostly in the resting state.

Indeed, a N_2OR preparation from another anaerobic growth/aerobic purification shows spectroscopic features that are intermediate between the "purple" and the "pink" forms described above (Figure 5.1 B). In particular, in this preparation, which will be named here as "anaerobic 1", the ferricyanide-oxidised form (Figure 5.1 B – i) presents a 550 nm absorption band / 640 nm absorption band ratio of 1.38, that is lower than that of the "aerobic" form (1.87) but higher than the "anaerobic 2" (1.11) (Figure 5.1 C). In addition, when N_2OR "anaerobic 1" is reduced with sodium ascorbate, it is observed a shoulder at 550 nm, similar to what is observed in the "aerobic" form. Similarly to what was observed for the ferricyanide-oxidised N_2OR, in the ascorbate reduced enzyme, the ratio of the absorption band at 550 nm and 640 nm, is smaller for the "anaerobic 1" N_2OR (1.38) than the one in "aerobic" N_2OR (1.87). In the "anaerobic 2" sample, it is only observed the band at 640 nm, which is sharper than the one obtained for the other two preparations. These results indicate that the 550 nm absorption band is due to the CuZ center in the [$2Cu^{2+}$-$2Cu^{+}$] state.

The EPR spectra of the different redox forms of these N_2OR preparations were analysed. The total spin was quantified for each form of the enzyme (Table 5.1), assuming that the dithionite-reduced N_2OR presents a total spin of 1 (in this state CuZ center contains one unpaired electron in the mixed-valence state $1Cu^{2+}$-$3Cu^{+}$) and CuA center is reduced ($Cu^{1.5+}$-$Cu^{1.5+}$) and thus does not contribute to the EPR spectrum [10].

In all the preparations, the as-isolated N_2OR shows EPR spectra dominated by the CuA center features, since this center is partially oxidised in different proportions (Figure 5.2 A, B, C – ii), as observed before in the visible spectra.

The EPR spectra of *Ps. nautica* N_2OR with CuA center fully oxidised (by ferricyanide) is characterized by the typical seven-line hyperfine splitting pattern (Figure 5,2 A, B, C – i). These EPR spectra are characterized by a $g_{\parallel} = 2.18$, $g_{\perp} = 2.04$ and $A_{\parallel} \approx 40$ G for all the preparations. In the case of the "anaerobic 2" N_2OR the seven-line hyperfine splitting is less resolved due to the larger contribution of the "resting" CuZ centre contribution [1]. Moreover, the dithionite reduced *Ps. nautica* N_2OR has a similar EPR spectrum for all enzyme preparations, and is characterized by a broad four-line splitted signal (Figure 5.2 A, B, C – iii), typical for the resting state. These EPR spectra are characterized by a $g_{\parallel} = 2.19$, $g_{\perp} = 2.05$ and $A_{\parallel} \approx 60$ G for all the preparations.

Finally, the EPR of the ascorbate-reduced N_2OR points out differences between the different preparations, not in the EPR spectrum shape, that is similar to the one of the resting state, but in the total spin quantification (Figure 5.2 A, B, C – iv and Table 5.1).

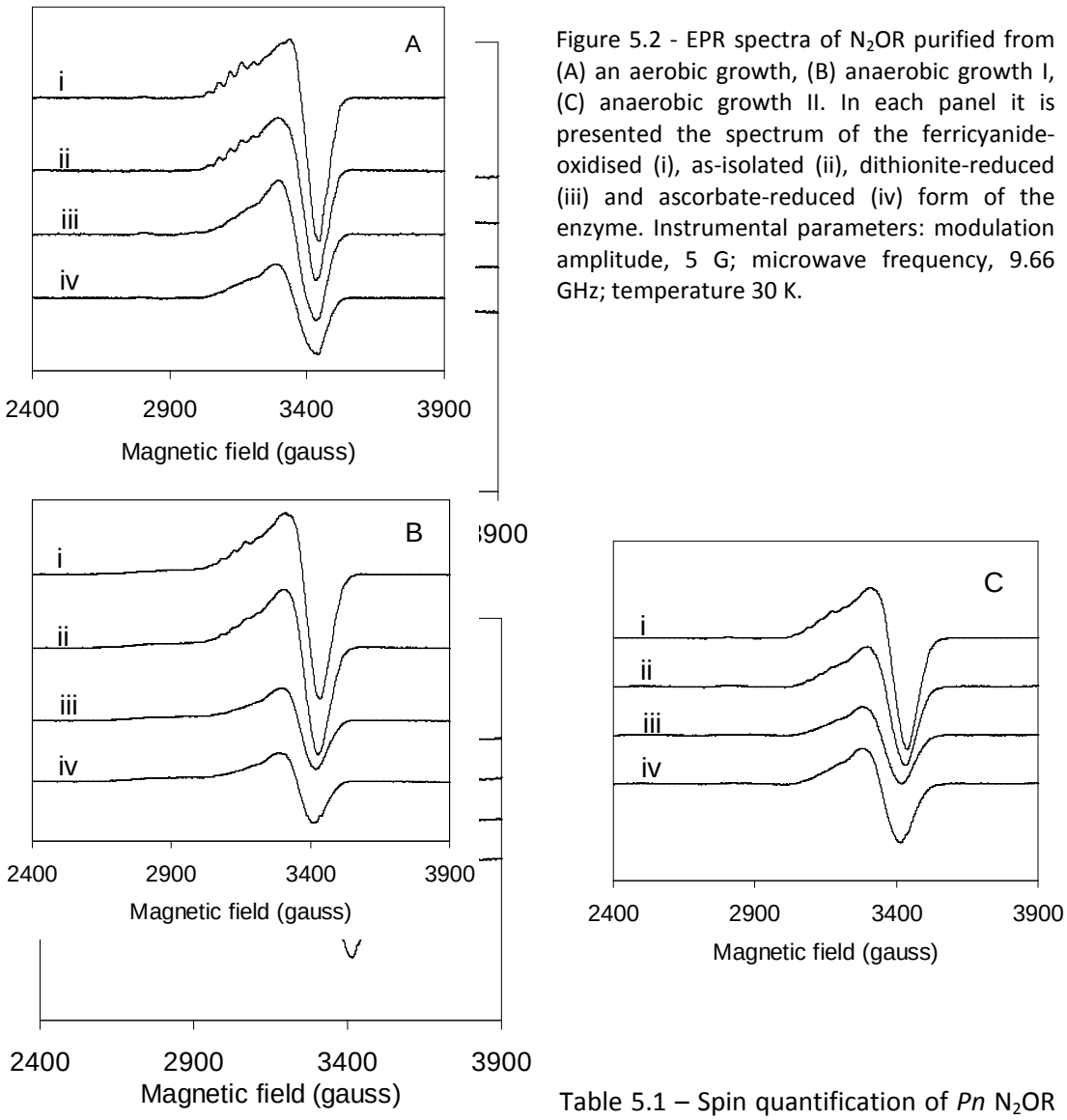

Figure 5.2 - EPR spectra of N_2OR purified from (A) an aerobic growth, (B) anaerobic growth I, (C) anaerobic growth II. In each panel it is presented the spectrum of the ferricyanide-oxidised (i), as-isolated (ii), dithionite-reduced (iii) and ascorbate-reduced (iv) form of the enzyme. Instrumental parameters: modulation amplitude, 5 G; microwave frequency, 9.66 GHz; temperature 30 K.

Table 5.1 – Spin quantification of *Pn* N_2OR from EPR spectra.

	Aerobic N_2OR	Anaerobic 1 N_2OR	Anaerobic 2 N_2OR
Fe^{III}-oxidised	1.9	2.5	2.2
As-Isolated	1.2	2.2	1.6
Asc.-reduced	0.7	0.8	1.1
Dth.-reduced	1.0	1.0	1.0

Asc – ascorbate reduced; Dth – dithionite reduced.

In the case of "aerobic" N_2OR, the ascorbate-reduced form of the enzyme has a total spin lower than 1 (0.7 – see Table 5.1), which means that the CuZ center is not completely in the

resting state (characterized by a total spin of 1). Thus, there is a second form of CuZ center contributing with as a diamagnetic state, which is the [$2Cu^{2+}$-$2Cu^{+}$] state, since ascorbate quickly reduces CuA center but the reduction of CuZ center in the $2Cu^{2+}$-$2Cu^{+}$ state is slow and not complete [8].

The "anaerobic 2" form does not present CuZ center in the [$2Cu^{2+}$-$2Cu^{+}$] state, since the ascorbate-reduced form is equal to the dithionite, both in the UV-visible and EPR spectroscopic analysis, attesting that the CuZ center is only present as the resting state (or CuZ* form).

However, the "anaerobic 1" preparation has a percentage of CuZ in the diamagnetic [$2Cu^{2+}$-$2Cu^{+}$] form, as shown by the total spin lower than 1 and by the visible spectra with contribution at 550 nm in the ascorbate-reduced form.

According to the definition used by Rasmussen *et al.* [7], the catalytic center, CuZ center, is always present in two different states, CuZ ($2Cu^{2+}$-$2Cu^{+}$ - diamagnetic) and CuZ* ($1Cu^{2+}$-$3Cu^{+}$ - paramagnetic). From the EPR spin quantification it is possible to estimate the ratio of these two forms of CuZ center. In the "aerobic" N_2OR there is the 30% of CuZ and 70% CuZ*; "anaerobic 1" N_2OR 20% of CuZ and 80% CuZ*; and in the "anaerobic 2" N_2OR CuZ is completely in the CuZ* state[1].

Therefore, this work presents the first report of the [$2Cu^{2+}$-$2Cu^{+}$] state of CuZ center from *Ps. nautica* N_2OR and the first time that this form of the enzyme has been isolated from an aerobic purification/microaerophilic growth.

ii) Specific activity of N_2OR in the different forms

In addition to the spectroscopic characterization, it is also important to evaluate the specific activity that is associated with the "purple" state of CuZ center. This state has been proposed to be redox active, in comparison with the non-active resting state of CuZ center.

The modified activity assay, described in Chapter 2 [21], will enable the separation of the slow activation, that is accomplished with reduced methylviologen, from the catalytic activity, and thus the determination of the specific activity of each of these enzyme forms.

The specific activity of the different forms of the enzyme is shown in Table 5.2, along with the main redox state of the CuZ center in those forms.

[1] The exact quantification of the percentage of CuZ and CuZ* in the EPR samples is still in progress, because in the time elapsed between the visible spectra and the freezing of the EPR tube (about 15 minutes) the ascorbate is able to reduce partially the CuZ to the CuZ* state.

Table 5.2 - Activity values (U/mg) of the forms of *Pn* N_2OR isolated from microaerobic and anaerobic growth.

	"Aerobic"		"Anaerobic 1"		"Anaerobic 2"	
	activity	**CuZ center redox state**	**Activity**	**CuZ center redox state**	**activity**	**CuZ center redox state**
Fe^{III} oxidised	0.4	$2Cu^{2+}$-$2Cu^{+}$	0.4	$2Cu^{2+}$-$2Cu^{+}$ / $1Cu^{2+}$-$3Cu^{+}$	1.1	$1Cu^{2+}$-$3Cu^{+}$
Asc-reduced	0.3	$2Cu^{2+}$-$2Cu^{+}$	0.3	$1Cu^{2+}$-$3Cu^{+}$	0.9	$1Cu^{2+}$-$3Cu^{+}$
Dth-reduced	0.2	$1Cu^{2+}$-$3Cu^{+}$	0.3	$1Cu^{2+}$-$3Cu^{+}$	0.2	$1Cu^{2+}$-$3Cu^{+}$
Fully-reduced	88.0	$4Cu^{+}$	96.1	$4Cu^{+}$	92.4	$4Cu^{+}$

Asc- ascorbate; Dth - dithionite

The analysis of Table 5.2 clearly shows that none of these N_2OR forms has an activity comparable with the maximum specific activity that is reached with the fully reduced form of the enzyme, and that there are no significant differences between the different preparations of N_2OR.

A similar result was obtained for *A. cycloclastes* and *P. pantotrophus* N_2OR [7, 12], where the specific activity of N_2OR with CuZ center in different redox states from both aerobic and anaerobic preparations is low compared to the high activity of the enzyme described more recently [11, 12], in which the CuZ center is in the fully reduced state.

In conclusion, the $2Cu^{2+}$-$2Cu^{+}$ species of CuZ center present in the "purple" form of N_2OR is not catalytically competent, even if it is redox active, and as proposed by other authors can be reversibly reduced to $1Cu^{2+}$-$3Cu^{+}$ [7].

In conclusion, N_2OR isolated either anaerobically or aerobically always requires an activation process. This activation process consists in the fully reduction of the CuZ center.

5.5 Conclusion

Here, we presented the first purification and characterization of a "purple" form of N_2OR from *Ps. nautica*. For the first time, N_2OR was isolated from a non-strictly anaerobic growth, using microaerobic conditions in the presence of nitrate. This indicates that in *Pseudomonas nautica* the denitrification pathway can take place simultaneously with the aerobic respiration in the presence of oxygen.

Moreover, the spectroscopic characterization of this N_2OR form enabled the comparison of the "purple" form *Ps. nautica* with the ones obtained from other bacterial sources, which is characterized by a diamagnetic state [$2Cu^{2+}$-$2Cu^{+}$] and an absorption band at 550 nm in the

UV-visible spectrum. The catalytic center is still present as a mixture of two species: [$2Cu^{2+}$-$2Cu^{+}$] (or CuZ) present at 30 % and [$1Cu^{2+}$-$3Cu^{+}$] (or CuZ*) (70%).

The activity assay allows us to conclude that the oxidised [$2Cu^{2+}$-$2Cu^{+}$] state of CuZ center is not catalytically competent, since the activity of the enzyme with CuZ center in that state ("purple" form) is much smaller than the one with CuZ center in the non-active resting state.

Up-to-now, only the fully reduced state ($4Cu^{+}$) and the CuZ° center states have been identified as catalytically competent, being CuZ° an intermediate in the catalytic cycle of N_2OR. However, it is important to point out that in the proposed catalytic cycle of N_2OR, there is a ($2Cu^{2+}$-$2Cu^{+}$) state of CuZ center, as the first intermediate after N_2O release, which has not yet been observed nor characterized.

5.6 References

1. Zumft WG, Kroneck PM (2007) Adv Microb Physiol 52:107-227
2. Tavares P, Pereira AS, Moura JJ, Moura I (2006) J Inorg Biochem 100:2087-2100
3. Brown K, Tegoni M, Prudencio M, Pereira AS, Besson S, Moura JJ, Moura I, Cambillau C (2000) Nat Struct Biol 7:191-195
4. Scott RA, Zumft WG, Coyle CL, Dooley DM (1989) PNAS 86:4082-4086
5. Kroneck PM, Antholine WE, Kastrau DH, Buse G, Steffens GC, Zumft WG (1990) FEBS Lett 268:274-276
6. Antholine WE, Kastrau DH, Steffens GC, Buse G, Zumft WG, Kroneck PM (1992) Eur J Biochem 209:875-881
7. Rasmussen T, Berks BC, Butt JN, Thomson AJ (2002) Biochem J 364:807-815
8. Farrar JA, Zumft WG, Thomson AJ (1998) PNAS 95:9891-9896
9. Prudencio M, Pereira AS, Tavares P, Besson S, Cabrito I, Brown K, Samyn B, Devreese B, Van Beeumen J, Rusnak F, Fauque G, Moura JJ, Tegoni M, Cambillau C, Moura I (2000) Biochemistry 39:3899-3907
10. Chen P, Gorelsky SI, Ghosh S, Solomon EI (2004) Angew Chem Int Ed Engl 43:4132-4140
11. Ghosh S, Gorelsky SI, Chen P, Cabrito I, Moura JJ, Moura I, Solomon EI (2003) J Am Chem Soc 125:15708-15709
12. Chan JM, Bollinger JA, Grewell CL, Dooley DM (2004) J Am Chem Soc 126:3030-3031
13. Dell'acqua S, Pauleta SR, Paes de Sousa PM, Monzani E, Casella L, Moura JJ, Moura I (2010) J Biol Inorg Chem 15:967-976
14. Coyle CL, Zumft WG, Kroneck PM, Korner H, Jakob W (1985) Eur J Biochem 153:459-467
15. Snyder SW, Hollocher TC (1987) J. Biol. Chem. 262:6515-6525
16. Ferretti S, Grossmann JG, Hasnain SS, Eady RR, Smith BE (1999) Eur J Biochem 259:651-659
17. Riester J, Zumft WG, Kroneck PM (1989) Eur J Biochem 178:751-762
18. Alvarez ML, Ai J, Zumft W, Sanders-Loehr J, Dooley DM (2001) J Am Chem Soc 123:576-587
19. Farrar JA, Thomson AJ, Cheesman MR, Dooley DM, Zumft WG (1991) FEBS Lett 294:11-15
20. Sproer C, Lang E, Hobeck P, Burghardt J, Stackebrandt E, Tindall BJ (1998) Int J Syst Bacteriol 48:1445-1448 DOI 10.1099/00207713-48-4-1445
21. Dell'acqua S, Pauleta SR, Monzani E, Pereira AS, Casella L, Moura JJ, Moura I (2008) Biochemistry 47:10852-10862

Chapter 6

. Biomimetic complex of CuZ – Copper-Sulfur chemistry

6.1 Abstract

The ultimate goal is to understand the copper-sulfur chemistry in enzymes and in particular to investigate the unique motif in the catalytic centre of nitrous oxide reductase, CuZ, a μ4-sulfido-tetranuclear copper cluster coordinated by multiple histidine donors. Reaction of mononuclear and binuclear $Cu^{I}(PF_6)$ complexes supported by N-donor ligands with S_8 yielded copper(II)-sulfur clusters, the structure of which is still to be clarified.

6.2 Introduction

Several examples of copper-sulfur enzymes are present in biological systems, which show a versatile and sometimes unusual coordination chemistry. In synthetic models, sulfur atoms from thiolates, thioethers or, more rarely, disulfide or inorganic sulfur have been shown to act as donor ligands in a variety of copper complexes. In biology, copper ions coordinated by multiple histidine N-donor and sulfur-containing thiolate or sulphide ligands comprise the active site of several metalloproteins. Much interest has been focused on the mononuclear type-1 copper site and on the binuclear CuA electron-transfer sites, in which the nature of highly covalent copper(II)-thiolate interaction has been demonstrated through detailed structural, spectroscopic and synthetic modelling studies (*1, 2*). Copper(I)-thiolates are also largely present in proteins involved in the copper transport and storage, as well as those that regulate gene transcription ensuring a proper copper ion homeostasis in the cell (*3-6*). Although proteins containing iron-sulfide clusters are widespread in biochemistry (*7, 8*), a copper-sulfide cluster has only been identified in the catalytic centre of nitrous oxide reductase (*9*). Recent structural (*9, 10*) and spectroscopic (*11-16*) studies have revealed that CuZ, the catalytic site of N_2OR, contains a novel μ4-sulfido tetranuclear copper cluster coordinated by multiple histidine donors. This cluster can exist in different redox states, however the fully reduced Cu_4^I form has been proposed to bind and reduce N_2O via pathways supported by theoretical calculations (*17, 18*). In higher oxidized states the electron delocalization is mediated through the μ4-sulfide cluster (*11, 16*).

Previous synthetic efforts have yielded sulfur-containing Cu(II) or Cu(III) compounds with either the S-S bond intact (e.g., disulfo(2-), Figure 6.1 – A and B (*19, 20*)), or disulfide (•1-) (Figure 6.1 – C (*21*)), or broken (e.g., sulfide, Figure 6.1 - D (*22*)), depending on the nature of the N-donor ligand and the reaction conditions.

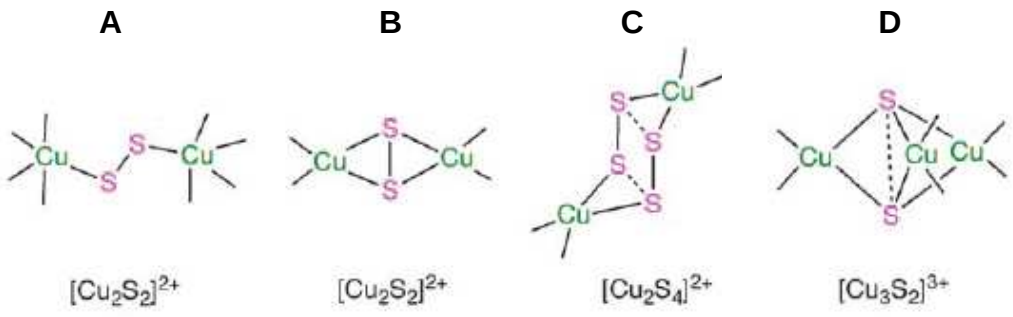

Figure 6.1 – Core structural motifs identified by X-ray crystallography for copper sulfur complexes supported by N-donor ligands (not shown) (adapted from ref. (*23*)).

The μ–η^1:η^1– and μ–η^2–η^2–disulfidodicopper complexes A (*19*) and B (*20*) are close counterparts of peroxodicopper analogs with identical tetra- or tridentate supporting ligands (*24-26*), and the bonding interactions in the Cu_2O_2 and Cu_2S_2 cores are similar as determined from comparative spectroscopic/theoretical studies (*27*). The side-on μ–η^2–η^2 complexes (B, and the its peroxo analogous) exhibit an intense charge-transfer (CT) electronic absorption bands and low S-S and O-O stretching frequencies of 500 and 760 cm^{-1}, respectively, that indicate weak bonds. These features have been rationalized by a common core-bonding model illustrated in Figure 6.2.

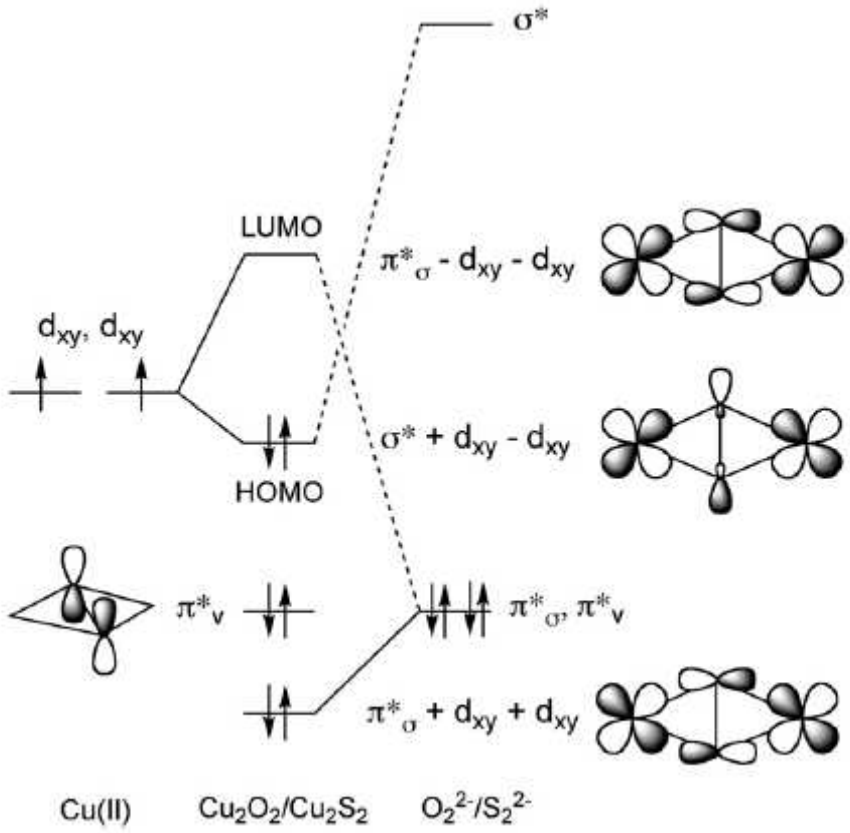

Figure 6.2 – Schematic molecular orbital energy-level diagram for the (μ–η^2–η^2-peroxo/sulfide)dicopper core (adapted from ref. (*28*)).

According to this picture, the O_2^{2-}/S_2^{2-} π^* orbital that lies in the plane of the Cu_2O_2/Cu_2S_2 core (π^*_σ) interacts strongly with the Cu d_{xy} orbitals, while the out-of-plane O_2^{2-}/S_2^{2-} π^* orbital (π^*_v) remains basically unperturbed (nonbonding with respect to the Cu ions). The Cu-O/S bonding is thus dominated by highly covalent, strong σ-donation from the filled O_2^{2-}/S_2^{2-} π^*_σ orbital into the Cu d_{xy} set. An additional interaction occurs between the Cu d_{xy} orbitals and the empty O_2^{2-}/S_2^{2-} σ^* orbital. It is, essentially, a backbonding interaction, it results in a lowering the HOMO energy predominantly based on Cu-orbitals and rationalizes the weakening of the O_2^{2-}/S_2^{2-}

bond. The electronic CT absorption bands derive from excitations of the π^* + xy + dxy and π^*_v orbitals, with the former being more intense and at higher energy. A detailed comparative study (*27*) showed that the Cu_2S_2 core of complex B exhibits greater metal-ligand covalency (π^*_σ/Cu) and backbonding (Cu/σ^*) than its peroxide analog, corresponding to a more significant weakening (activation) of the S-S bond.

Recently, the first complex able to bind and react with N_2O has been described (*29*). The complex presents a $[Cu_3S_2]^{2+}$ core having a localized mixed-valence cluster, supported by tertiary amine ligands. This complex presents a contribution at 395 nm that is a $S_2^{2-} \rightarrow Cu^{2+}$ charge transfer transition also present in the Cu_2-μ-S_2 and an additional band at 630 nm that is similar only in appearance to the CuZ resting typical spectroscopic feature. In this case the transition can be attributed to a metal-to-ligand charge transfer (MLCT) from the Cu^I centres into a π^* orbital of the S-S bond, while for the CuZ in the resting state, the transition is due to a $S \rightarrow Cu^I$ charge-transfer, as already mentioned. The experimental data, supported by DFT calculations, indicate that the cluster dissociates in a Cu^I fragment and a dicopper(I,II) species that binds N_2O by a μ-1,1-O coordination that promotes the N-O cleavage. This mechanism is different from the μ-1,3-O,N coordination proposed for the CuZ active site in the enzyme (*11, 30*).

Several Cu_2O_2 complexes were synthesized and characterized in Casella's lab in order to study the binding and activation of molecular dioxygen in copper-proteins such as hemocyanin and tyrosinase (*31-33*). In particular, a series of polibenzymidazolic ligands were used as histidine-mimetic donor ligands for the metal ions. This type of heterocyclic ligands bears the advantage with respect to the more widely employed amine or pyridine donors, of having similar donor properties to the natural imidazoles, and of being easily obtained from a synthetic viewpoint with respect to histidine containing molecules.

This work is focused on the synthesis of polynuclear complexes containing aromatic amines as ligands for the coppers, in order to mimic the seven Cu-bound histidines in the enzyme active site, and containing a μ-sulfido bridge.

6.2 Materials and methods

6.2.1 General procedures

All solvents and reagents were obtained from commercial sources and used as received unless otherwise noted. NMR spectra were recorded on a Bruker AVANCE 400 spectrofotometer. Optical spectra were measured on HP 8453 diode array spectrophotometer.

6.2.2 Synthesis of the ligands

The ligand Me-BB5 (Figure 6.3 – A) was prepared following a procedure similar to that previously described (*34*). Powdered KOH (0.3 g) was added to a stirred suspension of N,N-bis(benzimidazolyl-methyl)methylamine (0.3 g) in acetone (100 ml). The solution was stirred at room temperature for 5 min. Iodomethane (0.29 g) was added dropwise with vigorous stirring. Stirring the mixture for further 15 min, a fine precipitate of KI is formed. The solvent was removed under reduced pressure and the residue shaken with a mixture of water and CH_2Cl_2. Upon dissolution of all the solid, the organic phase was separated and the aqueous phase extracted again with CH_2Cl_2. The combined organic extracts were dried over $MgSO_4$, filtered, and the solvent removed under reduced pressure. The crude product was recrystallyzed from methanol-water to give white crystals of the monohydrate. ^{1}H NMR (400 MHz, $CDCl_3$, 20 °C, TMS): δ 7.70 (2H, m), 7.19 (6H, m), 3.78 (4H, s) 3.50 (6H, s), and 2.26 (3H, s).

The ligand BB6 (Figure 6.3 – B) was prepared following a procedure similar to that previously described (*35*). N,N'-bis[2-(1'-methyl-2'-benzimidazolyl)ethyl]amine (BB6) compound was obtained by refluxing a solution of 3,3'-iminodipropionitrile (12.5 mmol) and *N*-methyl-*o*-phenylenediamine (25.0 mmol) in 6 M hydrochloric acid for 100 h. The resulting brown solution was cooled in an ice bath and made basic by dropwise addition of ammonia (conc.). The precipitate thus formed was collected by filtration and washed several times with dilute ammonia. The product was crystallized from ethanol-water (1:1). ^{1}H NMR (400 MHz, $CDCl_3$, 20 °C, TMS): δ 2.5 (br, NH), 2.9-3.4 (t, ^{3}J(H,H)=7.8 Hz, 8H; N-CH_2-CH_2-benzimidazole), 3.68 (s, 4H; N-CH_2-phenyl), 7.1-7.3 (m, 6H; benzimidazole-H) and 7.6-7.8 (m, 2H; benzimidazole-H).

The ligand L55 (Figure 6.3 – C) was prepared following a procedure similar to that previously described (*36*). A mixture of a,a'-diamino-m-xylene dihydrochloride (0.38 g, 1.8 mmol), 2-(chloromethyl)-N-methylbenzimidazole (1.35 g. 7.4 mmol), anhydrous sodium carbonate (1.5 g, 14.2 mmol), and dry DMF (100 mL) was refluxed for about 8 h. After evaporation to dryness under vacuum, the solid residue was treated with chloroform and the inorganic salts were filtered off. The filtrate was concentrated to a small volume, and diethyl ether was added to precipitate the product (yield 70%). ^{1}H NMR (400 MHz, $CDCl_3$, 20 °C, TMS): δ (4H, CH2-phenyl), 3.94 (s, 8H, CH2-benzimidazolyl), 7.2-7.4 and 7.6-7.8 (m, 16H, Ph H + benzimidazolyl H).

The ligand Me-L66 (Figure 6.3 – D) was prepared following a procedure similar to that previously described (*31*). N,N'-bis[2-(1'-methyl-2'-benzimidazolyl)ethyl]amine (BB6), dry

Na_2CO_3, and 1,3-bis(bromomethyl)-5-methylbenzene were reacted at 85 °C under stirring for 55 h in dry DMF (freshly distilled over CaH_2) under an inert atmosphere. After cooling to room temperature, a precipitate was obtained by addition of cold water. The crude MeL66 product was purified by column chromatography on silica (4x40 cm), using an eluent mixture of CH_2Cl_2/MeOH 15:1 containing 1% NEt_3 (v/v). ^{1}H NMR (400 MHz, $CDCl_3$, 20 °C, TMS): δ 7.68 (m, 4H; benzimidazole-H), 7.20-7.24 (m, 12H; benzimidazole-H), 6.94 (s, 1H; phenyl-H), 6.92 (s, 2H; phenyl-H), 3.66 (s, 4H; N-CH_2-phenyl), 3.52 (s, 12H; N-CH_3), 3.13 (t, ^{3}J(H,H)=7.8 Hz, 8H; N-CH_2-CH_2-benzimidazole), 2.99 (t, ^{3}J(H,H)=7.8 Hz, 8H; N-CH_2-CH_2-benzimidazole), 2.14 (s, 3H; CH_3-phenyl).

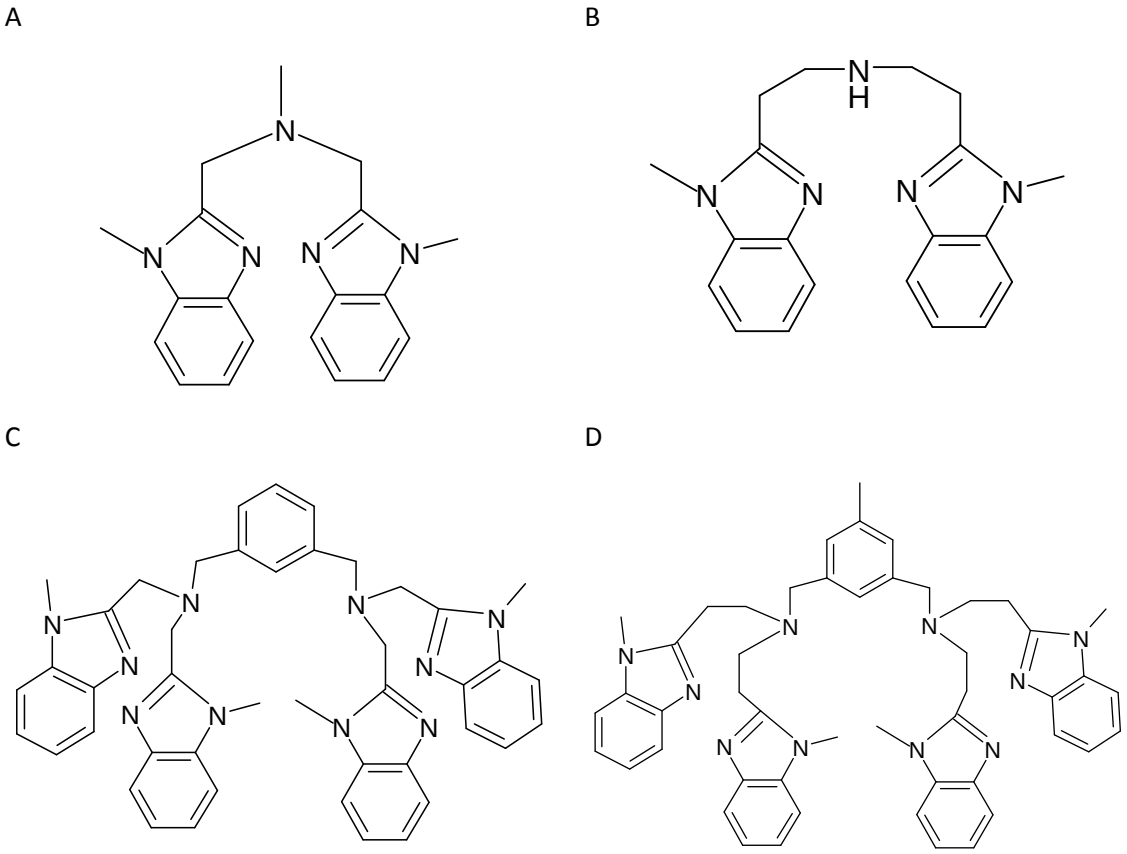

Figure 6.3 – Structures of the ligands used to form the copper complexes. In panel A, B, C, and D the mononuclear ligands MeBB5 and BB6 and the binuclear ligands L55 and MeL66 are represented, respectively.

6.2.3 Synthesis of copper(I) complexes and reaction with S_8

To a solution containing $[Cu(CH_3CN)_4]PF_6$ (1.0 or 2.0 equiv. depending on the nuclearity of the ligand used) in CH_2Cl_2 or CH_3CN was added the ligand and, subsequently, a stoichiometric amount of inorganic sulfur (S_8). The reaction was performed in anaerobic conditions using a

Schlenk apparatus and the progress of the reaction was monitored through the development of UV/Vis bands by using a home made fiber-optics immersion probe.

6.2.4 Reaction with triphenylphosphine (PPh_3)

Three equivalents of PPh_3 (4.6 mg, 0.018 mmol) were dissolved in CH_2Cl_2 (2 mL), and the mixture was added to compound Cu-BB6-S (5.0 mg, 0.006 mmol). After the mixture was stirred for 1 hour, ^{1}H and ^{31}P NMR spectra were recorded, which, showed formation of 1 equiv of triphenylphosphine sulfide ($S=PPh_3$) and 2 equivalents of $(L)Cu_4(PPh_3)_4$. ^{31}P NMR (CD_3Cl): 42.7, -5.65. A similar reaction of PPh_3 with compound Cu-BB6-S_2, using 4 equivalents of phosphine, yielded 2 equivalents of triphenylphosphine sulfide and 2 equivalents of $(L)Cu_4(PPh_3)_4$.

6.3. Results and discussion

Initially the reaction of Cu(I) complex with molecular S_8 was tested in the presence of the binuclear ligands L55 and MeL66 because, in the case of the analogue reaction with O_2, these complexes offer a better stabilization of the Cu_2O_2 core, due the preorganitazion of the ligand. In particular, the complex supported by the MeL66 ligand is able to form a stable Cu_2O_2 complex at very low temperature (-80°C) (*31*). However, the reaction with S_8 of the complexes containing Cu(I) and L55 or MeL66 do not show any coordination of sulfur to the copper ions.

We decided to use more flexible ligands and with less steric hindrance, in order to offer better coordination to the sulfur. The reaction of Cu(I)-MeBB5 complex with S_8 appears to occur into 2 steps. The first one is characterized by the formation of a sharp band at 640 nm, while in the second the absorption band becomes broader and shifts to 680 nm. The first intermediate is formed in the order of time of minutes and it is not stable. The final compound has been identified as Cu^{II}-MeBB5, without any sulfur coordinated, because it shows the same features in the UV-vis, NMR and EPR spectra. The first intermediate has not been fully characterized due to the transient nature of this species.

Another mononuclear N-donor was then used in the reaction with the correspondent Cu^{I}-compound and molecular sulfur. The reaction of Cu^{I}-BB6 with S_8 shows again the formation of a first intermediate characterized by a sharp absorption band at 640 nm (Figure 6.4 – black line). This intermediate species has a longer life-time than the one formed with the MeBB5 ligand; it is stable for 1 hour, then it slowly degrades to the mononuclear Cu^{II}MeBB5 that is characterized by a broad band centred at 680 nm (Figure 6.4 - blue and red lines).

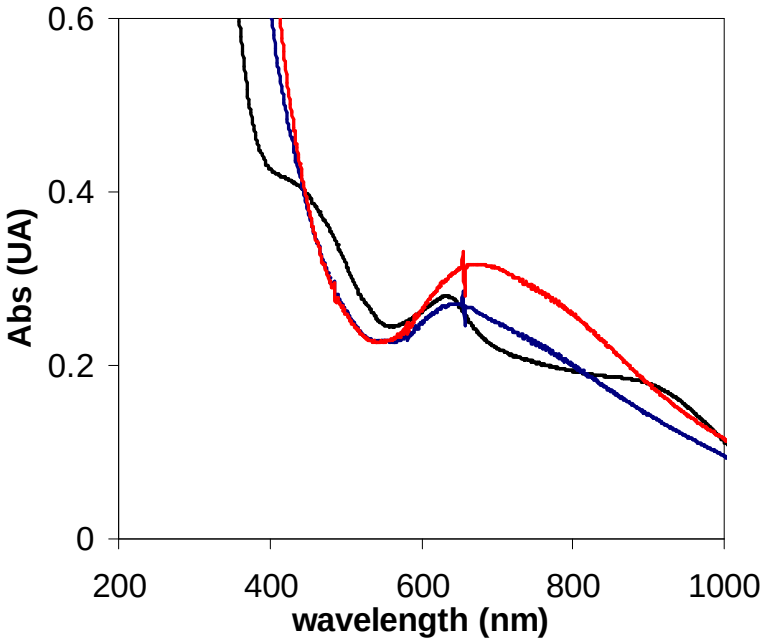

Figure 6.4 – Reaction between Cu^{I}-BB6(PF_6) and inorganic sulfur at different reaction times. Black line: 1 hour; blue line: 3 hours; red line: 24 hours.

In order to establish the presence of sulfur in the cluster and preliminary testing the reactivity in the S transfer, the reaction of the compound Cu-BB6-S with different amount of PPh_3 were explored. ^{1}H and ^{13}P NMR spectra showed that treatment of compound Cu-BB6-S with 3 equivalents of PPh_3 towards copper yielded 1 equivalent of $S{=}PPh_3$ and 1 equivalent of $Cu_2(PPh_3)_2$ adduct; if one more equivalent of PPh_3 was used, 2 equivalents of $S{=}PPh_3$ and 1 equivalent of $Cu_2(PPh_3)_2$ adduct were obtained. The reaction with phosphine suggests the presence of more than one sulfur atom per cluster.

Moreover ^{1}H-NMR spectra of the mononuclear Cu^{II}BB6 complex shows very broad signals according with its paramagnetic nature, whereas the Cu-BB6-S compound shows sharper signals probably due to coupling of the copper ions mediated by a bridging sulfur coordination.

The data reported suggest the formation, after addition of elemental sulfur to the mononuclear copper cluster, of a transient copper-sulfur species, where the sulfur is likely bridging two copper ions forming a binuclear centre. However, even if the solution is kept under anaerobic conditions, the product is not stable, which means that the coordination of the sulfur is labile and the complex slowly rearranges to the mononuclear Cu^{II} compound. We made several attempts to characterize the structure of this complex but the unstable and transient nature of this compound prevented the formation of crystals of appropriate size.

6.4 Conclusions

The complicated copper-sulfur chemistry has been explored by studying different mononuclear and binuclear N-donors ligands. The copper(I) complexes with binuclear ligands, that has been showed to form stable adducts with a bridging oxygen in the Cu_2O_2 complexes, do not react with sulfur. The copper(I) complexes with mononuclear ligands react with sulfur, even if the Cu-S species has a labile nature. The troubles connected to obtain crystals of appropriate size made difficult to understand the real structure of the cluster, and in particular the number of sulfur atoms bound to the copper complex. A preliminary reactivity study revealed a facile sulfur transfer to the added PPh_3.

Since the copper(II)-sulfur clusters have been synthesised as model compounds for nitrous oxide reductase, their further characterization will require the study of their reactivity versus the substrate of the enzyme. We plan to follow the spectral changes of the cluster upon addition of gaseous N_2O. Furthermore, attempted to transform the reaction from stoichiometric into catalytic will be performed by employing a reductant as co-substrate.

6.5 References

1. Tolman, W. B. (2006) Using synthetic chemistry to understand copper protein active sites: a personal perspective, *J Biol Inorg Chem 11*, 261-271.
2. Gray, H. B., Malmstrom, B. G., and Williams, R. J. (2000) Copper coordination in blue proteins, *J Biol Inorg Chem 5*, 551-559.
3. Turski, M. L., and Thiele, D. J. (2009) New Roles for Copper Metabolism in Cell Proliferation, Signaling, and Disease, *J. Biol. Chem. 284*, 717-721.
4. Boal, A. K., and Rosenzweig, A. C. (2009) Structural biology of copper trafficking, *Chem Rev 109*, 4760-4779.
5. Gaggelli, E., Kozlowski, H., Valensin, D., and Valensin, G. (2006) Copper homeostasis and neurodegenerative disorders (Alzheimer's, prion, and Parkinson's diseases and amyotrophic lateral sclerosis), *Chem Rev 106*, 1995-2044.
6. Henkel, G., and Krebs, B. (2004) Metallothioneins: zinc, cadmium, mercury, and copper thiolates and selenolates mimicking protein active site features--structural aspects and biological implications, *Chem Rev 104*, 801-824.
7. Beinert, H., Holm, R. H., and Munck, E. (1997) Iron-Sulfur Clusters: Nature's Modular, Multipurpose Structures, *Science 277*, 653-659.
8. Rees, D. C., and Howard, J. B. (2003) The Interface Between the Biological and Inorganic Worlds: Iron-Sulfur Metalloclusters, *Science 300*, 929-931.
9. Brown, K., Djinovic-Carugo, K., Haltia, T., Cabrito, I., Saraste, M., Moura, J. J. G., Moura, I., Tegoni, M., and Cambillau, C. (2000) Revisiting the Catalytic CuZ Cluster of Nitrous Oxide (N2O) Reductase. EVIDENCE OF A BRIDGING INORGANIC SULFUR, *J. Biol. Chem. 275*, 41133-41136.
10. Haltia, T., Brown, K., Tegoni, M., Cambillau, C., Saraste, M., Mattila, K., and Djinovic-Carugo, K. (2003) Crystal structure of nitrous oxide reductase from Paracoccus denitrificans at 1.6 A resolution, *Biochem J 369*, 77-88.
11. Chen, P., Gorelsky, S. I., Ghosh, S., and Solomon, E. I. (2004) N2O reduction by the mu4-sulfide-bridged tetranuclear CuZ cluster active site, *Angew Chem Int Ed Engl 43*, 4132-4140.
12. Rasmussen, T., Berks, B. C., Sanders-Loehr, J., Dooley, D. M., Zumft, W. G., and Thomson, A. J. (2000) The catalytic center in nitrous oxide reductase, CuZ, is a copper-sulfide cluster, *Biochemistry 39*, 12753-12756.
13. Alvarez, M. L., Ai, J., Zumft, W., Sanders-Loehr, J., and Dooley, D. M. (2001) Characterization of the copper-sulfur chromophores in nitrous oxide reductase by resonance raman spectroscopy: evidence for sulfur coordination in the catalytic cluster, *J Am Chem Soc 123*, 576-587.
14. Chen, P., Cabrito, I., Moura, J. J., Moura, I., and Solomon, E. I. (2002) Spectroscopic and electronic structure studies of the mu(4)-sulfide bridged tetranuclear Cu(Z) cluster in N(2)O reductase: molecular insight into the catalytic mechanism, *J Am Chem Soc 124*, 10497-10507.
15. Chen, P., DeBeer George, S., Cabrito, I., Antholine, W. E., Moura, J. J., Moura, I., Hedman, B., Hodgson, K. O., and Solomon, E. I. (2002) Electronic structure description of the mu(4)-sulfide bridged tetranuclear Cu(Z) center in N(2)O reductase, *J Am Chem Soc 124*, 744-745.
16. Oganesyan, V. S., Rasmussen, T., Fairhurst, S., and Thomson, A. J. (2004) Characterisation of [Cu4S], the catalytic site in nitrous oxide reductase, by EPR spectroscopy, *Dalton Trans 7*, 996-1002.
17. Ghosh, S., Gorelsky, S. I., Chen, P., Cabrito, I., Moura, J. J., Moura, I., and Solomon, E. I. (2003) Activation of N2O reduction by the fully reduced micro4-sulfide bridged tetranuclear Cu Z cluster in nitrous oxide reductase, *J Am Chem Soc 125*, 15708-15709.
18. Chan, J. M., Bollinger, J. A., Grewell, C. L., and Dooley, D. M. (2004) Reductively activated nitrous oxide reductase reacts directly with substrate, *J Am Chem Soc 126*, 3030-3031.
19. Helton, M. E., Chen, P., Paul, P. P., Tyeklar, Z., Sommer, R. D., Zakharov, L. N., Rheingold, A. L., Solomon, E. I., and Karlin, K. D. (2003) Reaction of elemental sulfur with a copper(I) complex forming a trans-mu-1,2 end-on disulfide complex: new directions in copper-sulfur chemistry, *J Am Chem Soc 125*, 1160-1161.
20. Helton, M. E., Maiti, D., Zakharov, L. N., Rheingold, A. L., Porco, J. A., and Karlin, K. D. (2006) A mu-eta2:eta2-disulfide dicopper(II) complex from reaction of S8 with a copper(I) precursor: reactivity of the bound disulfur moiety, *Angew Chem Int Ed Engl 45*, 1138-1141.

21. York, J. T., Brown, E. C., and Tolman, W. B. (2005) Characterization of a complex comprising a [Cu2(S2)2]2+ core: bis(mu-S2 2-)dicopperIII or bis(mu-S2).-)dicopperII?, *Angew Chem Int Ed Engl 44*, 7745-7748.
22. Brown, E. C., York, J. T., Antholine, W. E., Ruiz, E., Alvarez, S., and Tolman, W. B. (2005) [Cu3(mu-S)2]3+ clusters supported by N-donor ligands: progress toward a synthetic model of the catalytic site of nitrous oxide reductase, *J Am Chem Soc 127*, 13752-13753.
23. Tolman, W. B. Binding and activation of N2O at transition-metal centers: recent mechanistic insights, *Angew Chem Int Ed Engl 49*, 1018-1024.
24. Tyeklar, Z., Jacobson, R. R., Wei, N., Murthy, N. N., Zubieta, J., and Karlin, K. D. (1993) Reversible reaction of dioxygen (and carbon monoxide) with a copper(I) complex. X-ray structures of relevant mononuclear Cu(I) precursor adducts and the trans-(.mu.-1,2-peroxo)dicopper(II) product, *Journal of the American Chemical Society 115*, 2677-2689.
25. Kitajima, N., Fujisawa, K., Fujimoto, C., Morooka, Y., Hashimoto, S., Kitagawa, T., Toriumi, K., Tatsumi, K., and Nakamura, A. (1992) A new model for dioxygen binding in hemocyanin. Synthesis, characterization, and molecular structure of the .mu.-.eta.2:.eta.2 peroxo dinuclear copper(II) complexes, [Cu(HB(3,5-R2pz)3)]2(O2) (R = isopropyl and Ph), *Journal of the American Chemical Society 114*, 1277-1291.
26. Henson, M. J., Vance, M. A., Zhang, C. X., Liang, H.-C., Karlin, K. D., and Solomon, E. I. (2003) Resonance Raman Investigation of Equatorial Ligand Donor Effects on the Cu2O22+ Core in End-On and Side-On Î¼-Peroxo-Dicopper(II) and Bis-Î¼-oxo-Dicopper(III) Complexes, *Journal of the American Chemical Society 125*, 5186-5192.
27. Chen, P., Fujisawa, K., Helton, M. E., Karlin, K. D., and Solomon, E. I. (2003) Spectroscopy and bonding in side-on and end-on Cu2(S2) cores: comparison to peroxide analogues, *J Am Chem Soc 125*, 6394-6408.
28. York, J. T., Bar-Nahum, I., and Tolman, W. B. (2008) Copper-Sulfur Complexes Supported by N-Donor Ligands: Towards Models of the Cu(Z) Site in Nitrous Oxide Reductase, *Inorganica Chim Acta 361*, 885-893.
29. Bar-Nahum, I., Gupta, A. K., Huber, S. M., Ertem, M. Z., Cramer, C. J., and Tolman, W. B. (2009) Reduction of nitrous oxide to dinitrogen by a mixed valent tricopper-disulfido cluster, *J Am Chem Soc 131*, 2812-2814.
30. Gorelsky, S. I., Ghosh, S., and Solomon, E. I. (2006) Mechanism of N2O reduction by the mu4-S tetranuclear CuZ cluster of nitrous oxide reductase, *J Am Chem Soc 128*, 278-290.
31. Palavicini, S., Granata, A., Monzani, E., and Casella, L. (2005) Hydroxylation of phenolic compounds by a peroxodicopper(II) complex: further insight into the mechanism of tyrosinase, *J Am Chem Soc 127*, 18031-18036.
32. Battaini, G., De Carolis, M., Monzani, E., Tuczek, F., and Casella, L. (2003) The phenol ortho-oxygenation by mononuclear copper(I) complexes requires a dinuclear mu-eta2:eta2-peroxodicopper(II) complex rather than mononuclear CuO2 species, *Chem Commun (Camb)*, 726-727.
33. Monzani, E., Quinti, L., Perotti, A., Casella, L., Gullotti, M., Randaccio, L., Geremia, S., Nardin, G., Faleschini, P., and Tabbi, G. (1998) Tyrosinase Models. Synthesis, Structure, Catechol Oxidase Activity, and Phenol Monooxygenase Activity of a Dinuclear Copper Complex Derived from a Triamino Pentabenzimidazole Ligand, *Inorg Chem 37*, 553-562.
34. Crane, J. D., and Fenton, D. E. (1990) Tripodal Benimidazolate Complexes of Tricarbonylmolybdenum(0) and of Iron (III), *J. Chem. Soc. Dalton Trans. 12*, 3647-3653.
35. Casella, L., Gullotti, M., Radaelli, R., and Di Gennaro, P. (1991) A tyrosinase model system. Phenol ortho-hydroxylation by a binuclear three-coordinate copper(I) complex and dioxygen, *Journal of the Chemical Society, Chemical Communications*, 1611-1612.
36. Casella, L., Carugo, O., Gullotti, M., Garofani, S., and Zanello, P. (1993) Hemocyanin and tyrosinase models. Synthesis, azide binding, and electrochemistry of dinuclear copper(II) complexes with poly(benzimidazole) ligands modeling the met forms of the proteins, *Inorg. Chem. 32*, 2056-2067.

Chapter 7

Conclusions and future perspectives

The study of the enzyme N_2OR represents an open field in bioinorganic chemistry, especially after the resolution of the first structure of the enzyme from *Pseudomonas nautica* had revealed the unique motif of the catalytic centre CuZ.

The objectives of this thesis are linked with the need to investigate the reaction mechanism of the enzyme, the interaction with the electron donors, the active forms of the catalytic centre and its correlation with structural and electronic features.

In **Chapter 2**, the study of the interaction of *Pseudomonas nautica* N_2OR with its physiological electron donor was described. Activity tests in the presence of different *c*-type cytochromes, isolated from the same bacterial source, show that only cytochrome c_{552} has able to donate electrons to this enzyme and thus is its physiological electron donor. The first detailed kinetic treatment for N_2OR with its redox partner was performed and the comparison of the kinetic

parameters obtained when using cytochrome c_{552} or methylviologen (the artificial electron donor also used as reducing agent in the activation process) pointed out important differences in the mechanism of interaction of these two electron donors with the enzyme. The kinetic study also revealed the hydrophobic nature of the interaction and direct electron transfer studies showed that CuA center is the center that receives electrons from the physiological electron donor.

The electron transfer complex between cytochrome c_{552} and N2OR was then investigated by other techniques, such as ^{1}H-NMR protein-protein titrations and a molecular docking program, BiGGER, was used to obtain a model structure of the complex. The proposed docked complexes corroborated the ET studies, giving a large number of solutions in which cytochrome c_{552} is placed nearby a hydrophobic patch located around the CuA center of N_2OR.

Following the previous study, in **Chapter 3** the interaction of cytochrome c_{552} and N_2OR was studied by electrochemical methods, using a membrane configuration electrode. The intermolecular electron transfer was analysed by cyclic voltammetry, under catalytic conditions, and a second-order rate constant (k) of $(5.5 \pm 0.9) \times 10^5$ $M^{-1}s^{-1}$ was determined.

Moreover, the direct reaction of the activated form of *Pseudomonas nautica* nitrous oxide reductase with stoichiometric amounts of N_2O allowed the identification of a new reactive intermediate of the catalytic centre, CuZ°, in the turnover cycle, characterized by an intense absorption band at 680 nm. Both the reaction of stoichiometric amounts of substrate and the electrochemical studies showed that the active CuZ° species, generated in the absence of reductants, can rearrange to the resting non-active CuZ state. New aspects of the catalytic and activation/inactivation mechanism of the enzyme are discussed and represented here in an overall scheme (Figure 7.1). In perspective, the complete spectroscopic and electronic characterization of the CuZ° specie is imperative to understand its electronic properties and structure.

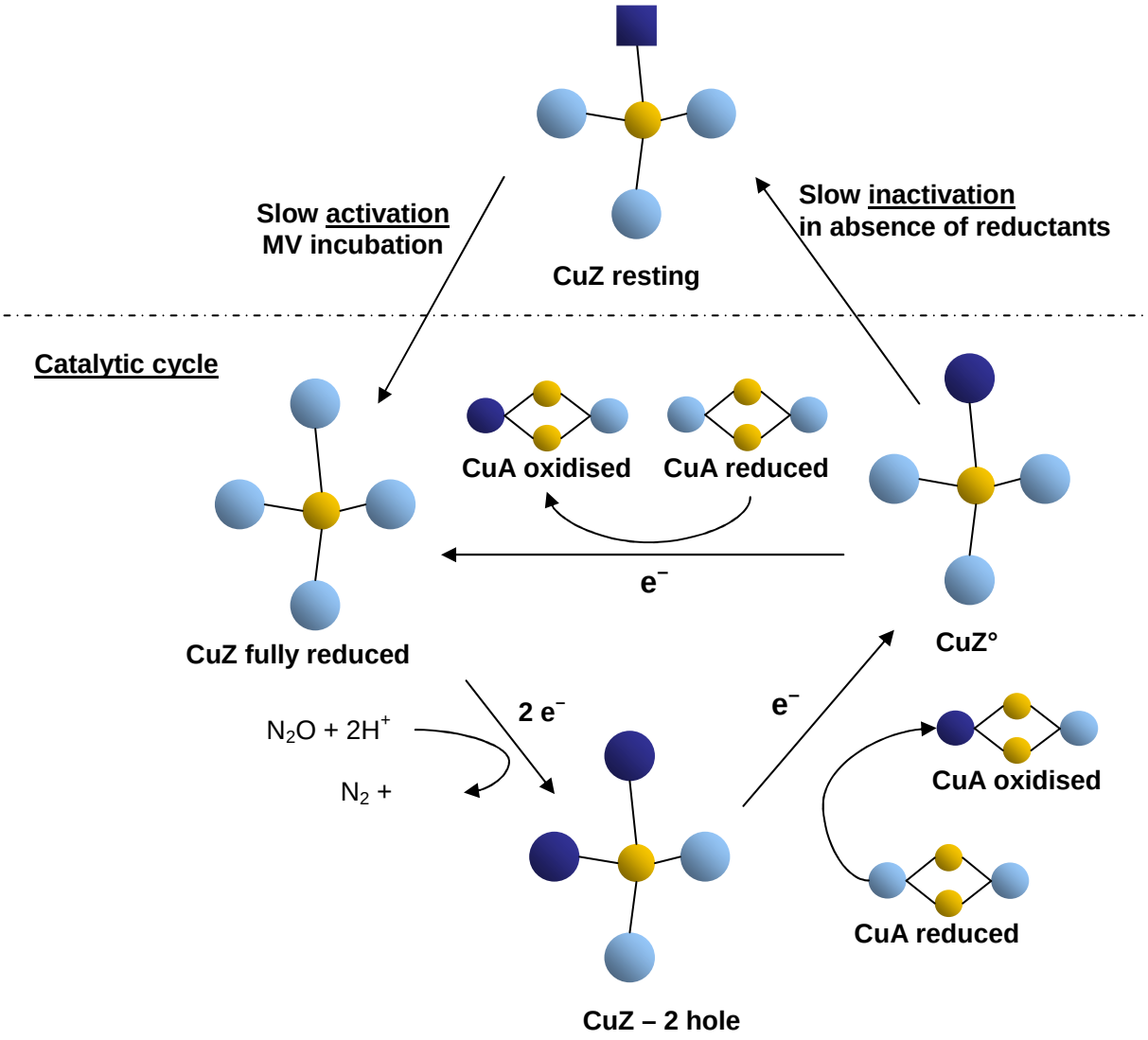

Figure 7.1 – Schematic diagram of the possible mechanism of reduction, catalysis and inactivation of the N_2OR catalytic centre – CuZ. Copper ions are blue colored spheres in the (II) oxidation state or light blue in the (I) oxidation state. In the CuZ resting form, the Cu(II) ion is represented as a blue square to indicate that this form is inactive. In both CuZ and CuA centers, the unpaired electrons are delocalized within the cluster through the sulfur atom.

In **Chapter 4**, the study of the model structure of the electron transfer complex between N_2OR and its electron donor was extended to enzymes from different bacterial sources. The comparison between the interaction of N_2OR from three different microorganisms, *Pseudomonas nautica*, *Paracoccus denitrificans* and *Achromobacter cycloclastes*, of which the three-dimensional structure is available, with their physiological electron donors was performed through the analysis of their primary sequence alignment, electrostatic surface and by molecular docking simulations using the BiGGER algorithm. The docking results were refined on the basis of experimental data, since the interaction is suggested to have either a

hydrophobic, in the case of *Pseudomonas nautica* N_2OR, or an electrostatic nature, in the case of *Paracoccus denitrificans* and *Achromobacter cycloclastes.*

The properties of the electron transfer complex were further investigated by focusing on the pathways for the electron transfer. A set of well conserved residues on the N_2OR surface were proposed to be involved in the electron pathway from the redox partner to nitrous oxide reductase (Ala495, Asp519, Val524, His566 and Leu568 in the case of *Pseudomonas nautica* N_2OR). Moreover, we built a model for *Wolinella succinogenes* N_2OR, an enzyme that presents an additional cytochrome *c* domain. The structure of both N_2OR – domain and cytochrome *c* – domain were modelled and the full length structure was obtained by molecular docking simulation of these two domains.

In **Chapter 5**, the first purification and characterization of the redox-active "purple" form of *Pseudomonas nautica* N_2OR was reported. This study showed that both the as-isolated form of N_2OR, the "blue" resting and the "purple" form, show a very low activity when compared with the high activity of the fully reduced state and also with the CuZ° intermediate state.

The strong reducing conditions required for N_2OR activation, which are also not available in the periplasm of a Gram-negative bacterium, suggests that MV can interact directly with CuZ over-passing the physiologic electron transfer pathway that goes through CuA centre.

However, the enzyme can have a high catalytic activity in the absence of reduced MV, as shown by the CuZ° that has the same catalytic activity as the fully reduced form. The full spectroscopic and electronic characterization of the CuZ° intermediate is necessary to understand the properties of this intermediate.

The first intermediate of the CuZ after the N_2O reduction should be a two-hole form that until now has not been trapped under turnover conditions, probably because of its short-life time due to the very fast delivery of one-electron from the CuA center. Therefore, stopped-flow kinetics and rapid-freeze quenching techniques will be required to trap this key intermediate of the turnover cycle.

In addition, structural data of N_2OR with CuZ in different redox states is also essential to obtain because the crystal structures available are of the resting non-active form of the enzyme. The prolonged incubation required to fully activate the enzyme suggests that there is a conformational change in the protein structure or in the cluster geometry in order to reach the optimal configuration of catalytically active CuZ center.

The biomimetic approach described in **Chapter 6** represents a valid alternative to study the complex copper-sulfur chemistry of the catalytic centre of N_2OR, CuZ center. A synthetic

method that exploits the capability of copper(I) complexes to react with molecular sulfur (S_8) was used. In particular, polybenzimidazole residues as histidine-mimetic were used as donor ligands for the copper ions.

In conclusion, in spite of the progress already achieved in the study about the enzymatic properties of *Pseudomonas nautica* N_2OR, several aspects remain unclear. Moreover, the full understanding of the CuZ center structure in N_2OR and its catalytic mechanism is urgent due to the high impact that the N_2O has towards the environment, as a potent greenhouse gas which plays a serious role in stratospheric ozone depletion.